Stream Temperature and Dissolved Oxygen Modeling in the Lower Flint River Basin, GA

by

Guoyuan Li

(Under the direction of C. Rhett Jackson)

Abstract

The tributaries of the Lower Flint River, southwest Georgia, are incised into the upper Floridan semi-confined limestone aquifer, and thus seepage of relatively old groundwater sustains baseflows and provides some influence over temperature and dissolved oxygen (DO) fluctuations. This hydrologic and geologic setting creates unique aquatic habitats. Groundwater withdrawals for center-pivot irrigation and proposed water supply municipal reservoirs threaten to exacerbate low flow conditions during summer droughts, which may negatively alter stream temperature and dissolved oxygen conditions. To evaluate possible effects of human modifications to stream habitat, we developed a one-dimensional Dynamic stream Dissolved Oxygen and Temperature (DDOT) model. DDOT was constructed with both Continuously Stirred Tank Reactor (CSTR) based and the one-dimensional Advection-Dispersion-Reaction Equation (ADRE) based formulations, and integrates the effects of dynamic streamflow and groundwater inputs, riparian shading, channel geometry, and channel hydraulics on the spatial and temporal dissolved oxygen and temperature dynamics. The major contributions of model DDOT to existing models include the integration of an easy-to-use SHADE module and a BED module. The SHADE module generates accurate estimation of riparian vegetation shading to direct solar radiation on stream water surface, while the BED module calculates the streambed layer vertical temperature and DO profiles that are necessary to account for groundwater input effect on surface water quality. The model was calibrated with field data collected in 2002 and evaluated with data from 2003, years in which flow and water quality behavior were very different. The two formulations provided nearly equivalent simulations. The model performed well and allowed robust exploration of system sensitivities and responses to management actions. With DDOT, we conducted sensitivity analysis of stream temperature and DO to the upstreamflow input, groundwater discharge, stream riparian vegetation shading, and stream width. It indicated that 1)reduced instreamflow rate leads to increased stream temperature and decreases stream DO in summer, 2)reduced groundwater input exacerbates stream temperature problems,especially during drought seasons, 3) reduced groundwater input does not exacerbate stream DO problems due to the fact that ground water itself has a DO concentration as low as 5 mg/L, 4)problematic DO levels occur only at very low flows, and 5)stream width and riparian vegetation have strong effects on stream temperature and DO levels. The model was then used to predict time series stream temperature and DO with long-term time series (1950 - 2003) streamflow data simulated by Hydrological Simulation Program - FORTRAN (HSPF) model and groundwater discharge data simulated by MODular Finite-Element (MODFE) model under three different agricultural pumping scenarios for Ichawaynochaway Creek and Spring Creek watersheds in the Lower Flint River Basin. The simulation indicated that the spatial patterns of water quality dynamics in the two watersheds were associated with groundwater input, stream aspect, and stream width.

Index words: Streamflow, Groundwater discharge, Water quality, Stream temperature, Dissolved oxygen, Dynamic modeling, CSTR, ADRE, Finite difference, Numerical solution

Stream Temperature and Dissolved Oxygen Modeling in the Lower Flint River Basin, GA

by

Guoyuan Li

B.A., Beijing Forestry University, 1998

M.S., Beijing Forestry University, 2001

A Dissertation Submitted to the Graduate Faculty
of The University of Georgia in Partial Fulfillment
of the
Requirements for the Degree

Doctor of Philosophy

Athens, Georgia

2006

Stream Temperature and Dissolved Oxygen Modeling in the Lower Flint River Basin, GA

by

Guoyuan Li

Approved:

Major Professor: C. Rhett Jackson

Committee: Todd C. Rasmussen
M. Bruce Beck
James T. Peterson
David E. Stooksbury

Electronic Version Approved:

Maureen Grasso
Dean of the Graduate School
The University of Georgia
August 2006

Dedication

With love and devotion

To my parents, who supported me for education

To my wife, Hong, who accompanies me

To my son, Gary, who makes life so meaningful to us

ACKNOWLEDGMENTS

I am greatly indebted to my major professor, Dr. C. Rhett Jackson, for his acceptance, support, guidance, and encouragement throughout my study. Dr. Jackson was always there to listen and to give advice. He taught me how to express my ideas, how to fulfill research goals, how to make scientific presentations, and how to write academic papers. This dissertation would not have been possible without his enlightening suggestions. I am also greatly indebted to Dr. Jackson for his friendship to me and to my family. He hosted warmhearted household parties to welcome the arrival of myself and my wife to the US. He threw a baby shower for the arrival of my son to this wonderful world. Dr. Jackson's kindness brought measureless brightness to our life here in Athens.

Sincere thanks are extended to Dr. Todd C. Rasmussen, for his always enthusiastic help with my study. I learned a lot from his extremely broad knowledge and very nice personality. Dr. Rasmussen guided me in use of Matlab and LaTeX, which became the major tools for my model development and dissertation writing. Dr. Rasmussen generously offered me both vehicle and furniture, which greatly improved my living and research at UGA.

I thank Dr. M. Bruce Beck, an eminent scholar at UGA, for instructing direct modeling techniques and his insightful thoughts and suggestions for my project. His gentlemanly and humorous style of conversation made it a great pleasure to take his classes, and his prudence and frugality influenced me deeply.

I would also like to thank other members of my advisory committee: Dr. James T. Peterson and Dr. David E. Stooksbury. I thank Dr. James T. Peterson, for his funding, advice, and helpful suggestions to my dissertation project. I thank Dr. David E. Stooksbury, for his help on my weather data manipulation.

Let me say “Thank you” to the hydrology group for their help and encouragement. Much gratitude is extended to Chris Holliday, Jenny Yearwood, Zhulu Lin, Denise Carroll, Feng Jiang, Joan Schneier, Jim White, Will Summer, and Josh Romeis.

Finally, I would like to extend my special thanks to my wife, Hong, for her love, support, patience, and sacrifice. Hong has been taking care of our little son Gary on her own through those days and nights when I was working on my dissertation project. The completion of my doctoral study is a joint accomplishment of both of us.

Table of Contents

List of Figures

List of Tables

Chapter 1

Introduction

Stream temperature and dissolved oxygen are two critical factors affecting survival, movement and the growth of fish (Beschta *et al.*, 1987; Coutant, 1987; Christie and Regier, 1988; Horne and Goldman, 1994; Karim *et al.*, 2003). During hot summer weather, high stream temperature and low dissolved oxygen problems often occur simultaneously and the resulting stress affects fish habitat use and survival (Matthews, 1998; Lind, 1985). These two water quality parameters are also key factors affecting freshwater mussel survival (Miller and Payne, 2004; Johnson *et al.*, 2001). Studies have shown that the instream flow rates play an important role in summer stream temperature and DO variations (Gaffield *et al.*, 2005; Lopes *et al.*, 2004; Sridhar *et al.*, 2004; Sinokrot and Gulliver, 2000; Chaudhury *et al.*, 1998; Caruso, 2002; Gilvear *et al.*, 2002; Sabo *et al.*, 1999), and the effects of groundwater discharge on stream summer temperature and DO can be significant (Moore *et al.*, 2005; Gaffield *et al.*, 2005; Power *et al.*, 1999; LeBlanc *et al.*, 1997). Accordingly, the preservation of a minimum amount of instream flow and maintenance of groundwater discharge can be critical to protect stream aquatic habitat.

In the state of Georgia, streamflow regulation has been one of the most important issues facing natural resource managers and planners. Increasing population, combined with increased water withdrawal for crop irrigation, has created conflicts in water resources management (Fanning, 1999). Increased water demand and use has been identified as one of the primary problems threatening stream fishes and other aquatic biota in the Southeastern United States (Richter *et al.*, 1997).

The Lower Flint River Basin, as one of the state's most important agricultural areas, has become a particular concern of resources managers, planners, and fishery scientists. Extremely low flow and severely degraded aquatic habitat problems have occurred during drought seasons. In the summer of 2000, extended drought and increased irrigation pumping brought record low flow to streams in the basin. New record low groundwater levels were recorded in more than 40 wells in the statewide ground-water monitoring network from January to August 2000, with most of these wells located in the lower Flint River Basin (USGS, 2000). Excessive groundwater withdrawal for center-pivot irrigation reduces groundwater discharge to streams (Hayes *et al.*, 1983; Torak *et al.*, 1996; Albertson and Torak, 2002), which may have exacerbated the drought's effect on stream water quality. These changes severely impacted stream aquatic habitat. Unionid mussels *Elliptio crassidens* were killed in Chickasawhatchee Creek, Baker County, GA in July 2000, mainly due to the low flow velocity ($<$0.01 m/s) and dissolved oxygen ($<$5 mg/L) (Johnson *et al.*, 2001). Major fish kills also occurred due to the loss of the aquatic habitat.

The state established the Flint River Drought Protection Act in March 2001 to protect instream flows in tributaries of the basin by limiting farmland irrigation from surface water during drought seasons. However, the efficiency of the Act depends on whether natural resource managers and planners are informed as to the nature and extent of potential impacts. Proposals to construct water-regulation dams may have adverse impacts on downstream aquatic habitat, especially on stream water temperature and dissolved oxygen. There is a need to develop models for natural resources managers and planners to have a clear understanding of the interactions between stream water quantity and quality.

Among the goals of such a model would be to evaluate the following hypotheses for the study area:

1. Decreased instream flow rate leads to elevated stream temperature and degraded stream dissolved oxygen;

2. Ground water, with its relatively low temperature, has a strong cooling effect on streams in the summer;

3. Stream oxygen concentration increases as a response to decreased stream temperature by increased groundwater addition and/or upstream flow input;

4. Stream width, by affecting direct solar radiation, has positive correlations to stream temperature and dissolved oxygen; while

5. Riparian vegetative shading has negative correlations to stream temperature and dissolved oxygen.

To fulfill our goals, we developed the one-dimensional process-based Dynamic Dissolved Oxygen and Temperature (DDOT) stream water quality model. The model consists of flow, temperature, and dissolved oxygen components, with the flow component generating necessary dynamic flow parameters, and temperature and DO components providing time series water quality outputs. The model DDOT has advantages compared with existing computer models by integrating a SHADE module and a one-dimensional vertical temperature profile module of the streambed and a DO profile module of the flow passing through the streambed.

DDOT was calibrated successfully with data collected from Ichawaynochaway Creek during late summer of the year 2002, and was evaluated with data collected from the same reach during the summer of 2003. Sensitivity analysis was conducted to examine the effects of factors such as instream flow and groundwater discharge, plus another two important factors, i.e., riparian vegetation and stream width.

The model was then used to perform long-term simulations. The long-term simulations were intended to provide stream temperature and DO dynamics in Ichawaynochaway Creek and Spring Creek for given flow scenarios. The input streamflow data were generated by Hydrological Simulation Program - FORTRAN (HSPF) model and the groundwater discharge/recharge data were by MODular Finite-Element model (MODFE) model. These flow data were available from the Georgia Department of Natural Resources (DNR) for the years from 1950 to 2003. The yearly maximum temperature and minimum DO data under each of three flow scenarios were selected to demonstrate water quality patterns, which helped identify the reaches that were mostly susceptible to high temperature and low DO problems.

Chapter 2

Literature Review

Dynamic stream water quality models involve both the efficient formulation of the basic model structures and the precise estimation of the mass/energy source and sink terms. In this chapter, Section One introduces available model structures and numerical solution schemes that have been using for longitudinal stream water quality modeling; Section Two discusses the available studies of the instream flow and groundwater discharge effects on stream water quality; Section Three discusses the associated techniques in estimating the source and sink components for stream water temperature and DO constituents; and Section Four discusses the application and limitations of the existing computer models. A summary is provided at the very end of the chapter.

2.1 General model structures and numerical solutions

2.1.1 General model structures

Basically, water quality models can be divided into two categories, with one being the mechanistic (internally descriptive) models and the other being black box (input-output or empirical) models. Mechanistic models provide descriptions of the internal mechanisms and explain more about the behavior of the systems, while the black box models make no such explicit reference and deal with only the inputs and outputs. However, these two categories of models are two ends of the spectrum of models (Beck, 1983, P_{20}). In practice, many mechanistic models are actually semi-empirical even though they do account for individual processes (Cox, 2003b). In this review, we focus on the mechanistic models that use a certain amount of empirical equations for estimating source/sink terms. These type models have been mostly used in stream water quality modeling studies. Based on the model formulation representations, three typical model structures are commonly used: 1) the Continuously Stirred Tank Reactor (CSTR) based models; 2) the one-dimensional Advection-Dispersion-Reaction Equation (ADRE) based models; and 3) the Lagrangian models (James, 1984, Chapter 5).

CSTR models

CSTR models, initially used in chemical engineering (Young and Beck, 1974), have been used in water quality modeling extensively due to the more utilitarian formulation of the ordinary differential equations (ODE) for model calibration and evaluation as compared to partial differential equations (PDE) (Cox, 2003a). Young and Beck (1974) assumed the River Cam, England, to be idealized as a series of continuously connected CSTRs to study the dynamic behavior of DO and Biological Oxygen Demand (BOD) interactions. Ahlert and Hsueh (1980) verified the performance of CSTR models against tracer data in the Passaic River of New Jersey. Whitehead *et al.* (1997) developed the well-known water quality simulation along river systems (QUASAR) model with CSTR based modeling structures. Sincock *et al.* (2003) conducted sensitivity analysis of CSTR based river water quality model under unsteady flow conditions. Zeng *et al.* (2005) conceptualized an agricultural pond as a CSTR for their biogeochemical model. In England, many stream water quality computer models, such as SIMCAT, TOMCAT, and etc., also adopted CSTR model structures (Cox, 2003a).

CSTR models bear several assumptions. The most important one is the perfect mixing assumption (Chapra, 1997, Lecture 3; Beck, 1983, P_{451}). For a longitudinal river system, the conceptualized CSTR is usually considered to be a feed-forward system, in which diffusion is considered negligible (Chapra, 1997, Lecture 5). These assumptions enable the easier formulations of the CSTR models. Because streamflow is included explicitly, CSTR models allow examination of streamflow effects on water quality constituents.

A typical computational representation of CSTR models usually take the following form (Sincock *et al.*, 2003; Chapra, 1997, Lecture 3; James, 1984, $P_{67,96}$; Young and Beck, 1974):

$$\frac{dC}{dt} = \frac{Q_{in}C_{in} - Q_{out}C}{V} + S_1 - S_2 \tag{2.1}$$

where, C is any state variable concentration of interest (ML^{-3}); t is time (T); Q_{in} is upstream incoming flow (L^3T^{-1}); C_{in} is the state variable concentration of the upstream inflow (ML^{-3}); Q_{out} is downstream outflow (L^3T^{-1}); V is the volume of the tank (L^3); S_1 denotes source terms and S_2 denotes sink terms ($ML^{-3}T^{-1}$).

ADRE models

ADRE models are generally used for stream water quality modeling studies (Gooseff *et al.*, 2005; Liu *et al.*, 2005; Lin *et al.*, 2005; De Smedt *et al.*, 2005; Lopes *et al.*, 2004; Sridhar *et al.*, 2004; Zheng *et al.*, 2004; Zeng and Beck, 2003; Sincock *et al.*, 2003; Campolo *et al.*, 2002; Sinokrot and Gulliver, 2000; Rauch *et al.*, 1998; Adrian *et al.*, 1994; Sinokrot and Stefan, 1993; Van Orden and Uchrin, 1993; Stamou, 1992; Park and Uchrin, 1988; Gulliver and Stefan, 1984; O'Loughlin and Bowmer, 1975). One-dimensional ADRE models are simplified forms of the full three-dimensional convective diffusion models. The one-dimensional ADRE models are justified for the reason that, in most natural streams, the longitudinal mass transport is more significant than lateral and vertical mass transport. The models are derived using the Eulerian equation and Fick's law (James, 1984). ADRE models explicitly incorporate streamflow and cross section area, which allows one to directly examine flow effects on state variables. The typical one-dimensional ADRE models take the following form based on Taylor dispersion (Taylor, 1953):

$$\frac{\partial AC}{\partial t} + \frac{\partial QC}{\partial x} = \frac{\partial}{\partial x}(AD\frac{\partial C}{\partial x}) + S_1 - S_2 \tag{2.2}$$

where, C is any state variable concentration of interest (ML^{-3}); t is time (T); Q is stream discharge (L^3T^{-1}); A is stream cross section area (L^2); D is dispersion coefficient ($L^2\ T^{-1}$); S_1 denotes source terms and S_2 denotes sink terms ($M\ L^{-1}T^{-1}$).

Lagrangian models

The Lagrangian formulation is an alternative approach for the continuity equation derivation. In Lagrangian models, streamflow is simulated as a series of blocks with fixed mass moving consecutively downstream (James, 1984, P_{92}). The dispersive mechanism is assumed to be negligible. The blocks are considered to be discrete and there is no mass exchange between blocks. Water quality studies using Lagrangian models include Wang *et al.* (2003), Williams *et al.* (2000), Rutherford *et al.* (1997), and Pearson and Crossland (1996). The typical mathematical representation takes the following form (James, 1984, P_{95}):

$$\frac{dC}{dt} = S_1 - S_2 \tag{2.3}$$

where, C is any state variable concentration of interest (ML^{-3}); t is time (T); S_1 denotes source terms and S_2 denotes sink terms ($M\ L^{-1}T^{-1}$).

Lagrangian formulation itself takes a simple ODE form and thus is succinct. However, because it does not explicitly account for streamflow information, it is inconvenient for evaluating flow effects on water quality.

2.1.2 Commonly used finite difference numerical solutions

Many different types of numerical solutions are available for differential equations, such as methods of finite difference, finite volume, finite element, and characteristics (Thomee, 2001; Morton and Mayers, 1994; Gerald and Wheatley, 1989; Ames, 1977). Among these methods, the finite difference methods, including both explicit and implicit schemes, are mostly used for one-dimensional problems such as longitudinal river systems (Sturm, 2001; Chapra, 1997; Beven and Kirkby, 1993; Chaudhry, 1993; James, 1984; Orlob, 1983).

Finite difference schemes for ODE

The simplest numerical method for solving ODE is the Euler's method (Chapra, 1997). Euler's method was derived by removing all the second and higher order derivatives of

Taylor series expansion. A mathematical representation of this method can be written as below (Sturm, 2001; Chapra, 1997; James, 1984):

$$C_{i+1} = C_i + f(h_i, C_i)\Delta h \tag{2.4}$$

where, C_{i+1} and C_i denote values of the state variables of interest at step $i+1$ and i respectively; $f(C_i)$ is the slope evaluated at step i, i.e., $\frac{dC}{dh}|_{h \to h_i}$; h_i is the value of h at location i; and Δh is the calculation step length.

The Euler method is a first-order approach (Chapra, 1997, P_{126}). It requires very small steps for nonlinear systems, and therefore considerable computational effort, to achieve acceptable accuracy (Sturm, 2001).

The Heun method, by using the mean of the slopes evaluated both at step i and $i+1$, improves the prediction accuracy (Sturm, 2001; Chapra, 1997). Because the slope at step $i+1$ is not known, it is first predicted by the Euler method. Thus this method is also known as the corrected Euler method or the predictor-corrector method. The method is a second-order approach (Chapra, 1997, P_{126}). The formulation of this method takes the following form,

$$C_{i+1}^0 = C_i + f(h_i, C_i)\Delta h \tag{2.5a}$$

$$C_{i+1} = C_i + \frac{f(h_i, C_i) + f(h_{i+1}, C_{i+1}^0)}{2}\Delta h \tag{2.5b}$$

Essentially, the Heun method is the simplest one of a larger class of solution techniques known as Runge-Kutta methods. The Runge-Kutta methods are a family of numerical methods that have been used extensively in water quality modeling (Chapra, 1997, Lecture 7). The most popular one is the classic fourth-order method, which requires four steps to obtain an improved average slope. The procedures can be represented as below,

$$C_{i+1} = C_i + \frac{k_1 + 2k_2 + 2k_3 + k_4}{6}\Delta h \tag{2.6}$$

Where,

$$k_1 = f(h_i, C_i)\Delta h$$
$$k_2 = f(h_i + \frac{\Delta h}{2}, C_i + \frac{\Delta h}{2}k_1)$$
$$k_3 = f(h_i + \frac{\Delta h}{2}, C_i + \frac{\Delta h}{2}k_2)$$
$$k_4 = f(h_i + \Delta h, C_i + \Delta h k_3)$$

Finite difference schemes for PDE

Because partial differential equations are extensively used in practice, numerous numerical schemes have been developed. Several commonly used schemes in water quality modeling studies include explicit schemes, such as the MacCormack scheme, the Saulyev scheme, the QUICK/QUICKEST schemes, and implicit schemes, such as the Backward-time/Centered-space scheme, the Crank-Nicolson Scheme, and the Preissmann scheme (Chapra, 1997; Sturm, 2001; Chaudhry, 1993; Leonard, 1979; Stamou, 1992; Dehghan, 2004a,b). A detailed review of these schemes can be found in Chapter 3.

2.2 Effects of instream flow and groundwater input on stream water quality

A large body of literature has examined the effects of instream flow rate and/or groundwater discharge on stream water quality constituents (Gaffield *et al.*, 2005; Sridhar *et al.*, 2004; Lopes *et al.*, 2004; Sinokrot and Gulliver, 2000; Chaudhury *et al.*, 1998; LeBlanc *et al.*, 1997; Hewlett and Fortson, 1982; Caruso, 2002; Gilvear *et al.*, 2002; Sabo *et al.*, 1999).

Sinokrot and Gulliver (2000) investigated the relationships of streamflow discharge rate and stream temperatures during sunny, hot summer days of the Central Platte River, western Nebraska. A 128-km reach of the river downstream of two hydropower dams was studied to determine the relationship between river summer water temperatures and river flow-rate, and the effects of instream flow requirements upon peak water temperatures. Hourly water temperatures were simulated using a modified dynamic numerical model MNSTREM (Stefan *et al.*, 1980) with and without instream flow requirements. The model used a one-dimensional advection-dispersion equation, plus heat fluxes at both stream surface and streambed. The groundwater inflow and streambed temperature profiles were considered independently. It was found that a clear relationship existed between river water temperatures and river flow-rate, and that the occurrence of high water temperatures could be attributed to low river flow rate. The high temperature could be reduced but not eliminated with minimum instream flow requirements.

Gaffield *et al.* (2005) examined how stream temperature was controlled by the complex interactions among meteorologic processes, channel geometry, and ground water inflow for streams in southwestern Wisconsin. An analytical solution of the Stream Network Temperature Model (SNTEMP) (Theurer *et al.*, 1984) was used to simulate steady state stream temperatures throughout the stream reach. It concluded that the distribution of groundwater inflow throughout a stream reach had an important influence on stream temperature, and springs were especially effective at providing thermal refuges for fish. The riparian vegetation shading and channel width were also among the most important factors controlling summer stream temperatures.

Lopes *et al.* (2004) conducted a case study of the effects of instream flow on water quality with data collected from a stream segment downstream of the Touvedo dam on the Lima river, in northern Portugal. The model included a dynamic flow model (Saint-Venant equations) and water quality model (ADRE), with the flow model solved using the Preissmann implicit scheme and the quality model using the explicit SMART algorithm. Water temperature and DO were simulated for different operational conditions of the dam discharges (water quantity and duration) and two levels of water withdrawal. By simulating the variation of DO and temperature downstream of the dam, it was found that water quality modified as a function of the outflow and discharge level from the dam, which caused adverse impacts to the migratory fish community, such as that salmonids fishes would be replaced by the more tolerant cyprinids.

2.3 Stream water quality modeling techniques

2.3.1 Stream temperature modeling

Stream temperature modeling has been studied extensively since Brown (1969). The modeling strategies used were either black box modeling using regression equations (Caissie *et al.*, 2001; Mohseni and Stefan, 1999, 1998; Stefan and Preudhomme, 1993; Maidment, 1993; Hostetler, 1991; Beschta and Taylor, 1988), or mechanistic modeling that internally described the system with differential equations (Gooseff *et al.*, 2005; Sridhar *et al.*, 2004; Chen *et al.*, 1998; LeBlanc *et al.*, 1997; Rutherford *et al.*, 1997; Whitehead *et al.*, 1997; Sinokrot and Stefan, 1993; Sullivan *et al.*, 1990; Jobson, 1977; Brown, 1970, 1969).

The stream temperature mechanistic models usually fall into two categories, either reach models or basin models (Sullivan *et al.*, 1990). Reach models predict water temperatures of relatively short individual reaches. Basin models attempt to predict temperatures at different locations of an entire watershed. Basin models usually initially use a reach model to predict temperatures at specific sites, then route water downstream to the next prediction site while adjusting temperatures based on the environmental conditions encountered. Essentially, basin models are integrated reach models. Several stream temperature modeling studies are reviewed below.

Brown (1969) employed energy budget techniques to predict small stream temperature changes. The energy fluxes considered included: the net all-wave thermal radiation flux measured with a net radiometer, the evaporative flux estimated with the Delton-type equation, the streambed conductive heat flux estimated based on measured streambed temperature gradient, the water surface convective flux estimated with the Bowen ratio, and the advective flux from upstream, tributary, or groundwater discharge estimated with a simple mixing ratio equation. Using this technique, Brown predicted hourly stream temperatures for a whole day, with 22 out of 24 predictions within 1 °F of the measured value. Brown was the first researcher to consider the effect of bottom conduction, which, as he pointed out, was essential for accurate temperature prediction.

Sinokrot and Stefan (1993) predicted hourly stream water temperatures by numerically solving the one-dimensional advection-dispersion unsteady heat equation. Factors such as solar radiation, air temperature, relative humidity, cloud cover, and wind speed were used to estimate the net rate of heat exchange through the water surface. Heat flux through the streambed was calculated by numerically simulating streambed vertical temperature profile with a one-dimensional unsteady heat conduction equation. Accuracies of the hourly and daily predictions were of the order of 0.2 to 1 °C. It was shown that, although solar radiation is the most important control of stream water temperature, the other heat fluxes, such as long-wave radiation, evaporation, convection, and streambed conduction, were not negligible.

LeBlanc *et al.* (1997) developed the critical urban stream temperature model (CrUSTe) to study the effects of land use change on urban stream temperatures. Model CrUSTe integrated four models, one of which was the stream temperature model, which considered heat gains and losses resulting from radiation, convection, evaporation, and advection. Streambed conduction was considered negligible so that it was not included in the model. However, groundwater input was included. The stream reach was divided into several shorter segments where a proportion of groundwater was attributed to the beginning of each segment. The proportion was calculated by assuming uniform groundwater infiltration over the entire reach. The sensitivity analysis indicated riparian vegetation shading, groundwater discharge, and stream width had the greatest influence on stream temperatures.

Rutherford *et al.* (1997) developed a computer model (STREAMLINE) to predict the effects of shade on water temperatures in small streams near Hamilton, New Zealand under steady stream discharge with a time step length of 15-minutes. The model quantified shading by riparian vegetation shade factor, hillsides angle, and stream bank angle. Heat fluxes by radiation, convection, evaporation, and streambed heat conduction were calculated based on the streambed vertical temperature profile, which was simulated by assuming a bed of several sediment layers of equal depth and solving the heat equations numerically.

Chen *et al.* (1998) investigated the effects of riparian shading and streambed conduction on watershed-scale stream water temperatures. A GIS based SHADE program was developed and integrated to Hydrologic Simulation Program - FORTRAN (HSPF) to generate hourly riparian vegetation and topography shading for available solar radiation at stream water surfaces. Heat exchange between water and streambed was estimated with the analytical solutions developed by Jobson (1977), assuming streambed to be a homogeneous medium insulated on the lower face and with the upper face always having a temperature equal to the overlying water.

Sridhar *et al.* (2004) studied streamside vegetation buffer effect on stream temperatures in forested headwater watersheds with a simple energy balance GIS based model. The model was designed for the application to *worst case* or maximum annual stream temperature under low flow condition and maximum annual solar radiation and air temperature. Their sensitivity analysis showed that increasing the buffer width beyond 30 m did not significantly decrease stream temperatures, and that other vegetation parameters, such as leaf area index and average tree height, more strongly affected maximum stream temperatures.

2.3.2 Stream dissolved oxygen modeling

The classic stream dissolved oxygen modeling has been attributed to Streeter-Phelps equations, which incorporate the two primary mechanisms governing the fates of DO and BOD along a river (Cox, 2003b). Since then, many modified or extended versions of the Streeter-Phelps equations have been used for stream DO mechanistic modeling (Young and Beck, 1974; Gulliver and Stefan, 1984; Van Orden and Uchrin, 1993; Stefan and Fang, 1994; Pearson and Crossland, 1996; Whitehead *et al.*, 1997; Chaudhury *et al.*, 1998; Parkhill and Gulliver, 1999; Williams *et al.*, 2000; Kayombo *et al.*, 2000; Moatar *et al.*, 2001; Wang *et al.*, 2003; Zheng *et al.*, 2004; Zeng *et al.*, 2005). In general, the dominant processes related to stream oxygen levels include atmospheric reaeration, algae/plant photosynthesis, algae/plant respiration, BOD decay, and sediment oxygen demand (SOD) decay, where BOD can be refined as carbonaceous and nitrogenous oxygen demand (Bennett and Rathbun, 1972). Nitrogenous oxygen demand can also be further refined into ammonia oxygen demand and nitrite oxygen demand in dissolved oxygen models (Chaudhury *et al.*, 1998; Zeng *et al.*, 2005). Several stream DO modeling studies are reviewed below.

Young and Beck (1974) investigated the modeling and control techniques of DO and BOD in a non-tidal river system, River Cam outside Cambridge in east England. By assuming the reach to be CSTRs, a simple ordinary differential equation model for DO-BOD interaction was verified against field data collected from a single reach of the river. The processes considered for DO balance included atmosphere reaeration, BOD decay, and a net DO removal from the reach by the combined effects of photosynthesis, respiration, and mud deposits. One of the conclusions was that the simple, lumped-parameter, dynamic model appeared to provide a potentially adequate description of the DO-BOD balance in a non-tidal river system.

Gulliver and Stefan (1984) developed a numerical Dissolved Oxygen Routing Model (DORM) to determine total stream community photosynthesis and community respiration rates through iterative routing of two-station diel DO measurements. The model used a complete one-dimensional stream DO transport equation (ADRE), which included longitudinal dispersion, dependence of respiratory rate on water temperature and DO, and wind dependent oxygen transfer through the water surface. The respiration rate was a combined effect of SOD, BOD, animal (fish, insects, etc.) and plant respiration. The model was claimed to be simple to apply and more accurate than the traditional graphical procedures of diel curve analysis.

Chaudhury *et al.* (1998) studied stream DO under dry weather conditions of the Blackstone River, Northeastern United States by calibrating and validating the Enhanced Stream Water QUALity Model (QUAL2E). A stepwise approach to simulate each source and sink of DO was used, which was accomplished by progressively defining atmospheric reaeration, algal photosynthesis and respiration, and oxygen depletion due to carbonaceous BOD, nitrification, and SOD. The study indicated that under 7Q10 (Seven day mean flow in ten years) flows, violations of the DO criteria of 5.0 mg/L occurred downstream of the waste-water treatment plant.

Sincock *et al.* (2003) investigated the identifiability of water quality parameters and the associated uncertainty in model simulations by presenting an improved flow component within the framework of the water quality model "QUAlity Simulation Along River Systems (QUASAR)". A Monte-Carlo analysis was used to evaluate the model performance with data collected on the Bedford Ouse River, UK. It was found that some supposedly important water quality parameters associated with algal activity, i.e., the algae respiration coefficient and the algae respiration coefficient directly proportional to chlorophyll-a, were completely insensitive and hence non-identifiable, while others (nitrification and sedimentation) had optimum values at or close to zero, indicating that those processes were not detectable from the dataset examined.

Zheng *et al.* (2004) developed a coupled three-dimensional physical and water quality model for the Satilla River Estuary, Georgia. The physical model was used to provide necessary hydrology parameters for water quality model. The water quality model was a modified three-dimensional conventional Water quality Analysis Simulation Program (WASP5). Water quality constituents simulated by the model included DO, nitrogen, phosphorus, and phytoplankton. The algal photosynthesis carbon fixation was one source of water DO. Atmospheric reaeration was considered either a source or a sink depending on the difference between actual water DO and the saturated water DO. Other associated processes, including SOD, phytophlankton respiration, nitrification, and oxidation of carbonaceous BOD (CBOD), acted as sink terms for DO.

2.4 Existing water quality computer models

TEMPEST was a reach scale stream temperature model developed by Sullivan and Adams. (1990). The model considered each of the heat transfer processes but with simplified variables. The associated factors were daily average solar radiation, air temperature, riparian vegetation shading, wind speed, relative humidity, and groundwater infiltration. The model was designed to perform sensitivity analysis of stream heating processes, but the full model could be used to predict hourly stream temperatures. TEMPEST was later expanded to a basin scale model called MODEL-Y (Sullivan *et al.*, 1990). MODEL-Y used the same energy balance equations as TEMPEST combined with travel time, stream depth, and regional air temperature, and provided a GIS interface. The model was specifically designed for the Timber-Fish-Wildlife project in Washington state and had very limited applicability since it had not been upgraded and tested for general use at other locations.

SNTEMP/SSTEMP (Stream Network TEMPerature model/Stream Segment TEMPerature model), developed by U.S. Fish and Wildlife Service, were mechanistic, one-dimensional heat transport models for stream branched networks/individual reaches that predicted the daily mean and maximum water temperatures as a function of stream distance and environmental heat fluxes (Theurer *et al.*, 1984). The spatial layout of the hydrologic network was defined by subdividing it into stream segments with homogeneous characteristics such as stream discharge, width, and shading. The heat transport model was based on the dynamic temperature, steady state flow equation, assuming that all input data, including meteorological and hydrological variables, could be represented by 24-hour averages. The heat exchange processes included solar radiation, long-wave atmospheric radiation, convection, evaporation, streamside vegetation (shading), streambed fluid friction, and the water's back radiation. Groundwater inflow effect was also incorporated. The models required MS-DOS environment to execute. Typical applications included predicting the consequences of stream manipulation, such as reservoir discharge or release temperature changes, irrigation diversions, riparian shading alteration, channel modifications, or thermal loading of water temperature. The major limitation of the model was that it did not have a hydrologic and hydraulic component to generate dynamic flow information for temperature simulation and could not simulate diurnal stream temperatures.

STREAM (Segment Travel River Ecosystem Autograph Model) was a multiconstituent stream ecosystem model designed for steep and shallow streams (Park and Lee, 1996). The moving segment approach conceptualizing the stream as a series of completely mixed flow reactors was used. The major constituents included DO, 5-day BOD, suspended solids, coliform bacteria, nitrogen species, phosphorus species, and phytoplankton. Although the model required observed temperature as an input to correct state variables, it did not predict stream temperatures. Rather, it used observed temperatures as input. The hydraulic regime was assumed to be steady-state and groundwater interactions were considered. The model was programmed in BASIC and executed on an MS-DOS environment. A demonstration application indicated that the model could effectively simulate water quality of steep and shallow streams where longitudinal dispersive transport was negligible.

QUAL2E (Enhanced Stream Water QUALity Model, Windows) was an integrated and comprehensive one-dimensional ADRE water quality model developed by United States Environmental Protection Agency (USEPA) (Brown and Barnwell, 1987). The channel was discretized into equally spaced segments with each of segment assumed to be well-mixed both vertically and laterally. The streamflow, although non-uniform among the segments, was considered to be steady state for each specific element. Thus, the model could not handle dynamic flow situations. Water quality constituents (up to 15) that could be simulated by the model included water temperature, DO, BOD, algae as chlorophyll a, organic nitrogen, ammonium, nitrite, nitrate, organic phosphorus, dissolved phosphorus, and coliform. The kinetics of these constituents were all on a diurnal time scale. Although the model contained a detailed heat budget and transport module, it did not contain a provision for riparian or topographic shading (Sullivan *et al.*, 1990).

QUAL2K (or Q2K) was another river and stream water quality model that was intended to represent a modernized version of the QUAL2E model (Chapra and Pelletier, 2003). The model was programmed in the Windows macro language: Visual Basic for Applications (VBA) with Excel used as the graphical user interface (GUI). Several major improvements included: 1) Unequally-spaced reaches, with multiple loadings and abstractions possible for any reach; 2) Sediment-water fluxes of dissolved oxygen and nutrients simulated as a function of settling particulate organic matter, reactions within the sediments, and the concentrations of soluble forms in the overlying waters; 3) Simulated anoxia by reducing oxidation reactions to zero at low oxygen levels; and 4) Two forms of carbonaceous BOD to represent organic carbon, e.g., a slowly oxidizing form (slow CBOD) and a rapidly oxidizing form (fast CBOD). Q2K had the same limitations as QUAL2E.

WASP6 (Water Quality Analysis Simulation Program), developed by the USEPA, was a dynamic compartment-modeling program for aquatic systems, including both the water column and the underlying benthos (Wool *et al.*, 2001). The model was an enhancement of the original WASP by Di Toro *et al.* (1983). WASP6 used advection-dispersion equations and consisted of two stand-alone computer programs, DYNHYD5 and WASP6. These two programs could be run conjunctly or separately. The hydrodynamics program, DYNHYD5, simulated water movement, which provided the base for the water quality program, WASP6, to simulate the movement and interaction of pollutants within the water. WASP6 allowed the user to investigate one-, two-, and three-dimensional systems, and a variety of pollutant types. The state variables simulated by the model included tracer transport, sediment transport, DO, eutrophication, toxicants, and organic chemicals. Advection, dispersion, point and diffuse mass loading, and boundary exchange, which vary over time, were represented in the model. WASP6 itself did not account for either stream temperature predictions or the groundwater discharge effects on water quality.

QUASAR (Quality Simulation Along River Systems) was a one-dimensional CSTR based river quality model (Whitehead *et al.*, 1997). The model combined a flow module and a process based water quality module, and was designed to simulate water quality parameters including DO, BOD, temperature, nitrate, ammonium, pH, and a conservative water quality determinant. The model was later enhanced by incorporating two aggregated dead-zone (ADZ) parameters (Lees *et al.*, 1998). However, QUASAR still had some limitations. Water temperature was modeled as a conservative variable, implying that heat exchange at the surface was negligible. This is not the case for most streams according to numerous stream temperature studies. Stream DO was modeled as a result of photosynthetic oxygen production, benthic oxygen demand, reaeration (natural or due to presence of a weir), nitrification, and BOD decay. The effect of groundwater discharge was not considered.

SWAT (Soil and Water Assessment Tool) was a quasi physically-based basin-scale water quality simulation model that operated on a daily time step developed by Arnold *et al.* (1998). SWAT was developed to predict the impact of land management practices on water, sediment and agricultural chemical yields in complex watersheds with varying soils, land use and management conditions over long periods of time. An ArcView based interface was available to input GIS into SWAT, which enabled the integration of SWAT to BASINS (Better Assessment Science Integrating Point and Nonpoint Sources). SWAT used an empirical equation developed by Stefan and Preudhomme (1993) to calculate average daily water temperatures from air temperatures for a well-mixed stream, assuming that the effect of all the other variables, such as solar radiation, relative humidity, wind speed, water depth, ground water inflow, thermal conductivity of the sediments, were not significant to water temperatures. Limited by its time step length, the SWAT model did not simulate diurnal variations.

Summary

The literature review indicates that factors such as streamflow, groundwater discharge, riparian vegetation shading, and stream width have strong effects on dynamic stream temperatures and DO concentrations. These factors are particularly important on water quality of the forested tributaries in the Lower Flint River Basin, where extremely low flow and severely degraded aquatic habitat problems have occurred during drought seasons, and where excessive groundwater withdrawal for agricultural irrigation may have exacerbated the drought impacts.

Natural resources managers and planners need models to provide a quantitative understanding of the effects of these factors on stream water quality, especially the effects of instream flow rate and groundwater discharge rate. However, the existing models are incomplete and thus limited in their use by failing to include the dynamic flow module component, the groundwater discharge effect, accurate riparian vegetation shading estimates, and/or the temperature and DO constituents. Such situations necessitate the development of our model DDOT, a new integrated water quality models, to meet our goals.

References

Adrian, D. D., F. X. Yu, and D. Barbe, 1994. Water quality modeling for a sinusoidally varying waste discharge concentration. *Water Research*, 28(5):1167–1174.

Ahlert, R. C. and S.-F. Hsueh, 1980. A reactor network model of the Passaic River. *Ecological Modelling*, 10(1):47–61.

Ames, W. F., 1977. *Numerical Methods for Partial Differential Equations, 2nd Edition.* Academic Press, New York, 365 pp.

Arnold, J., R. Srinivasan, R. Muttiah, and J. Williams, 1998. Large area hydrologic modeling and assessment. Part I: Model development. *Journal of the American Water Resources Association*, 34(1):73–89.

Beck, M. B., 1983. A procedure for modeling. In Orlob, G. T., editor, *Mathematical Modeling of Water Quality: Streams, Lakes, and Reservoirs*, International series on applied systems analysis. Wiley, Chichester [West Sussex], New York, pp. 11-41.

Bennett, J. P. and R. E. Rathbun, 1972. Reaeration in Open-Channel Flow. U.S. Geological Survey Professional Paper 737, U.S. Govt. Print. Off., Washington, 75 pp.

Beschta, R. L. and R. L. Taylor, 1988. Stream temperature increases and land use in a Forested Oregon Watershed. *Water Resources Bulletin*, 24(1):19–25.

Beven, K. J. and M. J. Kirkby, 1993. *Channel Network Hydrology.* Wiley, Chichester, New York, 319 pp.

Brown, G., 1969. Predicting temperatures of small streams. *Water Resources Research*, 5(1):68–75.

Brown, G., 1970. Predicting the effect of clearcutting on stream temperature. *Soil and Water Conservation*, 25:11–13.

Brown, L. and T. Barnwell, 1987. Computer program documentation for the enhanced Stream Water Quality Model QUAL2E and QUAL2E-UNCAS. Technical Report Rep. No. EPA-600/3-87/007, Environmental Research Laboratory, U.S. EPA, Athens, GA.

Caissie, D., N. El-Jabi, and M. G. Satish, 2001. Modelling of maximum daily water temperatures in a small stream using air temperatures. *Journal of Hydrology*, 251(1-2):14–28.

Campolo, M., P. Andreussi, and A. Soldati, 2002. Water quality control in the river Arno. *Water Research*, 36(10):2673–2680.

Caruso, B. S., 2002. Temporal and spatial patterns of extreme low flows and effects on stream ecosystems in Otago, New Zealand. *Journal of Hydrology*, 257(1-4):115–133.

Chapra, S. C., 1997. *Surface Water-Quality Modeling*. McGraw-Hill, New York, 844 pp.

Chapra, S. C. and G. J. Pelletier, 2003. QUAL2K: A Modeling Framework for Simulating River and Stream Water Quality Documentation and Users Manual. Civil and Environmental Engineering Dept., Tufts University, Medford, MA, 121pp. Web: `http://www.epa.gov/ATHENS/wwqtsc/html/qual2k.html`.

Chaudhry, M. H., 1993. *Open-Channel Flow*. Prentice-Hall, Englewood Cliffs, N.J., 483 pp.

Chaudhury, R. R., J. A. H. Sobrinho, R. M. Wright, and M. Sreenivas, 1998. Dissolved oxygen modeling of the Blackstone River (northeastern United States). *Water Research*, 32(8):2400–2412.

Chen, Y. D., R. F. Carsel, S. C. McCutcheon, and W. L. Nutter, 1998. Stream temperature simulation of forested riparian areas: I. Watershed-scale model development. *Journal of Environmental Engineering*, 124(4):304–315.

Cox, B. A., 2003a. A review of currently available in-stream water-quality models and their applicability for simulating dissolved oxygen in lowland rivers. *The Science of The Total Environment*, 314-316:335–377.

Cox, B. A., 2003b. A review of dissolved oxygen modelling techniques for lowland rivers. *The Science of The Total Environment*, 314-316:303–334.

De Smedt, F., W. Brevis, and P. Debels, 2005. Analytical solution for solute transport resulting from instantaneous injection in streams with transient storage. *Journal of Hydrology*, 315(1-4):25–39.

Dehghan, M., 2004a. Numerical schemes for one-dimensional parabolic equations with non-standard initial condition. *Applied Mathematics and Computation*, 147(2):321–331.

Dehghan, M., 2004b. Weighted finite difference techniques for the one-dimensional advection-diffusion equation. *Applied Mathematics and Computation*, 147(2):307–319.

Di Toro, D. M., J. J. Fitzpatrick, R. V. Thomann, and I. Hydroscience, 1983. Water Quality Analysis Simulation Program (WASP) and Model Verification Program (MVP) - Documentation. Technical Report EPA-600/3-81-044, Hydroscience, Inc., Westwood, NJ. for USEPA, Duluth, MN, Contract No. 68-01-3872, 156 pp. Web: `http://dspace.udel.edu:8080/dspace/handle/19716/1450`.

Gaffield, S. J., K. W. Potter, and L. Z. Wang, 2005. Predicting the summer temperature of small streams in Southwestern Wisconsin. *Journal of the American Water Resources Association*, 41(1):25–36.

Gerald, C. F. and P. O. Wheatley, 1989. *Applied numerical analysis*. Addison-Wesley Pub. Co., Reading, Mass. 679 pp.

Gilvear, D. J., K. V. Heal, and A. Stephen, 2002. Hydrology and the ecological quality of Scottish river ecosystems. *The Science of The Total Environment*, 294(1-3):131–159.

Gooseff, M., K. Strzepek, and S. Chapra, 2005. Potential effect of climate change on water temperature downstream of a reservoir: Lower Madison River, Montana. *Climatic Change*, 68(3):331–353.

Gulliver, J. S. and H. G. Stefan, 1984. Stream productivity analysis with dorm–I : Development of computational model. *Water Research*, 18(12):1569–1576.

Hewlett, J. D. and J. C. Fortson, 1982. Stream temperature under an inadequate buffer strip in the Southeast Piedmont. *Water Resources Bulletin*, 18(6):983–988.

Hostetler, S. W., 1991. Analysis and modeling of long-term stream temperatures on the Steamboat Creek Basin, Oregon. *Journal of the American Water Resources Association*, 27(4):637–647.

James, A., 1984. *An Introduction to Water Quality Modelling*. Wiley, Chichester, West Sussex, New York, 234 pp.

Jobson, H., 1977. Bed conduction computation for thermal models. *Journal of the Hydraulics Division, American Society of Civil Engineers*, 103(HY10):1213–1217.

Kayombo, S., T. S. A. Mbwette, A. W. Mayo, J. H. Y. Katima, and S. E. Jorgensen, 2000. Modelling diurnal variation of dissolved oxygen in waste stabilization ponds. *Ecological Modelling*, 127(1):21–31.

LeBlanc, R. T., R. D. Brown, and J. E. FitzGibbon, 1997. Modeling the effects of land use change on the water temperature in unregulated urban streams. *Journal of Environmental Management*, 49(4):445–469.

Lees, M., L. Camacho, and P. Whitehead, 1998. Extension of the QUASAR river water quality model to incorporate dead-zone mixing. *Hydrology and Earth System Sciences*, 2:353–365.

Leonard, B. P., 1979. A stable and accurate convective modelling procedure based on quadratic upstream interpolation. *Comput. Meth. Appl. Mech. Eng.*, 19:59–98.

Lin, Y. C., M. S. Chang, and J. M. A. Medina, 2005. A methodology for solute transport in unsteady, nonuniform streamflow with subsurface interaction. *Advances in Water Resources*, 28(8):871–883.

Liu, W. C., S. Y. Liu, M. H. Hsu, and A. Y. Kuo, 2005. Water quality modeling to determine minimum instream flow for fish survival in tidal rivers. *Journal of Environmental Management*, 76(4):293–308.

Lopes, L. F. G., J. S. A. Do Carmo, R. M. Vitor Cortes, and D. Oliveira, 2004. Hydrodynamics and water quality modelling in a regulated river segment: application on the instream flow definition. *Ecological Modelling*, 173(2-3):197–218.

Maidment, D. R., 1993. *Handbook of Hydrology.* McGraw-Hill, New York, 1424 pp.

Moatar, F., J. Miquel, and A. Poirel, 2001. A quality-control method for physical and chemical monitoring data. Application to dissolved oxygen levels in the river Loire (France). *Journal of Hydrology*, 252(1-4):25–36.

Mohseni, O. and H. Stefan, 1998. A non-linear regression model for weekly stream temperatures. *Water Resources Research*, 34(10):2685–2692.

Mohseni, O. and H. G. Stefan, 1999. Stream temperature/air temperature relationship: a physical interpretation. *Journal of Hydrology*, 218(3-4):128–141.

Morton, K. and D. Mayers, 1994. *Numerical Solution of Partial Differential Equations: An introduction.* Cambridge University Press, Cambridge, New York, 227 pp.

O'Loughlin, E. M. and K. H. Bowmer, 1975. Dilution and decay of aquatic herbicides in flowing channels. *Journal of Hydrology*, 26(3-4):217–235.

Orlob, G. T., 1983. *Mathematical modeling of water quality: streams, lakes, and reservoirs*. Wiley, Chichester, New York.

Park, S. S. and Y. S. Lee, 1996. A multiconstituent moving segment model for water quality predictions in steep and shallow streams. *Ecological Modelling*, 89(1-3):121–131.

Park, S. S. and C. G. Uchrin, 1988. A numerical mixing zone model for water quality assessment in natural streams: Conceptual development. *Ecological Modelling*, 42(3-4):233–244.

Parkhill, K. L. and J. S. Gulliver, 1999. Modeling the effect of light on whole-stream respiration. *Ecological Modelling*, 117(2-3):333–342.

Pearson, N. and N. O. Crossland, 1996. Measurement of community photosynthesis and respiration in outdoor artificial streams. *Chemosphere*, 32(5):913–919.

Rauch, W., M. Henze, L. Koncsos, P. Reichert, P. Shanahan, L. Somlyody, and P. Vanrolleghem, 1998. River water quality modelling: I. State of the art. *Water Science and Technology*, 38(11):237–244.

Rutherford, J. C., S. Blackett, C. Blackett, L. Saito, and R. J. Davies-Colley, 1997. Predicting the effects of shade on water temperature in small streams. *New Zealand Journal of Marine and Freshwater Research*, 31:707–721.

Sabo, M. J., C. F. Bryan, W. E. Kelso, and D. A. Rutherford, 1999. Hydrology and aquatic habitat characteristics of a riverine swamp: I. Influence of flow on water temperature and chemistry. *Regulated Rivers: Research and Management*, 15(6):505–523.

Sincock, A. M., H. S. Wheater, and P. G. Whitehead, 2003. Calibration and sensitivity analysis of a river water quality model under unsteady flow conditions. *Journal of Hydrology*, 277(3-4):214–229.

Sinokrot, B. A. and J. S. Gulliver, 2000. In-stream flow impact on river water temperatures. *Journal of Hydraulic Research*, 38(5):339–349.

Sinokrot, B. A. and H. Stefan, 1993. Stream temperature dynamics: Measurements and modeling. *Water Resources Research*, 29(7):2299–2312.

Sridhar, V., A. L. Sansone, J. LaMarche, T. Dubin, and D. P. Lettenmaier, 2004. Prediction of stream temperature in forested watersheds. *Journal of the American Water Resources Association*, 40(1):197–213.

Stamou, A. I., 1992. Improving the numerical modeling of river water quality by using high order difference schemes. *Water Research*, 26(12):1563–1570.

Stefan, H. G. and X. Fang, 1994. Dissolved oxygen model for regional lake analysis. *Ecological Modelling*, 71(1-3):37–68.

Stefan, H. G., J. S. Gulliver, M. G. Hahn, and A. Y. Fu, 1980. Water Temperature Dynamics in Experimental Field Channels: Analysis and Modeling,. Project report no. 193, Prepared for Environmental Research Laboratory, EPA, Duluth, 171 pp.

Stefan, H. G. and E. B. Preudhomme, 1993. Stream Temperature Estimation from Air-Temperature. *Water Resources Bulletin*, 29(1):27–45.

Sturm, T. W., 2001. *Open Channel Hydraulics*. McGraw-Hill, Boston, 493 pp.

Sullivan, K. and T. A. Adams., 1990. An analysis of temperature patterns in stream environments based on physical principles and field data. Weyerhaeuser tech. report.

Sullivan, K., J. Tooley, K. Doughty, J. Caldwell, and P. Knudsen, 1990. Evaluation of prediction models and characterization of stream temperature regimes in Washington. Timber/Fish/Wildlife Rep. No. TFW-WQ3-90-006, Washington Dept. Nat. Resources, Olympia, Washington, 224 pp.

Taylor, G. I., 1953. Dispersion of Soluble Matter in Solvent Flowing Slowly through a Tube. *Royal Society of London Proceedings Series A*, 219:186–203.

Theurer, F., K. Voos, and W. Miller, 1984. Instream water temperature model. Instream flow information paper no. 16, USDA Fish and Wildlife Service, Cooperative Instream Flow Service Group, Fort Collins, CO.

Thomee, V., 2001. From finite differences to finite elements: A short history of numerical analysis of partial differential equations. *Journal of Computational and Applied Mathematics*, 128(1-2):1–54.

Van Orden, G. N. and C. G. Uchrin, 1993. The study of dissolved oxygen dynamics in the Whippany river, New Jersey using the QUAL2E model. *Ecological Modelling*, 70(1-2):1–17.

Wang, H., M. Hondzo, C. Xu, V. Poole, and A. Spacie, 2003. Dissolved oxygen dynamics of streams draining an urbanized and an agricultural catchment. *Ecological Modelling*, 160(1-2):145–161.

Whitehead, P. G., R. J. Williams, and D. R. Lewis, 1997. Quality simulation along river systems (QUASAR): model theory and development. *Science of The Total Environment*, 194-195:447–456.

Williams, R. J., C. White, M. L. Harrow, and C. Neal, 2000. Temporal and small-scale spatial variations of dissolved oxygen in the Rivers Thames, Pang and Kennet, UK. *The Science of The Total Environment*, 251-252:497–510.

Wool, T. A., R. B. Ambrose, J. L. Martin, and E. A. Comer, 2001. Water Quality Analysis Simulation Program (WASP) Version 6.0 - DRAFT: User's Manual. Technical report, US Environmental Protection Agency, Atlanta, GA, 267 pp. Web: `http://www.epa.gov/athens/wwqtsc/html/wasp.html`.

Young, P. and B. Beck, 1974. The modelling and control of water quality in a river system. *Automatica*, 10(5):455–468.

Zeng, W. and M. B. Beck, 2003. STAND, a dynamic model for sediment transport and water quality. *Journal of Hydrology*, 277(1-2):125–133.

Zeng, X., T. C. Rasmussen, M. B. Beck, A. K. Parker, and Z. Lin, 2005. A biogeochemical model for metabolism and nutrient cycling in a Southeastern Piedmont impoundment. *Environmental Modelling and Software*, In Press.

Zheng, L., C. Chen, and F. Y. Zhang, 2004. Development of water quality model in the Satilla River Estuary, Georgia. *Ecological Modelling*, 178(3-4):457–482.

Chapter 3

Simple, Efficient, and Accurate Revisions to the MacCormack and Saulyev Schemes: High Peclet Numbers [1]

[1] Li, G. and C. Rhett Jackson. For submission to *Applied Mathematics and Computation.*

Abstract

Stream water quality modeling often involves numerical methods to solve the dynamic one-dimensional advection-dispersion-reaction equations (ADRE). There are numerous explicit and implicit finite difference schemes for solving these problems, and two commonly used schemes are the MacCormack and Saulyev schemes. This paper presents simple revisions to these schemes that make them more accurate without significant loss of computational efficiency. Using advection dominated (high Peclet number) problems as test cases, performances of the revised schemes are compared to performances of five classic schemes: forward-time/centered-space (FTCS); backward-time/centered-space (BTCS); Crank-Nicolson; and the traditional MacCormack and Saulyev schemes. These seven numerical schemes were tested against analytical solutions for pulse and step inputs of mass to a steady flow in a channel, and performances were considered with respect to stability, accuracy, and computational efficiency. Results indicated that both the modified Saulyev and the MacCormack schemes, which are named the Saulyev$_c$ and MacCormack$_c$ schemes respectively, greatly improved the prediction accuracy over the original ones. The computational efficiency in terms of computer Central Processing Unit (CPU) time was not affected for the Saulyev$_c$ scheme. The MacCormack$_c$ scheme demonstrated increased time consumption but was still much faster than implicit schemes.

Keywords

Finite differences, Numerical methods, One-dimensional, Advection-Dispersion-Reaction equation, Partial differential equation

3.1 Introduction

In stream water quality modeling studies, the commonly used governing equations are the dynamic one-dimensional Advection-Dispersion-Reaction equations (ADRE) based on Taylor dispersion (Taylor, 1953). A simplified representation of such an equation is shown in equation (3.1) (O'Loughlin and Bowmer, 1975; Stamou, 1992; Chen *et al.*, 2001; Zeng and Beck, 2003; Lin *et al.*, 2005). This equation will be further used for formulation demonstration of numerical schemes in the subsequent sections.

$$\frac{\partial C}{\partial t} + U\frac{\partial C}{\partial x} = D\frac{\partial^2 C}{\partial x^2} - KC \tag{3.1}$$

where, C is mass concentration (mg/L); U is flow velocity (m/s); D is the system dispersion coefficients (m^2/s); K is the mass decay rate (s^{-1}); x is longitudinal distance along the stream (m); and t is time (s).

Numerous numerical methods for solving such partial differential equations with appropriate boundary and initial conditions are available (Ames, 1977; Morton and Mayers, 1994; Chapra, 1997; Gerald and Wheatley, 2004). Generally, these numerical methods are classified into three groups, e.g., finite difference methods, finite volume methods, and finite element methods (Thomee, 2001). Among these methods, the finite difference methods, including both explicit and implicit schemes, are mostly used for one-dimensional problems such as in longitudinal river systems (Chapra, 1997).

Studies on finite difference schemes have focused on computation accuracy and numerical stability. Many complex numerical schemes, such as QUICK/QUICKest schemes (Leonard, 1979), Lax-Wendroff scheme (Sousa and Sobey, 2002), Crandall scheme (Dehghan, 2004a), and Dufort-Frankel scheme (Dehghan, 2005) have been developed to improve model performance. These schemes have the advantages in terms of stability and high order accuracy and are desirable for advection dominated systems. However, the specific boundary and initial conditions required by these schemes make them difficult to use. In addition, they require more computing effort since iterations or more grids are involved in each computation step.

For example, the QUICKest scheme uses a three-point upstream-weighted quadratic interpolation, and requires the stop criteria controlled iterations for each grid in order to improve the accuracy (Sousa and Sobey, 2002). The scheme apparently enforces a heavy computing burden. Besides, since it involves two upstream points, the upstream boundary conditions need to be defined carefully before starting the computation. Similarly, the Dufort-Frankel scheme requires two backward-time points (Dehghan, 2005), which require special care for initial values at the beginning of the computation.

Considering the tradeoffs between the advantages and disadvantages of the above schemes, the simple finite difference schemes become more attractive for general model use. The typical simple explicit schemes include Forward-Time/Centered-Space (FTCS) scheme, the MacCormack scheme, and the Saulyev scheme, and the typical implicit schemes include the Backward-Time/Centered-Space (BTCS) scheme and the Crank-Nicolson scheme (Chapra, 1997). These schemes are either first or second order accurate and have the advantages of simplicity in coding and time effectiveness in computing without losing too much accuracy, and thus are preferred for many model applications.

This paper proposes and explores simple revisions to the MacCormack and Saulyev schemes that improve their accuracy for high Peclet number problems. The revised schemes are denoted as MacCormack_c and Saulyev_c. Prediction accuracies of these alternative schemes are comparable with complex schemes.

To identify the best one from these simple schemes, comparative studies of these schemes are necessary. Dehghan (2004a,b) tested the performances of FTCS scheme, the BTCS scheme, the Crank-Nicolson scheme, and the Saulyev scheme. However, these tests did not consider advection and reaction terms, and thus may not be applicable to dynamic stream water quality systems where advection is usually predominant over diffusion. This paper presents a complete comparison of all these schemes and the revised schemes for 1-D stream modeling of step and pulse inputs of a water quality constituent.

In the following sections, the formulations of the typical schemes are reviewed; the proposed revisions are then described; the numerical testing scenarios are described; and the accuracy and efficiency of these schemes are compared and evaluated.

3.2 Review of commonly used simple finite difference schemes

3.2.1 General concerns

Finite difference schemes discretize continuous space and time into a grid system, and the values of the state variables are evaluated at each node of the grids (Figure 3.1). For the simple finite difference schemes, the first order derivatives are approximated with either central-, backward-, or forward-discretization, while the second order derivatives are always approximated with central-discretization. Two practical problems require special attention in finite difference schemes. One is stability, and the other is numerical dispersion.

Stability problem exists only in explicit schemes, and different explicit schemes may have different stability restraints. The most rigorous stability requirements for the simple explicit schemes are by the FTCS scheme, with the stability requirements as below (Thomee 2001; Chapra 1997, $P_{214,216}$; Ames 1977, $P_{45,195}$):

$$\lambda = \frac{D\Delta t}{\Delta x^2} < \frac{1}{2} \tag{3.2a}$$

$$\gamma = \frac{U\Delta t}{\Delta x} < 1 \tag{3.2b}$$

where, λ is the diffusion number (dimensionless); γ is the advection number or Courant number (dimensionless); Δx is space step length (m); and Δt is time step length (s).

The explicit MacCormack scheme has more flexible restraints than the above (Chapra, 1997, P_{229}). Although the Saulyev scheme is also an explicit scheme, it does not have stability problems for its special formulation method (Dehghan, 2004a).

If a derivative approximation during discretization is not centered, then numerical dispersion will be introduced. The dispersion coefficients used in the model should take the value obtained by subtracting the numerical dispersion from the real dispersion of the interested system. The amounts of numerical dispersion introduced by backward-space (denoted as Dn_1) and forward-time (denoted as Dn_2) schemes are shown in equation (3.3a) and (3.3b) respectively (Chapra, 1997, P_{217}).

$$Dn_1 = \frac{\Delta x}{2} U \tag{3.3a}$$

$$Dn_2 = -\frac{\Delta t}{2} U^2 \tag{3.3b}$$

Initial and boundary conditions are required to solve the partial differential equations with numerical methods. The initial condition and the upper boundary conditions are usually determined by direct measurements. For the lower boundary conditions, it is considered as a Neumann type in this paper, that is, the derivative of the concentration is assumed to be a constant (Chapra, 1997, P_{194}). Specifically, at the lower boundary, the following relationships are assumed (Zeng, 2000):

$$C_{I+1}^{j+1} = 2C_I^{j+1} - C_{I-1}^{j+1} \tag{3.4a}$$

$$C_{I+1}^{j} = 2C_I^{j} - C_{I-1}^{j} \tag{3.4b}$$

where, C is state variable of interest; I is the lower boundary space node; and j is the j^{th} time node.

3.2.2 Implicit schemes

Backward-time/Centered-space scheme

The BTCS scheme approximates the temporal and spacial derivatives and the decay term in equation (3.1) with the following discretization:

$$\frac{\partial C}{\partial t} \cong \frac{C_i^{j+1} - C_i^j}{\Delta t} \tag{3.5a}$$

$$\frac{\partial C}{\partial x} \cong \frac{C_{i+1}^{j+1} - C_{i-1}^{j+1}}{2\Delta x} \tag{3.5b}$$

$$\frac{\partial^2 C}{\partial x^2} \cong \frac{C_{i+1}^{j+1} - 2C_i^{j+1} + C_{i-1}^{j+1}}{\Delta x^2} \tag{3.5c}$$

$$C \cong C_i^{j+1} \tag{3.5d}$$

Substitute the equations (3.5) and (3.2) into equation (3.1), and rearrange to yield the BTCS scheme,

$$-(\lambda+\frac{\gamma}{2})C_{i-1}^{j+1}+(1+2\lambda+K\Delta t)C_i^{j+1}-(\lambda-\frac{\gamma}{2})C_{i+1}^{j+1}=C_i^j \tag{3.6}$$

For $i=1$, move the measured upper boundary C_0^{j+1} in equation (3.6) to the right hand side and rearrange to get the upper boundary formulation,

$$(1+2\lambda+K\Delta t)C_1^{j+1}-(\lambda-\frac{\gamma}{2})C_2^{j+1}=C_1^j+(\lambda+\frac{\gamma}{2})C_0^j \tag{3.7}$$

For $i=I$, plug equation (3.4a) into (3.6), and rearrange to get the lower boundary formulation,

$$-\gamma C_{I-1}^{j+1}+(1+\gamma+K\Delta t)C_I^{j+1}=C_I^j \tag{3.8}$$

Equations (3.6) - (3.8) form a linear system of equations that can be expressed in matrix format as below,

$$\mathbf{A}\vec{C}^{j+1}=\vec{C}^j+(\lambda+\frac{\gamma}{2})\vec{C_0^{j+1}} \tag{3.9}$$

where,

$$\mathbf{A}=\begin{pmatrix} (1+2\lambda+K\Delta t) & -(\lambda-\frac{\gamma}{2}) & 0 & \cdots & 0 & 0 & 0 \\ -(\lambda+\frac{\gamma}{2}) & (1+2\lambda+K\Delta t) & -(\lambda-\frac{\gamma}{2}) & \cdots & 0 & 0 & 0 \\ \vdots & \vdots & \vdots & \ddots & \vdots & \vdots & \vdots \\ 0 & 0 & 0 & \cdots & -(\lambda+\frac{\gamma}{2}) & (1+2\lambda+K\Delta t) & -(\lambda-\frac{\gamma}{2}) \\ 0 & 0 & 0 & \cdots & 0 & -\gamma & (1+\gamma+K\Delta t) \end{pmatrix}_{I\times I}$$

$$\vec{C}^j=\begin{pmatrix} C_1 \\ C_2 \\ \vdots \\ C_{I-1} \\ C_I \end{pmatrix}^j_{I\times 1} \qquad \vec{C_0}^{j+1}=\begin{pmatrix} C_0 \\ 0 \\ \vdots \\ 0 \\ 0 \end{pmatrix}^{j+1}_{I\times 1}$$

The solution of equation (3.9) can then be obtained with the following equation,

$$\vec{C}^{j+1}=\mathbf{A}^{-1}\vec{C}^j+\mathbf{A}^{-1}(\lambda+\frac{\gamma}{2})\vec{C}_0^{j+1} \tag{3.10}$$

The BTCS is unconditionally stable (Chapra, 1997, P_{231}). However, because it uses a biased time derivative approximation, it generates a time-dependent numerical dispersion as mentioned previously. This numerical dispersion should be subtracted from the true dispersion coefficient in the numerical model.

Crank-Nicolson scheme

The Crank-Nicolson scheme corrects the deficiency of biased slope evaluation in the BTCS scheme by using both centered-time and centered-space method. The discretization of equation (3.1) under this scheme is as below (Ames, 1977, P_{49-54}; Chapra, 1997, P_{227}),

$$\frac{\partial C}{\partial t} \cong \frac{C_i^{j+1} - C_i^j}{\Delta t} \tag{3.11a}$$

$$\frac{\partial C}{\partial x} \cong \frac{\frac{C_{i+1}^j - C_{i-1}^j}{2\Delta x} + \frac{C_{i+1}^{j+1} - C_{i-1}^{j+1}}{2\Delta x}}{2} \tag{3.11b}$$

$$\frac{\partial^2 C}{\partial x^2} \cong \frac{\frac{C_{i+1}^j - 2C_i^j + C_{i-1}^j}{\Delta x^2} + \frac{C_{i+1}^{j+1} - 2C_i^{j+1} + C_{i-1}^{j+1}}{\Delta x^2}}{2} \tag{3.11c}$$

$$C \cong \frac{C_i^j + C_i^{j+1}}{2} \tag{3.11d}$$

Substitute the above equations into equation (3.1), and rearrange to yield the Crank-Nicolson scheme,

$$\begin{aligned} &-(\lambda + \frac{\gamma}{2})C_{i-1}^{j+1} + 2(1 + \lambda + K\Delta t)C_i^{j+1} - (\lambda - \frac{\gamma}{2})C_{i+1}^{j+1} \\ &\qquad = (\lambda + \frac{\gamma}{2})C_{i-1}^j + 2(1 - \lambda - K\Delta t)C_i^j + (\lambda - \frac{\gamma}{2})C_{i+1}^j \end{aligned} \tag{3.12}$$

For $i = 1$, move the measured upper boundary C_0^{j+1} in equation (3.13) to the right hand side and rearrange to get the upper boundary formulation,

$$\begin{aligned} &2(1 + \lambda + K\Delta t)C_1^{j+1} - (\lambda - \frac{\gamma}{2})C_2^{j+1} \\ &\qquad = 2(1 - \lambda - K\Delta t)C_1^j + (\lambda - \frac{\gamma}{2})C_2^j + (\lambda + \frac{\gamma}{2})(C_0^j + C_0^{j+1}) \end{aligned} \tag{3.13}$$

For $i = I$, plug the lower boundary equations (3.4a) and (3.4b) into (3.13), and rearrange, getting the lower boundary formulation,

$$-\gamma C_{I-1}^{j+1} + 2(1 + \frac{\gamma}{2} + K\Delta t)C_I^{j+1} = \gamma C_{I-1}^j + 2(1 - \frac{\gamma}{2} - K\Delta t)C_I^j \tag{3.14}$$

Similar to the BTCS scheme, the above equations (3.13) - (3.14) form a linear system of equations that can be represented in matrix format as below,

$$\mathbf{A}\vec{C}^{j+1} = \mathbf{B}\vec{C}^{j} + (\lambda + \frac{\gamma}{2})\vec{C}_0^{j,j+1} \tag{3.15}$$

where,

$$\mathbf{A} = \begin{pmatrix} 2(1+\lambda+K\Delta t) & -(\lambda-\frac{\gamma}{2}) & 0 & \cdots & 0 & 0 & 0 \\ -(\lambda+\frac{\gamma}{2}) & 2(1+\lambda+K\Delta t) & -(\lambda-\frac{\gamma}{2}) & \cdots & 0 & 0 & 0 \\ \vdots & \vdots & \vdots & \ddots & \vdots & \vdots & \vdots \\ 0 & 0 & 0 & \cdots & -(\lambda+\frac{\gamma}{2}) & 2(1+\lambda+K\Delta t) & -(\lambda-\frac{\gamma}{2}) \\ 0 & 0 & 0 & \cdots & 0 & -\gamma & 2(1+\frac{\gamma}{2}+K\Delta t) \end{pmatrix}_{I\times I}$$

$$\mathbf{B} = \begin{pmatrix} 2(1-\lambda-K\Delta t) & (\lambda-\frac{\gamma}{2}) & 0 & \cdots & 0 & 0 & 0 \\ (\lambda+\frac{\gamma}{2}) & 2(1-\lambda-K\Delta t) & (\lambda-\frac{\gamma}{2}) & \cdots & 0 & 0 & 0 \\ \vdots & \vdots & \vdots & \ddots & \vdots & \vdots & \vdots \\ 0 & 0 & 0 & \cdots & (\lambda+\frac{\gamma}{2}) & 2(1-\lambda-K\Delta t) & (\lambda-\frac{\gamma}{2}) \\ 0 & 0 & 0 & \cdots & 0 & \gamma & 2(1-\frac{\gamma}{2}-K\Delta t) \end{pmatrix}_{I\times I}$$

$$\vec{C}^{j+1} = \begin{pmatrix} C_1 \\ C_2 \\ \vdots \\ C_{I-1} \\ C_I \end{pmatrix}^{j+1}_{I\times 1} \qquad \vec{C}^{j} = \begin{pmatrix} C_1 \\ C_2 \\ \vdots \\ C_{I-1} \\ C_I \end{pmatrix}^{j}_{I\times 1} \qquad \vec{C}_0^{\,j,j+1} = \begin{pmatrix} C_0^j + C_0^{j+1} \\ 0 \\ \vdots \\ 0 \\ 0 \end{pmatrix}_{I\times 1}$$

Accordingly, the solution of equation (3.15) can then be expressed with the following formulation,

$$\vec{C}^{j+1} = \mathbf{A}^{-1}\mathbf{B}\vec{C}^{j} + \mathbf{A}^{-1}(\lambda + \frac{\gamma}{2})\vec{C_0^{j,j+1}} \tag{3.16}$$

The Crank-Nicolson scheme is unconditionally stable. It also effectively removes the temporal- and spatial-dependent numerical dispersion and thus is expected to work much better than BTCS scheme. However, since equation (3.11d) becomes impracticable for non-first-order decay, the scheme applies only to linear systems (Chapra, 1997, P_{231}).

3.2.3 Explicit schemes

Forward-time/Centered-space scheme

The FTCS scheme approximates the temporal and spacial derivatives in equation (3.1) with the following discretization:

$$\frac{\partial C}{\partial t} \cong \frac{C_i^{j+1} - C_i^j}{\Delta t} \tag{3.17a}$$

$$\frac{\partial C}{\partial x} \cong \frac{C_{i+1}^j - C_{i-1}^j}{2\Delta x} \tag{3.17b}$$

$$\frac{\partial^2 C}{\partial x^2} \cong \frac{C_{i+1}^j - 2C_i^j + C_{i-1}^j}{\Delta x^2} \tag{3.17c}$$

$$C \cong C_i^j \tag{3.17d}$$

Substitute the equations 3.17 into equation (3.1) and rearrange to yield the FTCS scheme,

$$C_i^{j+1} = (\lambda + \frac{\gamma}{2})C_{i-1}^j + (1 - 2\lambda - K\Delta t)C_i^j + (\lambda - \frac{\gamma}{2})C_{i+1}^j \tag{3.18}$$

For $i = I$, plug equation (3.4b) into (3.18), and rearrange, getting the lower boundary formulation,

$$C_I^{j+1} = \gamma C_{I-1}^j + (1 - \gamma - K\Delta t)C_I^j \tag{3.19}$$

The FTCS is conditionally stable subject to constraints in equation (3.2). Strict stability requirements are the main disadvantage of this scheme. It generates time-dependent numerical dispersion with the amount shown in equation (3.3b), and thus requires small time steps to obtain accurate solutions for highly advective systems (Chapra, 1997, P_{231}).

MacCormack scheme

The MacCormack scheme is an explicit scheme with predictor-corrector two-step evaluations. The first step is a modified FTCS by changing the centered-space evaluation at time j to a forward-space evaluation. This step is actually a foward-time/forward-space (FTFS) scheme. That is, in equation group (3.17a) - (3.17d), equation (3.17b) now changes to the following equation:

$$\frac{\partial C}{\partial x} \cong \frac{C_{i+1}^{j} - C_{i}^{j}}{\Delta x} \tag{3.20}$$

Substitute the difference equations into equation (3.1), and then define slope s_{i_1} as,

$$s_{i_1} = -U\frac{C_{i+1}^{j} - C_{i}^{j+1}}{\Delta x} + D\frac{C_{i+1}^{j} - 2C_{i}^{j} + C_{i-1}^{j}}{\Delta x^2} - KC_{i}^{j} \tag{3.21}$$

Defining $\gamma' = \frac{U}{\Delta x} = \frac{\gamma}{\Delta t}$, $\lambda' = \frac{D}{\Delta x^2} = \frac{\lambda}{\Delta t}$, equation (3.21) takes the following simplified form,

$$s_{i_1} = (\lambda' - \gamma')C_{i+1}^{j} - (2\lambda' - \gamma' + K)C_{i}^{j} + \lambda' C_{i-1}^{j} \tag{3.22}$$

For the lower boundary, where $i = I$, plug equation (3.4b) into (3.22), and rearrange to get,

$$s_{I_1} = -(\gamma' + K)C_{I}^{j} + \gamma' C_{I-1}^{j} \tag{3.23}$$

Use Euler's formula to get the McCormack predictor step formulation,

$$C_{i}^{j+1} = C_{i}^{j} + s_{i_1}\Delta t \tag{3.24}$$

The second step is a modified BTCS scheme by changing the centered-space evaluation at time j with a backward-space evaluation. It is essentially a backward-time/backward-space (BTBS) scheme. That is, in equation group (3.5a) $\sim$ (3.5d), equation (3.5b) now changes to the following equation:

$$\frac{\partial C}{\partial x} \cong \frac{C_{i}^{j+1} - C_{i-1}^{j+1}}{\Delta x} \tag{3.25}$$

Since the values at time $j+1$ are already calculated in preditor step 1, the second step is still an explicit scheme. Then another slope based on these predictors can be evaluated as:

$$s_{i_2} = \lambda' C_{i+1}^{j+1} - (2\lambda' + \gamma' + K)C_{i}^{j+1} + (\lambda' + \gamma')C_{i-1}^{j+1} \tag{3.26}$$

For $i = I$, plug equation (3.4a) into (3.26), and rearrange to get the slope equation,

$$s_{I_2} = -(\gamma' + K)C_{I}^{j+1} + \gamma' C_{I-1}^{j+1} \tag{3.27}$$

With the above two steps, the final MacCormack scheme takes the following form,

$$C_i^{j+1} = C_i^j + \frac{s_{i_2} + s_{i_2}}{2}\Delta t \tag{3.28}$$

The MacCormack scheme has advantages compared with FTCS. Although it is still conditionally stable, constraints becomes more liberal (Chapra, 1997, P_{231}). By taking the average of the FTFS and BTBS schemes, the MacCormack scheme is free from numerical dispersion. The actual dispersion can be used in the model.

Saulyev scheme

The Saulyev scheme converts a seemingly implicit scheme into an explicit scheme. Based on the computation direction, the scheme calculating from left to right is called a downstream type formula, while the scheme from right to left is called an upstream type formula. For both formulae, the state variable C in the decay term is evaluated at node (i, j). To save space, only the downstream formulation is presented here:

$$\frac{\partial C}{\partial t} \cong \frac{C_i^{j+1} - C_i^j}{\Delta t} \tag{3.29a}$$

$$\frac{\partial C}{\partial x} \cong \frac{C_{i+1}^j - C_{i-1}^{j+1}}{2\Delta x} \tag{3.29b}$$

$$\frac{\partial^2 C}{\partial x^2} \cong \frac{C_{i+1}^j - C_i^j - C_i^{j+1} + C_{i-1}^{j+1}}{\Delta x^2} \tag{3.29c}$$

$$C \cong C_i^j \tag{3.29d}$$

Plug the above equations into equation (3.1), and rearrange to yield,

$$C_i^{j+1} = \frac{1}{1+\lambda}[(\lambda + \frac{\gamma}{2})C_{i-1}^{j+1} + (1 - \lambda - K\Delta t)C_i^j + (\lambda - \frac{\gamma}{2})C_{i+1}^j] \tag{3.30}$$

Equation (3.30) is an explicit scheme if calculating from upstream to downstream.
Slightly different from that in equation (3.4a) and (3.4b), the lower boundary assumption for Saulyev scheme takes the following form:

$$C_{I+1}^j = C_I^j + C_I^{j+1} - C_{I-1}^{j+1} \tag{3.31}$$

Plug equation (3.31) into (3.30), where $i = I$, and rearrange to get,

$$C_I^{j+1} = \frac{1}{1+\frac{\gamma}{2}}[\gamma C_{I-1}^{j+1} + (1 + \frac{\gamma}{2} - K\Delta t)C_I^j] \tag{3.32}$$

The Saulyev scheme is unconditionally stable. It is also simple to implement and economical to use (Dehghan, 2004a).

3.3 Proposed revised schemes

3.3.1 Revised MacCormack scheme

Each of the above mentioned schemes has minor deficiencies in terms of either stability, accuracy, or efficiency. For instance, the original MacCormack scheme exhibits excessive dispersion effects for large time/space step lengths, significantly decreasing the efficiency of the MacCormack scheme (Figures 3.2(d) and 3.3(d)). Because the scheme uses the FTFS difference for prediction, and the BTBS difference for correction, temporal and spacial numerical dispersion exists in both predictor and corrector steps. From equation (3.3a) and (3.3b), it can be seen that the numerical dispersion introduced is as much as shown in equation (3.33a) for the FTFS prediction step, and (3.33b) for the BTBS correction step.

$$D_{n_{prd}} = -\frac{\Delta x}{2}U - \frac{\Delta t}{2}U^2 \tag{3.33a}$$

$$D_{n_{crc}} = \frac{\Delta x}{2}U + \frac{\Delta t}{2}U^2 \tag{3.33b}$$

To eliminate the numerical dispersion effect, the modified MacCormack scheme, termed MacCormack$_c$, uses a corrected dispersion, rather than the actual dispersion coefficients for calculation in both steps,

$$D_1 = D_{true} - D_{n_{prd}} \tag{3.34a}$$

$$D_2 = D_{true} - D_{n_{crc}} \tag{3.34b}$$

where, D_1 is the dispersion coefficient used in the prediction step; and D_2 is the dispersion coefficient used in the correction step.

The above correction is easy to formulate and has the potential to greatly improve accuracy.

3.3.2 Revised Saulyev scheme

The traditional Saulyev scheme tends to accelerate the propagation of a moving front, which makes the front occur earlier in time for the downstream scheme and later for the upstream scheme (Figures 3.2(c) and 3.3(c)). The relative time differences of these two schemes from the analytical solution are equal. In addition, both curves match each other exactly, after shifting certain calculating grids along the time axis. It is desirable to improve the prediction accuracy through removing the phase mismatch by a simple shifting operation. The test indicated that the number of time steps required to make the shift for a node varies with the distance of the node from the upper boundary. It was tested that, for the predictions at the I^{th} space node from the upper boundary, the necessary shifting steps, n_I, could be calculated as below,

$$n_I = \frac{I}{2} \tag{3.35}$$

So we propose a modified Saulyev scheme, named as Saulyev$_c$, to improve the prediction accuracy by adding the above mentioned shifting operation to the original Saulyev schemes. The modification, which only requires slightly more computing effort, is expected to remove the phase mismatch that occurs in original Saulyev schemes. By the shifting operation, Saulyev$_c$ makes either the first or the last n values unknown after shifting. However, such unknown values can be obtained by using Auto-Regressive Moving Average (ARMA) models or other extrapolation methods when necessary.

3.4 Numerical test

All schemes were tested against analytical solutions for step and pulse inputs of a mass concentration into a river. The problem is defined as follows. Suppose we want to predict mass concentration C at the lower boundary of a rectangular uniform stream reach as a response to an impulse input and a step input respectively from the upper boundary. Suppose the reach system has the characteristics as shown in Table 3.1. For convenience, the stream reach is considered to be a homogeneous system, so that all parameters such as U, D, and K, hold constant values over time and space. The initial and boundary conditions are defined as:

Initial conditions:

$C(x,0) = 0\ \forall x;$

Upstream boundary:

1. impulse input

   $C(0,t) = \frac{M}{U}\delta(t)\quad \text{for } 0 < t \leq t_0$

   Where, $\delta(t)$ is the Dirac function (Jury and Roth, 1990).

   $C(0,t) = 0 \qquad \text{for } t > t_0$

2. step input

   $C(0,t) = 0 \qquad \text{for } t \leq 0$

   $C(0,t) = C_0 \quad \text{for } t > 0$

Downstream boundary:

$C(\infty,t) = 0.$

The governing equation for such a system can be formulated exactly as shown in equation (3.1). The analytical solutions of the governing equation are shown below in equation (3.36a) for the impulse input, and in equation (3.36b) for the step input (O'Loughlin and Bowmer, 1975; Chapra, 1997):

$$C(x,t) = \frac{M}{2\sqrt{\pi D t}} \cdot exp[-\frac{(x-Ut)^2}{4Dt} - Kt] \times 1000 \tag{3.36a}$$

$$\begin{aligned} C(x,t) = \frac{C_0}{2} \cdot [exp(\frac{Ux(1-\Gamma)}{2D}) \cdot erfc(\frac{x-Ut\Gamma}{2\sqrt{Dt}}) \\ + exp(\frac{Ux(1+\Gamma)}{2D}) \cdot erfc(\frac{x+Ut\Gamma}{2\sqrt{Dt}})] \end{aligned} \tag{3.36b}$$

In equation (3.36a), the coefficient 1000 converts the unit of concentration from kg/m^3 to mg/L; $erfc()$ is the complementary error function; and $\Gamma = \sqrt{1 + \frac{4KD}{U^2}}$ (Chapra, 1997, $\mathrm{P}_{183-184}$).

For the numerical testing, the time step was set to 15 min (e.g., 900 s), which is a common interval for time series water quality data. The space step was set to 500 m. The definitions gave $\lambda = 0.072$, $\gamma = 0.9$. The above setup met the stability standards as in equation (3.2a) and (3.2b). The Peclet number was $P_e = \frac{U\Delta x}{D} = 12.5 > 10$, which indicated the stream system was advection dominated (Chapra, 1997, $\mathrm{P}_{163-164}$).

While the upper boundary location of the numerical schemes for step input was set equal to that for analytical solutions, it was reset to the middle of the entire stream reach, e.g., at location $x = \frac{L}{2}$, for impulse input. The new boundary location ensured a complete breakthrough curve passing through this boundary and then feeding into the numerical schemes. All the lower boundary conditions for the numerical schemes were set to a Neumann type as described in the review section.

To better address the numerical scheme performances, the modified schemes including FTCS-BTCS, $\mathrm{Saulyev}_{12}$, $\mathrm{Crank\text{-}Nicolson}_B$, and $\mathrm{Crank\text{-}Nicolson}_F$, were also tested. The FTCS-BTCS scheme uses FTCS to predict and BTCS to correct. The $\mathrm{Saulyev}_{12}$ scheme takes the Saulyev downstream scheme as predictor and the Saulyev upstream scheme as corrector. Schemes of $\mathrm{Crank\text{-}Nicolson}_B$ and $\mathrm{Crank\text{-}Nicolson}_F$ evaluate the reaction term at j and $j+1$ respectively.

3.5 Test results

The model outputs of the tested numerical schemes are plotted against the analytical solutions in Figures 3.2 and 3.3. The sum of square errors (SSE) are shown in Figure 3.4(a), and the computation efficiency in terms of CPU time are presented in Figure 3.4(b).

The FTCS scheme gave much better predictions than the BTCS scheme for both impulse and step inputs (Figures 3.2(a) and 3.3(a)). The BTCS scheme tended to generate over-dispersion for impulse input. The combined form FTCS-BTCS scheme gave similar predictions to FTCS, but generated overshooting at peak values under step input. The three types of Crank-Nicolson schemes performed about the same. These predictions looked more accurate than BTCS scheme under impulse input. However, they fail to reach the peak values, especially under the step input (Figure 3.3(b)). In addition, the Crank-Nicolson schemes began to oscillate since the system was advection dominated. For the Saulyev down/upstream schemes, although oscillation also occurred, the main problem had been the phase mismatch (Figures 3.2(c) and 3.3(c)). The performance of the combined down/up-stream scheme was similar to the BTCS scheme. The Sauleve$_c$ scheme greatly improved the original Saulyev scheme simply by an additional phase shifting operation. The original MacCormack scheme demonstrated even more over-dispersion than the BTCS scheme. However, the MacCormack$_c$ scheme provided very accurate predictions under both impulse and step inputs (Figures 3.2(d) and 3.3(d)). In general, the schemes such as the FTCS, MacCormack$_c$, and Saulyev$_c$ tended to provide very accurate results (Figures 3.2(e) and 3.3(e)); and the BTCS, Saulyev, and MacCormack schemes tended to generate over dispersion (Figures 3.2(f) and 3.3(f)).

Analysis of SSE for each individual scheme (Figure 3.4(a)) indicated that, Saulyev down/up-stream gave much larger errors than the other schemes. Overall, the FTCS, Saulyev$_c$, and MacCormack$_c$ schemes were the most accurate schemes among all the tested numerical schemes.

Computational efficiency is another important factor in evaluating the superiority of the schemes. It was shown that, in general, explicit schemes executed much faster than implicit schemes (Fig. 3.4(b)). The proposed explicit MacCormack$_c$ scheme took more time than the other explicit schemes, but still much less than the implicit schemes. All the other explicit schemes consumed similar computation time.

3.6 Discussion and conclusion

In general, under the same scenarios, implicit schemes require much longer computing time than explicit ones. For this reason, explicit schemes are preferable to implicit ones if their accuracy is acceptable. However, the typical explicit schemes, such as FTCS, Saulyev, and MacCormack schemes, have limitations with respect to accuracy and/or stability. The FTCS scheme requires the most rigorous stability constraints; the Saulyev down/up-scheme tends to generate phase acceleration/lag in time; and the MacCormack gives over-dispersive predictions. For this reason, we proposed Saulyev$_c$ and MacCormack$_c$ schemes by adding simple revisions to the original Saulyev and MacCormack schemes. The revisions demonstrated great improvements in accuracy over the original schemes. The computation efficiency was not decreased for the Saulyev$_c$ scheme. Although the MacCormack$_c$ scheme became less efficient than the original MacCormack scheme, it was still much faster than the implicit schemes.

References

Ames, W. F., 1977. *Numerical Methods for Partial Differential Equations, 2nd Edition.* Academic Press, New York, 365 pp.

Chapra, S. C., 1997. *Surface Water-Quality Modeling.* McGraw-Hill, New York, 844 pp.

Chen, J. Y., C. H. Ko, S. Bhattacharjee, and M. Elimelech, 2001. Role of spatial distribution of porous medium surface charge heterogeneity in colloid transport. *Colloids and Surfaces A: Physicochemical and Engineering Aspects*, 191(1-2):3–15.

Dehghan, M., 2004a. Numerical schemes for one-dimensional parabolic equations with non-standard initial condition. *Applied Mathematics and Computation*, 147(2):321–331.

Dehghan, M., 2004b. Weighted finite difference techniques for the one-dimensional advection-diffusion equation. *Applied Mathematics and Computation*, 147(2):307–319.

Dehghan, M., 2005. Efficient techniques for the second-order parabolic equation subject to nonlocal specifications. *Applied Numerical Mathematics*, 52(1):39–62.

Gerald, C. F. and P. O. Wheatley, 2004. *Applied Numerical Analysis.* Pearson/Addison-Wesley, Boston, 609 pp.

Jury, W. A. and K. Roth, 1990. *Transfer Functions and Solute Movement Through Soil : Theory and Applications.* Birkhuser Verlag, Basel, Boston, 226 pp.

Leonard, B. P., 1979. A stable and accurate convective modelling procedure based on quadratic upstream interpolation. *Comput. Meth. Appl. Mech. Eng.*, 19:59–98.

Lin, Y. C., M. S. Chang, and J. M. A. Medina, 2005. A methodology for solute transport in unsteady, nonuniform streamflow with subsurface interaction. *Advances in Water Resources*, 28(8):871–883.

Morton, K. and D. Mayers, 1994. *Numerical Solution of Partial Differential Equations: An introduction*. Cambridge University Press, Cambridge, New York, 227 pp.

O'Loughlin, E. M. and K. H. Bowmer, 1975. Dilution and decay of aquatic herbicides in flowing channels. *Journal of Hydrology*, 26(3-4):217–235.

Sousa, E. and I. Sobey, 2002. On the influence of numerical boundary conditions. *Applied Numerical Mathematics*, 41(2):325–344.

Stamou, A. I., 1992. Improving the numerical modeling of river water quality by using high order difference schemes. *Water Research*, 26(12):1563–1570.

Taylor, G. I., 1953. Dispersion of Soluble Matter in Solvent Flowing Slowly through a Tube. *Royal Society of London Proceedings Series A*, 219:186–203.

Thomee, V., 2001. From finite differences to finite elements: A short history of numerical analysis of partial differential equations. *Journal of Computational and Applied Mathematics*, 128(1-2):1–54.

Zeng, W., 2000. *A Model For Understanding And Managing The Impacts Of Sediment Behavior On River Water Quality*. PhD thesis, University of GA, Athens, GA, 244 pp. Web: `http://getd.galib.uga.edu/public/zeng_wei_200012_phd/zeng_wei_200012_phd.pdf`.

Zeng, W. and M. B. Beck, 2003. STAND, a dynamic model for sediment transport and water quality. *Journal of Hydrology*, 277(1-2):125–133.

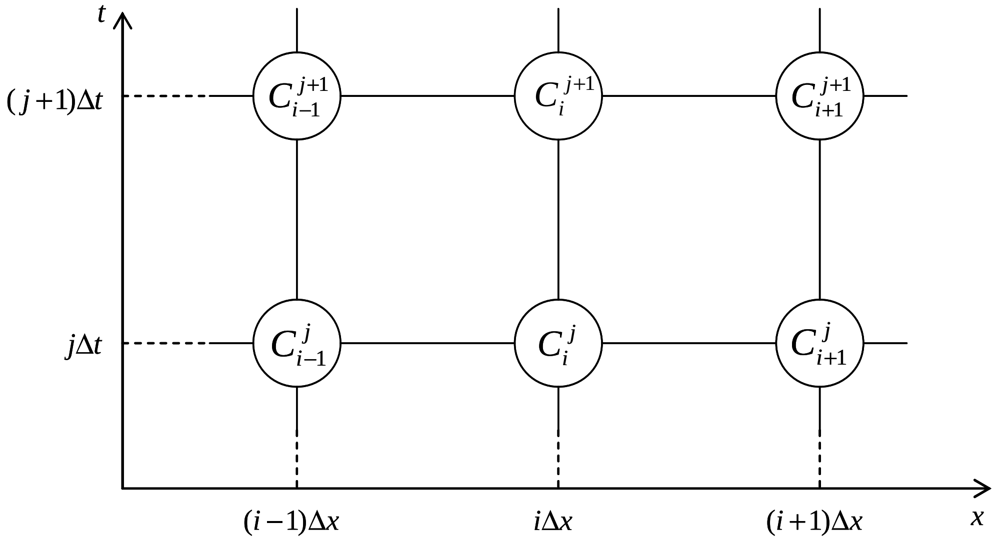

Figure 3.1: Discretization of finite difference schemes. where, C is the relevant state variable; Δx is space step length and Δt is time step length, while i denotes the i^{th} space node and j denotes the j^{th} time node.

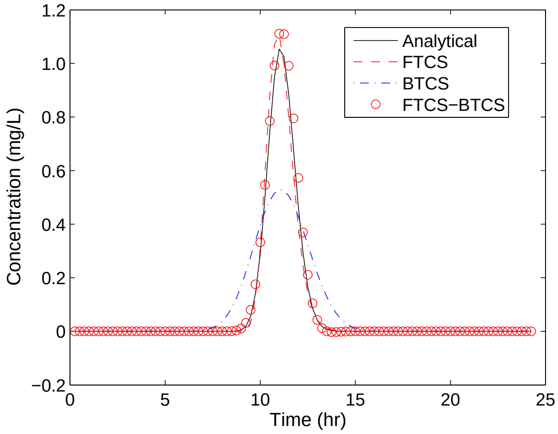

(a) FTCS, BTCS schemes

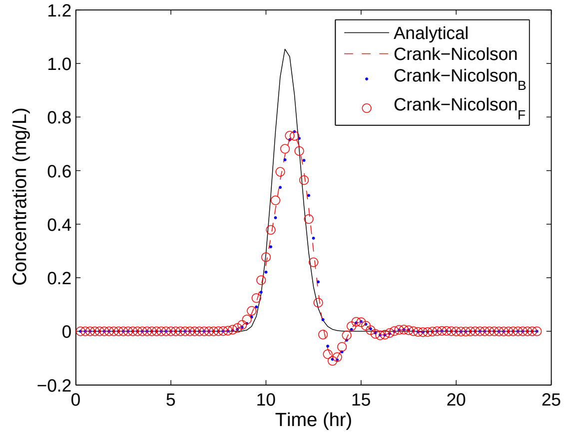

(b) Crank-Nicolson schemes

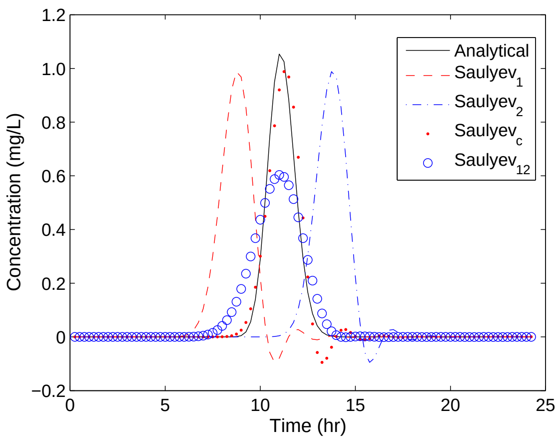

(c) Saulyev schemes

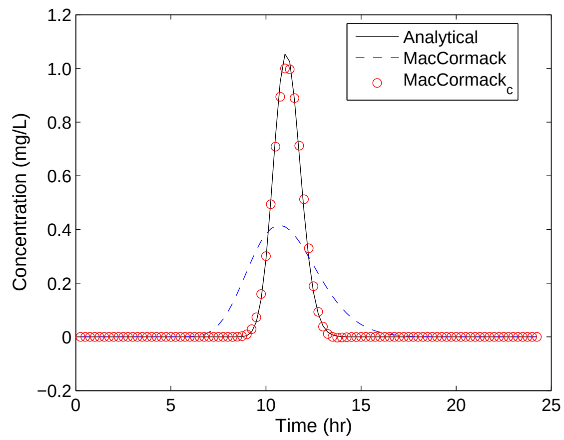

(d) MacCormack schemes

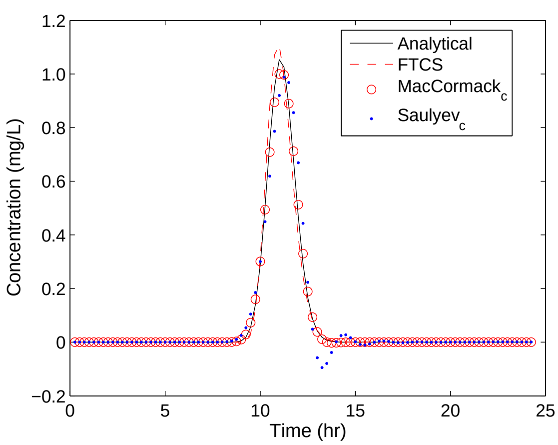

(e) More accurate schemes

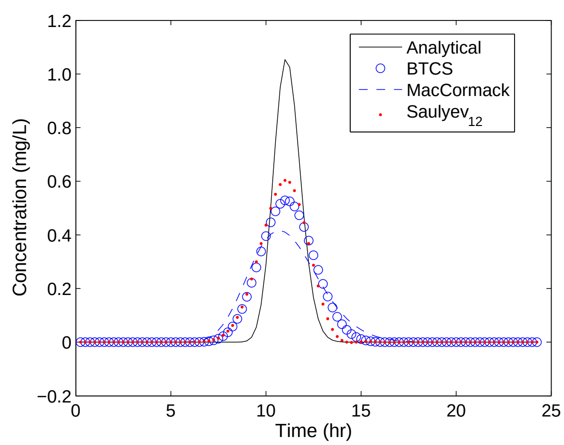

(f) More stable schemes

Figure 3.2: Performances of finite difference schemes under impulse input scenario

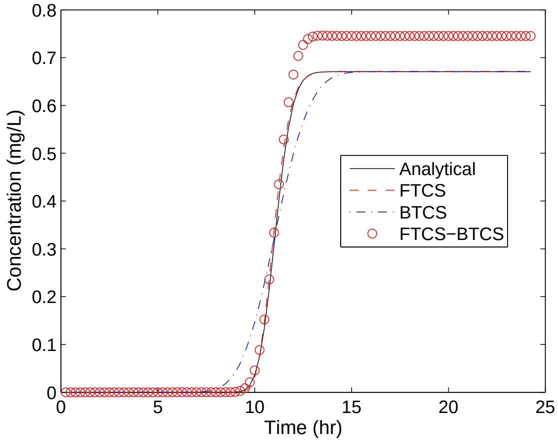

(a) FTCS, BTCS schemes

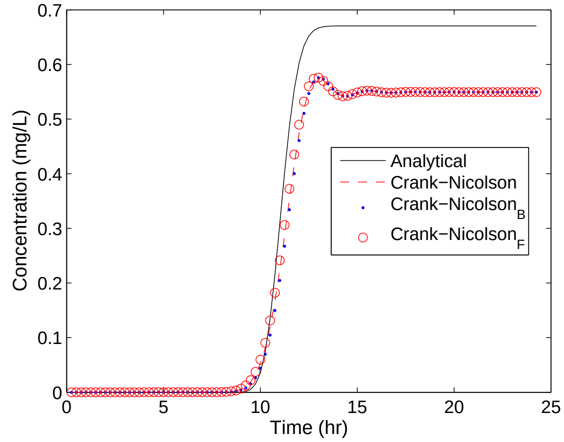

(b) Crank-Nicolson schemes

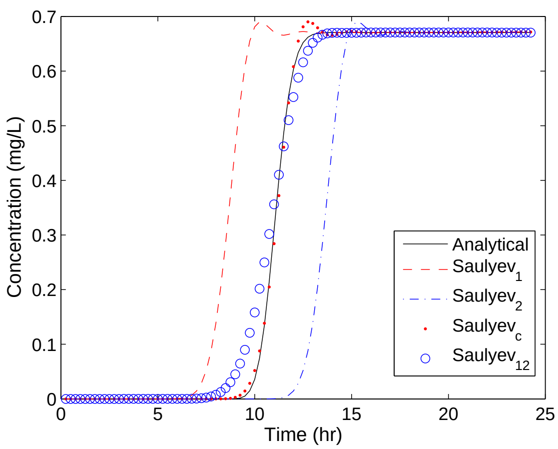

(c) Saulyev schemes

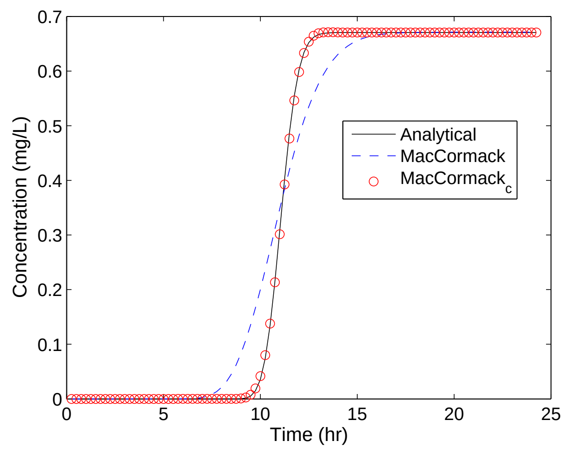

(d) MacCormack schemes

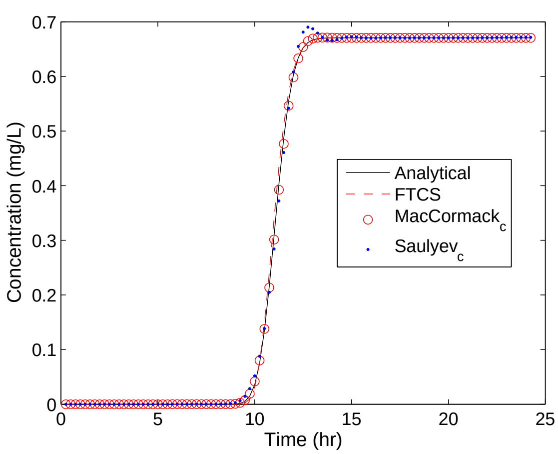

(e) More accurate schemes

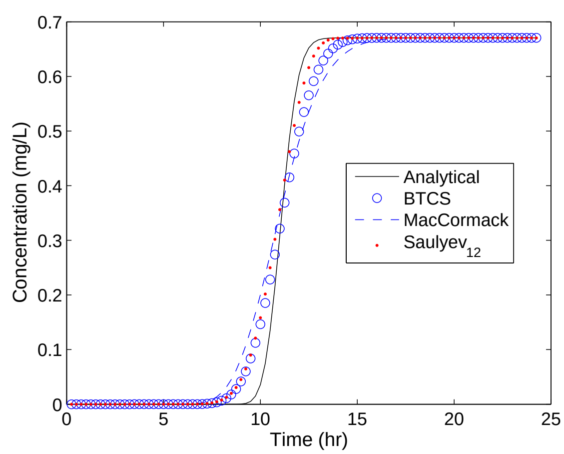

(f) More stable schemes

Figure 3.3: Performances of finite difference schemes under step input scenario

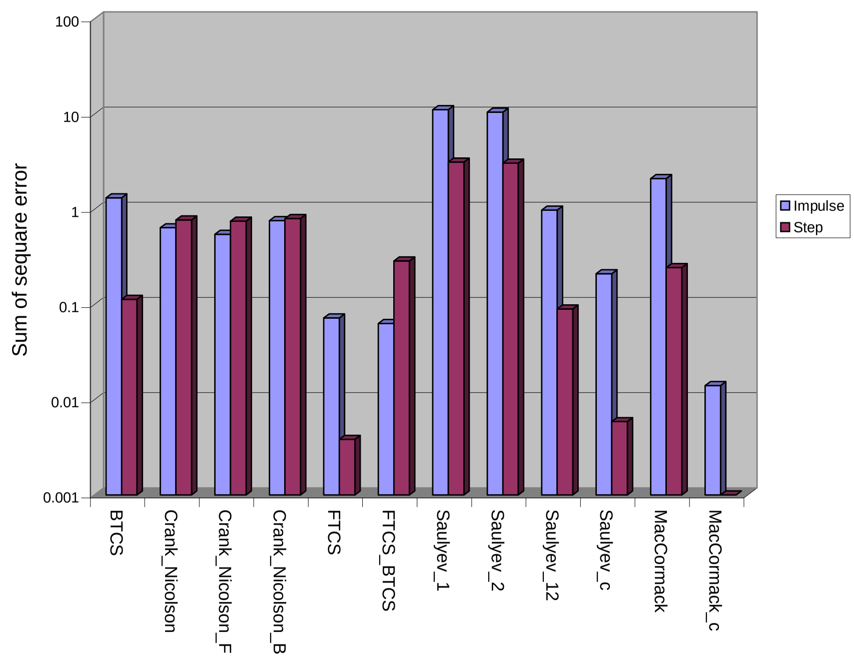

(a) Sum of Square Error (SSE)

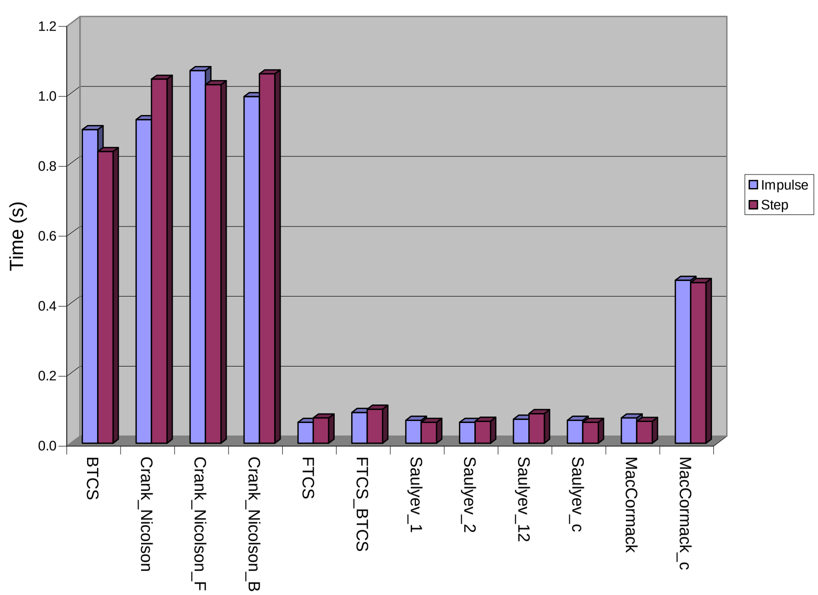

(b) CPU Time consumption

Figure 3.4: Comparison of different numerical schemes in terms of a) SSE and b) CPU time

Table 3.1: Stream system characteristics

Symbol	Description	Unit	Value
X	Stream reach length	2000	m
W	Stream reach width	2	m
h	Stream water depth	1	m
U	Streamflow velocity	0.5	m/s
D	Streamflow dispersivity	20	m^2/s
K	First order reaction rate	10^{-5}	s^{-1}
M	Impulse input amount	5	Kg/m^2
C_0	Step input concentration	1	mg/L

Chapter 4

Development of a Dynamic Dissolved Oxygen and Temperature Model with Groundwater Interactions[1]

[1] Li, G. and C. Rhett Jackson. For submission to *Water Resources Research.*

Abstract

The tributaries of the Lower Flint River, southwest Georgia, are incised into the upper Floridan semi-confined limestone aquifer, and thus seepage of relatively old groundwater sustains baseflows and provides some influence over temperature and dissolved oxygen fluctuations. This hydrologic and geologic setting creates unique aquatic habitats. Groundwater withdrawals for center-pivot irrigation and proposed water supply reservoirs threaten to exacerbate low flow conditions during summer droughts, which may adversely affect stream temperature and dissolved oxygen conditions. To evaluate possible effects of human modifications to stream habitat, we developed a one-dimensional Dynamic stream Dissolved Oxygen and Temperature (DDOT) model. DDOT was constructed with both CSTR (Continuously Stirred Tank Reactor) based and the one-dimensional ADRE (Advection-Dispersion-Reaction) based formulations, and integrates the effects of upstream flow input, groundwater discharge, riparian shading, channel geometry, and channel hydraulics on the spatial and temporal dissolved oxygen and temperature dynamics. The major contribution of model DDOT to existing models lies at the integration of an easy-to-use SHADE module and a BED module. The SHADE module generates accurate estimation of riparian vegetation shading to direct solar radiation on stream water surface, while the BED module calculates the streambed layer vertical temperature and DO profiles that are necessary to account for groundwater input effect on surface water quality. The model was calibrated with field data collected in 2002 and evaluated with data from 2003, years in which flow and water quality behavior were very different. The two formulations provided nearly equivalent simulations. The model performed well and allows robust exploration of system responses to management actions. The model sensitivity analysis using local method indicated that stream temperature is most sensitive to long wave radiation, and stream DO is most sensitive to SOD exchange rate. Companion paper shows the application of the model under different management scenarios.

Keywords

Time series, Stream temperature, Dissolved oxygen, CSTR, ADRE, Finite difference, Numerical solution

4.1 Introduction

Stream temperature and dissolved oxygen are two critical factors affecting survival, movement and the growth of fish (Beschta *et al.*, 1987; Coutant, 1987; Christie and Regier, 1988; Horne and Goldman, 1994; Karim *et al.*, 2003). During hot summer weather, high stream water temperature and low dissolved oxygen problems often occur simultaneously and the resulting stress affects fish habitat use and survival (Matthews, 1998; Lind, 1985). These two water quality parameters are also key factors affecting freshwater mussel survival (Miller and Payne, 2004; Johnson *et al.*, 2001). Studies have shown that the stream discharge play an important role in summer stream temperature and DO variations (Gaffield *et al.*, 2005; Lopes *et al.*, 2004; Sridhar *et al.*, 2004; Sinokrot and Gulliver, 2000; Chaudhury *et al.*, 1998; Caruso, 2002; Gilvear *et al.*, 2002; Sabo *et al.*, 1999), and the effects of groundwater discharge on stream summer temperature and DO can be significant (Moore *et al.*, 2005; Gaffield *et al.*, 2005; Power *et al.*, 1999; LeBlanc *et al.*, 1997). Accordingly, the preservation of a certain amount of upstream inflow and maintenance of groundwater discharge can be critical to protect stream aquatic habitat.

In the state of Georgia, streamflow regulation has been one of the most important issues facing natural resource managers and planners. Increasing population, combined with increased water withdrawal for crop irrigation, has created conflicts in water resources management (Fanning, 1999). Increased water demand and use has been identified as one of the primary problems threatening stream fishes and other aquatic biota in the Southeastern United States (Richter *et al.*, 1997).

The Lower Flint River Basin (Figure 4.1), as one of the state's most important agricultural areas, has become a particular concern of resources managers, planners, and fishery scientists due to the reduced stream discharge (Figure 4.2). Extremely low flow and severely degraded aquatic habitat problems have occurred during drought seasons. During summer 2000, extended drought and increased irrigation pumping brought record low flow to streams in the basin. New record low groundwater levels were recorded in more than 40 wells in the statewide ground-water monitoring network from January to August 2000, among which most of the wells were located in the lower Flint River Basin (USGS, 2000). Excessive ground-water withdrawal for center-pivot irrigation reduces groundwater discharge to streams (Hayes *et al.*, 1983; Torak *et al.*, 1996; Albertson and Torak, 2002), which may have exacerbated the drought's effect on stream water quality. These changes severely affected stream aquatic habitat. Unionid *Elliptio crassidens* were found killed in Chickasawhatchee Creek, Baker County, GA in July 2000, mainly due to the low flow velocity (< 0.01 m/s) and dissolved oxygen (< 5 mg/L) (Johnson *et al.*, 2001). Major fish kills also occurred due to the loss of the aquatic habitat.

The state established the Flint River Drought Protection Act in March 2001 to protect streamflows in tributaries of the basin by limiting farmland irrigation from surface water during droughts. However, the efficiency of the Act depends on whether natural resource managers and planners are informed as to the nature and extent of potential impacts. Proposals to construct water-regulation dams may have adverse impact on downstream aquatic habitat, especially on stream water temperature and dissolved oxygen. There is a need to develop models for natural resources managers and planners to have a clear understanding of the interactions between stream water quantity and quality. Among the goals of such a model would be to evaluate the following hypotheses for the study area:

1. Decreased stream discharge leads to elevated stream temperature and degraded stream dissolved oxygen;

2. Ground water, with its relatively low temperature, has a strong cooling effect on streams in the summer;

3. Stream oxygen concentration increases as a response to decreased stream temperature by increased groundwater addition and/or upstream flow input;

4. Stream width, by affecting direct solar radiation, has positive correlations to stream temperature and dissolved oxygen; while

5. Riparian vegetative shading has negative correlations to stream temperature and dissolved oxygen.

In our study area, surface and ground water interactions are usually large due to the incision of streams into the Upper Floridan Aquifer (Albertson and Torak, 2002; Mosner, 2002). It was therefore necessary for us to develop a more comprehensive Dynamic Dissolved Oxygen and Temperature (DDOT) stream water quality model. DDOT uses a one-dimensional advection-diffusion module to simulate vertical temperature profiles of the streambed and vertical DO profiles of the streambed infiltration flow, which accounts for both diffusion and advection terms that coexist for our sites and is more accurate than existing models. Although the land use of the study area was agriculture dominated, streams had riparian vegetation buffers along both stream banks, which play an important role on stream water quality. It was necessary to account for the riparian vegetation shading effect. A new SHADE routine is introduced to DDOT to give fast and accurate shading estimation, which enables the model to address canopy shading effects not only on stream temperature by blocking direct solar radiation, but also on stream DO by affecting algae photosynthesis. Meanwhile, the consideration of both CSTR based and ADRE based model structures provides a double check on the model performances.

This paper describes the water quality modeling background, model representation, calibration, and evaluation. A companion paper shows the application of the model under different management scenarios. The goals of this research are to provide an accurate simulation tool to guide management decisions and to evaluate the previously stated hypotheses.

4.2 Background

4.2.1 Review of stream temperature modeling

Stream temperature modeling has been studied extensively since Brown (1969). Stream temperature variability is caused by temporal and spatial variation in energy transfer and storage. Energy transfer can be categorized as being either advection terms, or source and sink terms. The advection terms are the ones that involve streamflow, which include surface water flow from upstream and tributaries, and groundwater flow through the streambed. The source and sink terms include fluxes by solar radiation, atmosphere long wave radiation, convection, evaporation/condensation, and streambed conduction. Among these components, streambed conduction and canopy shading are two important factors that affect stream water heat balance (Brown and Krygier, 1967; Jobson, 1977).

Streambed conduction has been included in numerous temperature modeling studies. However, none of these studies has incorporated both the streambed heat diffusion and the groundwater infiltration advection that coexist in porous streambed systems. Brown (1969) included a streambed heat conduction component calculated using Fourier's law based on field measurements of streambed vertical temperature gradient, but assumed there was no groundwater flow through the streambed since it was a solid rock bottom. Brown (1970) further suggested that possible groundwater additions could be treated as a tributary and the mixing ratio method could be used to account for the groundwater effect, but this effect was not actually included in his model. Jobson (1977) stressed the effect of streambed energy storage on water temperature with an analytical solution of the one-dimensional diffusion model assuming a homogeneous streambed, and indicated that temperatures at a depth of three meters below the streambed surface still had important effects on stream water temperatures. Jobson's method was reused by Chen *et al.* (1998) for temperature simulation in forested streams. Sinokrot and Stefan (1993) assumed the streambed to be a "semi-infinite solid body" and used a one-dimensional diffusion equation to predict streambed vertical temperature profiles with numerical solutions, and then used Fourier's law to account for the streambed heat conduction. Their calculation indicated that sediment temperature at a depth of no less than four meters still imposed important effects on stream water temperatures. Rutherford *et al.* (1997) and Gooseff *et al.* (2005) used the same method in their small stream temperature modeling studies. All these studies tended to consider pure diffusion in streambed and thus could not account for groundwater advection effect that exists in porous streambed systems. Studies by LeBlanc *et al.* (1997) and Sridhar *et al.* (2004) did include the heat flux by groundwater input to the stream using the temperature difference method and complete mixing method. However, streambed conduction was neglected. Due to the fact that the quantification of streambed effects on stream temperature was incomplete, available temperature models failed to allow us to fully test our assumptions.

Riparian zone canopy shading may intercept available solar insolation into forested streams and thus plays an important role on stream water temperatures. Brown and Krygier (1967, 1970) reported large increases in stream temperatures after clear-cutting. LeBlanc *et al.* (1997) concluded that water temperature was very sensitive to stream shading. Although on-site measurements of solar radiation with a pyranometer could be used to estimate solar insolation into streams, such as in Gooseff *et al.* (2005), it may not be reliable for streams that experience large diurnal variation of canopy shading, especially for wide streams. For stream temperature time series modeling, accurate real-time riparian vegetation shading efficiency is always critical. Several modeling studies did consider the canopy shading factor (Sinokrot and Stefan, 1993; LeBlanc *et al.*, 1997; Sridhar *et al.*, 2004), but detailed shading calculations were not reported. The most comprehensive studies of canopy and topography shading on stream temperature modeling were found in Rutherford *et al.* (1997) and Chen *et al.* (1998). Rutherford *et al.* (1997) provided a detailed method to estimate solar insolation to streams. However, their method only involved three shading scenarios, i.e., no direct sunlight, full direct sunlight, and a fixed percent of direct sunlight regardless of solar altitude, which becomes inaccurate when shadow length on stream surface changes over time. In addition, the determination of two key factors, that is, the “canopy angle” and “topography angle,” which vary by stream aspect and time, was not fully addressed. The GIS-integrated SHADE program in Chen *et al.* (1998) was very comprehensive and accounted for all the possible scenarios. However, the way it represented riparian vegetation as polygons was a GIS adaption and too complex for general model use. The formulation for "hour angle" was over parameterized and could have been simplified to reduce the computation burden.

4.2.2 Review of stream DO modeling

Published dissolved oxygen models encompass a range of physical completeness. The classic Streeter-Phelps equations used an analytical solution to describe water oxygen and biochemical oxygen demand (BOD) profiles along a river (Cox, 2003). The equations use BOD decay as the only sink, and reaeration as the only source for DO, which was not sufficient for most river systems because other source and sink terms, such as algal photosynthesis and respiration, were found significant on stream DO levels in subsequent studies in the 1960s (Cox, 2003). In the early seventies, Bennett and Rathbun (1972) proposed the dominant processes related to stream oxygen levels as being atmospheric reaeration, algae/plant photosynthesis, algae/plant respiration, BOD decay, and sediment oxygen demand (SOD) decay, where BOD was defined as carbonaceous and nitrogenous oxygen demand. Nitrogenous oxygen demand can also be further refined into ammonium oxygen demand and nitrite oxygen demand in dissolved oxygen modelings (Chaudhury *et al.*, 1998; Zeng *et al.*, 2005). Other modeling studies have used all or part of these components for oxygen balance analysis (Gulliver and Stefan, 1984; Stefan and Fang, 1994; Pearson and Crossland, 1996; Parkhill and Gulliver, 1999; Williams *et al.*, 2000; Kayombo *et al.*, 2000; Moatar *et al.*, 2001; Wang *et al.*, 2003; Zheng *et al.*, 2004). However, none of the above studies integrated the advection component by groundwater, which monitoring studies found significant for dissolved oxygen levels for streams with groundwater additions (Schreier *et al.*, 1980; Power *et al.*, 1999). Canopy shading can decrease photosynthesis by blocking available solar input and also affect oxygen levels (Parr *et al.*, 2002). However, our literature review indicated none of the stream oxygen modeling studies have mentioned this effect.

4.3 Model description

The components considered in model DDOT are illustrated in Figure 4.3. Based on the components analysis, DDOT integrates three modules plus two submodules (Figure 4.4). The three modules are, respectively, the streamflow module, temperature module, and dissolved oxygen module. The two submodules are SHADE submodule and BED submodule. The flow module calculates time series flow rate, stream velocity, and water depth for each stream reach segment at each time node. These results are fed into temperature and oxygen modules to give predicted stream temperature and oxygen respectively. The SHADE submodule generates time series shading efficiency. The BED submodule simulates vertical temperature and oxygen profiles in a porous streambed. The outputs of the submodules are used for source and sink terms estimation. The specific governing equations for both the CSTR and ADRE model structures are provided in Appendix A.

In this section, the BED submodule and SHADE submodule are presented respectively. Then the detailed quantification methods of source and sink terms are followed. Finally the numerical solution schemes are briefly described.

4.3.1 BED submodule

The BED submodule simulates the temperature profile of the saturated streambed and oxygen profile of infiltration flow through the streambed. The streambed is considered as a homogeneous porous media (Rutherford *et al.*, 1997; Chen *et al.*, 1998) inside which infiltration between stream and the underlying aquifer occurs perpendicular to the streambed. Infiltration rate, although variable over time, is assumed to be distributed homogeneously along the reach. It is assumed there are only advection and diffusion terms in the infiltration flow, without any other source or sink terms being considered. Although studies have shown that the hyporheic zone plays an important role in solute exchange and transportation (Martinez and Wise, 2003; Hinkle *et al.*, 2001; Runkel, 1998), it is not explicitly considered in this study due to the extreme difficulty in data collection. The effects of hyporheic zone are believed at least partly to be alternatively accounted for by the dispersion coefficients in the BED submodule and the decay rate of SOD in the dissolved oxygen module. Based on the assumptions, the BED submodule is described by two pure one-dimensional advection-dispersion partial differential equations that are responsible for streambed temperature and DO profiles respectively (Taniguchi *et al.*, 1999a,b):

$$\frac{\partial T_g}{\partial t} - U_g \frac{\partial T_g}{\partial z} = D_{T_g} \frac{\partial^2 T_g}{\partial z^2} \tag{4.1a}$$

$$\frac{\partial C_g}{\partial t} - U_g \frac{\partial C_g}{\partial z} = D_{C_g} \frac{\partial^2 C_g}{\partial z^2} \tag{4.1b}$$

where, t is time (s); z is the downward depth from the top of streambed (m); subscript g means the indicated variables are for groundwater passing through the streambed; T is temperature (°C), C is oxygen concentration (mg/L); D is effective diffusivity (m^2/s); and U_g is Darcy flow velocity in direction of z (m/s), positive for a gaining stream, and negative for a losing stream.

The submodule requires both upper and lower boundaries to be solvable. The upper boundary, located at the interface between stream water and streambed, is set to the temperature and oxygen of the overlying stream (Chen *et al.*, 1998; Sinokrot and Stefan, 1993). The lower boundary is set to the temperature and oxygen of the aquifer (Chen *et al.*, 1998; Rutherford *et al.*, 1997). The location of this boundary is relatively flexible and usually set to a depth where temperature and oxygen are constant.

With streambed temperature and oxygen profiles simulated by the BED submodule, the following equations are used to account for streambed effects on stream temperature and oxygen dynamics.

$$\frac{\partial T}{\partial t} = \frac{D_{T_g}}{h} \frac{\partial T_g}{\partial z}|_{z\to 0} + \frac{U_g}{h} T_{g|z\to 0} \tag{4.2a}$$

$$\frac{\partial C}{\partial t} = \frac{D_{C_g}}{h} \frac{\partial C_g}{\partial z}|_{z\to 0} + \frac{U_g}{h} C_{g|z\to 0} \tag{4.2b}$$

where, state variables T and C without subscript g are for stream water, and those with subscript g are for streambed and infiltration flows; h is stream water hydraulic mean depth.

4.3.2 SHADE submodule

The submodule SHADE is used to generate time series data of riparian canopy shading efficiency (%) over the stream surface. The required input variables include solar altitude, solar azimuth, site latitude, stream orientation angle, stream width, water depth, bank height, and riparian vegetation height. The formula for calculating solar altitude can be found in a variety of sources such as Chen *et al.* (1998), Rutherford *et al.* (1997), Garg and Datta (1993), TVA (1972), and Penrod and Prasanna (1962). We proposed a modified version to calculate solar altitude (Equation (4.3)). Detailed derivation of this equation is in Appendix C.2. This formulation defines the hour angle, ωt, to be the angle from due north, other than from solar noon as in Chen *et al.* (1998) and Rutherford *et al.* (1997). The new definition allows ωt to be calculated as $2\pi \times J_D$, where J_D is day of the year with its decimal part denoting the hour. Thus it is more efficient to code than methods used in Chen *et al.* (1998) and Rutherford *et al.* (1997). In equation 4.3, the term $\sin\Psi$ is negative for the time period from sunset to sunrise. In practical applications, these negative values are set to zero, which leads to $\arcsin(\sin\Psi)$ being within the range of $[0, \frac{\pi}{2}]$.

$$\sin\Psi = \sin\alpha\sin\beta - \cos\alpha\cos\beta\cos\omega t \tag{4.3}$$

where,

$\Psi =$	solar altitude angle	(rad)
$\alpha =$	solar declination angle	(rad)
$\beta =$	site latitude	(rad)
$\omega =$	earth angular velocity	$(\frac{\pi}{12}\ \mathrm{h}^{-1})$
$t =$	local time $[0, 24)$	(h)

The solar declination angle, which is the angle between the ecliptic plane and the equatorial plane, takes values within $[-23.45°, 23.45°]$ from the Southern Hemisphere to the Northern Hemisphere and varies with day of the year. Two formulas are available for estimating solar declination. One can be found in Garg and Datta (1993) or Bourges (1985); the other can be found in Chen *et al.* (1998) or Rutherford *et al.* (1997). The second one was chosen for our model:

$$\alpha = 23.45\frac{2\pi}{360}\cos\left[\frac{2\pi(172 - J_D)}{365}\right] \tag{4.4}$$

Solar azimuth, the angle between the projection of the solar beam on a horizontal plane and due south or due north, is another key factor for shading calculation. It is a function of solar altitude, solar declination, and hour angle. The specific formulation can be slightly different depending on definitions of hour angle and solar azimuth angle (Chen *et al.*, 1998; Diasty, 1998; Rutherford *et al.*, 1997). We redefined the solar azimuth angle, with symbol Φ, as the angle from due east to the projection of the solar beam on the horizontal plane (Figure 4.5). With the new definition of the two angles, we proposed the following formulation (Appendix C.2):

$$\Phi = \arccos\left(\frac{\cos\alpha \times \sin\omega t}{\cos\Psi}\right) \tag{4.5}$$

The above equation gives values of the azimuth angle Φ that increase from 0 to π when the Sun moves from due east to due west, and decrease from π to 0 when the Sun moves from due west to due east. For the time period when the Sun moves from due west to due east, which, depending on the season, contains part or all of night time period, the formula needs to be adjusted as below:

$$\Phi = \pi - \arccos\left(\frac{\cos\alpha \times \sin\omega t}{\cos\Psi}\right) \tag{4.6}$$

Stream orientation angle, denoted by ϕ, is another critical factor for shading calculation. The angle ϕ is defined as the angle from due east, clockwise, to the stream orientation with the range of $[0, \pi)$ (Figure 4.5). Let H_t, H_a, and H_e denote riparian vegetation height plus bank height above water surface, the actual shadow length, and the effective shadow length that is perpendicular to stream orientation respectively, and define δ, within $[0, \pi/2]$, as the angle between stream orientation and solar azimuth. The effective shadow length can be calculated as below:

$$H_e = H_a \times \sin\delta = H_t \times \cot\Psi \times \sin\delta \tag{4.7}$$

In the above equation 4.7, the calculation of the angle δ require special attention because it varies with both stream orientation and solar azimuth. Analysis shown in Figure 4.5 indicates that the following equation works for all possible spatial situations:

$$\sin\delta = \sin(|\Phi - \phi|) \tag{4.8}$$

With the effective shade length, the shading percent over a stream surface can be easily calculated as the ratio of the difference between this shade length and the sum of the stream width and and the distance of the riparian tree to the edge of stream water over stream width. It is possible to get ratio > 1, which means complete shading. At this situation the ratio is reset to 1, so that shading efficiency is within $[0, 1]$. This situation applies at night when the sun is on the other side of the earth.

With the shading ratio given by SHADE, the effective solar radiation to the stream is adjusted as below:

$$I = I_0 \times (1 - r_{shade}) \tag{4.9}$$

where, I is the available solar radiation to the stream; I_0 is observed or theoretical solar radiation at an open place; and r_{shade} is the shading ratio.

4.3.3 Sources and Sinks

In model DDOT, the source and sink terms for the stream temperature module include solar radiation, atmosphere long wave radiation, convection, evaporation/condensation, streambed conduction, and groundwater advection 4.3(a). Those terms for oxygen include atmospheric reaeration, algae/plant photosynthesis, algae/plant respiration, BOD decay, SOD decay, and groundwater advection 4.3(b). The detailed calculation methods for the components are presented below.

E_S — SOLAR RADIATION FLUX (J M^{-2} S^{-1})

Solar radiation flux is usually available from local weather station. The actual solar radiation input to the stream was considered as below (Anderson, 1954; LeBlanc *et al.*, 1997):

$$E_S = I(1 - r_{shd})(1 - r_{albedo\_S}) \tag{4.10}$$

where,

$$r_{albedo\_S} = \begin{cases} 1.18\Psi^{-0.77} & if \quad \Psi > 1.24^\circ \\ 1 & otherwise \end{cases}$$

$I =$ solar radiation from weather station (J m^{-2} s^{-1})

$r_{shd} =$ canopy shading (%)

E_L — LONG WAVE RADIATION FLUX (J M^{-2} S^{-1})

Using Stefan-Boltzman equation (Tang *et al.*, 2004; Chapra 1997, P_{570}):

$$E_L = \sigma\{\varepsilon_a T_a^4(1 - r_{albdedo\_L}) - \varepsilon_w T_w^4\} \tag{4.11}$$

where,

$T_a =$ air temperature (K)

$T_w =$ water temperature (K)

$\varepsilon_a =$ $0.7 + 0.031\sqrt{e_{air/133.3}}$, emissivity of air

$\varepsilon_w =$ 0.97, emissivity of water

$r_{albedo\_L} =$ 0.065, water surface reflection to long wave radiation

$\sigma =$ 5.67×10^{-8}, Stefan-Boltzman constant (W m^{-2} K^{-4})

E_H — EVAPORATION FLUX (LATENT HEAT) (J M^{-2} S^{-1})

Using empirical equation (Tang and Etzion, 2004; Chapra 1997, P_{567}, P_{571}):

$$E_H = f(W)(e_a - e_w) \tag{4.12}$$

where,

$$\begin{aligned} f(W) = &\quad 0.0887 + 0.07815 \times W \text{ (m/s)} \\ W = &\quad \text{wind speed (m/s)} \\ e_a = &\quad 4.596 \exp\left(\tfrac{17.27T_a}{237.3+T_a}\right) \times 133.3 \times R_h \text{ (N/m}^2) \\ e_w = &\quad 4.596 \exp\left(\tfrac{17.27T_w}{237.3+T_w}\right) \times 133.3 \text{ (N/m}^2) \\ T_a = &\quad \text{air temperature (°C)} \\ T_w = &\quad \text{water temperature (°C)} \\ R_h = &\quad \text{Relative humidity (\%)} \end{aligned}$$

E_C — CONVECTION FLUX (SENSIBLE HEAT) (J M^{-2} S^{-1})

Using empirical equation (Krajewski *et al.*, 1982; LeBlanc *et al.*, 1997):

$$E_C = f(W)(T_a - T_w) \tag{4.13}$$

where,

$$\begin{aligned} f(W) = &\quad 0.0228 \times p \times W \text{ (J m}^{-2}\text{ °C }^{-1}) \\ p = &\quad \text{air pressure (KPa)} \\ W = &\quad \text{wind speed (m s}^{-1}) \end{aligned}$$

P_k — REAERATION RATE (MG L^{-1} S^{-1})

Atmospheric reaeration rate of oxygen to streams is usually modeled with the Dalton type equation:

$$P_k = K_a(C_s - C) \tag{4.14}$$

where,

$$\begin{aligned} K_a = &\quad \text{Reaeration coefficient (s}^{-1}) \\ \theta_k = &\quad \text{1.024, Arrhenius coefficient (Bowie \textit{et al.} 1985, P}_{125}) \\ C_s = &\quad \text{Saturated DO concentration (mg L}^{-1}) \\ C = &\quad \text{Actural DO concentration (mg L}^{-1}) \end{aligned}$$

Oxygen saturation depends on water temperature (°C). The frequently used equation for C_s (Cox, 2003; Bowie *et al.* 1985, P$_{91}$) is as below:

$$C_s = 14.652 - 0.41022T + 0.007991T^2 - 7.7774 \times 10^{-5}T^3 \tag{4.15}$$

The reaeration coefficient K_a is related to streamflow velocity and stream water depth. A collection of available empirical equations can be found in Cox (2003) and Bowie *et al.* (1985, P$_{103}$). The one developed by Owens and Gibbs (1964) (Cox, 2003) for streams with depth from 0.12 - 0.73 m and velocity from 0.03-0.55 m/s was chosen for the model. In the model application, the units were converted from day^{-1} to s^{-1}.

$$K_a = 5.32\frac{U^{0.67}}{h^{1.85}} \cdot \frac{1}{24 \times 3600} \tag{4.16}$$

P_a — ALGAL PHOTOSYNTHESIS RATE (MG L^{-1} S^{-1})

Algal photosynthesis is assumed to be directly proportional to the available solar radiation, and then corrected by the stream temperature with the Arrhenius coefficient (Darley 1982, P_{26}; Cox 2003; Zeng 2001, P$_{184-186}$):

$$P_a = K_{a2p} \times G_M \times \theta_p^{T-20} \times I \times [Alg] \tag{4.17}$$

where,

$K_{a2p} = \frac{138\times32}{106\times12}$, conversion coefficient from algae to oxygen (Zeng, 2001; Chapra and Pelletier, 2003)

$G_I =$ Algal growth rate per unit solar radiation at 20 °C (m^2 J^{-1})

$\theta_p =$ 1.036, Arrhenius coefficient (Parkhill and Gulliver, 1999)

$[Alg] =$ Algal concentration (mg L^{-1})

R_a — ALGAL RESPIRATION RATE (MG L^{-1} S^{-1})

Algal respiration is computed as (Parkhill and Gulliver, 1999; Zeng 2001,P$_{184-186}$):

$$R = K_{a2r} \times R_{20} \times \theta_r^{T-20} \times [Alg] \tag{4.18}$$

where,

$K_{a2r} =$ $\frac{38\times 32}{106\times 12}$, conversion coefficient from algae to oxygen (Zeng, 2001)

$R_{20} =$ Algal respiration rate at 20 °C (s^{-1})

$\theta_r =$ 1.045, Arrhenius coefficient (Parkhill and Gulliver, 1999)

R_b — BOD decay rate (mg L^{-1} s^{-1})

A simple way to model BOD decay is to use the following equation (Zeng 2001, $P_{188-190}$; Knowles and Wakeford, 1978):

$$R_b = K_b \times \theta_b^{T-20} \times L_b \tag{4.19}$$

where,

$K_b =$ BOD decay coefficient at 20 °C (s^{-1})

$\theta_b =$ 1.047, Arrhenius coefficient (Knowles and Wakeford, 1978)

$L_b =$ BOD concentration (mg L^{-1})

R_s — SOD decay rate (mg L^{-1} s^{-1})

SOD decay can be modeled with equation shown below (Cox, 2003; Zeng, 2001):

$$R_s = \frac{K_s \times \theta_s^{T-20}}{h} \times 0.001 \tag{4.20}$$

where,

$K_s =$ SOD exchange rate at 20 °C (mg m^{-2} s^{-1})

$\theta_s =$ 1.035 (Park and Jaffe, 1999) or 1.065 (Cox 2003)

$h =$ hydraulic mean depth (m)

$0.001 =$ converts unit from mg/m^3 to mg/L

4.3.4 Numerical solutions

The numerical solution strategies are different for the two different model formulations used in DDOT. The CSTR based formulations take the form of ordinary differential equations, which are solved by using the built in ODE solver in Matlab. The ADRE based formulations take the form of partial differential equations, in which the flow module uses Saint-Venant equations which are solved by the implicit Preissman method (Sturm, 2001, $P_{313-319}$; Zeng, 2000), and the temperature and oxygen module are solved with explicit MacCormack schemes (Chapra, 1997, P_{229}). The detailed finite difference numerical solutions are attached in Appendix B.

While numerical stability is not a concern for implicit schemes, explicit schemes can suffer from instability problems if the lengths of space step and time step are not appropriate (Chapra, 1997, $P_{223-232}$). Although the explicit MacCormack scheme requires more liberal stability constraints (Chapra 1997, $P_{214,216}$), the time and step lengths in DDOT are designed to meet both the diffusion number and the advection number or CFL (Courant-Friedrichs-Levy) number requirements for simple explicit finite difference schemes. These requirements are:

$$\lambda = \frac{D\Delta t}{\Delta x^2} < \frac{1}{2} \tag{4.21a}$$

$$\gamma = \frac{U\Delta t}{\Delta x} < 1 \tag{4.21b}$$

where, λ is the diffusion number, γ is the advection number, D is the dispersion number (m^2/s); U is the streamflow velocity (m/s); Δx is the space step (m); and Δt is the time step (s).

4.4 Study site

The study site is located on the Dougherty plain in the Lower Flint River Basin, Southwest GA, where karst physiography controls hydrology (Hyatt and Jacobs, 1996). Land use in the study area is predominantly agricultural (Warner *et al.*, 2002). Streams across the area are mostly buffered with riparian forests. In this karstic system, streams are hydraulicly connected to the Upper Floridan aquifer, resulting in active water exchanges between streams and the aquifer (Hyatt and Jacobs, 1996; Adams, 2005). Low flows in these streams occur from June to October, coincident with late summer high temperature and low dissolved oxygen conditions (Figure 4.6 and Table 4.1).

Since the 1970s, water use has been dominated by agricultural irrigation, comprising up to 90% of the water used in the Flint River Basin during the April-September growing season (Adams, 2005). Overall, a total of approximately 160,000 acres are irrigated from surface water and approximately 403,000 acres from Floridan aquifer wells in this area. In the peak month (July) of a typical irrigation season during a drought year, approximately 250 mgd are used by agricultural surface water users, and approximately 950 mgd are withdrawn from Floridan aquifer irrigation wells (Adams, 2005).

The water use distribution varies over the area. In the Kinchafoone-Muckalee Creek watershed, with lesser amounts of land under irrigation, is dominated by surface water withdrawals; in the Ichawaynochaway watershed, the southern half is supplied mostly by aquifers, and the northern half by both surface and wells; while the Spring Creek watershed, irrigation is almost exclusively supplied by groundwater (Adams, 2005).

The stream reach selected for data collection and model development was between the cities of Morgan and Milford on Ichawaynochaway Creek (Figure 4.7). This stream reach had two major advantages over the other reaches. The reach had U.S. Geological Survey flow gages installed at both boundaries, and there was only one significant tributary, Pachitla Creek, joined to this reach, which also had a flow gage, although relatively far from its confluence with the main reach. In total three locations were selected for time series water quality monitoring: 1) upper boundary Ichawaynochaway Creek at Morgan (Ichi2) ; 2) lower boundary Ichawaynochaway Creek at Milford (Ichi3); and 3) Pachitla Creek close to its confluence with the main reach (Pach). The reach length was 25,200 m, and Pachitla Creek converged into the reach at a location 8,611 m below the upper boundary.

4.5 Model test

4.5.1 Data collection

We monitored stream water quality time series data for our study sites during the summers of the years 2002 - 2004 with Hydrolabs. In each summer, we deployed the Hydrolabs to each selected locations for about 10 days. Data was collected every 15 minutes to capture short term temporal variations in water quality variables. This interval also matched flow data frequency of the USGS, which made it convenient to integrate the datasets. The deployment time period was limited by battery life and memory storage, but also by the accumulation of algae and sediment, which could decrease probe sensitivities and lead to unreliable measurements. Due to the extreme difficulty of collecting time series of stream algae and BOD concentrations, we tested grab samples only once for the sites. Stream SOD, another component in DDOT, was determined by model calibration.

Time series streamflow data were downloaded from the USGS website. Because no direct groundwater discharge and recharge data were available, a water balance method was used to estimate groundwater flows. The difference of discharge between the upper and lower boundaries was considered to be the groundwater discharge rate. The time series weather data were from the nearest weather station located at Newton, GA.

Among the available datasets, the one collected during 9/5/2002 - 9/15/2002 was chosen for model calibration. There were two reasons to choose this dataset: 1) the time period was late summer, during which stream temperature was high and became a concern of fishery scientists; 2) no precipitation occurred during that time period aiding calibration because our model is not designed to handle precipitation inputs. The dataset collected during 10/03/2003 - 10/11/2003 for was chosen for model evaluation. Although the time period was about one month later than that for the model calibration, this was also a clean dataset.

4.5.2 Calibration

The study reach in Ichawaynochaway Creek had channel widths ranging from 12 to 28 m from upper to lower boundaries, with a mean discharge of 21.43 m^3/s at the lower boundary computed from USGS data (1940 - 2003). Streambed gradient was approximately 0.058% based on site survey. For such streams, the dispersion coefficients are usually less than 100 m^2/s (Chapra 1997, P_{236}). The time interval of data collection was 15 minutes. The streamflow velocity varied from 0.3 - 0.5 m/s. The above criteria requires a space step Δx larger than 500 m. During model calibration, a fixed space step Δx equal to 1000 m was used, which turned out to be an appropriate value for the stream system. Our calibration indicated that CSTR based formulations did not encounter stability problems. To make the comparison convenient between the two model structures, the same step size was chosen for CSTR formulations.

The stream reach was then divided into 25 segments, which generated 25 CSTRs and 26 nodes including both boundaries. The tributary converged to the main reach at a location between nodes 9 and 10, but closer to node 10. For easier model calculation manipulation, it was assumed that the tributary joined the main reach exactly at node 10 or the upper boundary of CSTR 10 (Figure 4.8).

Among the three submodules, the flow module affects both the temperature and DO modules, while the temperature module also affects the DO module; no other interactions were considered. For this reason, the modules were calibrated individually but strictly by the order of flow module calibration - temperature module calibration - DO module module calibration.

Assumptions necessary to calibrate the model include the stream reach to be longitudinally smooth, so that parameters such as stream width, streambed gradient, Manning's roughness coefficient, riparian zone vegetation height, for segments in between the upper and lower boundaries could be linearly interpolated from the boundary values.

Automatic and manual calibration were used alternately for model parameter optimization. Automatic parameter search were conducted with the Matlab built-in classical optimization toolbox that calculates the smallest Sum of Square Error (SSE). It was found that the automatically optimized parameters did not give very good prediction results. We doubted that the automatic optimization searched the globally optimized parameter set, as for non-linear models, several locally optimum parameter sets often exist (Figure 4.9). So the trial and error manual calibration was followed until SSE was minimized. Input parameters with their final values were summarized in Table 4.2.

The calibrated Manning's n was reasonable for a medium size stream flowing through forested lands. The groundwater flow corrector, q_{gc}, was introduced for groundwater flow estimation. The flow module generated very accurate simulations.

During model calibration, it was found necessary to introduce correction coefficients for the source/sink terms of the temperature module to dampen the large amplitude of diurnal variations. The simulated results would not fit the observed data until these correctors were introduced. These corrections were considered reasonable as stream reaches were densely forested, which could significantly block the vertical fluxes through the stream water surface and dampen out diurnal variations of temperatures. Although forest shading effect was included in both models, the canopy of these riparian trees was assumed not to overhang the stream, while actually it might provide additional shading effect. On the other hand, these correctors might have reflected some energy and mass flows through the hyporheic zone, which was not included in the models. In contrast to groundwater discharge/recharge flows, hyporheic flow usually does not change flow volume of the stream reach. However, it can greatly accelerate the mass and energy exchange of surface water with the streambed (Supriyasilp *et al.*, 2003; Jonsson *et al.*, 2003; Hendricks and White, 1988), where temperature and DO levels might be quite different from those in surface water. While reasonable causes for the above corrections were discussed, the coefficients for convective flux in both formulation types were well above the mentioned ranges, and even larger than the one in the ADRE based formulation. Most likely, this might be a compensatory response for errors induced by other parameters, or, it might be an indicator that the original empirical convective flux equation, although commonly used in research, should be modified for our specific site. The latter possibility could be true, since "The resulting vertical convective air currents ... might be expected to achieve much higher rates of heat and mass transfer from the water surface [even in the absence of wind] than would be possible by molecular diffusion alone (Edinger et al, 1974)" (Chapra and Pelletier, 2003).

In the DO module, two parameters were calibrated with values that are quite different from the literature: the reaeration coefficient and the respiration rate. The reaeration coefficient was greatly reduced by a correction coefficient 0.03. This could be an effect of dense canopy cover, or a compensation for possible errors from overall lower oxygen demand of the system. The very high respiration coefficient, which is larger than 1 day^{-1}, is probably due to the extremely low algae concentration observed in the stream. In most natural stream systems, algae chlorophyll a concentration were in the range of 1 mg/L (Zeng *et al.*, 2005; Skidmore *et al.*, 1998). However, it was measured in this river at only 0.001 mg/L, which resulted in a very high respiration rate during calibration in order to get a reasonable respiration effect that was calculated as the product of the two variables.

With these calibrated parameters, the simulated values fitted the observed data very well (Figures 4.10, 4.11, and 4.12). High correlations existed between simulated and observed data for both CSTR and ADRE based formulations (Figure 4.13). The scatter plots indicated that there was no apparent difference between CSTR formulations and ADRE formulations (Figure 4.18, Calibration). During model calibration, the groundwater flows were adjusted to be 60% of the difference between the upper boundary input and lower boundary output to achieve a good fit of the flow module. This adjustment was reasonable since some unknown local water input or withdrawal could occur.

4.5.3 Evaluation

Both calibrated models were tested against second year data. The parameters for the flow module, such as n in Manning's equation, and a and b in the experiential flow equation, were re-calibrated during the model evaluation period. These adjustments were necessary because the test flow regime was much higher than the calibration period. The groundwater flow rate was reset to exactly equal the differences between output and input discharges, which generated good fits for observed discharge and water stage. The very small magnitude of the adjustments indicated the efficiency of the flow module.

All the other parameters were kept constant during model evaluation. The model fit for the evaluation datasets indicated that flow module in both models provided very close predictions to observed flow (Figure 4.14). The temperature module also gave very accurate predictions (Figure 4.15). The oxygen module in the ADRE based formulations predicted fairly well, while some underestimation observed in the CSTR based formulations, with the maximum underestimation around $0.8mg/L$ (Figure 4.16). However, the overall trend was the same, so such underestimation does not significantly degrade the module performance.

The scatter plots between simulated and observed data during the evaluation period indicated that the temperature module worked fairly well for both CSTR and ADRE based formulations (Figure 4.17). The ADRE based oxygen module produced acceptable evaluation results, while the CSTR based oxygen module had a relatively low correlation between simulated and observed data. The relatively poor evaluation results in oxygen simulation might be due to relatively large errors by the flow module. As expected, the scatter plots of simulation results between CSTR and ADRE based formulations indicated that there was no apparent difference between the CSTR based and the ADRE based temperature module, while some differences were observed for the flow module and oxygen module (Figure 4.18, Evaluation).

4.5.4 Sensitivity analysis

The local method sensitivity analysis (Saltelli, 2004) was conducted to examine the sensitive model parameters. That is, each time only one parameter was allowed to change certain amount from its calibrated value. The averaged ratio of the relative change of a state variable over that of a parameter was used as the sensitivity index. Specifically, the following equation (4.22) was used as the quantification of model sensitivities.

$$S_{i,\beta_j} = \frac{1}{n}\sum_{t=1}^{n}\left(\frac{\beta_j}{C_i^t}\frac{dC_i^t}{d\beta_j}\right) \cong \frac{1}{n}\sum_{t=1}^{n}\left(\frac{\beta_j}{C_i^t}\frac{\Delta C_i^t}{\Delta\beta_j}\right) = \frac{1}{n}\sum_{t=1}^{n}\left(\frac{\beta_j}{C_i^t}\frac{C_{i,\beta_j}^t - C_{i,\hat{\beta}_j}^t}{\beta_j - \hat{\beta}_j}\right) \tag{4.22}$$

where, S_{i,β_j} is Sensitivity of the i^th state variable against the j^th parameter; C_i^t is the i^th state variable at time t; β_j is the j^th parameter of interest; n is total number of time series data observations.

The tested parameters and their sensitivities were shown in Figure 4.19. The results indicated that, 1) stream discharge is most sensitive to Manning's roughness coefficient; 2) stream temperature is most sensitive to long wave radiation; and 3) stream DO is most sensitive to SOD exchange rate.

4.6 Discussion and conclusion

Both streambed and groundwater discharge have important effects on stream water temperatures. However, the available stream temperature modeling studies considered either streambed conduction or groundwater discharge individually. None of them integrated both the diffusion and advection effects which are more meaningful for streams with groundwater and surface water interactions such as our study sites. Similarly, ground water discharge also buffers stream oxygen variations in monitoring studies. It seems that this buffer ability has been omitted in available stream oxygen models. While it was reasonable not to include all of these effects, the available models were inadequate for our study sites in the Lower Flint River Basin, southwest Georgia.

The unique hydrologic and geologic settings of the study area required a water quality numerical model able to address the effects of streamflow and ground water infiltration on stream water temperature and dissolved oxygen dynamics. Model DDOT is designed to meet such requirements by integrating a one-dimensional advection-dispersion temperature submodule that dynamically solved vertical temperature and oxygen profiles of groundwater flows passing through a porous streambed.

Riparian canopy shading also has a significant effect on stream temperature dynamics. Although Rutherford *et al.* (1997) provided comprehensive shading predictions, only three scenarios were considered in their methods, which were not appropriate for high frequency time series models. Another comprehensive study by Chen *et al.* (1998) summarized detailed formulations of time series shading calculations in their GIS-integrated SHADE program. However, the program was too complex for general model use. Our submodule SHADE provides a new way to account for riparian shading effect, which gives fast and accurate results.

DDOT also enhances its modeling ability by taking both CSTR-based and ADRE-based structures. The very close simulation results by the two different methods increases confidence in the model performance. For model application, users can employ both structures for comparison purposes, or just select either one of them depending on their individual preference. The calibration and evaluation indicated negligible differences between the two formulations in the flow submodule and the temperature submodule. The CSTR-based oxygen submodule was slightly low during the model evaluation period. However, the overall trend was the same as the observed data.

The very high correlations between simulated and observed data during model calibration indicated successful model structure selection and parameterization. Model evaluation verified the reliable performance of the model for brand new time series datasets. By taking streamflow, groundwater inputs, riparian shading, channel geometry, and channel hydraulics, the model addresses the effects of variation of these factors on stream temperature and oxygen dynamics, which enables it to be an accurate simulation tool to guide management decisions.

References

Adams, J. L., 2005. Recommendations for the Flint River Basin Water Development and Conservation Plan. Presented to the Georgia Environmental Protection Division Director, the Flint River Basin Stakeholder Advisory Committee, 227 pp. Web: `http://www.gadnr.org/frbp/Assets/Documents/Plan17.pdf`.

Albertson, P. N. and L. J. Torak, 2002. Simulated effects of ground-water pumpage on stream-aquifer flow in the vicinity of federally protected species of freshwater mussels in the lower Apalachicola-Chattahoochee-Flint River basin (Subarea 4), southeastern Alabama, northwestern Florida, and southwestern Georgia. Water-Resources Investigations Report 02-4016, U.S. Geological Survey, 54 pp. Web: `http://ga.water.usgs.gov/pubs/wrir/wrir024016/`.

Anderson, E. R., 1954. Water-Loss Investigations: Lake Hefner Studies. Professional Paper 269, U.S. Geological Survey, Washington, D.C., 71 pp.

Becker, M. W., T. Georgian, H. Ambrose, J. Siniscalchi, and K. Fredrick, 2004. Estimating flow and flux of ground water discharge using water temperature and velocity. *Journal of Hydrology*, 296(1-4):221–233.

Bennett, J. P. and R. E. Rathbun, 1972. Reaeration in Open-Channel Flow. U.S. Geological Survey Professional Paper 737, U.S. Govt. Print. Off., Washington, 75 pp.

Beschta, R., R. Bilby, G. Brown, L. Holtby, and T. Hofstra, 1987. Chapter 6. stream temperature and aquatic habitat: Fisheries and forestry interactions. In Salo, E. and T. Cundy, editors, *Streamside Management: Forestry and Fishery Interactions*. University of Washington, Institute of Forest Resources. Contribution No. 57, pp. 191-232.

Bourges, B., 1985. Improvement in solar declination computation. *Solar Energy*, 35(4):367–369.

Bowie, G. L., W. B. Mills, D. B. Porcella, C. L. Campbell, J. R. Pagenkopf, G. L. Rupp, K. M. Johnson, P. W. Chan, and S. A. Gherini, 1985. Rates, Constants, and Kinetics Formulations in Surface Water Quality Modeling (Second Edition). Technical Report EPA/600/3-85/040, Environmental Research Laboratory, Office of Research and Development, U.S. Environmental Protection Agency,, Athens, GA 30613, 455 pp.

Brown, G., 1969. Predicting temperatures of small streams. *Water Resources Research*, 5(1):68–75.

Brown, G., 1970. Predicting the effect of clearcutting on stream temperature. *Soil and Water Conservation*, 25:11–13.

Brown, G. W. and J. T. Krygier, 1967. Changing water temperatures in small mountain streams. *Soil and Water Conservation*, (11-12):242–244.

Brown, G. W. and J. T. Krygier, 1970. Effects of clear-cutting on stream temperature. *Water Resources Research*, 6(4):1133–1139.

Caruso, B. S., 2002. Temporal and spatial patterns of extreme low flows and effects on stream ecosystems in Otago, New Zealand. *Journal of Hydrology*, 257(1-4):115–133.

Chapra, S. C., 1997. *Surface Water-Quality Modeling*. McGraw-Hill, New York, 844 pp.

Chapra, S. C. and G. J. Pelletier, 2003. QUAL2K: A Modeling Framework for Simulating River and Stream Water Quality Documentation and Users Manual. Civil and Environmental Engineering Dept., Tufts University, Medford, MA, 121pp. Web: `http://www.epa.gov/ATHENS/wwqtsc/html/qual2k.html`.

Chaudhury, R. R., J. A. H. Sobrinho, R. M. Wright, and M. Sreenivas, 1998. Dissolved oxygen modeling of the Blackstone River (northeastern United States). *Water Research*, 32(8):2400–2412.

Chen, Y. D., R. F. Carsel, S. C. McCutcheon, and W. L. Nutter, 1998. Stream temperature simulation of forested riparian areas: I. Watershed-scale model development. *Journal of Environmental Engineering*, 124(4):304–315.

Christie, C. and H. Regier, 1988. Measurements of optimal habitat and their relationship to yields for four commercial fish species. *Canadian Journal of Fisheries and Aquatic Science*, 45:301–314.

Coutant, C. C., 1987. Thermal preference - When does an asset become a liability. *Environmental Biology of Fishes*, 18(3):161–172.

Cox, B. A., 2003. A review of dissolved oxygen modelling techniques for lowland rivers. *The Science of The Total Environment*, 314-316:303–334.

Crittenden, R. N., 1978. Sensitivity analysis of a theoretical energy balance model for water temperatures is small streams. *Ecological Modelling*, 5(3):207–224.

Darley, W. M., 1982. *Algal biology : A physiological approach*. Blackwell Scientific Publications, Blackwell Mosby Book Distributors, Oxford, Boston, St. Louis, MO, 168 pp.

Diasty, R. E., 1998. Variable positioning of the sun using time duration. *Renewable Energy*, 14(1-4):185–191.

Fanning, J. L., 1999. Water use in coastal Georgia by county and source, 1997; and water-use trends, 1980-97. Georgia Geologic Survey Information Circular 104, U.S. Geological Survey, Atlanta, GA, 37 pp. Web: http://ga.water.usgs.gov/pubs/other/ggs-ic104/.

Gaffield, S. J., K. W. Potter, and L. Z. Wang, 2005. Predicting the summer temperature of small streams in Southwestern Wisconsin. *Journal of the American Water Resources Association*, 41(1):25–36.

Garg, H. P. and G. Datta, 1993. Fundamentals and characteristics of solar radiation. *Renewable Energy*, 3(4-5):305–319.

Gilvear, D. J., K. V. Heal, and A. Stephen, 2002. Hydrology and the ecological quality of Scottish river ecosystems. *The Science of The Total Environment*, 294(1-3):131–159.

Gooseff, M., K. Strzepek, and S. Chapra, 2005. Potential effect of climate change on water temperature downstream of a reservoir: Lower Madison River, Montana. *Climatic Change*, 68(3):331–353.

Gulliver, J. S. and H. G. Stefan, 1984. Stream productivity analysis with dorm–I : Development of computational model. *Water Research*, 18(12):1569–1576.

Hayes, L., M. Maslia, and W. Meeks, 1983. Hydrology and model evaluation of the principal artesian aquifer, Dougherty Plain, southwest Georgia. Georgia Geologic Survery Bulletin 97, 93 pp.

Hendricks, S. P. and D. S. White, 1988. Hummocking by Lotic Chara: Observations on alterations of hyporheic temperature patterns. *Aquatic Botany*, 31(1-2):13–22.

Higashino, M. and H. G. Stefan, 2005. Sedimentary microbial oxygen demand for laminar flow over a sediment bed of finite length. *Water Research*, 39(14):3153–3166.

Hinkle, S. R., J. H. Duff, F. J. Triska, A. Laenen, E. B. Gates, K. E. Bencala, D. A. Wentz, and S. R. Silva, 2001. Linking hyporheic flow and nitrogen cycling near the Willamette River – a large river in Oregon, USA. *Journal of Hydrology*, 244(3-4):157–180.

Horne, A. J. and C. R. Goldman, 1994. *Limnology, 2nd Edition.* McGraw-Hill, New York, 576 pp.

Hyatt, J. A. and P. M. Jacobs, 1996. Distribution and morphology of sinkholes triggered by flooding following Tropical Storm Alberto at Albany, Georgia, USA. *Geomorphology*, 17(4):305–316.

Jobson, H., 1977. Bed conduction computation for thermal models. *Journal of the Hydraulics Division, American Society of Civil Engineers*, 103(HY10):1213–1217.

Johnson, P. M., A. E. Liner, S. W. Golladay, and W. K. Michener, 2001. Effects of drought on freshwater mussels and instream habitat in Coastal Plain tributaries of the Flint River, southwest Georgia (July-October, 2000). Presented to The Nature Conservancy Apalachicola River and Bay Project, Jones Ecological Research Center, Route 2 Box 2324, Newton, GA, 34 pp. Web: `http://www.jonesctr.org/research/aquatics_research/final_report2.pdf`.

Jonsson, K., H. Johansson, and A. Worman, 2003. Hyporheic exchange of reactive and conservative solutes in streams–tracer methodology and model interpretation. *Journal of Hydrology*, 278(1-4):153–171.

Karim, M. R., M. Sekine, and M. Ukita, 2003. A model of fish preference and mortality under hypoxic water in the coastal environment. *Marine Pollution Bulletin*, 47(1-6):25–29.

Kayombo, S., T. S. A. Mbwette, A. W. Mayo, J. H. Y. Katima, and S. E. Jorgensen, 2000. Modelling diurnal variation of dissolved oxygen in waste stabilization ponds. *Ecological Modelling*, 127(1):21–31.

Knowles, G. and A. C. Wakeford, 1978. A mathematical deterministic river-quality model. Part 1: Formulation and description. *Water Research*, 12(12):1149–1151.

Krajewski, W. F., A. K. Kraszewski, and W. J. Grenney, 1982. A graphical technique for river water temperature predictions. *Ecological Modelling*, 17(3-4):209–224.

LeBlanc, R. T., R. D. Brown, and J. E. FitzGibbon, 1997. Modeling the effects of land use change on the water temperature in unregulated urban streams. *Journal of Environmental Management*, 49(4):445–469.

Lind, O. T., 1985. *Handbook of Common Methods in Limnology, 2nd Edition*. Kendall/Hunt Pub. Co., Dubuque, Iowa, 199 pp.

Lopes, L. F. G., J. S. A. Do Carmo, R. M. Vitor Cortes, and D. Oliveira, 2004. Hydrodynamics and water quality modelling in a regulated river segment: application on the instream flow definition. *Ecological Modelling*, 173(2-3):197–218.

Martinez, C. J. and W. R. Wise, 2003. Analysis of constructed treatment wetland hydraulics with the transient storage model OTIS. *Ecological Engineering*, 20(3):211–222.

Matthews, W. J., 1998. *Patterns in Freshwater Fish Ecology*. Chapman and Hall, New York, 756 pp.

McCuen, R. H., 1998. *Hydrologic analysis and design*. Prentice Hall, Upper Saddle River, N.J.

Miller, A. C. and B. S. Payne, 2004. Reducing risks of maintenance dredging on freshwater mussels (Unionidae) in the Big Sunflower River, Mississippi. *Journal of Environmental Management*, 73(2):147–154.

Moatar, F., J. Miquel, and A. Poirel, 2001. A quality-control method for physical and chemical monitoring data. Application to dissolved oxygen levels in the river Loire (France). *Journal of Hydrology*, 252(1-4):25–36.

Moore, R. D., D. L. Spittlehouse, and A. Story, 2005. Riparian microclimate and stream temperature response to forest harvesting: A review. *Journal of the American Water Resources Association*, 41(4):813–834.

Mosner, M. M., 2002. Stream-Aquifer Relations and the Potentiometric Surface of the Upper Floridan Aquifer in the Lower Apalachicola-Chattahoochee-Flint River Basin in parts of Georgia, Florida, and Alabama, 1999-2000. Water-Resources Investigations Report 02-4244, U.S. Geological Survey, 51 pp. Web: http://ga.water.usgs.gov/pubs/wrir/wrir02-4244/.

Park, S. S. and P. R. Jaffe, 1999. A numerical model to estimate sediment oxygen levels and demand. *Journal of Environmental Quality*, 28(4):1219–1226.

Parkhill, K. L. and J. S. Gulliver, 1999. Modeling the effect of light on whole-stream respiration. *Ecological Modelling*, 117(2-3):333–342.

Parr, L. B., R. G. Perkins, and C. F. Mason, 2002. Reduction in photosynthetic efficiency of *Cladophora glomerata*, induced by overlying canopies of *Lemna spp*. *Water Research*, 36(7):1735–1742.

Pearson, N. and N. O. Crossland, 1996. Measurement of community photosynthesis and respiration in outdoor artificial streams. *Chemosphere*, 32(5):913–919.

Penrod, E. B. and K. V. Prasanna, 1962. Design of a flat-plate collector for a solar earth heat pump. *Solar Energy*, 6(1):9–22.

Power, G., R. Brown, and J. Imhof, 1999. Groundwater and fish - Insights from northern North America. *Hydrological Processes*, 13(3):401–422.

Richter, B. D., D. P. Braun, M. A. Mendelson, and L. L. Master, 1997. Threats to imperiled freshwater fauna. *Conservation Biology*, 11(5):1081–1093.

Runkel, R. L., 1998. One-dimensional transport with inflow and storage (OTIS): a solute transport model for streams and rivers. Water-Resources Investigations Report 98-4018, U.S. Geological Survey, Denver, Colorado, 80 pp. Web: http://co.water.usgs.gov/otis/documentation/primary/wrir98-4018.pdf.

Rutherford, J. C., S. Blackett, C. Blackett, L. Saito, and R. J. Davies-Colley, 1997. Predicting the effects of shade on water temperature in small streams. *New Zealand Journal of Marine and Freshwater Research*, 31:707–721.

Sabo, M. J., C. F. Bryan, W. E. Kelso, and D. A. Rutherford, 1999. Hydrology and aquatic habitat characteristics of a riverine swamp: I. Influence of flow on water temperature and chemistry. *Regulated Rivers: Research and Management*, 15(6):505–523.

Saltelli, A., 2004. *Sensitivity analysis in practice : a guide to assessing scientific models*. Wiley, Hoboken, NJ.

Schreier, H., W. Erlebach, and L. Albright, 1980. Variations in water quality during winter in two Yukon rivers with emphasis on dissolved oxygen concentration. *Water Research*, 14(9):1345–1351.

Sinokrot, B. A. and J. S. Gulliver, 2000. In-stream flow impact on river water temperatures. *Journal of Hydraulic Research*, 38(5):339–349.

Sinokrot, B. A. and H. Stefan, 1993. Stream temperature dynamics: Measurements and modeling. *Water Resources Research*, 29(7):2299–2312.

Skidmore, R. E., S. C. Maberly, and B. A. Whitton, 1998. Patterns of spatial and temporal variation in phytoplankton chlorophyll a in the River Trent and its tributaries. *The Science of The Total Environment*, 210-211:357–365.

Sridhar, V., A. L. Sansone, J. LaMarche, T. Dubin, and D. P. Lettenmaier, 2004. Prediction of stream temperature in forested watersheds. *Journal of the American Water Resources Association*, 40(1):197–213.

Stefan, H. G. and X. Fang, 1994. Dissolved oxygen model for regional lake analysis. *Ecological Modelling*, 71(1-3):37–68.

Sturm, T. W., 2001. *Open Channel Hydraulics*. McGraw-Hill, Boston, 493 pp.

Supriyasilp, T., A. J. Graettinger, and S. R. Durrans, 2003. Quantitatively directed sampling for main channel and hyporheic zone water-quality modeling. *Advances in Water Resources*, 26(9):1029–1037.

Tang, R. and Y. Etzion, 2004. Comparative studies on the water evaporation rate from a wetted surface and that from a free water surface. *Building and Environment*, 39(1):77–86.

Tang, R., Y. Etzion, and I. A. Meir, 2004. Estimates of clear night sky emissivity in the Negev Highlands, Israel. *Energy Conversion and Management*, 45(11-12):1831–1843.

Taniguchi, M., J. Shimada, T. Tanaka, I. Kayane, Y. Sakura, Y. Shimano, S. Dapaah-Siakwan, and S. Kawashima, 1999a. Disturbances of temperature-depth profiles due to surface climate change and subsurface water flow: 1. An effect of linear increase in surface temperature caused by global warming and urbanization in the Tokyo metropolitan area, Japan. *Water Resources Research*, 35(5):1507–1517.

Taniguchi, M., D. R. Williamson, and A. J. Peck, 1999b. Disturbances of temperature-depth profiles due to surface climate change and subsurface water flow: 2. An effect of step increase in surface temperature caused by forest clearing in southwest Western Australia. *Water Resources Research*, 35(5):1519–1529.

Torak, L. J., G. S. Davis, G. Strain, and J. Herndon, 1996. Geohydrology and evaluation of stream-aquifer relations in the Apalachicola-Chattahoochee-Flint River Basin, southeastern Alabama, northwestern Florida, and southwestern Georgia. Water-Supply Paper 2460, U.S. Geological Survey, 95 pp. Web: `http://ga.water.usgs.gov/publications/abstracts/wsp2460.html`.

TVA, 1972. Heat and mass transfer between a water surface and the atmosphere. Water Resources Laboratory Report 14, Norris, Tennessee Valley Authority.

USGS, 2000. Droughts in Georgia. Technical report. Web: `http://ga.water.usgs.gov/publications/ofr00-380.pdf`.

Van Orden, G. N. and C. G. Uchrin, 1993. The study of dissolved oxygen dynamics in the Whippany river, New Jersey using the QUAL2E model. *Ecological Modelling*, 70(1-2):1–17.

Wang, H., M. Hondzo, C. Xu, V. Poole, and A. Spacie, 2003. Dissolved oxygen dynamics of streams draining an urbanized and an agricultural catchment. *Ecological Modelling*, 160(1-2):145–161.

Warner, D., J. A. Easoz, and S. Priest, 2002. Ground-Water-Quality Data for Albany and Surrounding Areas, Southwest Georgia, 1951-99. U.S. Geological Survey Open-File Report 02-124, in cooperation with Albany Water, Gas, and Light Commission, Atalanta, GA, 11 pp. Web: `http://ga.water.usgs.gov/publications/ofr02-124/ofr02-124.pdf`.

Warner, D. and S. J. Lawrence, 2005. Ground-Water Flow and Water Quality in the Upper-Floridan Aquifer, Southwestern Albany Area, Georgia, 1998 - 2001. Scientific Investigations Report 2005-5047, U.S. Department of the Interior, U.S. Geological Survey, 77 pp. Web: `http://pubs.usgs.gov/sir/2005/5047/`.

Williams, R. J., C. White, M. L. Harrow, and C. Neal, 2000. Temporal and small-scale spatial variations of dissolved oxygen in the Rivers Thames, Pang and Kennet, UK. *The Science of The Total Environment*, 251-252:497–510.

Zeng, W., 2000. *A Model For Understanding And Managing The Impacts Of Sediment Behavior On River Water Quality*. PhD thesis, University of GA, Athens, GA, 244 pp. Web: `http://getd.galib.uga.edu/public/zeng_wei_200012_phd/zeng_wei_200012_phd.pdf`.

Zeng, X., 2001. *Water Quality Modeling in Southeastern Lake Management: A Case Study of Lake Lanier, Georgia*. PhD thesis, University of GA, Athens, GA, 345 pp. Web: `http://getd.galib.uga.edu/hold5yr/zeng_xiao-qing_200112_phd/zeng_xiao-qing_200112_phd.pdf`.

Zeng, X., T. C. Rasmussen, M. B. Beck, A. K. Parker, and Z. Lin, 2005. A biogeochemical model for metabolism and nutrient cycling in a Southeastern Piedmont impoundment. *Environmental Modelling and Software*, In Press.

Zheng, L., C. Chen, and F. Y. Zhang, 2004. Development of water quality model in the Satilla River Estuary, Georgia. *Ecological Modelling*, 178(3-4):457–482.

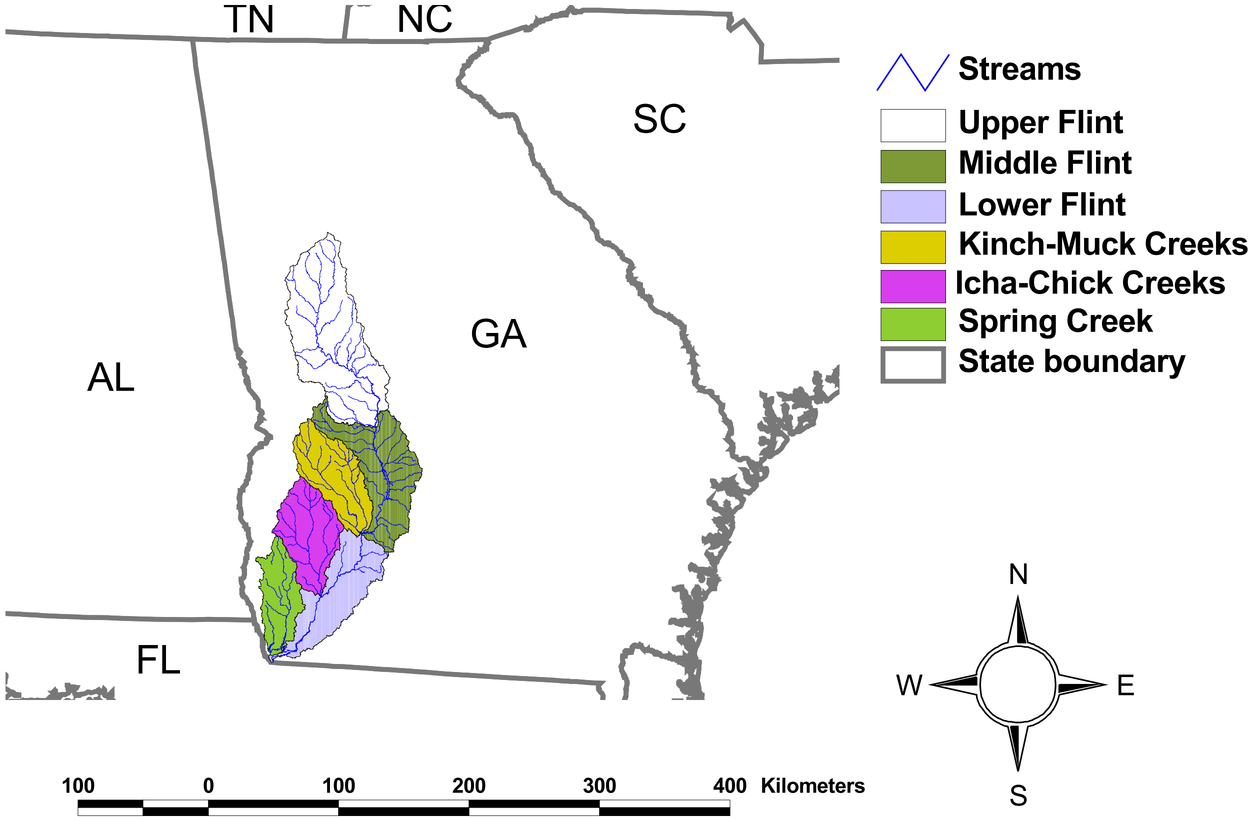

Figure 4.1: The Lower Flint River Basin consists of three watersheds: Kinch-Muck Creeks watershed, Icha-Chick Creeks watershed, and Spring Creek watershed. The Dougherty plain is located predominately within Icha-Chick Creeks watershed

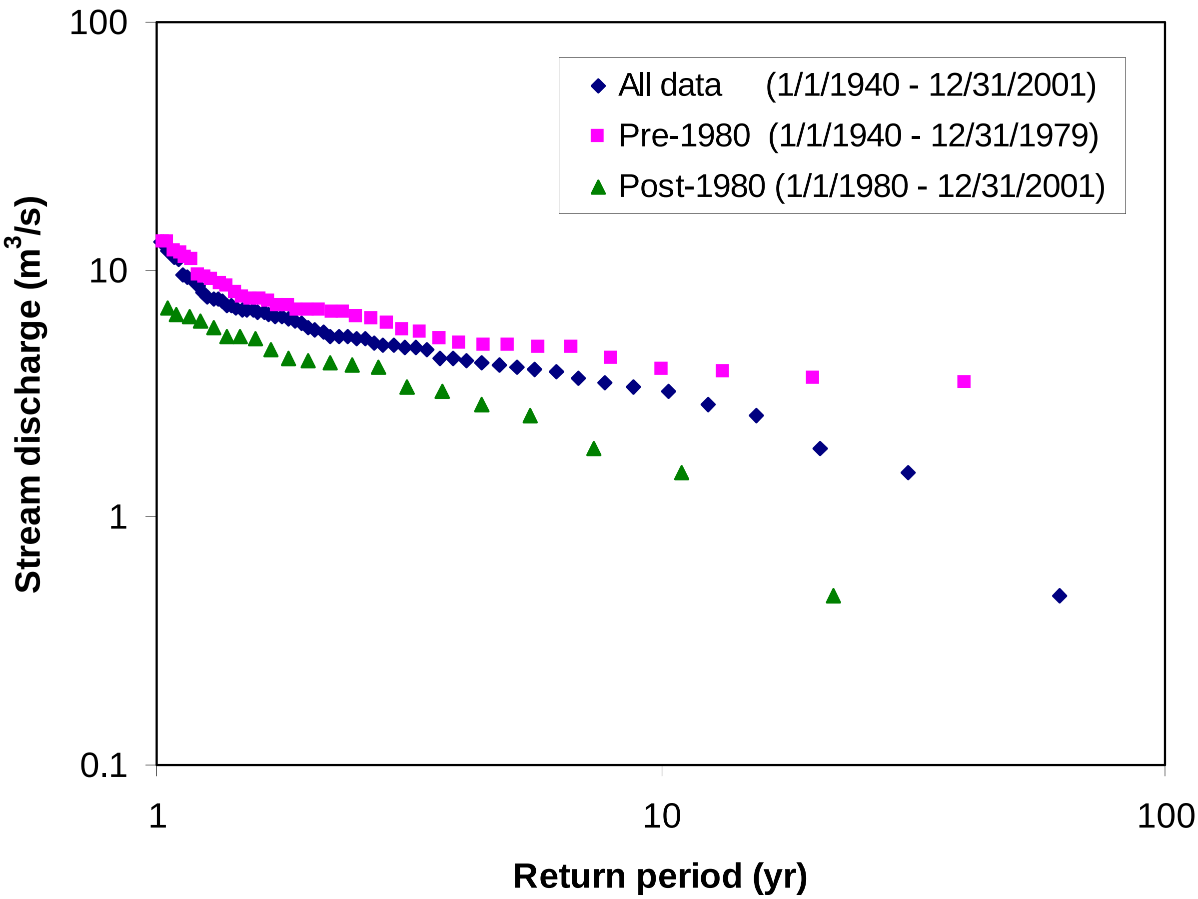

Figure 4.2: Stream seven day low flow vs. return period for Ichawaynochaway Creek near Milford. Data from USGS 01/01/1940 - 12/31/2001. Major fish and mussel kills occurred in August 2000 due to severe drought conditions. Since 1980, low streamflow events occurred more frequently, possibly due to agricultural irrigation pumping.

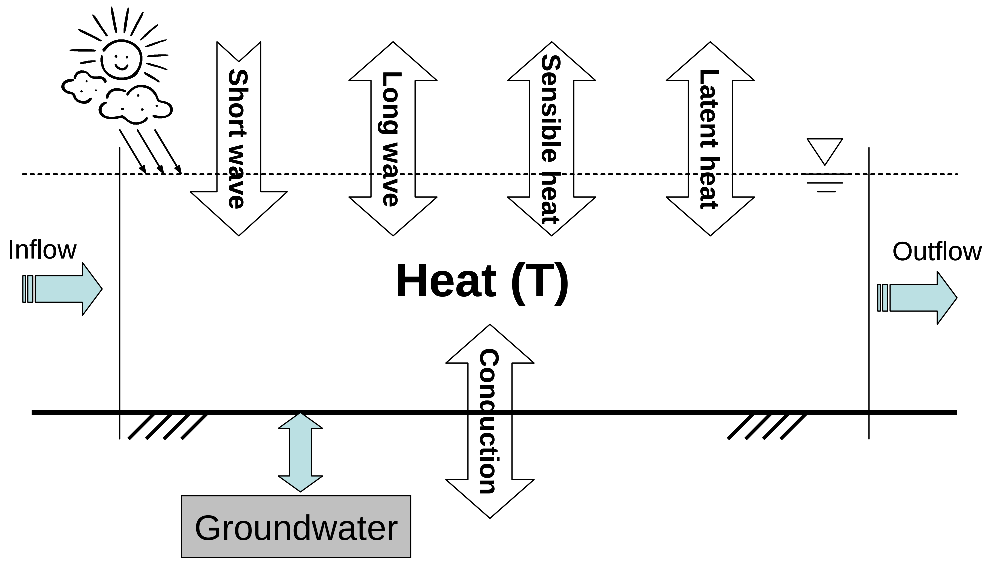

(a) Temperature

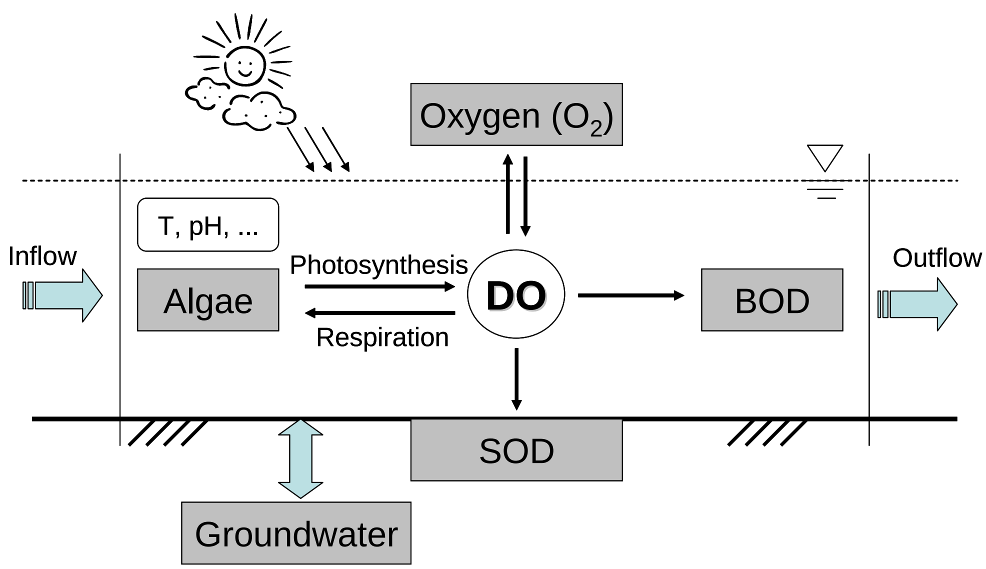

(b) Dissolved oxygen

Figure 4.3: Schematic of stream temperature and DO dynamic systems. Stream temperature dynamics is dominated by streamflow advection, groundwater discharge advection, solar radiation, long wave radiation, convection, evaporation, and streambed conduction; Stream DO dynamics is dominated by the same advection terms plus atmosphere reaeration, algal photosynthesis and respiration, BOD decay, and SOD decay.

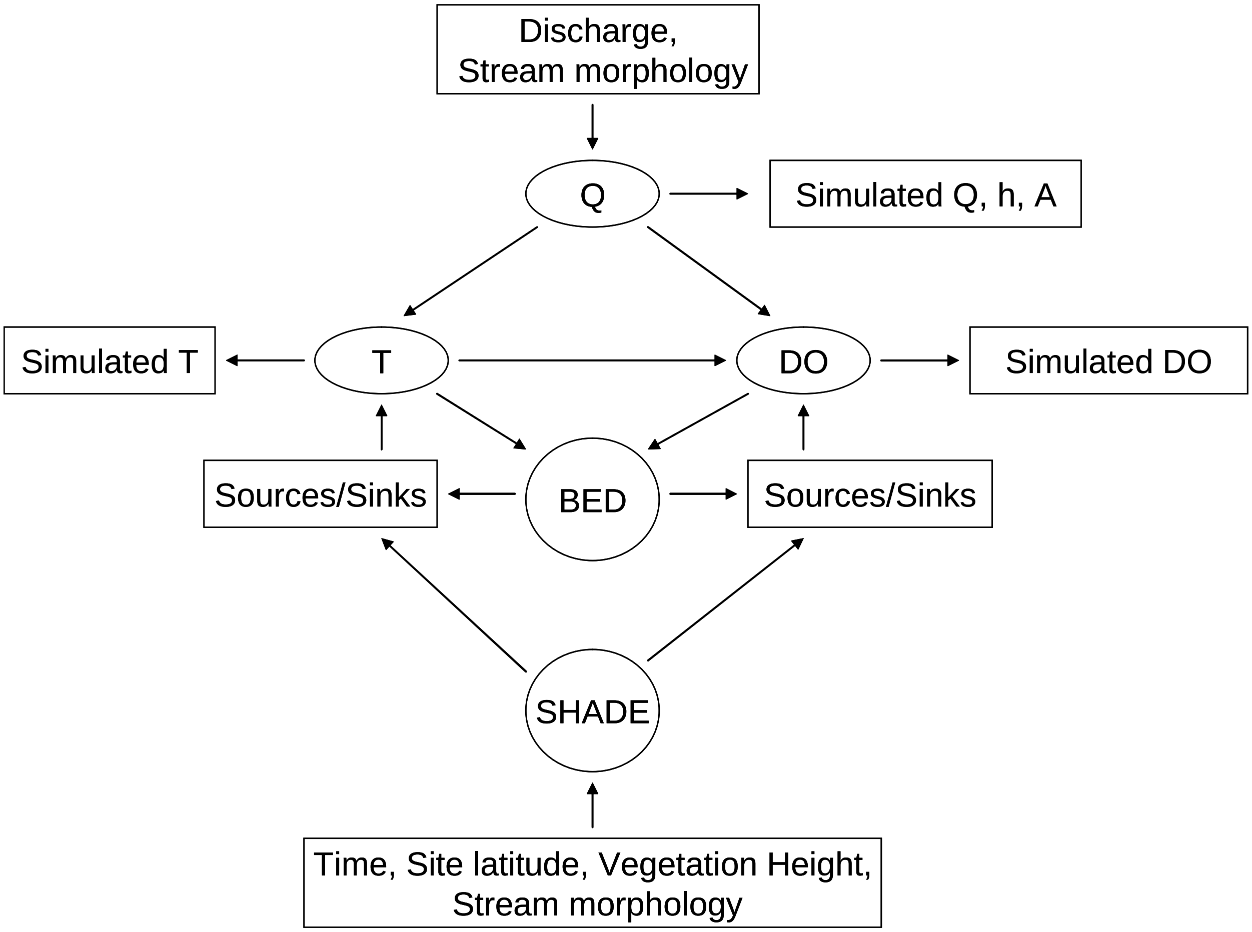

Figure 4.4: The modeling system of DDOT, where Q is flow module, T is temperature module, DO is dissolved oxygen module, BED is is BED submodule, SHADE is SHADE submodule, h is water depth, A is stream cross section area.

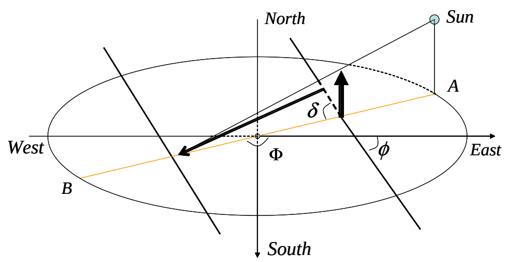

(a) $\phi < \frac{\pi}{2}$ and $\frac{\pi}{2} < \Phi < \pi \Longrightarrow \delta = \pi - (\Phi - \phi)$

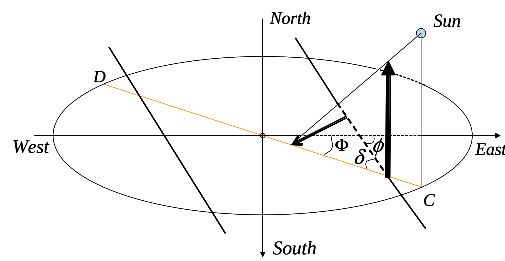

(b) $\phi < \frac{\pi}{2}$ and $\Phi < \frac{\pi}{2} \Longrightarrow \delta = \phi - \Phi$

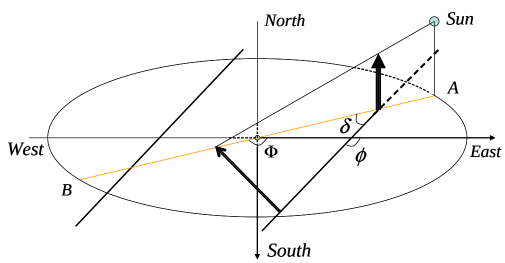

(c) $\frac{\pi}{2} < \phi < \pi$ and $\frac{\pi}{2} < \Phi < \pi \Longrightarrow \delta = \Phi - \phi$

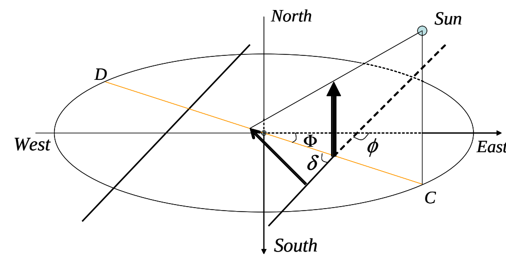

(d) $\frac{\pi}{2} < \phi < \pi$ and $\Phi < \frac{\pi}{2} \Longrightarrow \delta = \pi - (\phi - \Phi)$

Figure 4.5: Illustration of riparian vegetation shading over stream surface at different hours of day in summer at a location with latitude higher than solar declination. The two parallel thick lines denote stream banks. The thicker vertical arrow represents riparian trees, and the thinner horizontal arrow represents effective shade length on the stream surface. If solar location changes from A to B, or from C to D, the angle relationships will be exactly the same as before being changed. For latitude lower than solar declination, the angle relationships would be the same as that shown in (a) and (c).

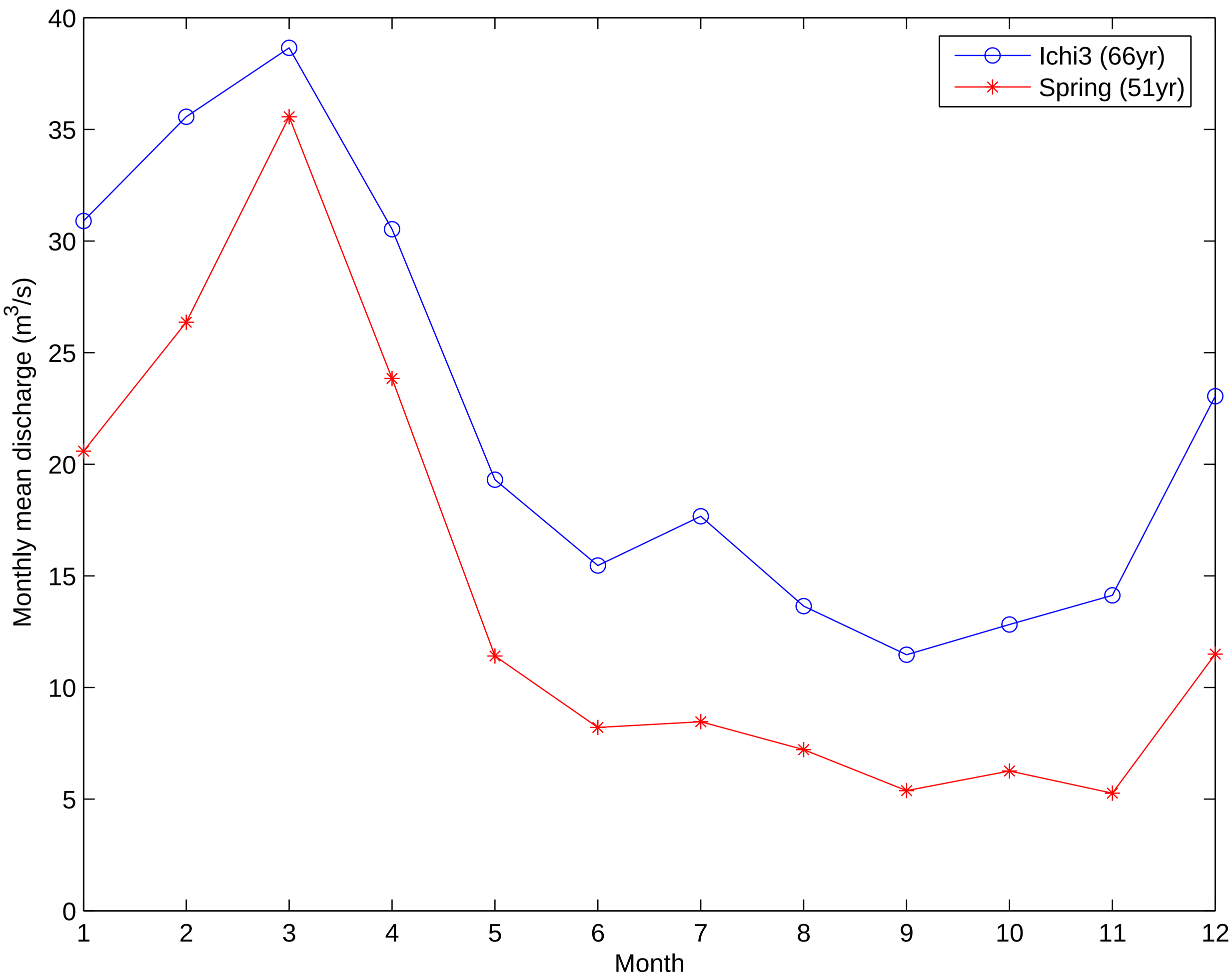

Figure 4.6: Monthly mean stream discharge distribution. Ichi3 is the location of the lower boundary of the selected reach. Spring is another site on Spring Creek in the study area adjacent to Ichaway Creek.

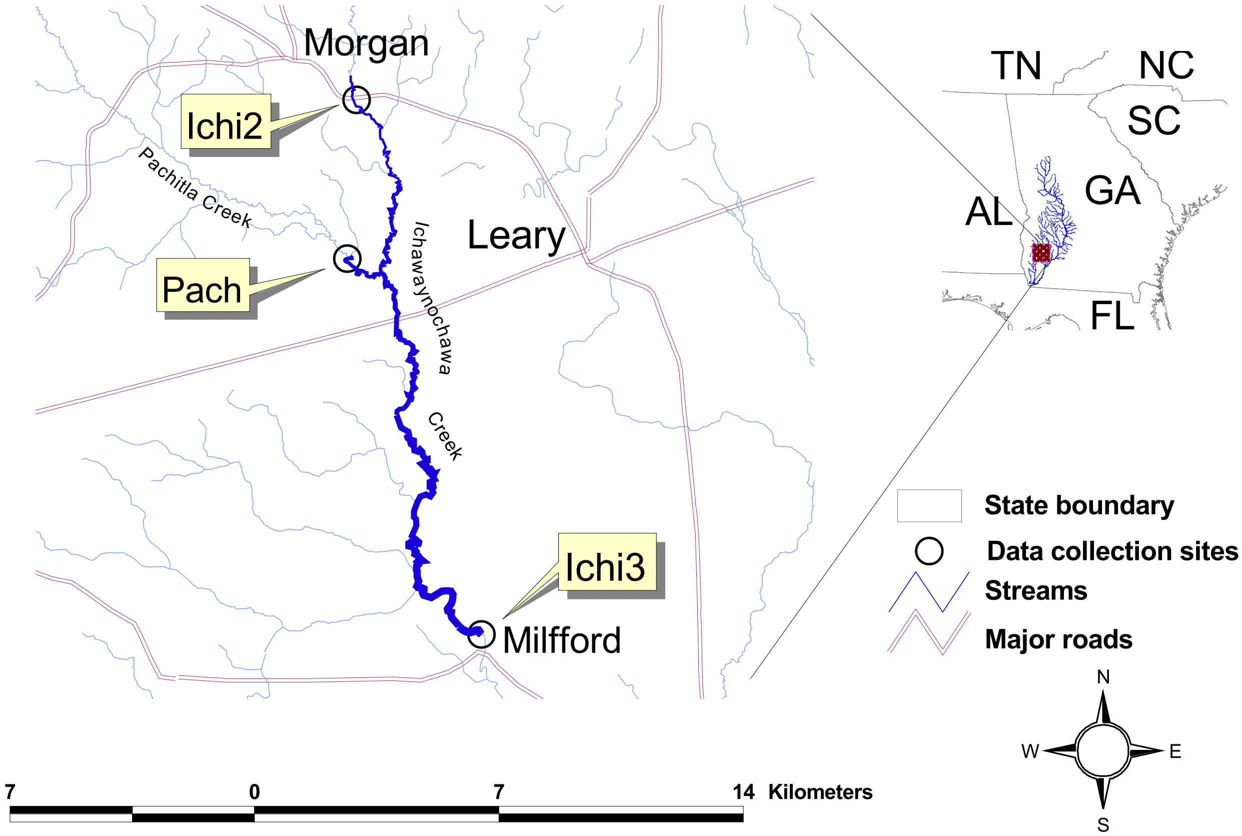

Figure 4.7: Water quality data collection sites. Stream flows southward. Ichi2 is the upper boundary; Ichi3 is the lower boundary; and Pach is a tributary to the main reach. The top right state map indicates the entire Flint River and the study site location in the Lower Flint River Basin.

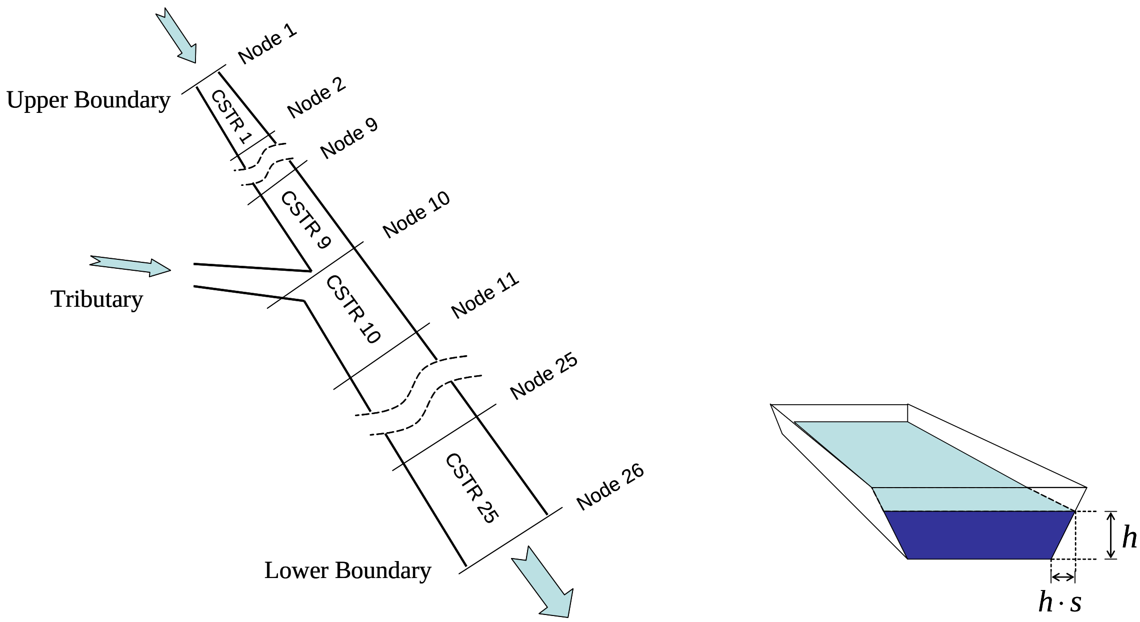

(a) Stream segmentation

(b) Trapezoidal cross section

Figure 4.8: Schematic of stream segmentation. Stream reach are evenly segmented into 25 CSTRs with 26 nodes.

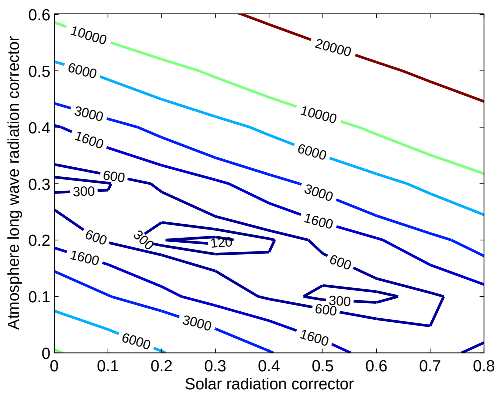

(a)

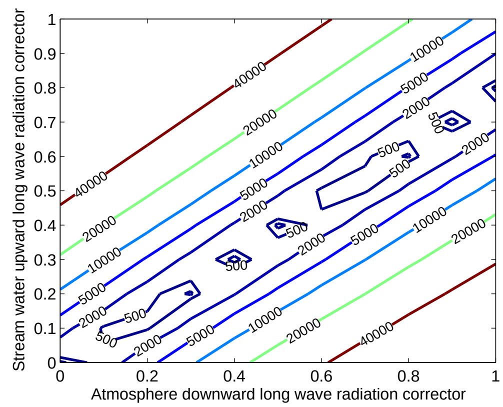

(b)

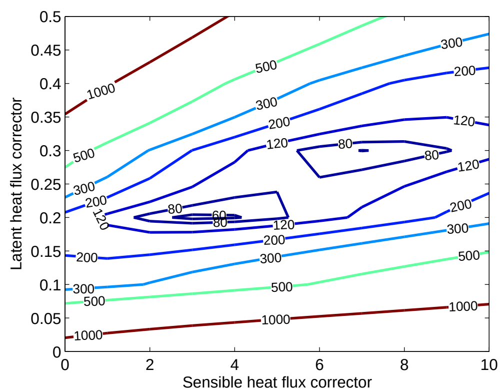

(c)

Figure 4.9: Model Sum of Square Errors (SSE) by ADRE based model formulation under selected parameter combination scenarios. Figure (a) indicates the smallest SSE obtained at parameter values around 0.3 for short wave radiation correction and around 0.2 for atmosphere long wave radiation correction. Figure (b) indicates multiple acceptable parameter sets. However, from Figure (a), parameter value for atmosphere long wave radiation was around 0.2. So if the results in Figure (a) were taken, then parameter value for stream water backward radiation should be around 0.1. Figure (c) indicated two parameter regions that might both fit the model. Since the bottom left region was expected to contain a smaller SSE, this region was chosen, which provided parameter values around 4 for sensible heat flux correction and around 0.2 for latent heat flux correction.

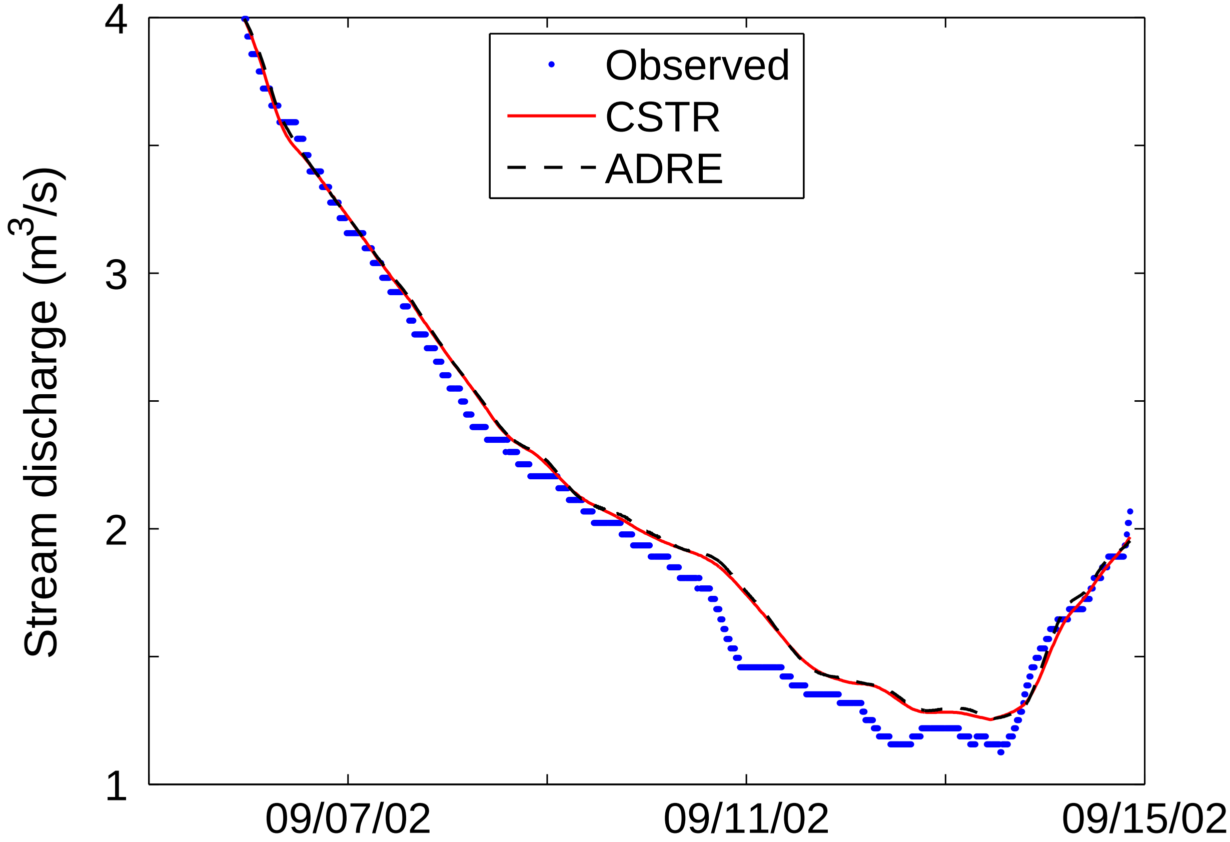

Figure 4.10: Flow module calibration results of both Continuously Stirred Tank Reactor (CSTR) and Advection-Dispersion-Reaction Equation (ADRE) based formulations

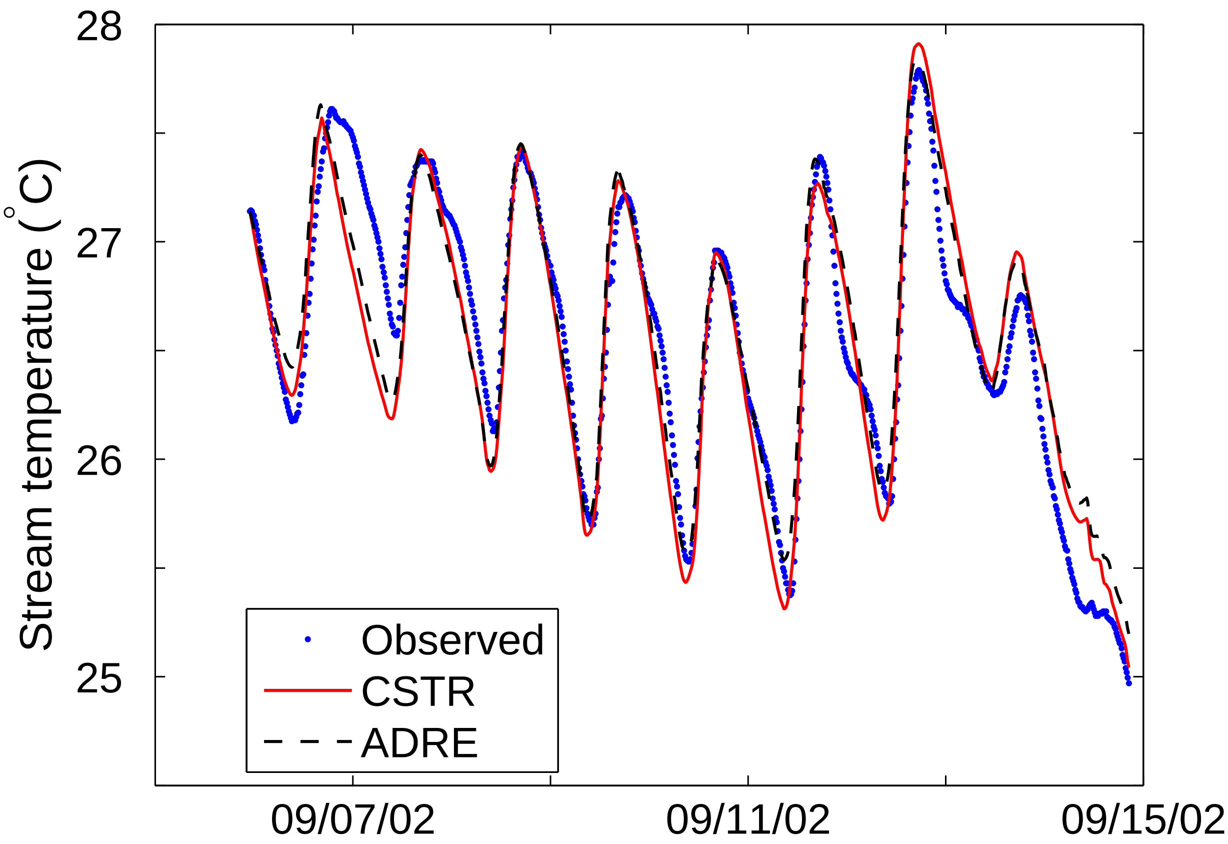

Figure 4.11: Temperature module calibration results of both Continuously Stirred Tank Reactor (CSTR) and Advection-Dispersion-Reaction Equation (ADRE) based formulations

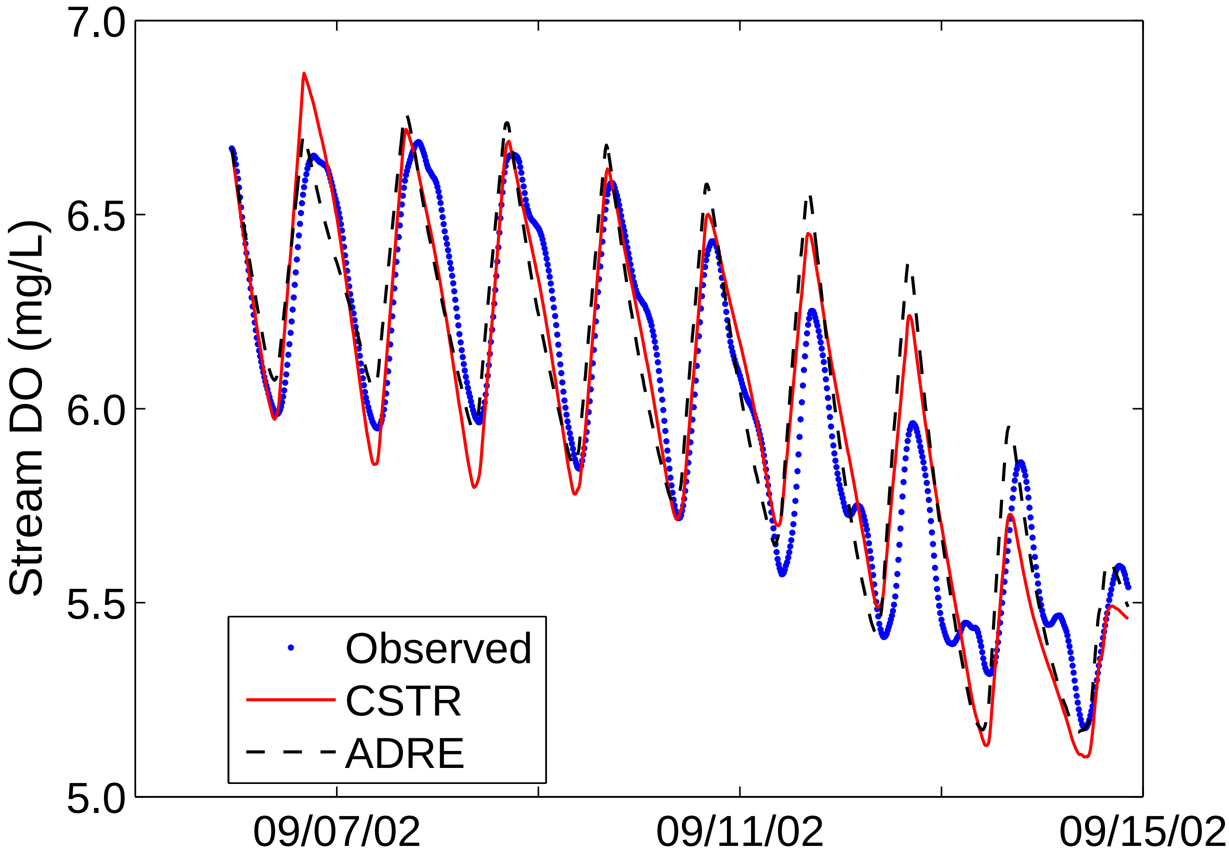

Figure 4.12: Dissolved oxygen module calibration results of both Continuously Stirred Tank Reactor (CSTR) and Advection-Dispersion-Reaction Equation (ADRE) based formulations

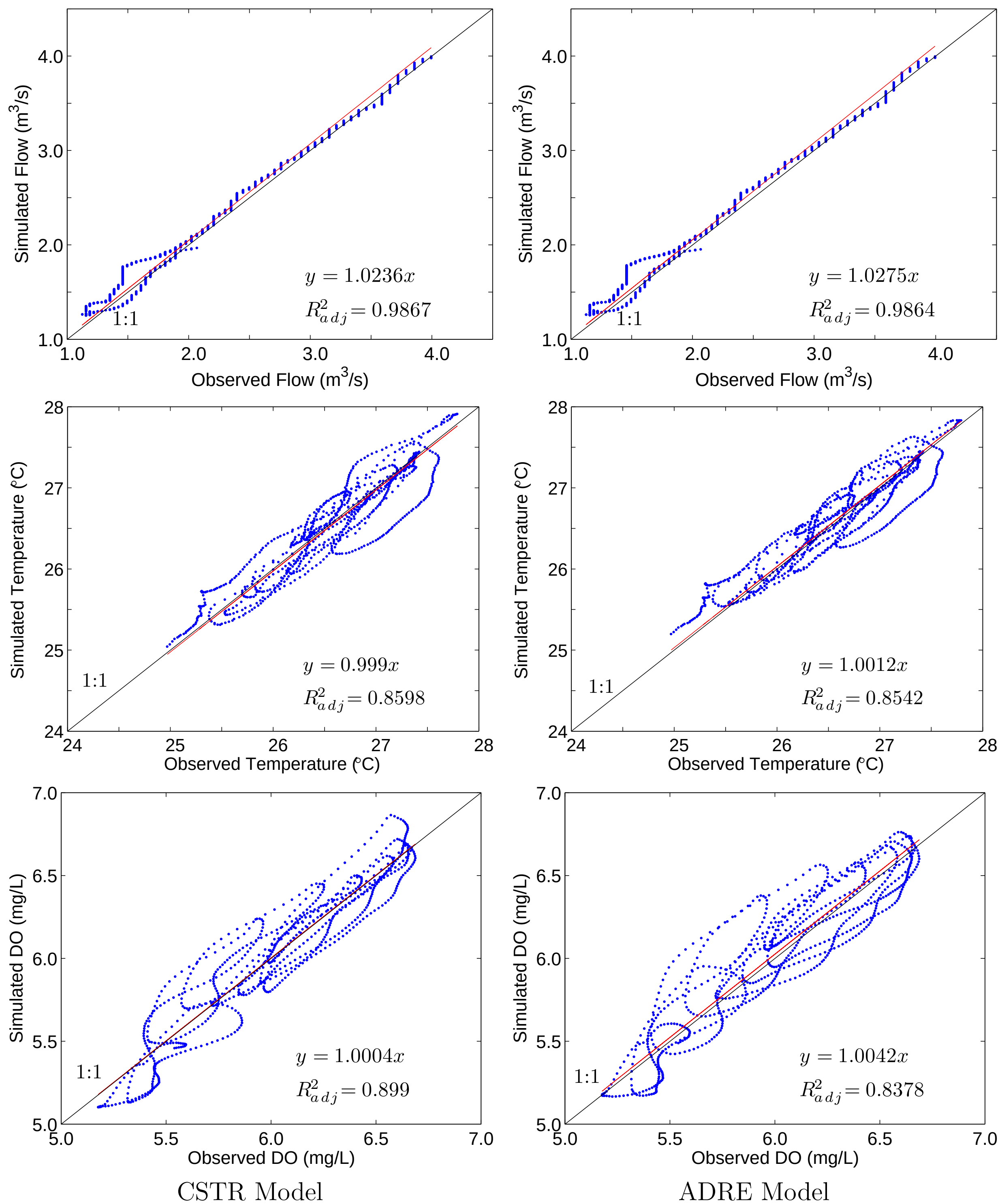

Figure 4.13: Calibration: Scatter plots of simulated vs. observed data. The left column is by CSTR based formulations, and the right column is by ADRE based formulations. The intercept of the regression equation is set to zero.

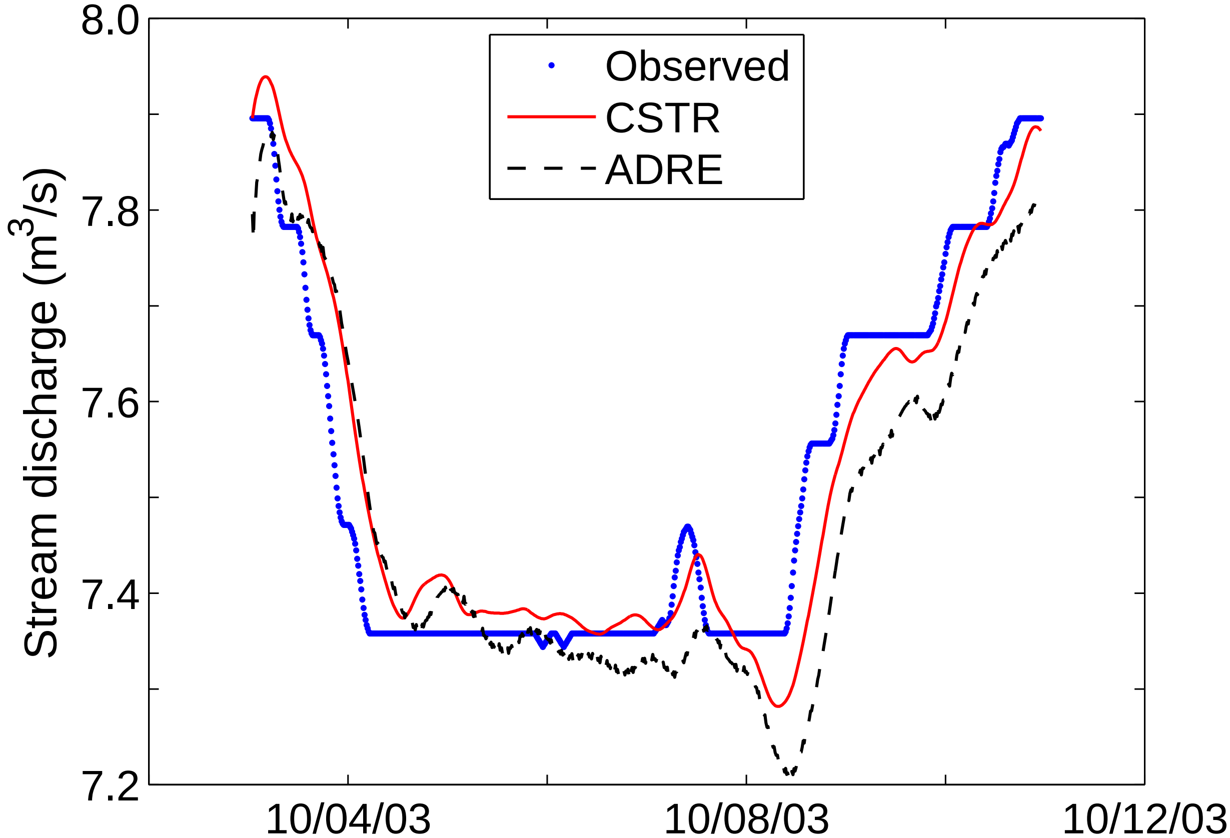

Figure 4.14: Flow module evaluation results of both Continuously Stirred Tank Reactor (CSTR) and Advection-Dispersion-Reaction Equation (ADRE) based formulations

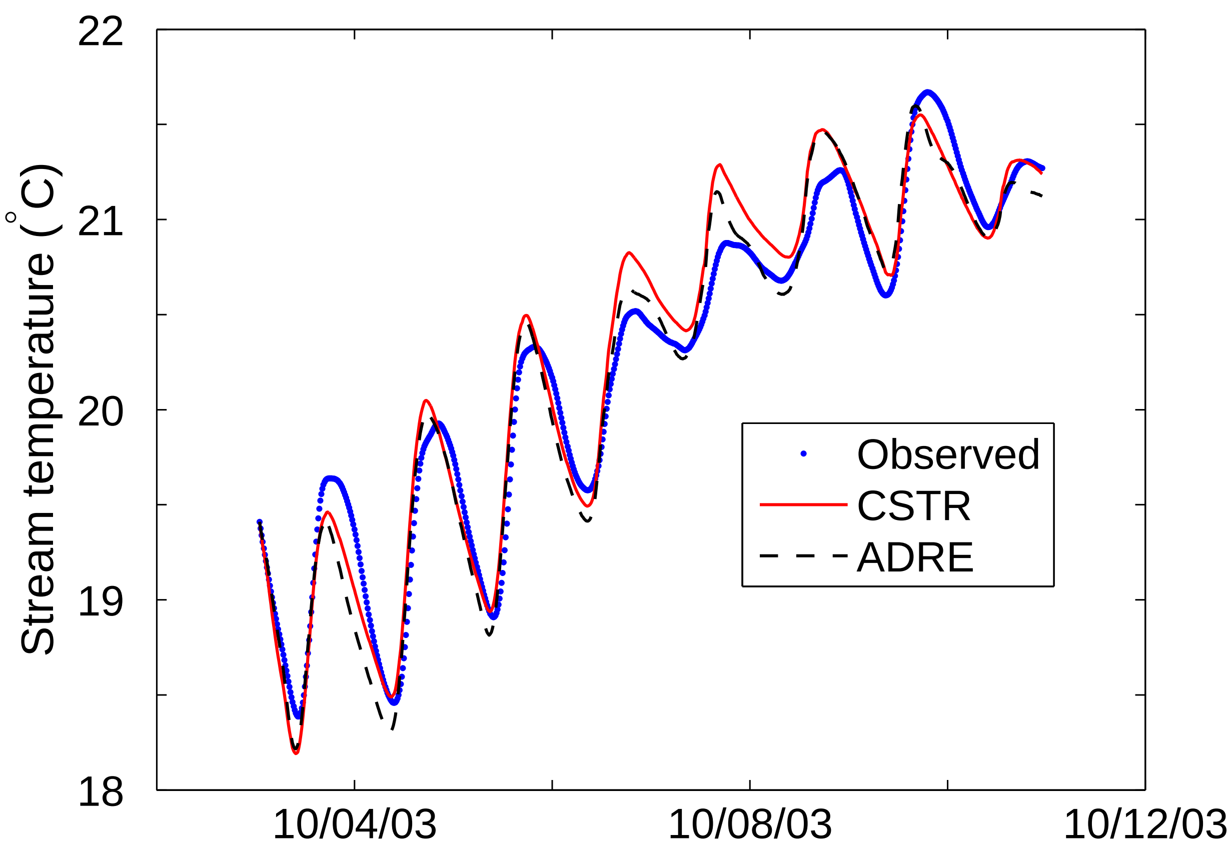

Figure 4.15: Temperature module evaluation results of both Continuously Stirred Tank Reactor (CSTR) and Advection-Dispersion-Reaction Equation (ADRE) based formulations

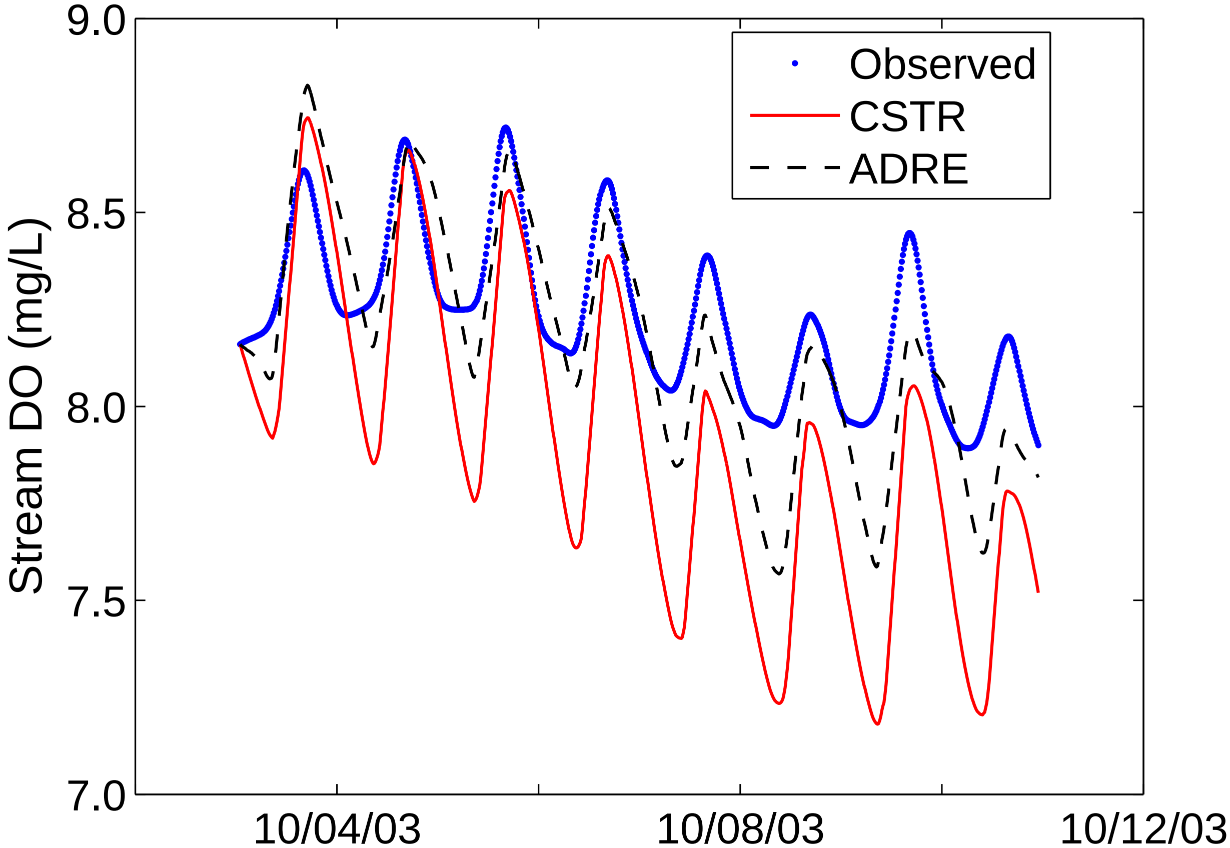

Figure 4.16: Dissolved oxgyen module evaluation results of both Continuously Stirred Tank Reactor (CSTR) and Advection-Dispersion-Reaction Equation (ADRE) based formulations

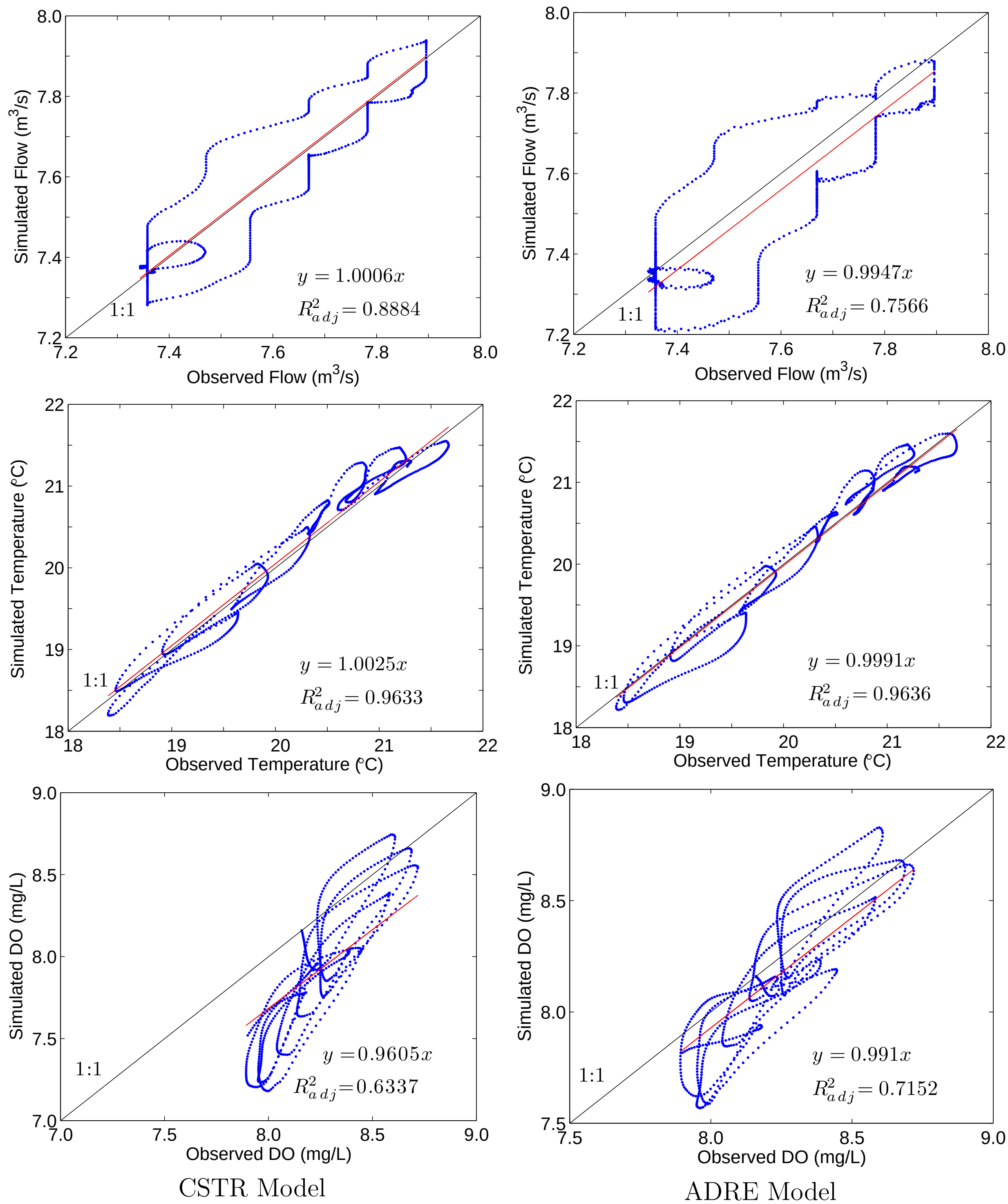

Figure 4.17: Evaluation: Scatter plots of simulated vs. observed data. The left column is by CSTR based formulations, and the right column is by ADRE based formulations. The intercept of the regression equation is set to zero.

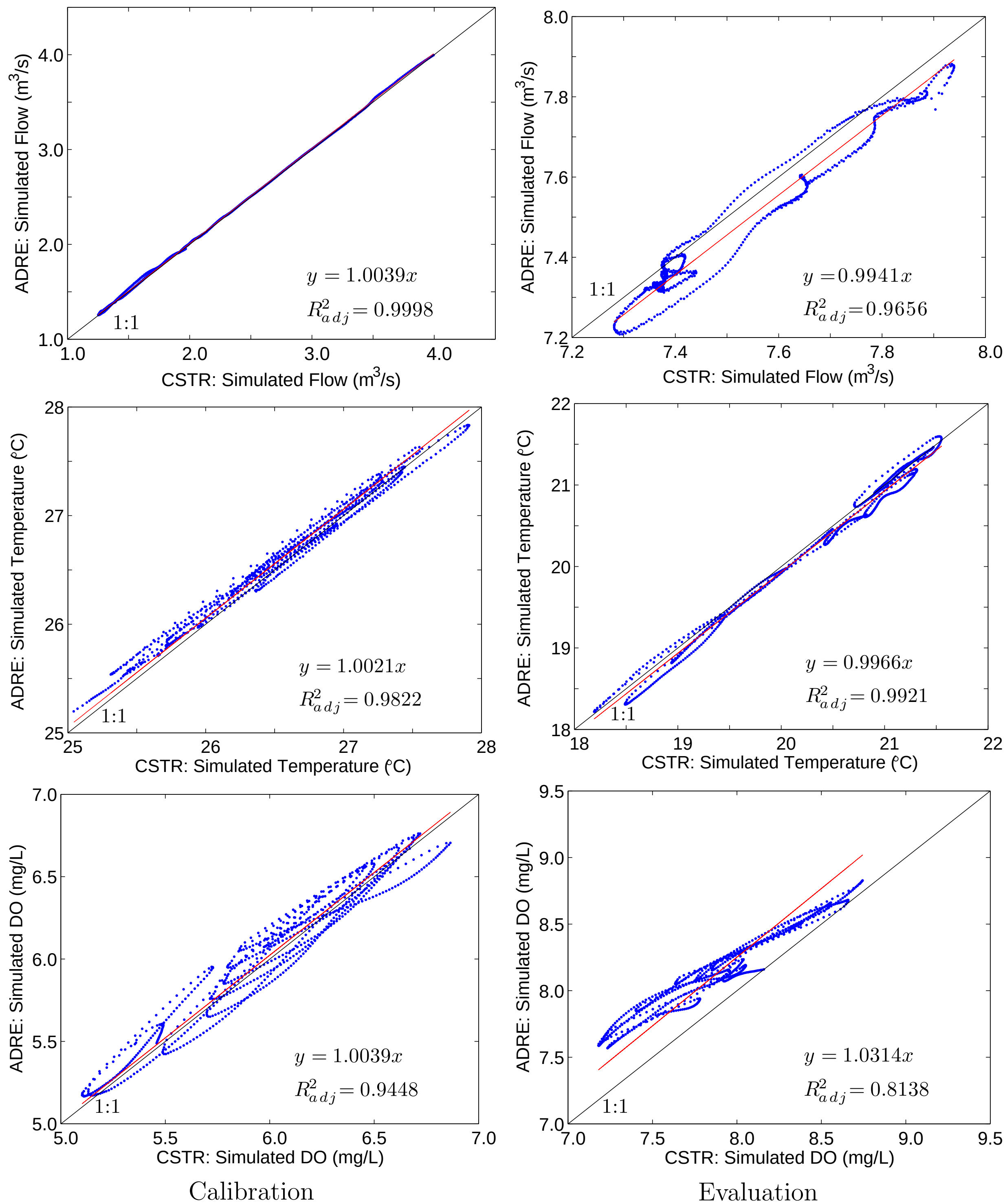

Figure 4.18: Algorithm comparison: Scatter plots of simulations between CSTR based formulation and ADRE based formulation. The left column is for the calibration period, and the right column is for the evaluation period.

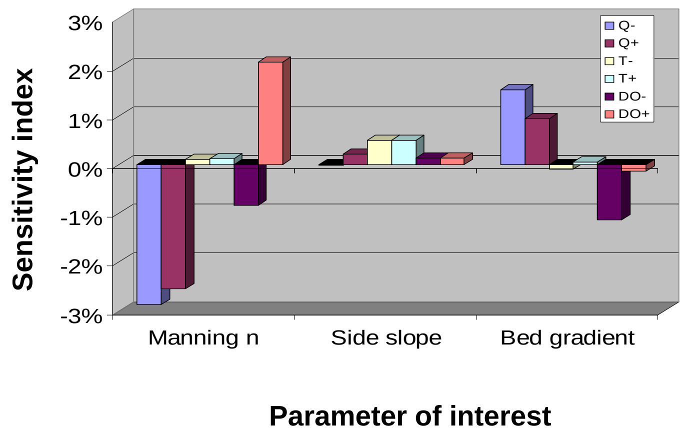

(a) Model sensitivity to flow module

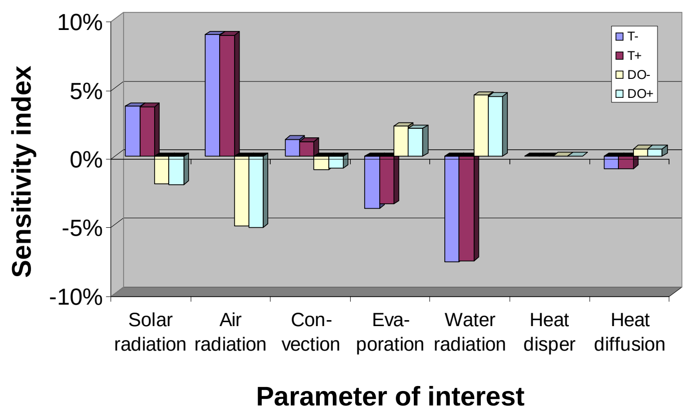

(b) Model sensitivity to temperature module

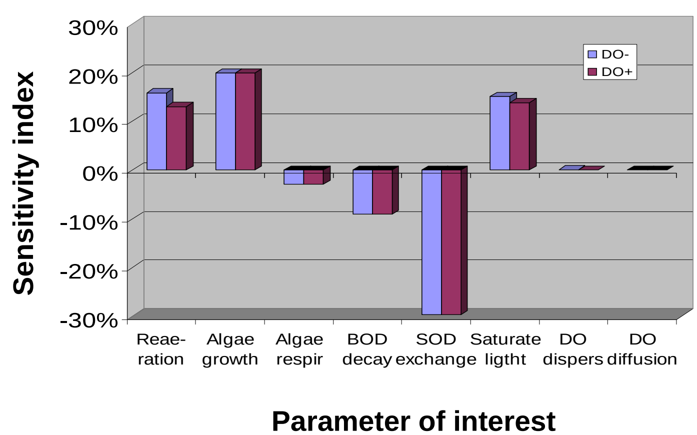

(c) Model sensitivity to DO module

Figure 4.19: Model sensitivity analysis

Table 4.1: Stream water quality statistics summary

Stream	**Time period**	**Max_Q** (m^3/s)	**Min_Q** (m^3/s)	**Max_T** (°C)	**Mean_T** (°C)	**Min_DO** (mg/L)	**Mean_DO** (mg/L)
Ichi1	06/30/02 - 07/12/02			26.54	24.44		
Ichi1	08/05/02 - 08/15/02			26.29	23.35	5.24	6.11
Ichi1	09/05/02 - 09/19/02			25.22	23.52	6.40	7.00
Ichi2	09/05/02 - 09/19/02	10.75	0.79	27.18	25.55	6.3	6.58
Ichi3	09/05/02 - 09/19/02	31.35	1.13	27.79	26.01	6.66	7.25
Ichi3	07/03/03 - 07/22/03	34.26	7.67	27.32	25.60	6.09	6.88
Ichi2	10/02/03 - 10/16/03	5.24	3.57	22.23	20.48	7.11	7.78
Ichi3	10/02/03 - 10/16/03	10.68	7.25	22.19	20.52	7.44	8.06
Ichi4	10/02/03 - 10/16/03			22.15	20.74	6.03	7.16
Ichi2	06/30/04 - 07/27/04	14.53	1.53	27.91	25.57	5.54	5.99
Ichi3	06/30/04 - 07/27/04	16.65	1.50	28.27	26.27	5.17	5.95
Ichi4	06/30/04 - 07/27/04	31.15	1.93	28.16	26.16	4.26	5.46
Spring2	06/30/02 - 07/12/02	2.95*	0.48*	28.27	26.18	4.67	6.64
Spring2	08/05/02 - 08/15/02			26.80	25.20	6.15	6.72
Spring1	06/10/04 - 06/29/04			26.56	24.53	4.69	5.36
Spring2	06/10/04 - 06/29/04			26.75	24.85	5.73	6.46
Spring3	06/10/04 - 06/29/04	18.29	5.81	27.08	25.09	4.87	5.79

Note: Q — flow rate; T — temperature, DO — dissolved oxygen. * means averaged daily flow. Blank means no data or data were apparently corrupted by instrument malfunction.

Table 4.2: Input parameters and values

Notation	Description	Upstream CSTR|ADRE	Downstream CSTR|ADRE	Unit	Source
Stream morphology					
L	Stream reach length	0	25200	m	M
W_{bed}	Streambed width	12	28	m	M
S_b	Stream bank slope	0.5			M
S_0	Streambed slope	0.058%			M
$canopy$	Canopy cover density	0.65			C
h_{tree}	Riparian tree height	20		m	M
h_{bank}	Bankful depth	2	3	m	M
β	Latitude	31.383	31.527	°	M
n in ADRE	Manning's n	0.068(0.068)	0.068(0.057)		C; (9)
a in CSTR	Coefficients in $U = aQ^b$	0.247(0.239)	0.188(0.199)		C
b in CSTR	Coefficients in $U = aQ^b$	0.460(0.431)	0.345(0.393)		C; (9)
L_{trib}	Tributary joint location	8611		m	M
$W_{bed_{trib}}$	Tributary bed width	8			M
φ	Trib angle with main reach	45		°	M
ϕ	River angle from east direction	90		°	M
Z_{bed}	streambed thickness	2		m	C
Groundwater charateristics					
q_{gc}	Groundwater flow correction	0.6(1)			C
T_g	Groundwater T	20.5		°C	(8)
C_g	Groundwater DO	5		mg L^{-1}	(8)
C_{p_g}	Streambed heat capacity	3350000		J m^{-3} °C	C; (1); (2); (3); (9)
λ_{bed}	Streambed thermal conductivity	2		W m^{-1} °C	C; (1); (2); (3); (9)
Numerical scheme parameters					
tol	Relative tolerance error in iteration	0.0001			A
θ	Weight coefficient in Preissmann scheme	0.6			A
Δx	CSTR size or node distance	1000		m	A
Δz	streambed vertical space interval	0.1		m	A
Δt	Time interval	900		s	A
D_T	Heat flux dispersion in stream	100		m^2 s^{-1}	C
D_{DO}	Mass flux dispersion in stream	100		m^2 s^{-1}	C
$D_{T_{bed}}$	Streambed thermal diffusivity	5.97015E-07		m^2 s^{-1}	C; (1); (2); (3)
$D_{DO_{bed}}$	Streambed DO diffusivity	1.19403E-07		m^2 s^{-1}	C; (1); (2); (3)
Engergy flux correctors					
$p(1)$	Solar radiation corrector	0.25|0.26			C
$p(2)$	Air long wave radiation corrector	0.34|0.21			C
$p(3)$	Water long wave radiation corrector	0.20|0.15			C
$p(4)$	Sensible heat flux corrector	0.98|4.79			C
$p(5)$	Latent heat flux corrector	0.21|0.23			C
Mass flux rates					
$p(6)$	Reaeration rate corrector	0.03			C
I_{growth}	"Saturation" light intensity for growth	211.26		W m^{-2}	C; (7); (10)
G_I	Alge growth rate at 20 °C	[5.98|4.83]E-05		m^2 J^{-1}	C; (7);(10)
R_a	Alge respiration rate at 20 °C	*3.76E-04		s^{-1}	C; (7);(10)
R_b	BOD decay rate at 20 °C	[2.31|9.84]E-07		s^{-1}	C; (7);(10)
R_s	SOD exchange rate at 20 °C	[8.65|3.48]E-03		mg O_2 m^{-2} s^{-1}	C;(7);(10);(11)
Arrhenius coefficient					
θ_k	Reaeration rate corrector	1.024			(7)
θ_p	Photosynthesis rate corrector	1.036			(4)
θ_r	Respriation rate corrector	1.045			(4)
θ_b	BOD decay rate corrector	1.047			(5)
θ_s	SOD decay rate corrector	1.065			(6);(7)
Unsimulated state variables					
$[Alg]$	Algae concentration	0.001		mg L^{-1}	M
$[BOD]$	BOD concentration	4.0		mg L^{-1}	M

Note: Blanks in downstream column possess the same values as in upstream column. Numbers in round brackets were for flow submodule evaluation. * indicated a very high coefficients due to very low algal concentration measurements. Parameters for segments in between the two boundaries were interpolated linearly before and after the tributary convergence. In the source column, if both C and reference numbers appear together, the calibrated value was within literature value ranges. Notations of sources: A – Assigned; C – Calibrated; M – Measured; (1) Becker *et al.*, 2004; (2) Chen *et al.*, 1998; (3) Crittenden, 1978; (4) Parkhill and Gulliver, 1999; (5) Knowles and Wakeford, 1978; (6) Cox, 2003; (7) Bowie *et al.*, 1985; (8) Warner and Lawrence, 2005; (9) McCuen, 1998;(10) Zeng *et al.*, 2005; (11) Higashino and Stefan, 2005; Van Orden and Uchrin, 1993; Zheng *et al.*, 2004; Stefan and Fang, 1994

Chapter 5

Application of Dynamic Dissolved Oxygen and Temperature Model to Ground and Surface Water Management Issues[1]

[1]Li, G. and C. Rhett Jackson. For submission to *Water Resources Research.*

Abstract

The tributaries of the Lower Flint River, southwest Georgia, are incised into the upper Floridan semi-confined limestone aquifer, and thus seepage of relatively old groundwater sustains baseflows and provides some control over temperature and dissolved oxygen fluctuations. This hydrologic and geologic setting creates aquatic habitat that is unique in the state of Georgia. Excessive agricultural irrigation pumpage from both streams and aquifers threatens to exacerbate low flow conditions during summer droughts, which may force stream temperature and dissolved oxygen to unacceptable levels. To evaluate the possible effects of human modifications to stream habitat, we developed the one-dimensional Dynamic Dissolved Oxygen and Temperature model (DDOT). Companion paper: Model Development provided a detailed description of model DDOT. In this paper, we analyzed the sensitivity of stream temperature and DO to upstream flow inputs, groundwater discharge, stream riparian vegetation shading, and stream width. It indicated that 1)reduced instream flow rate leads to increased stream temperature and decreases stream DO in summer, 2)reduced groundwater input exacerbates stream temperature problems,especially during drought seasons, 3) reduced groundwater input does not exacerbate stream DO problems due to the fact that ground water itself has a DO concentration as low as 5 mg/L, 4)problematic DO levels occur only at very low flows, and 5)stream width and riparian vegetation have strong effects on stream temperature and DO levels. The model was then run with long-term time series (1950 - 2003) streamflow data simulated by HSPF model and groundwater discharge data simulated by MODFE model under three different agricultural pumping scenarios for Ichawaynochaway Creek and Spring Creek watersheds in the Lower Flint River Basin. The simulation indicated that the spatial patterns of water quality dynamics in the two watersheds were associated with groundwater input, stream aspect, and stream width.

Keywords

Stream temperature, Dissolved oxygen, DDOT, Streamflow, Groundwater discharge, Agricultural pumping

5.1 Introduction

Stream temperature and dissolved oxygen are two critical factors that affect fish survival, movement and the growth (Beschta *et al.*, 1987; Coutant, 1987; Christie and Regier, 1988; Horne and Goldman, 1994; Karim *et al.*, 2003). High temperatures and low oxygen concentrations may also cause freshwater mussel mortality (Miller and Payne, 2004; Johnson *et al.*, 2001). These two water quality constituents vary seasonally and diurnally, driven primarily by fluctuation in solar radiation, but streamflow is also a controlling variable affecting the thermal and oxygen mass as well as the reaeration rate (Caruso, 2002; Gilvear *et al.*, 2002; Sabo *et al.*, 1999). Accordingly, the preservation of a certain amount of streamflow is critical to maintain temperature and dissolved oxygen levels suitable for native aquatic fauna.

In the state of Georgia, streamflow regulation is an important issues facing natural resource managers and planners. Increasing population, combined with increased water withdrawal for crop irrigation, has created conflicts in water resources management (Fanning, 1999). Increased water demand and use has been identified as one of the primary problems threatening stream fishes and other aquatic biota in the Southeastern United States (Richter *et al.*, 1997).

The Lower Flint River Basin (Figure 5.1), home to one of the state's most important agricultural areas, became a region of particular concern for resources managers, planners, and fishery scientists. Extremely low flow and severely degraded aquatic habitat problems have occurred during drought seasons. In summer 2000, extended drought and increased irrigation pumping brought record low flow to streams in the basin (Figure 5.2). New record low groundwater levels were recorded in more than 40 wells in the statewide ground-water monitoring network from January to August 2000, and many of these record-low levels were measured in the Lower Flint River Basin (USGS, 2000). Excessive groundwater withdrawal for center-pivot irrigation reduces groundwater discharge to streams (Hayes *et al.*, 1983; Torak *et al.*, 1996; Albertson and Torak, 2002), and may have exacerbated the drought's effect on stream water quality. These changes severely impacted stream aquatic habitat.

Unionid *Elliptio crassidens* were killed in Chickasawhatchee Creek, Baker County, GA in July 2000, mainly due to the low flow velocity (< 0.01 m/s) and dissolved oxygen (< 5 mg/L) (Johnson *et al.*, 2001). Major fish kills also occurred at the same time.

To evaluate effects of agricultural irrigation pumping effects from both streams and aquifers on streamflow rates in this area, the Environmental Protection Division (EPD) of Georgia simulated long-term (1950 - 2003) time series daily streamflows using the HSPF model for Ichawaynochaway Creek and Spring Creek watersheds. The simulations were performed under three management options, which were, respectively, 1) the Current irrigation scenario, which accounts for the approved permit applications received by EPD during the permit moratorium; 2) the Backlog irrigation scenario, which accounts for the option of approving all of the permit applications received by EPD; and 3) the 125Backlog irrigation scenario, which is the 1.25×Backlog Scenario. These long-term simulations provided stream discharges to evaluate how different water allocation strategies affect the occurrence of low dissolved oxygen and high temperature events.

To help assess the potential impacts of reduced streamflow and groundwater discharge on stream aquatic habitat, we developed the Dissolved Oxygen and Temperature Time Series model (DDOT). The model is intended to serve as a tool for fishery scientists and water resource managers by providing stream water temperature and dissolved oxygen time series data for any flow and climate scenario. In a previous paper (Li and Jackson, 2006), we presented the detailed model development and evaluation of DDOT. In this paper, we show the results of both the sensitivity analysis and a long-term simulation by model DDOT.

The sensitivity analysis was intended to analyze the sensitivity of stream temperature and DO as a response to the variation of upstream inflow rate, groundwater discharge, stream width, and riparian vegetation shading. Specifically, the following hypotheses were tested:

1. Decreased stream discharge leads to elevated stream temperature and degraded stream dissolved oxygen;

2. Ground water, with its relatively low temperature, has a strong cooling effect on streams in the summer;

3. Stream oxygen concentration increases as a response to decreased stream temperature by increased groundwater addition and/or upstream flow input;

4. Stream width, by affecting direct solar radiation, has positive correlations to stream temperature and dissolved oxygen; while

5. Riparian vegetative shading has negative correlations to stream temperature and dissolved oxygen.

The long-term simulation was intended to help identify stream reaches in Ichawaynochaway Creek and Spring Creek most susceptible to high temperature and low DO problems under the three GA EPD water use management options. Using DDOT, the hourly time series temperature and DO of the selected reaches were simulated for the time period from June 1^{st} to October 1^{st} of each year. The application results were also reported to fishery scientists for fish assemblage research.

5.2 Methods

5.2.1 Methods for sensitivity analysis

The sensitivity analysis was conducted using the same stream reach settings as for model calibration (Figure 5.3). Specifically, stream morphology and hydraulic characteristics, the weather conditions, the upper boundary and aquifer water qualities, and the simulation time period were kept unchanged from model calibration. We imposed different scenarios for the factors of interest, which include upstream inflow, groundwater discharge, stream width, and riparian vegetation height. We designed two experiments for the tests (summarized in Table 5.1). Experiment 1 was designed to test the effects of upstreamflow inputs and groundwater discharges, which were the focus of our research. Experiment 2 was designed to test the effects of stream width and riparian tree height for given upstreamflow input scenarios, due to their important roles in stream temperature and DO dynamics.

In Experiment 1, the twelve upstream input flow situations were based on flow metrics developed from USGS flow records at the lower boundary of the reach, with specific values shown in Table 5.2. The 13 groundwater discharge scenarios were based on the twelve flow metrics used for upstream inputs plus one zero groundwater discharge situation. Stream width and riparian vegetation height were the same as those used for calibration.

In Experiment 2, increments in stream width and riparian tree height were both set to two meters, which generated eleven scenarios for both of the two factors (Table 5.3). The sensitivity tests of water quality to riparian vegetation shading and stream width were considered together because the shading ratio is closely associated with stream width. Similarly, the sensitivity tests of these two factors were designed to combine with different instream flow scenarios, as the instream flow rate always plays a very important role. The instream flow scenarios were set to the same as shown from Table 5.2. In this experiment, the stream width was considered longitudinally constant, and the instream flow was considered to be from upstream flow inputs only. Groundwater discharge and tributary addition were neglected. In total there were 1452 combined testing scenarios.

The model was run with each of the proposed simulation scenarios. The maximum temperature and minimum DO were selected from the output time series of each model run. These results were then visualized using contour graphs to examine the sensitivity of stream temperature and DO to interested factors.

5.2.2 Methods for long-term simulation

Long-term (1950 - 2003) stream temperature and DO simulations were conducted for Ichawaynochaway Creek and Spring Creek watersheds, which were divided into sub-basins based on the 12 digits USGS Hydrologic Unit Code (USGS HUC12) with selected reaches being highlighted in blue (Figures 5.4 and 5.5). The stream morphology characteristics of these reaches were shown in Tables 5.4 and 5.5. The input long-term streamflow and groundwater discharge/recharge data for the simulation were generated by GA EPD using the HSPF model and the MODFE model for the three agricultural irrigation scenarios (Figures 5.6 and 5.7). The yearly maximum temperature and minimum DO data simulated by DDOT for each of the three flow scenarios were presented using Box-Whisker plots to show the water quality patterns.

We assumed that all calibrated parameters, such as photosynthesis rate, respiration rate, and etc, were unchanged over the whole simulation time period. For the upper boundary conditions, since we did not have the long-term water quality time series monitored at the boundary, we created an imaginary far away above the upper boundary, where the input temperature time series equalled the smoothed air temperature time series and the dissolved oxygen time series equalled 80% of the saturation oxygen time series based on the estimated water temperature time series. The imaginary long reach then allowed the flow to equilibrate to local climatic and hydraulic conditions. The simulated outputs from the imaginary long reach were used as the original upper boundary conditions.

The precipitation effect was not explicitly considered in model DDOT. Although precipitation did occur for long-term simulations, we assumed that the precipitation did not significantly affect the instream water quality since the generated runoff had become a part of instream flow by HSPF model before the water quality was simulated by our model.

5.3 Results

5.3.1 Results of sensitivity analysis

Sensitivity to upstream flow input and groundwater discharge

The sensitivity of stream temperature to streamflow scenarios is illustrated in Figure 5.8. Stream temperature is elevated (up to 28.5 °C) when both groundwater addition and upstream inflow rates fall to extremely low level (99.99% exceedance flow, or 0.311 m^3/s).

In this hydrologic environment, stream temperatures are far more sensitive to groundwater inputs than to upstream flow inputs. The sensitivity is nonlinear and increases greatly at lower flows and lower groundwater inputs, and the overall sensitivity of stream temperature to flows indicates interaction effects of groundwater discharge and upstream flow input scenarios.

With the addition of groundwater to the stream, the stream temperature decreases regardless upstream input flows. The groundwater cooling effect is most important during summer droughts when streamflow is low and stream temperature is high. For groundwater discharge rates within the range of 0 - 2.5 m^3/s, an increase of 1 m^3/s of groundwater discharge rate to the reach has the potential to decrease stream temperature about 1.6 °C if the upstream flow input rate is fixed to the 99.99% exceedance flow rate of the reach.

The effects of the upstream inflow on stream temperature is not as strong as that of groundwater discharge. However, it still shows a negative relationship between upstream input flow rate and stream temperature for the zero groundwater discharge scenario. In other words, decreased instream flow rates leads to elevated stream temperature, as stated in our first hypothesis. The upstream input flow effects become complex if groundwater is added. When groundwater flow discharges at a rate lower than the 99.5% exceedance instream flow rate (2.379 m^3/s), stream temperature decreases with the increase of upstream flow input. When groundwater discharges at the rate of 99.5% exceedance inflow, stream temperature tends to stay constant even though the upstream flow input varies. And when groundwater discharges more than the 99.5% exceedance inflow rate, stream temperature increases with the increase of the upstream flow input.

The sensitivity of stream DO to streamflow scenarios are shown in Figure 5.9. Not unexpectedly, stream DO levels increase with increasing upstream inflows, predominately due to higher reaeration rates at faster flow velocities. On the other hand, because of low DO levels in groundwater, groundwater inputs (larger than 1 m^3/s) decrease DO levels even though they also decrease stream temperatures. However, when upstream inflow rate is small (less than 7Q10, or 3.255 m^3/s), the addition of a small amount (< 1 m^3/s) of groundwater discharge increased stream DO levels. Stream DO will fall to below the GA water quality standard (<5 mg/L) when instream flow is lower than $Q_{99.9}$, or 0.736 m^3/s.

Sensitivity to riparian tree height and stream width

Stream water quality sensitivity to riparian tree height and stream width are dependent on the stream discharge. We have investigated and illustrated sensitivities at three different flow scenarios: the $Q_{99.9}$, an extremely low flow, 7Q10, a typical regulatory threshold, and Q_{50}, the median discharge. At high flows, there is very little sensitivity of temperature and DO to channel width and riparian tree height, and their values are uniformly good. At low flow rates, temperature and DO are very sensitive to channel width or riparian tree height, and unacceptable DO and temperature levels occur for various width and tree height scenarios (Figure 5.10).

Increasing riparian tree height blocks direct solar radiation to the stream surface, strongly reduces maximum stream temperatures under all flow scenarios, especially for low flows (Figures 5.10(a), 5.10(c), and 5.10(e)). Stream width, in general, positively correlates with stream temperature for all the flow scenarios, as wide streams increase exposure to direct solar radiation. However, stream width effects become complicated when streamflow rate is relatively high. Figure 5.10(e) shows that, at the Q_{50} discharge, stream temperature decreases first and then increases with the variation of stream width from 10 m to 30 m. However, absolute temperature sensitivity is very low at high discharges. Thus, at high discharges, the effect of stream width and riparian vegetation shading becomes less predominant. The integrated effects from all the other factors becomes apparent.

Stream DO sensitivities to riparian tree height and stream width are shown in Figures 5.10(b), 5.10(d), and 5.10(f)). When instream flow is extremely low, stream DO tends to be sensitive only to stream width, with wider streams having lower DO concentrations, while riparian vegetation shows little effect. Under 7Q10 flow rate, stream DO becomes sensitive to both factors. The increase of riparian trees leads to decreased stream DO due to the reduced solar energy to the stream. Wider streams have lower DO concentrations due to reduced stream velocity. At moderately high streamflow, the shading effect is significant only for wider streams, and the stream width effect becomes less significant on DO patterns.

5.3.2 Results of long-term simulation

Figures 5.11 and 5.12 shows the distributions of the annual temperature and DO extremes for each management scenario for various reaches of the two creeks. Overall, these graphs indicated very little temperature increase and DO decrease with increased irrigation pumpage, as the differences of streamflows between the pumpage scenarios were actually very slight (Figures 5.6 and 5.7).

In Ichawaynochaway Creek, from reach 27 to reach 35, stream temperature showed a slight increase trend. This was reasonable since from upstream to downstream, stream temperature usually increases for this area (Li and Jackson, 2003). The much lower temperatures in reach 43 indicated the stream orientation effect on available solar radiation energy. Accordingly, relatively low temperatures in reach 19 were expected as the confluence of reach 43 brought in cooler water. Reach 29, with its almost east-west direction, had relatively low temperatures. However, since it was just a first order stream, the heat buffer capacity of this reach was low. Thus, the water temperatures in this reach were higher than those in reach 43. Water temperatures of reach 42, with its very short reach length, were dominated by those in reach 19 and 20. There was a decreasing trend of temperatures from reach 42 to 41 to 40. The reason for this could only be the relatively cold groundwater discharge to the reaches, since the other factors tended to lead to a reverse trend. Reach 24 had a rather wide stream cross section (5.4) with a moderate discharge, thus its temperatures were relatively high.

The spatial patterns of stream DO in Ichawaynochaway Creek were rather obvious (Figures 5.11(d, e, f)). From reach 27 to reach 35, stream DO decreased, indicating an increased oxygen demand by the stream, which was often true for this area (Li and Jackson, 2003).

Reach 43 had very low DO due to low availability of direct solar radiation that was essential for oxygen reproduction through algal photosynthesis. There was a sudden increase of DO in reach 19, which was higher than that in both reach 35 and 43. We attributed this elevation to its low stream temperature (Figures 5.11(a, b, c)), wide stream width (Table 5.4), and the due-south stream aspect (Figure 5.4). It was not surprising that reach 20 had the lowest stream DO concentrations due to adverse stream aspect. The decreased pattern of DO from reach 42 to 41 was similar as that from reach 27 to 35. The relatively high DO in reach 24 was a reflection of high photosynthesis in wide streams with a large percentage of direct solar radiation. The high stream DO levels in reach 40 were mostly due to the mixing effect of reach 41 and 24, while the due-south orientation also had some positive effect on DO concentrations.

In Spring Creek, stream water temperature showed a decreasing trend from reach 18, to 20, to 21, and to 25 among all three flow scenarios. This was mostly a combined effect of stream orientation and groundwater input. Reach 26, which was wider than the upstream reaches, tended to be the most susceptible to higher temperatures problems than all the other reaches under current and backlog scenarios. Under 125Backlog scenario, temperatures in reach 26 were slightly lower than those in reaches 28-30, while still higher than that of all the other reaches. Temperatures in reach 28 - 30 were apparently higher under the 125backlog scenario than those in current and backlog scenarios, indicating the enhanced effects of extremely low-flow situations on water temperature.

The spatial patterns of stream DO showed slight differences between different flow scenarios. Under the current flow scenario, stream DO levels were about the same for reach 18, 20, and 21, roughly with similar median at 4.5 mg/L. Reach 25, due to the east-west aspect and also probably low stream discharge, had the lowest DO levels among all the reaches. DO levels in reach 26 were the highest among all the reaches. This was mostly because discharge increased a lot after the confluence of reach 20 and 21, with little groundwater discharge added. Although DO levels were similar along reaches 28, 29, and 30, a slightly increasing pattern was found. This pattern indicated increased algae photosynthesis rate as reaches become wider downstream. Under the Backlog scenario, there was almost no difference of spatial patterns from the Current scenario, except that the medians were slightly lower than those in current scenario for reaches 28, 29, and 30. Under the 125Backlog scenario, the range between 25% and 75% percentiles became wider compared with those under the Current and Backlog scenarios, indicating increased sensitivity to flows under extremely low-flow situations after excessive pumpage. The spatial variations became a little more apparent as well. Along reach 18, 20, 21, 25, there was a clear decreasing trend in median values, which could be due to the stream orientation, decreased instream flow rate, and probably increased groundwater addition. At the same time, the increasing trend in median values along reaches 28, 29, 30 became more apparent than those under the other two scenarios. Reach 25 was once again most susceptible to low DO problems.

5.4 Discussion and conclusion

In this paper, we applied model DDOT to both sensitivity analysis and long-term stream temperature and DO simulations. The sensitivity analysis simulation provided stream water temperature and DO sensitivity characteristics with respect to the factors of upstream input flow, groundwater discharge, riparian vegetation shading, and stream width. The long-term simulation enabled us to show spatial patterns of temperature and DO under different flow scenarios. The simulation also allowed us to quantify how different flow management scenarios affected the frequency and number of low DO and high temperature events.

The sensitivity analysis demonstrated the stream temperature and DO dynamics of the streams in the Lower Flint River Basin under typical summer weather conditions. Extremely low streamflow can lead to very low stream DO levels below Georgia EPA water quality standard (5 mg/L). As the stream DO becomes very sensitive to flows, the maintenance of a slightly higher flow rate would nearly eliminate stream DO stresses on aquatic habitat. Stream temperatures increases to 28.5 °C when the instream flow falls to the 99.99%

exceedance flow rate, or 0.311 m^3/s, of the reach. Stream temperature becomes most sensitive to stream discharge at extremely low-flow situations when high temperatures usually occur. Thus the maintenance of a certain amount of stream discharge rate is critical to protect available aquatic habitat in hot summer. Groundwater, by its very strong cooling effect, effectively helps protect available aquatic habitat in summer, especially during drought seasons.

Although groundwater discharge is expected to relieve stream DO stresses at low flows by its cooling effect on water temperature during hot summer, this effect is noticeable only when both groundwater discharge rate and the instream flow rate are very low (below 99.9% exceedance discharge rate for groundwater and below 7Q10 discharge rate for upstream inflow). It becomes either overwhelmed by the relatively low groundwater DO levels (Schreier *et al.*, 1980), or negligible when upstream inflow rate is much higher than groundwater addition rate.

Stream temperature and DO patterns under different tree height, stream width, and flow rate scenarios indicated the dynamic behavior of these two water quality constituents. Riparian vegetation shading, by blocking direct solar insolation to the stream, tends to protect stream temperatures from rising for all the flow scenarios. For a given discharge rate, wider streams have higher stream temperatures due to increased exposure to solar radiation and usually slower flow velocity. At low flow scenarios when water became very shallow, the SOD decay, which was negatively associated with water depth, became the dominant factor controlling stream oxygen levels. During moderate flow situations, when the SOD decay effect was no longer as strong as that in low-flow situations, the riparian tree height, by affecting direct solar radiation to the stream, began to act as a significant control on stream DO by regulating algal photosynthesis rate. For high flow situations, the effects of stream water depth and flow velocity variations induced by stream width change became even less important, which enabled algal photosynthesis to become the dominant factor in DO levels.

The non-monotonic trend of DO versus stream width indicated the complex nonlinear effects of the different scenarios.

The long-term simulation showed that there were only slight differences of stream temperature and DO levels between the three different flow scenarios, since the differences in flows between the scenarios were not large. However, spatial patterns existed from upstream to downstream of both watersheds for all flow scenarios. The patterns were mostly determined by stream orientation, groundwater input, and stream cross section. The reduced groundwater discharge due to increased pumpage rate from aquifers would very slightly increase both stream temperature DO.

Overall, the results indicate that low DO problems occur only during extreme low flow events. In these streams, a minimum instream flow policy makes sense. Furthermore, the results indicate that direct surface water withdrawals during droughts are more likely to cause problems than groundwater withdrawals. These model results indicated that, in order to keep water temperature and DO from being constraints for fish and mussels, water management policies should focus on eliminating direct surface water withdrawals during droughts.

References

Albertson, P. N. and L. J. Torak, 2002. Simulated effects of ground-water pumpage on stream-aquifer flow in the vicinity of federally protected species of freshwater mussels in the lower Apalachicola-Chattahoochee-Flint River basin (Subarea 4), southeastern Alabama, northwestern Florida, and southwestern Georgia. Water-Resources Investigations Report 02-4016, U.S. Geological Survey, 54 pp. Web: `http://ga.water.usgs.gov/pubs/wrir/wrir024016/`.

Beschta, R., R. Bilby, G. Brown, L. Holtby, and T. Hofstra, 1987. Chapter 6. stream temperature and aquatic habitat: Fisheries and forestry interactions. In Salo, E. and T. Cundy, editors, *Streamside Management: Forestry and Fishery Interactions*. University of Washington, Institute of Forest Resources. Contribution No. 57, pp. 191-232.

Caruso, B. S., 2002. Temporal and spatial patterns of extreme low flows and effects on stream ecosystems in Otago, New Zealand. *Journal of Hydrology*, 257(1-4):115–133.

Christie, C. and H. Regier, 1988. Measurements of optimal habitat and their relationship to yields for four commercial fish species. *Canadian Journal of Fisheries and Aquatic Science*, 45:301–314.

Coutant, C. C., 1987. Thermal preference - When does an asset become a liability. *Environmental Biology of Fishes*, 18(3):161–172.

Fanning, J. L., 1999. Water use in coastal Georgia by county and source, 1997; and water-use trends, 1980-97. Georgia Geologic Survey Information Circular 104, U.S. Geological Survey, Atlanta, GA, 37 pp. Web: `http://ga.water.usgs.gov/pubs/other/ggs-ic104/`.

Gilvear, D. J., K. V. Heal, and A. Stephen, 2002. Hydrology and the ecological quality of Scottish river ecosystems. *The Science of The Total Environment*, 294(1-3):131–159.

Hayes, L., M. Maslia, and W. Meeks, 1983. Hydrology and model evaluation of the principal artesian aquifer, Dougherty Plain, southwest Georgia. Georgia Geologic Survery Bulletin 97, 93 pp.

Horne, A. J. and C. R. Goldman, 1994. *Limnology, 2nd Edition*. McGraw-Hill, New York, 576 pp.

Johnson, P. M., A. E. Liner, S. W. Golladay, and W. K. Michener, 2001. Effects of drought on freshwater mussels and instream habitat in Coastal Plain tributaries of the Flint River, southwest Georgia (July-October, 2000). Presented to The Nature Conservancy Apalachicola River and Bay Project, Jones Ecological Research Center, Route 2 Box 2324, Newton, GA, 34 pp. Web: `http://www.jonesctr.org/research/aquatics_research/final_report2.pdf`.

Karim, M. R., M. Sekine, and M. Ukita, 2003. A model of fish preference and mortality under hypoxic water in the coastal environment. *Marine Pollution Bulletin*, 47(1-6):25–29.

Li, G. and C. R. Jackson, 2003. Physical and chemical characteristics of streams in the dougherty plain. In Hatcher, K. J., editor, *Proceedings of the 2003 Georgia Water Resources Conference, April 23-24, 2003*, University of Georgia.

Li, G. and C. R. Jackson, 2006. *Development of a Dynamic Dissolved Oxygen and Temperature Model with Groundwater Interactions*. Ph.D. Dissertation, University of Georgia, Athens, GA.

Miller, A. C. and B. S. Payne, 2004. Reducing risks of maintenance dredging on freshwater mussels (Unionidae) in the Big Sunflower River, Mississippi. *Journal of Environmental Management*, 73(2):147–154.

Richter, B. D., D. P. Braun, M. A. Mendelson, and L. L. Master, 1997. Threats to imperiled freshwater fauna. *Conservation Biology*, 11(5):1081–1093.

Sabo, M. J., C. F. Bryan, W. E. Kelso, and D. A. Rutherford, 1999. Hydrology and aquatic habitat characteristics of a riverine swamp: I. Influence of flow on water temperature and chemistry. *Regulated Rivers: Research and Management*, 15(6):505–523.

Schreier, H., W. Erlebach, and L. Albright, 1980. Variations in water quality during winter in two Yukon rivers with emphasis on dissolved oxygen concentration. *Water Research*, 14(9):1345–1351.

Torak, L. J., G. S. Davis, G. Strain, and J. Herndon, 1996. Geohydrology and evaluation of stream-aquifer relations in the Apalachicola-Chattahoochee-Flint River Basin, southeastern Alabama, northwestern Florida, and southwestern Georgia. Water-Supply Paper 2460, U.S. Geological Survey, 95 pp. Web: `http://ga.water.usgs.gov/publications/abstracts/wsp2460.html`.

USGS, 2000. Droughts in Georgia. Technical report. Web: `http://ga.water.usgs.gov/publications/ofr00-380.pdf`.

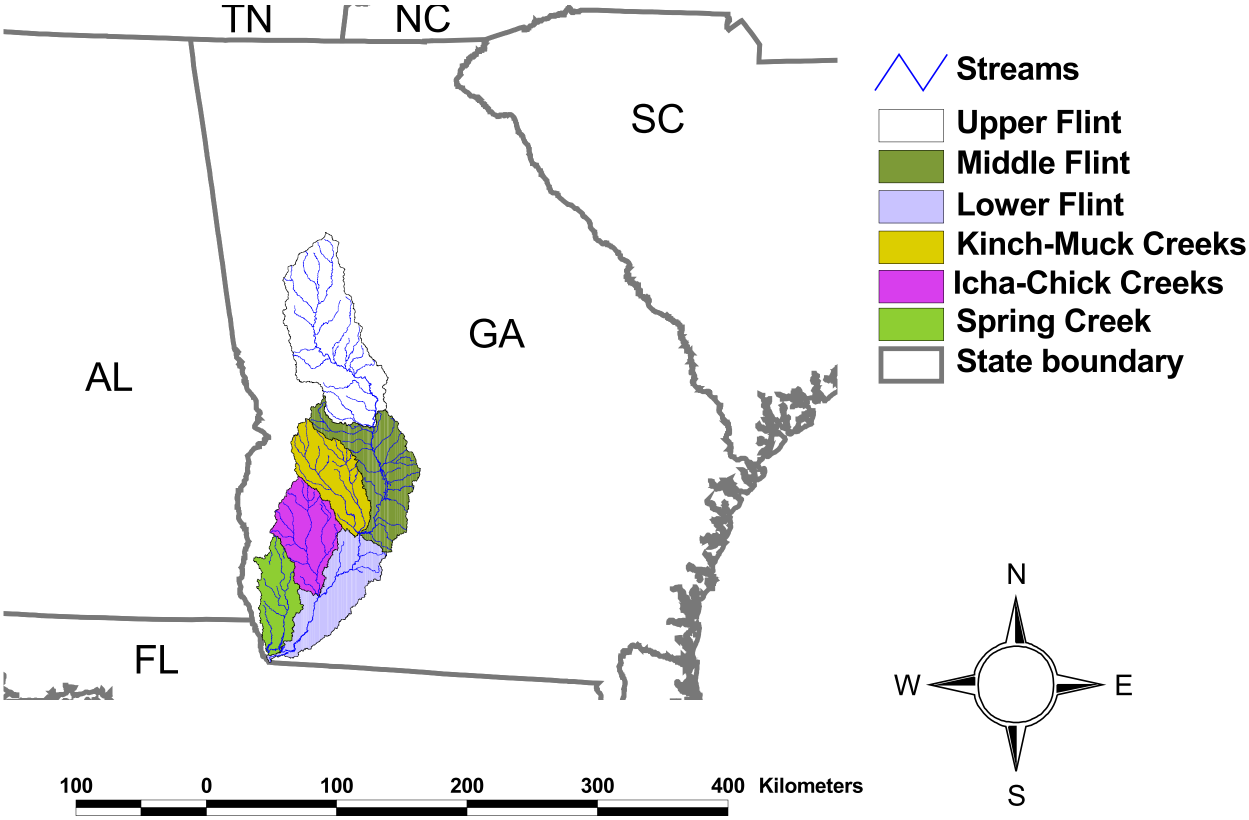

Figure 5.1: Study site - the Lower Flint River Basin.

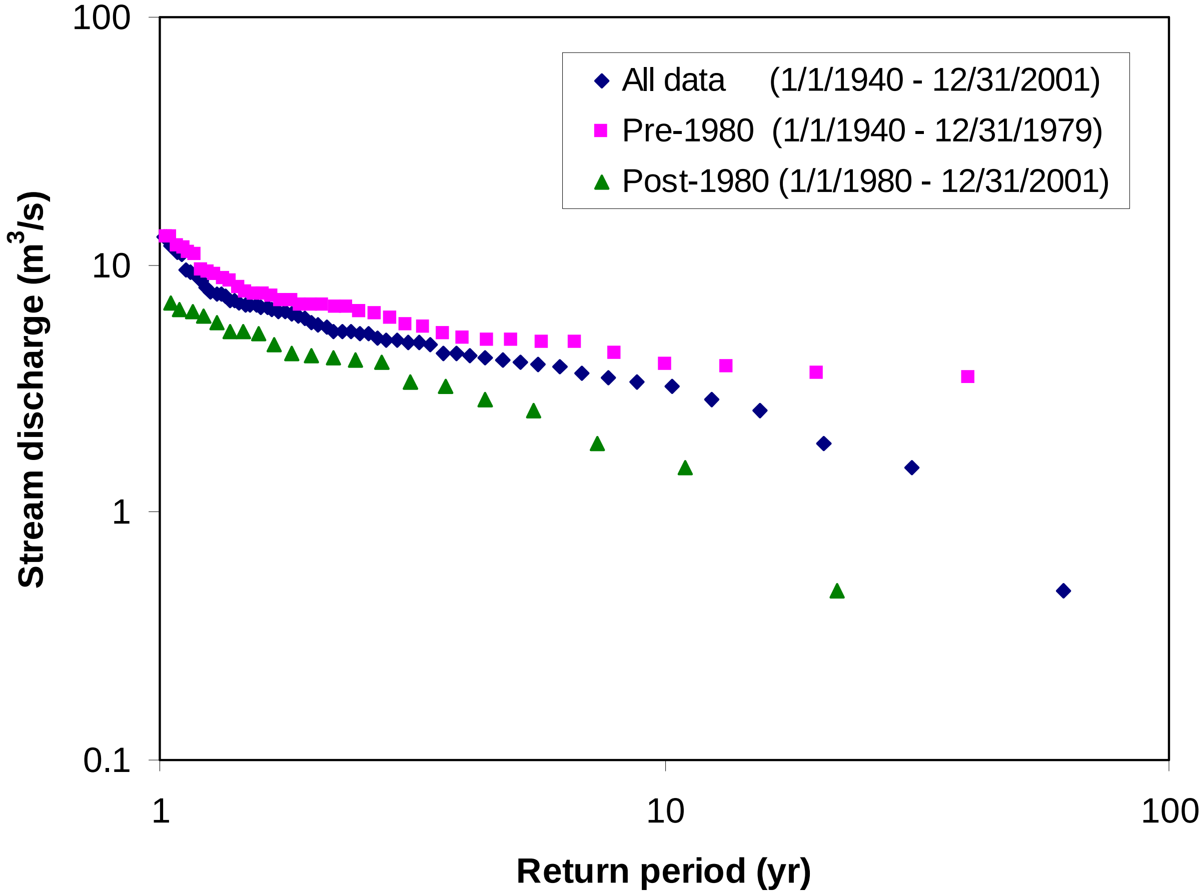

Figure 5.2: Stream Seven day low flow vs. return period for Ichawaynochaway Creek near Milford (Ichi3). Data from USGS 01/01/1940 - 12/31/2001. Since 1980, low streamflow events occur more frequently. The lowest 7-day flow on the graph occurred August 2000 when major fish and mussel kills occurred due to severe drought conditions. Agricultural irrigation pumping was suspected to exacerbate the drought.

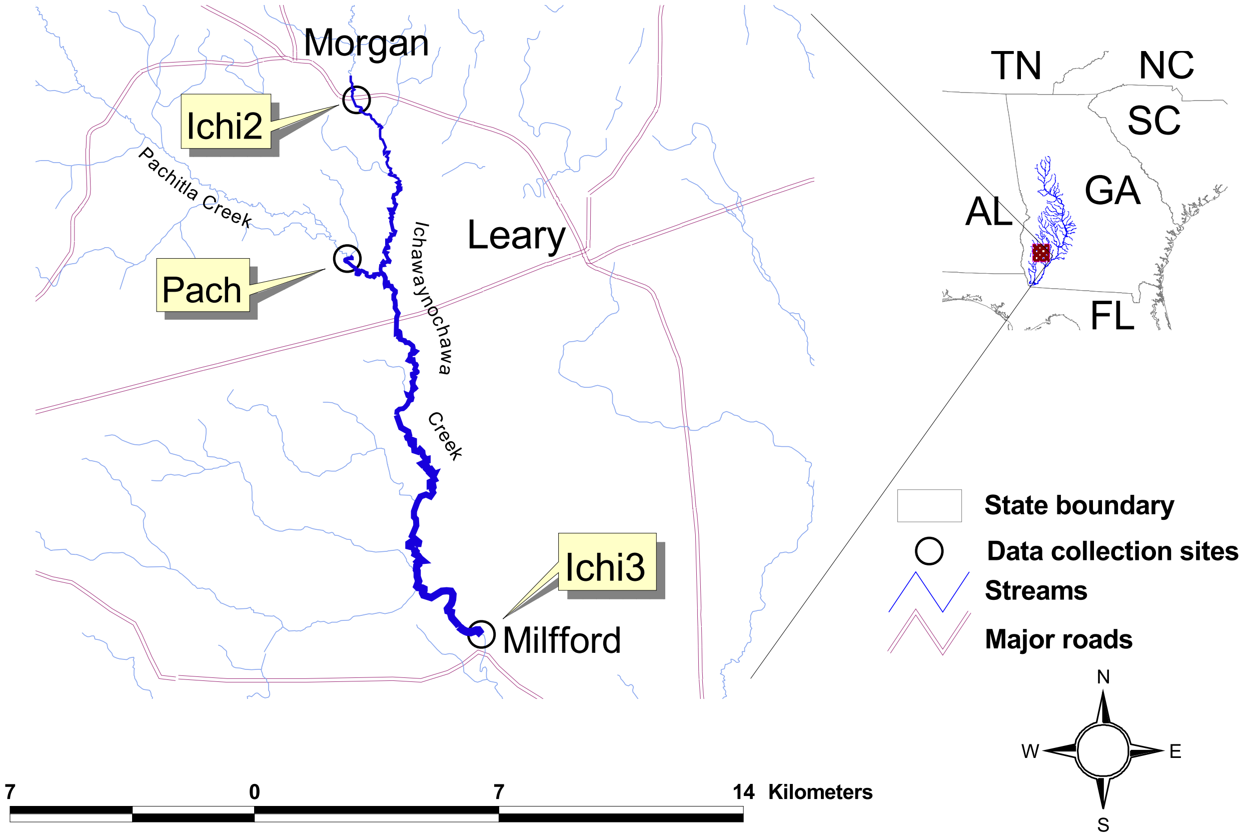

Figure 5.3: Sensitivity analysis - Stream reach settings.

Ichawaynochaway Creek

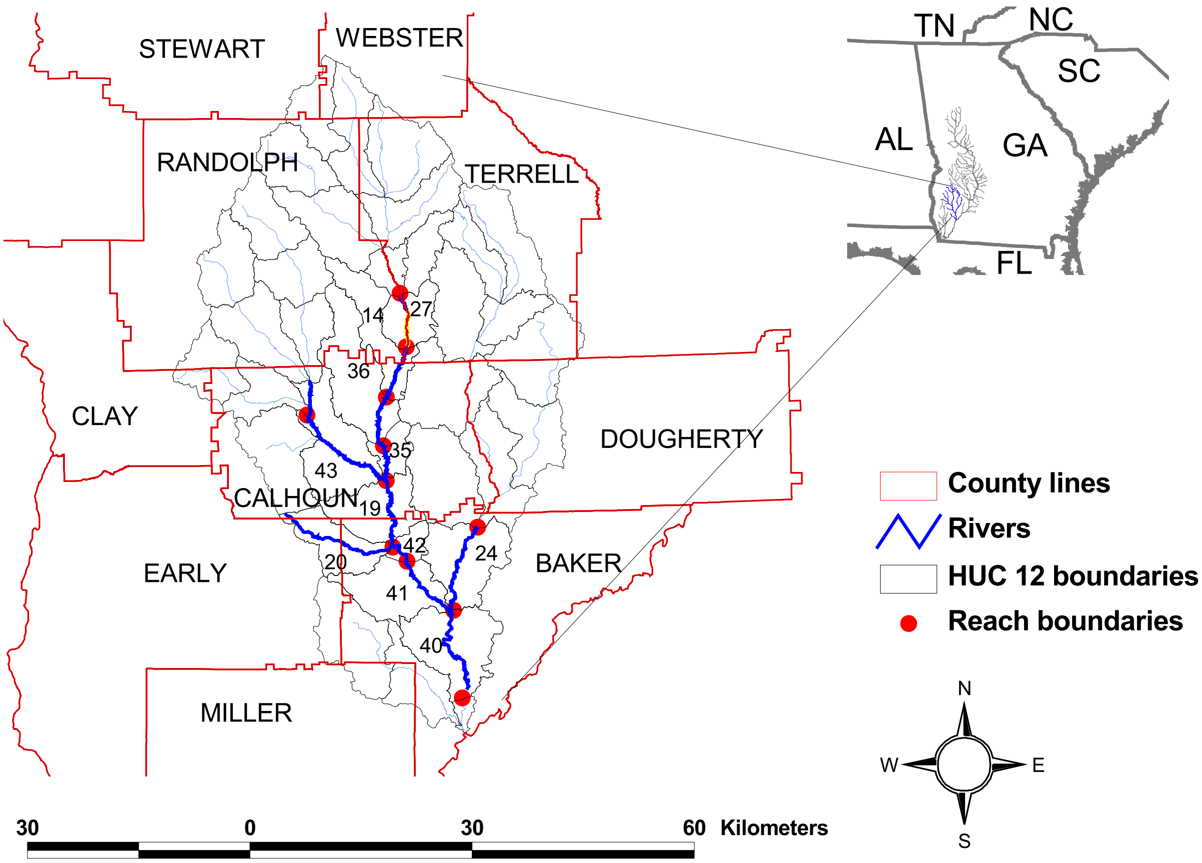

Figure 5.4: Long-term simulation - Selected reaches (highlighted in blue) in Ichawaynochaway Creek watershed. Sub-watersheds are delineated under 12 digits USGS Hydrologic Unit Code.

Spring Creek

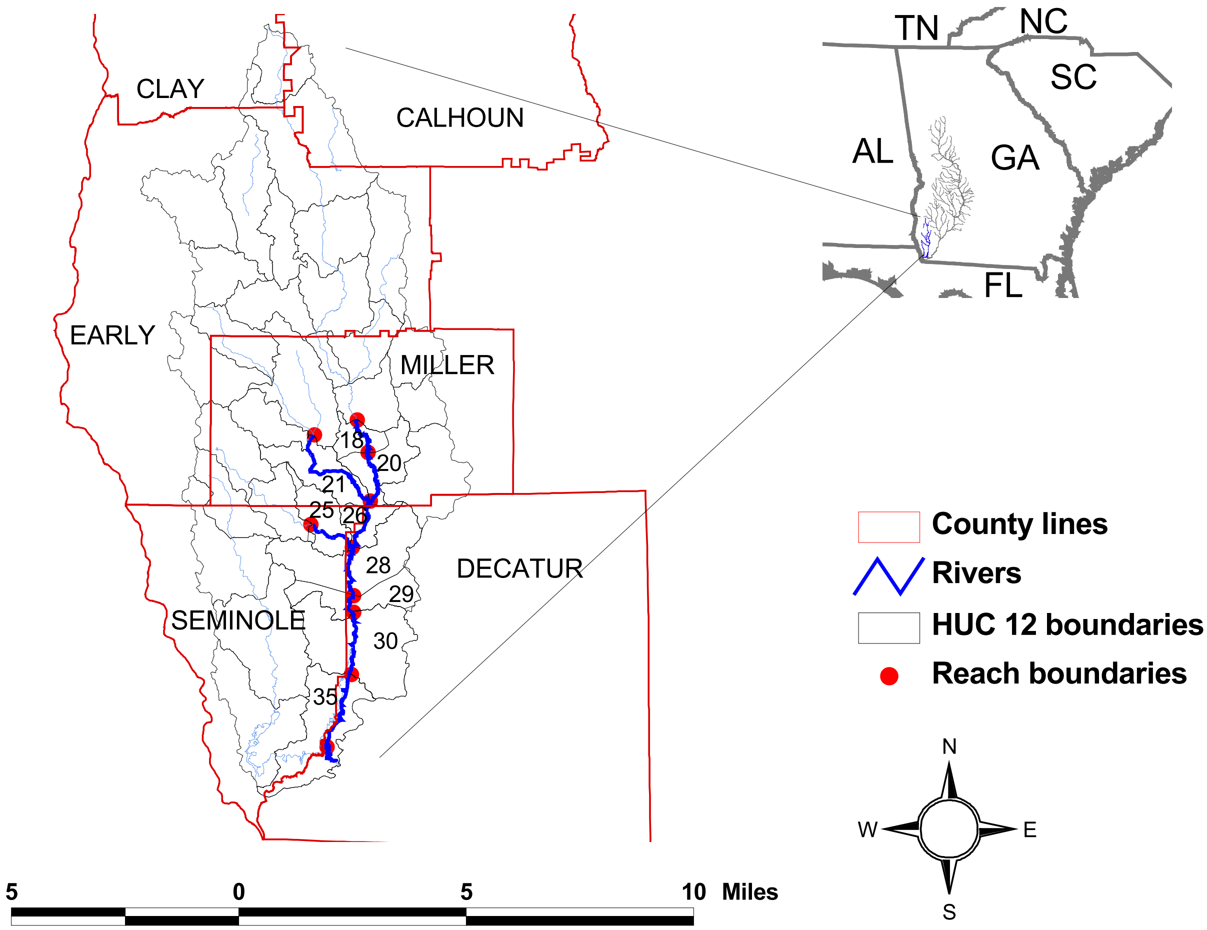

Figure 5.5: Long-term simulation - Selected reaches (highlighted in blue) in Spring Creek watershed. Sub-watersheds are delineated under 12 digits USGS Hydrologic Unit Code.

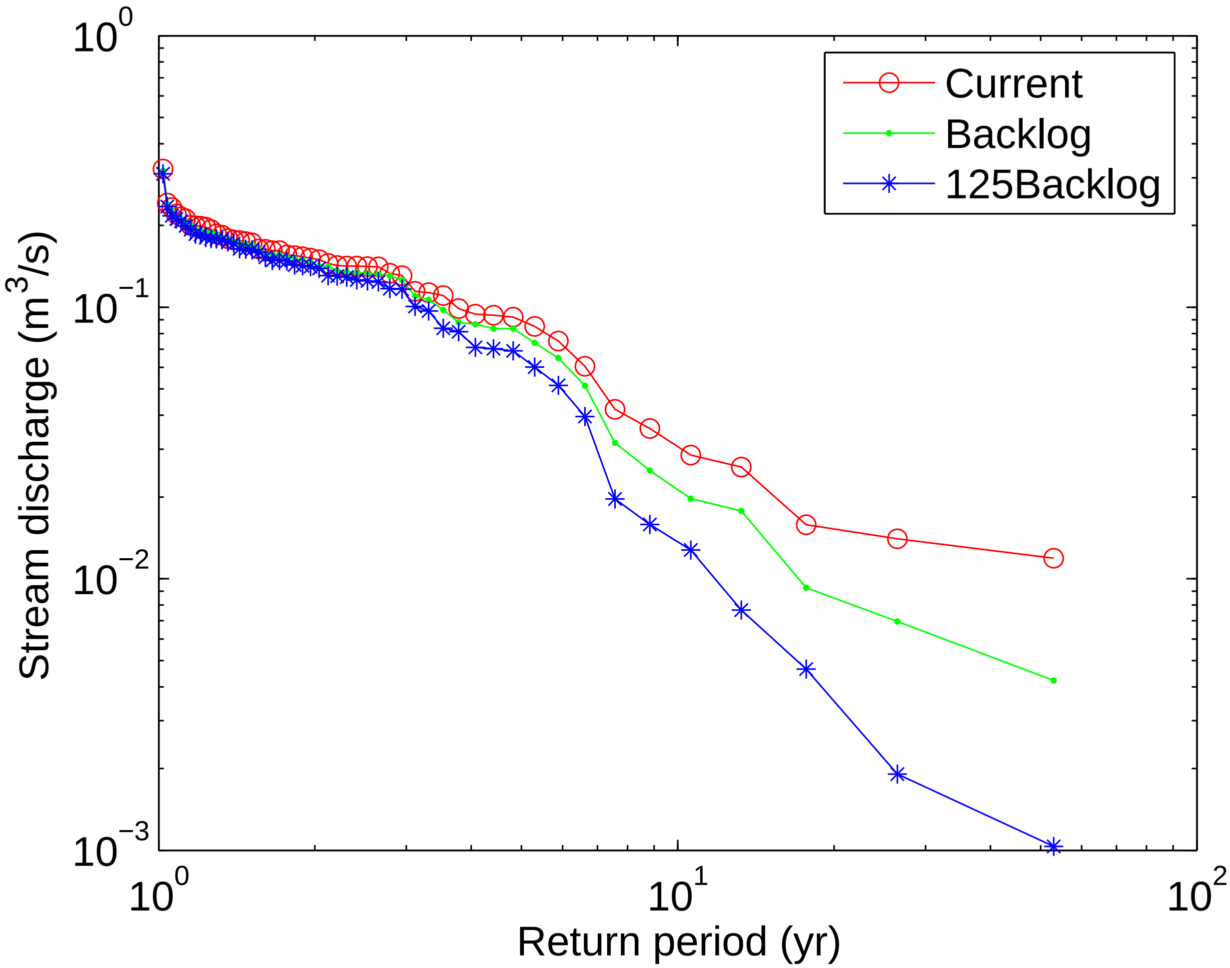

Figure 5.6: Stream Seven day low flow vs. return period - HSPF simulation of rch42 in Ichawaynochaway Creek (Figure 5.4) (1950 -2003).

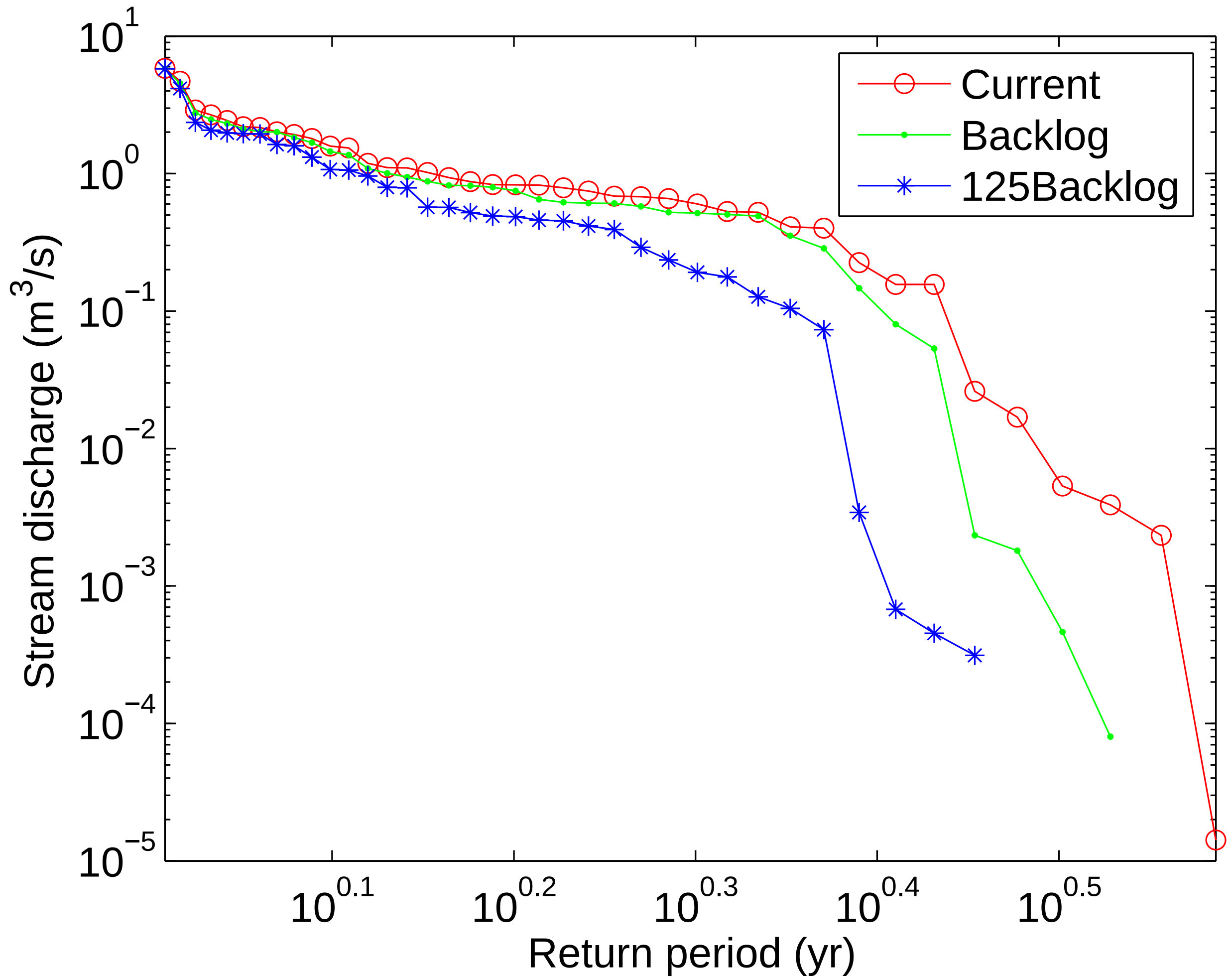

Figure 5.7: Stream Seven day low flow vs. return period - HSPF simulation of rch28 in Spring Creek (Figure 5.5) (1950 -2003).

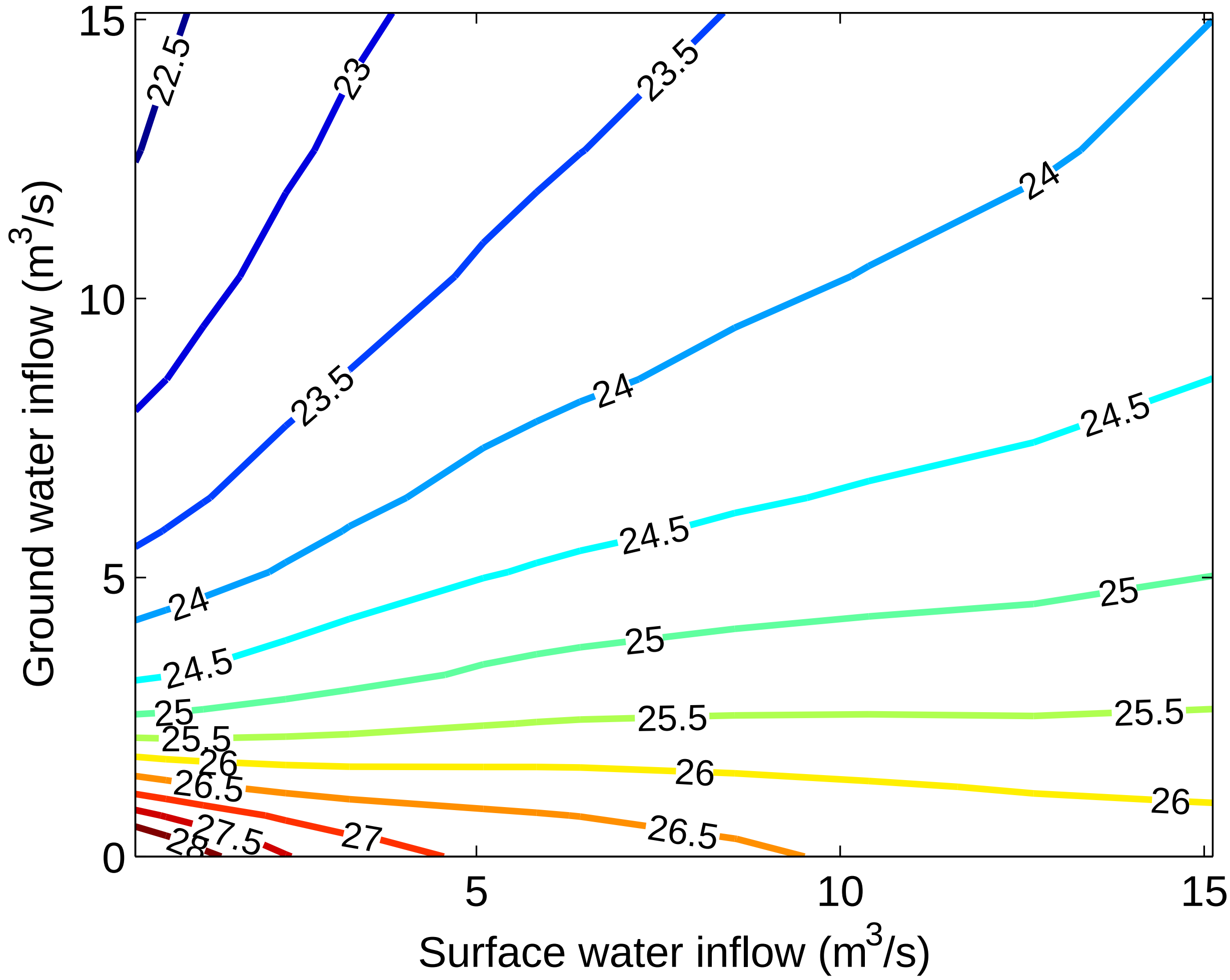

Figure 5.8: Sensitivity analysis - Stream temperature at downstream boundary of the reach vs. upstream flow input and groundwater discharge

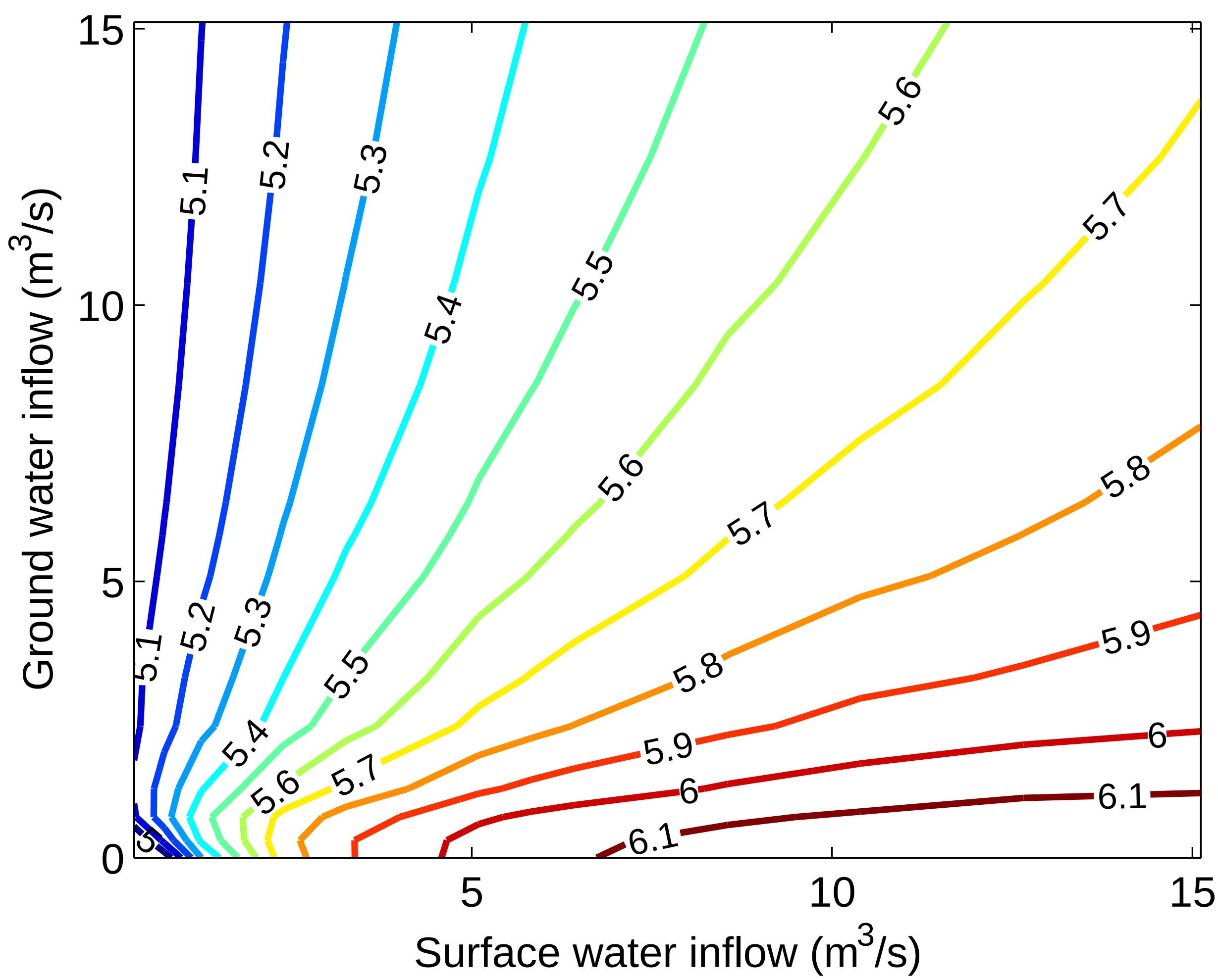

Figure 5.9: Sensitivity analysis - Stream DO at downstream boundary of the reach vs. upstream flow input and groundwater discharge

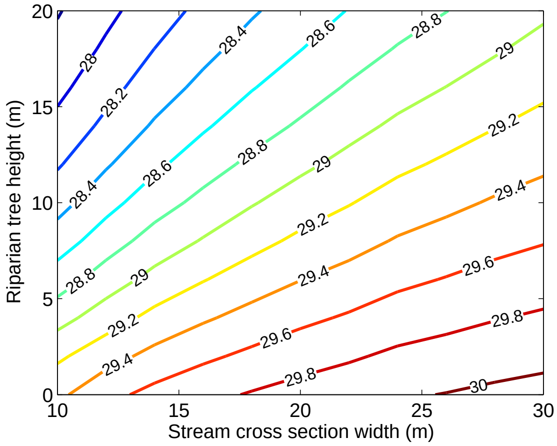

(a) T at $Q_{99.9}$ flow rate

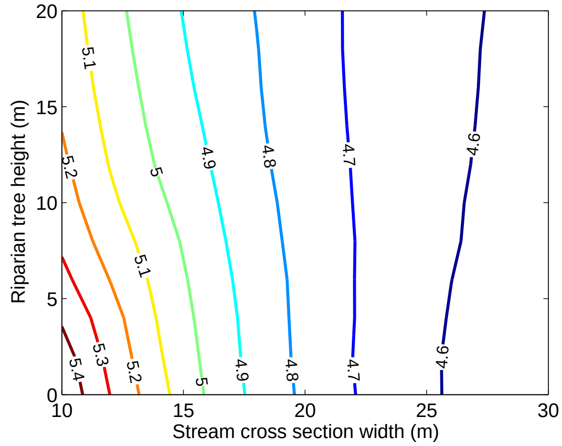

(b) DO at $Q_{99.9}$ flow rate

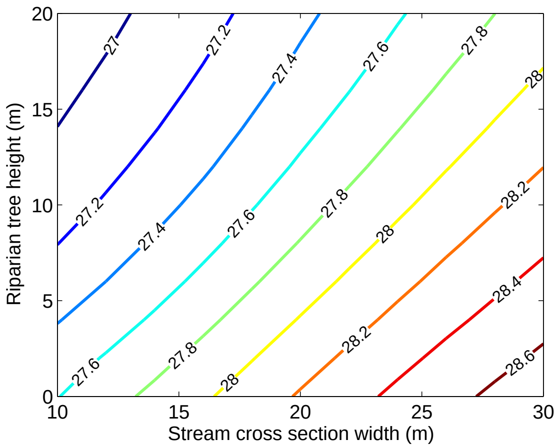

(c) T at 7Q10 flow rate

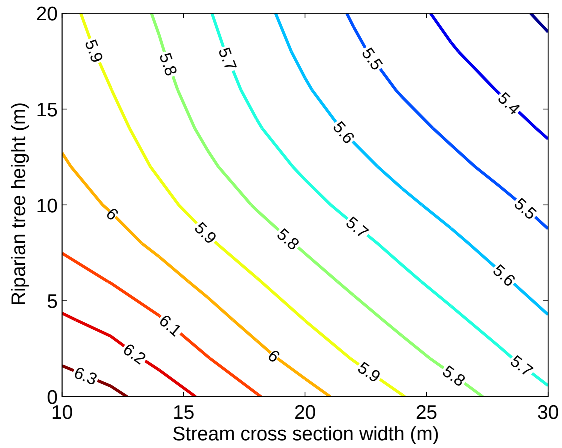

(d) DO at 7Q10 flow rate

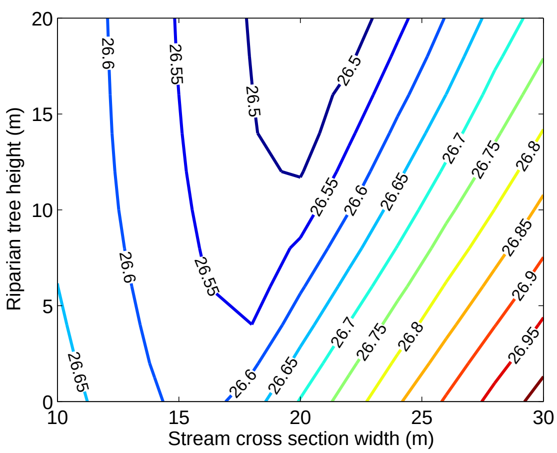

(e) T at Q_{50} flow rate

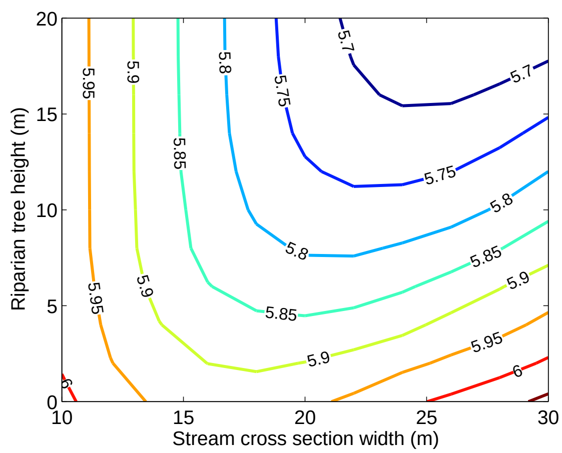

(f) DO at Q_{50} flow rate

Figure 5.10: Sensitivity analysis - Effects of riparian tree height and stream width on stream temperature and DO of selected flow scenarios

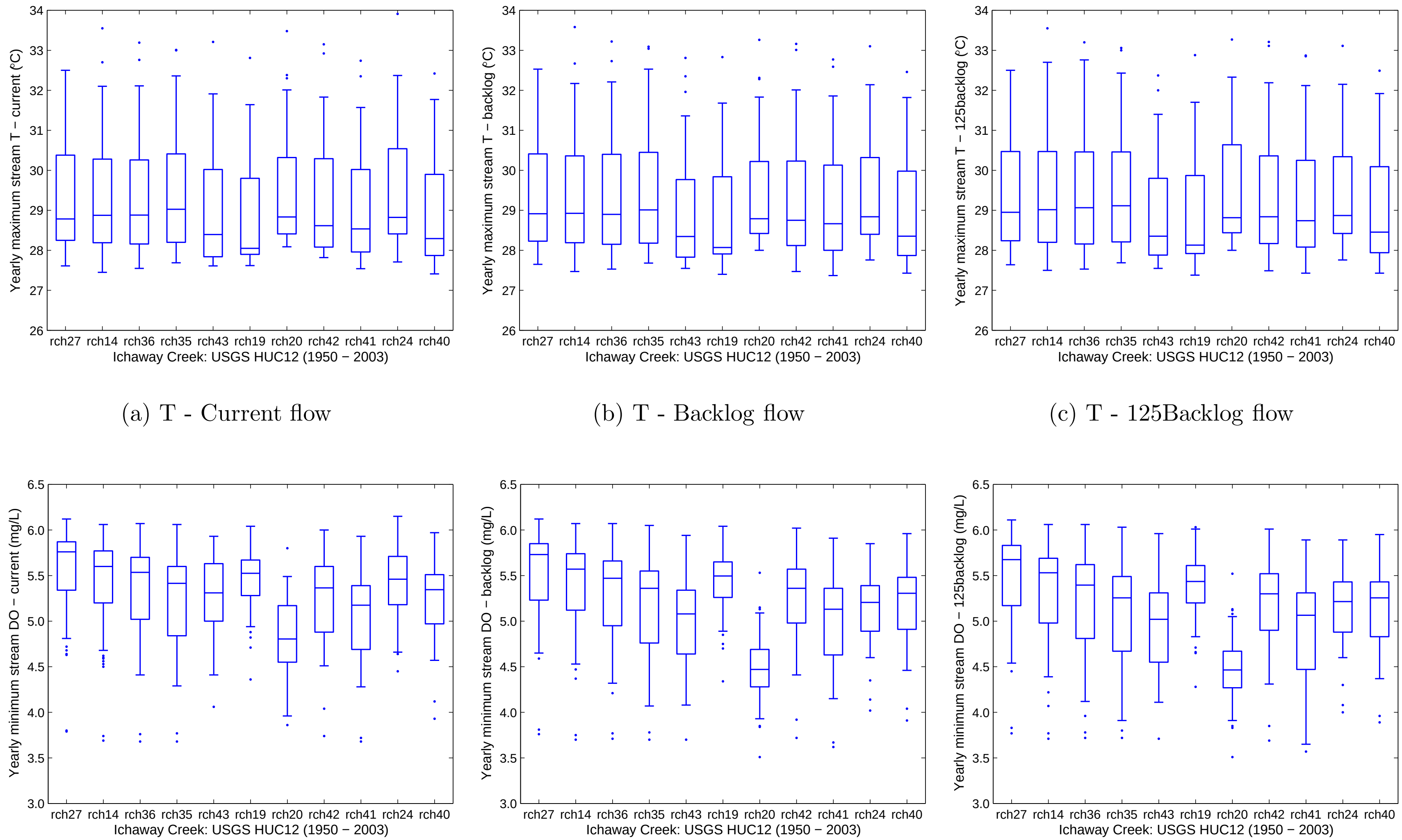

(a) T - Current flow

(b) T - Backlog flow

(c) T - 125Backlog flow

(d) DO - Current flow

(e) DO - Backlog flow

(f) DO - 125Backlog flow

Figure 5.11: Long-term simulation - Results for reaches in Ichawaynochaway Creek. Where, Current flow accounts for flow under the approved permit applications received by EPD during the permit moratorium; Backlog flow accounts for flow under the option of approving all of the permit applications received by EPD; and 125Backlog flow is flow under the 1.25×Backlog Scenario.

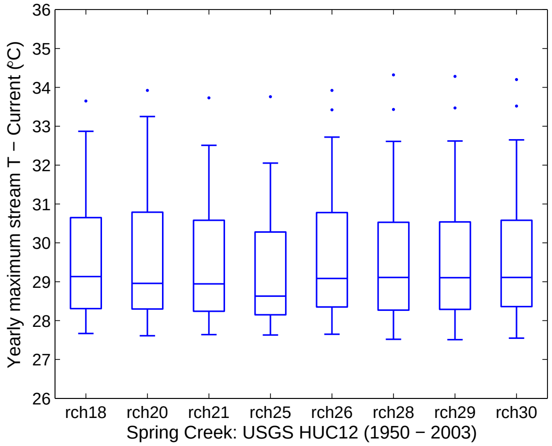

(a) T - Current flow

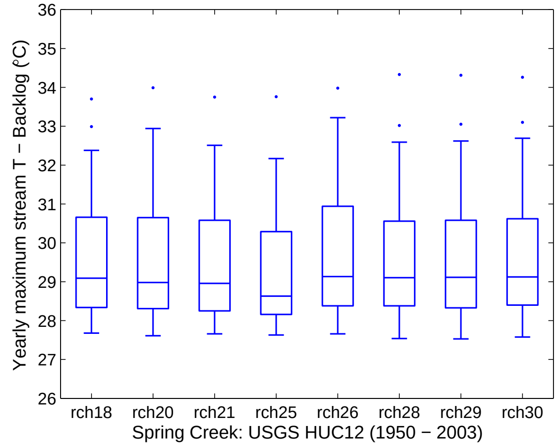

(b) T - Backlog flow

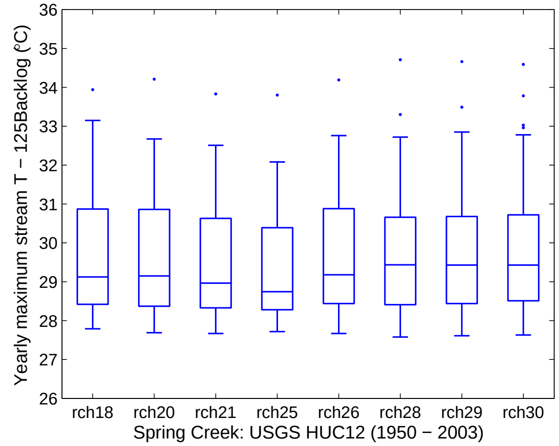

(c) T - 125Backlog flow

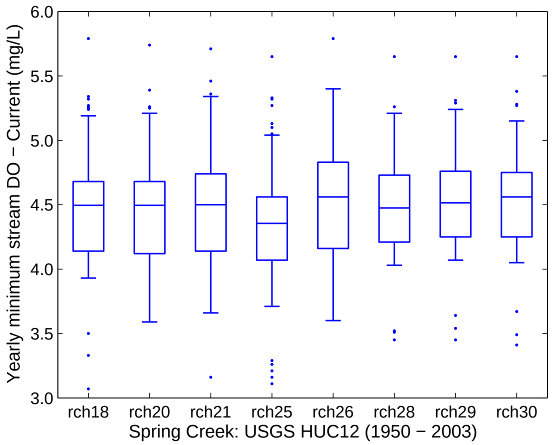

(d) DO - Current flow

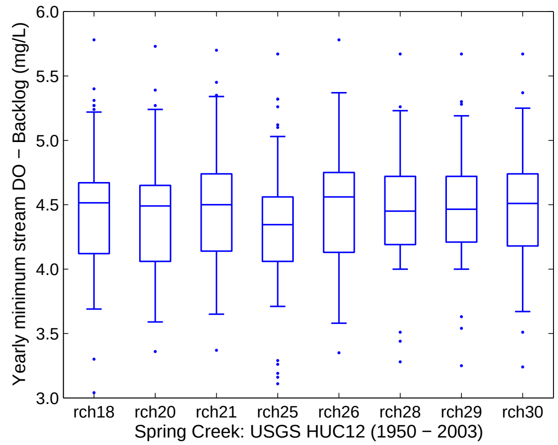

(e) DO - Backlog flow

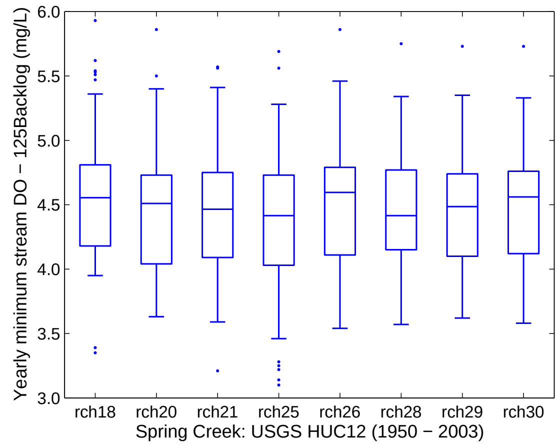

(f) DO - 125Backlog flow

Figure 5.12: Long-term simulation - Results for reaches in Spring Creek. Where, Current flow accounts for flow under the approved permit applications received by EPD during the permit moratorium; Backlog flow accounts for flow under the option of approving all of the permit applications received by EPD; and 125Backlog flow is flow under the 1.25×Backlog Scenario.

Table 5.1: Sensitivity analysis - Reach description and sensitivity experiments

Simulation reach:	Ichawaynochaway Creek	
Channel length:	25200 m	
Channel width:	12-28 m from upper to lower boundaries	
Basin area:	1608.26 km^2	
Aspect:	North-South	
Experiment 1: Effects of upstream flow inputs and groundwater discharge		
Range of upstream flows (m^3/s): 0.311 - 15.121		# of gradations: 12
Range of groundwater discharges (m^3/s): 0 - 15.121		# of gradations: 13
Total # of experiment combinations: 156		
Experiment 2: Effects of stream width and riparian tree height under given flow		
Range of stream width (m): 10 - 30		# of gradations: 11
Range of tree height (m): 0 - 20		# of gradations: 11
Range of instream flows (m^3/s): 0.311 - 15.121		# of gradations: 12
Total # of experiment combinations: 1452		

Table 5.2: Sensitivity analysis - Scenarios of upstream flow input and groundwater discharge

ID	Symbol	Description	Value (m^3/s)
1	$Q_{99.99}$	99.99% Exceedance flow	0.311
2	$Q_{99.9}$	99.9% Exceedance flow	0.736
3	$Q_{99.8}$	99.8% Exceedance flow	1.246
4	$Q_{99.5}$	99.5% Exceedance flow	2.379
5	7Q10	7 day, 10 year low flow	3.255
6	Q_{95}	95% Exceedance flow	5.097
7	7Q2	7 day, 2 year low flow	5.829
8	Q_{90}	90% Exceedance flow	6.428
9	Q_{80}	80% Exceedance flow	8.552
10	Q_{70}	70% Exceedance flow	10.392
11	Q_{60}	60% Exceedance flow	12.658
12	Q_{50}	50% Exceedance flow	15.121

Table 5.3: Sensitivity analysis - Scenarios of stream width and riparian vegetation shading

ID	Tree height (m)	Stream width (m)
1	0	10
2	2	12
3	4	14
4	6	16
5	8	18
6	10	20
7	12	22
8	14	24
9	16	26
10	18	28
11	20	30

Table 5.4: Long-term simulation - Stream morphology of Ichawaynochaway Creek

Reach	Length(m)	Width(m)		Latitudes (°)	
		upstream	downstream	upstream	downstream
rch27	8981	8	9	31.69	31.64
rch14	10067	9	10	31.64	31.59
rch36	8324	10	11	31.57	31.54
rch35	7695	11	12	31.51	31.48
rch19	14290	20	26	31.48	31.40
rch42	5001	26	28	31.40	31.38
rch41	10572	28	35	31.38	31.33
rch40	18275	35	40	31.32	31.22
rch43	18526	8	10	31.56	31.49
rch20	17343	3	6	31.44	31.38
rch24	15291	22	26	31.42	31.35

Table 5.5: Long-term simulation - Stream morphology of Spring Creek

Reach	Length(m)	Width(m)		Latitudes (°)	
		upstream	downstream	upstream	downstream
rch18	8227	14	16	31.16	31.12
rch20	7950	16	20	31.12	31.07
rch21	15883	4	6	31.15	31.07
rch25	6533	2	3	31.05	31.02
rch26	7687	20	25	31.07	31.02
rch28	8601	25	28	31.02	30.92
rch29	3361	28	29	31.00	30.92
rch30	9472	29	32	31.00	30.79

Chapter 6

Conclusions

The tributaries of the karstic Lower Flint River, southwest Georgia, are incised into the upper Floridan semi-confined limestone aquifer (Priest, 2004). The seepage of relatively old groundwater sustains baseflows and provides some influence over stream temperature and dissolved oxygen fluctuations. This hydrologic and geologic setting creates unique aquatic habitats.

In recent years, rapidly growing population has led to increased water demands from agriculture, industry, and municipalities in the state of Georgia (Fanning, 1999). Nowhere is this more evident than in the Lower Flint River Basin, where extremely low flow and severely degraded aquatic habitat issues occurred during summer droughts (USGS, 2000; Johnson *et al.*, 2001). Excessive groundwater withdrawal for center-pivot irrigation reduced groundwater input to tributaries (Torak *et al.*, 1996; Albertson and Torak, 2002), which exacerbated the droughts' effect on water quality.

The State established the Flint River Drought Protection Act to protect streamflows. To provide natural resource managers and planners a clear understanding of the effects of streamflow and channel morphology on stream water quality, and to help evaluate the potential adverse effect of reduced streamflow and groundwater discharge on stream aquatic habitat, we developed the dynamic water quality model DDOT. DDOT integrates stream dynamic flow, temperature , and DO components, and is enhanced by integrating the SHADE and BED modules. The SHADE module is a compact, accurate, and efficient program that calculates the percentage of the stream surface that does not receive direct solar radiation due to riparian vegetation shading. The BED module uses one-dimensional advection-diffusion equations to generate dynamic temperature and DO vertical profiles of the saturated porous streambed. This technique, although previously used to describe disturbances of temperature-depth profiles induced by subsurface water flow passing through the streambed (Taniguchi *et al.*, 1999a,b), has not been used in the existing stream temperature and DO models.

DDOT uses finite difference method to solve the governing equations. To choose the the most appropriate numerical schemes for the model, the comparison of several commonly used finite difference schemes were conducted, and the modified MacCormack and Saulyev schemes were proposed. It was shown that the modified MacCormack scheme, MacCormack$_c$, is superior to the others in terms of accuracy and efficiency. This scheme was used to solve ADRE based temperature and DO modules.

The model was calibrated successfully using data collected on Ichawaynochaway Creek in late summer of the year 2002. The model evaluation using data collected in summer of the year 2003 verified the reliability of the model. By integrating the streamflow, groundwater input, riparian shading, channel geometry, and channel hydraulics, the model is able to address the effects of these factors on stream temperature and oxygen dynamics, and to guide management decisions.

The sensitivity analysis indicated that, in the Lower Flint River Basin, both temperature and stream DO are very sensitive to upstream inflow, especially during low flow conditions. Extremely low stream discharge (99.9% exceedance flow, or 0.736 m^3/s) can increase stream temperature above 28 °C and decrease stream DO below Georgia EPA water quality standard (5 mg/L). Thus the maintenance of a minimum amount of upstream inflow is critical to eliminate stream temperature and DO stresses on fresh water fish and mussels in hot summer.

Groundwater discharge has a very strong cooling effect on stream water summer temperatures. This cooling effects effectively helps protect available aquatic habitat during summer droughts. Although groundwater discharge is expected to relieve stream DO stress by its cooling effect, this effect is noticeable only if both the groundwater input and the upstream discharge are very low (< 99.9% exceedance flow, or 0.736 m^3/s, for groundwater and < 7Q10 discharge rate for upstream inflow). Under other situations, this effect becomes either overwhelmed by the relatively low groundwater DO level, or negligible when upstream discharge rate is much higher than that of the groundwater.

Riparian vegetation shading protects stream temperature from increasing regardless of the instream discharge. With fixed stream discharge, wider streams have higher stream temperatures due to increased exposure to direct solar radiation and shallower water depth.

The long-term simulation shows only very slight differences between the three simulation scenarios. However, spatial patterns existed from upstream to downstream of both watersheds for all these scenarios. These patterns were mostly due to the stream aspect, groundwater discharge, and stream cross section morphology. Although very slightly, the reduced groundwater discharge due to increased agricultural pumpage from aquifers increased both the stream temperature and dissolved oxygen. The result that the reduced groundwater input increased stream DO level was not contradictory to our justification of the positive stream discharge effect on stream DO, because this result was actually due to the lower DO level of groundwater itself (Schreier *et al.*, 1980). Once the groundwater had been staying in the stream for some longer time, its effect on stream DO would eventually become positive.

Overall, the results indicate that, in the Lower Flint River Basin, stream low DO problems occur only during extremely low flow events. In these streams, a minimum instream flow policy makes sense. Furthermore, the results indicate that direct surface water withdrawals during droughts are more likely to cause problems in terms of stream temperature and dissolved oxygen than groundwater withdrawals. Based on these model results, water management policies should focus on eliminating direct surface water withdrawals during droughts.

Bibliography

Adams, J. L., 2005. Recommendations for the Flint River Basin Water Development and Conservation Plan. Presented to the Georgia Environmental Protection Division Director, the Flint River Basin Stakeholder Advisory Committee, 227 pp. Web: `http://www.gadnr.org/frbp/Assets/Documents/Plan17.pdf`.

Adrian, D. D., F. X. Yu, and D. Barbe, 1994. Water quality modeling for a sinusoidally varying waste discharge concentration. *Water Research*, 28(5):1167–1174.

Ahlert, R. C. and S.-F. Hsueh, 1980. A reactor network model of the Passaic River. *Ecological Modelling*, 10(1):47–61.

Albertson, P. N. and L. J. Torak, 2002. Simulated effects of ground-water pumpage on stream-aquifer flow in the vicinity of federally protected species of freshwater mussels in the lower Apalachicola-Chattahoochee-Flint River basin (Subarea 4), southeastern Alabama, northwestern Florida, and southwestern Georgia. Water-Resources Investigations Report 02-4016, U.S. Geological Survey, 54 pp. Web: `http://ga.water.usgs.gov/pubs/wrir/wrir024016/`.

Ames, W. F., 1977. *Numerical Methods for Partial Differential Equations, 2nd Edition*. Academic Press, New York, 365 pp.

Anderson, E. R., 1954. Water-Loss Investigations: Lake Hefner Studies. Professional Paper 269, U.S. Geological Survey, Washington, D.C., 71 pp.

Arnold, J., R. Srinivasan, R. Muttiah, and J. Williams, 1998. Large area hydrologic modeling and assessment. Part I: Model development. *Journal of the American Water Resources Association*, 34(1):73–89.

Beck, M. and B. Finney, 1987. Operational Water Quality Management: Problem Context and Evaluation of a Model for River Quality . *Water Resources Research*, 23(11):2030–2042.

Beck, M. B., 1983. A procedure for modeling. In Orlob, G. T., editor, *Mathematical Modeling of Water Quality: Streams, Lakes, and Reservoirs*, International series on applied systems analysis. Wiley, Chichester [West Sussex], New York, pp. 11-41.

Becker, M. W., T. Georgian, H. Ambrose, J. Siniscalchi, and K. Fredrick, 2004. Estimating flow and flux of ground water discharge using water temperature and velocity. *Journal of Hydrology*, 296(1-4):221–233.

Bennett, J. P. and R. E. Rathbun, 1972. Reaeration in Open-Channel Flow. U.S. Geological Survey Professional Paper 737, U.S. Govt. Print. Off., Washington, 75 pp.

Beschta, R., R. Bilby, G. Brown, L. Holtby, and T. Hofstra, 1987. Chapter 6. stream temperature and aquatic habitat: Fisheries and forestry interactions. In Salo, E. and T. Cundy, editors, *Streamside Management: Forestry and Fishery Interactions*. University of Washington, Institute of Forest Resources. Contribution No. 57, pp. 191-232.

Beschta, R. L. and R. L. Taylor, 1988. Stream temperature increases and land use in a Forested Oregon Watershed. *Water Resources Bulletin*, 24(1):19–25.

Beven, K. J. and M. J. Kirkby, 1993. *Channel Network Hydrology*. Wiley, Chichester, New York, 319 pp.

Bourges, B., 1985. Improvement in solar declination computation. *Solar Energy*, 35(4):367–369.

Bowie, G. L., W. B. Mills, D. B. Porcella, C. L. Campbell, J. R. Pagenkopf, G. L. Rupp, K. M. Johnson, P. W. Chan, and S. A. Gherini, 1985. Rates, Constants, and Kinetics Formulations in Surface Water Quality Modeling (Second Edition). Technical Report

EPA/600/3-85/040, Environmental Research Laboratory, Office of Research and Development, U.S. Environmental Protection Agency,, Athens, GA 30613, 455 pp.

Brown, G., 1969. Predicting temperatures of small streams. *Water Resources Research*, 5(1):68–75.

Brown, G., 1970. Predicting the effect of clearcutting on stream temperature. *Soil and Water Conservation*, 25:11–13.

Brown, G. W. and J. T. Krygier, 1967. Changing water temperatures in small mountain streams. *Soil and Water Conservation*, (11-12):242–244.

Brown, G. W. and J. T. Krygier, 1970. Effects of clear-cutting on stream temperature. *Water Resources Research*, 6(4):1133–1139.

Brown, L. and T. Barnwell, 1987. Computer program documentation for the enhanced Stream Water Quality Model QUAL2E and QUAL2E-UNCAS. Technical Report Rep. No. EPA-600/3-87/007, Environmental Research Laboratory, U.S. EPA, Athens, GA.

Caissie, D., N. El-Jabi, and M. G. Satish, 2001. Modelling of maximum daily water temperatures in a small stream using air temperatures. *Journal of Hydrology*, 251(1-2):14–28.

Campolo, M., P. Andreussi, and A. Soldati, 2002. Water quality control in the river Arno. *Water Research*, 36(10):2673–2680.

Caruso, B. S., 2002. Temporal and spatial patterns of extreme low flows and effects on stream ecosystems in Otago, New Zealand. *Journal of Hydrology*, 257(1-4):115–133.

Chapra, S. C., 1997. *Surface Water-Quality Modeling*. McGraw-Hill, New York, 844 pp.

Chapra, S. C. and G. J. Pelletier, 2003. QUAL2K: A Modeling Framework for Simulating River and Stream Water Quality Documentation and Users Manual. Civil and Environmental Engineering Dept., Tufts University, Medford, MA, 121pp. Web: `http://www.epa.gov/ATHENS/wwqtsc/html/qual2k.html`.

Chaudhry, M. H., 1993. *Open-Channel Flow*. Prentice-Hall, Englewood Cliffs, N.J., 483 pp.

Chaudhury, R. R., J. A. H. Sobrinho, R. M. Wright, and M. Sreenivas, 1998. Dissolved oxygen modeling of the Blackstone River (northeastern United States). *Water Research*, 32(8):2400–2412.

Chen, J. Y., C. H. Ko, S. Bhattacharjee, and M. Elimelech, 2001. Role of spatial distribution of porous medium surface charge heterogeneity in colloid transport. *Colloids and Surfaces A: Physicochemical and Engineering Aspects*, 191(1-2):3–15.

Chen, Y. D., R. F. Carsel, S. C. McCutcheon, and W. L. Nutter, 1998. Stream temperature simulation of forested riparian areas: I. Watershed-scale model development. *Journal of Environmental Engineering*, 124(4):304–315.

Christie, C. and H. Regier, 1988. Measurements of optimal habitat and their relationship to yields for four commercial fish species. *Canadian Journal of Fisheries and Aquatic Science*, 45:301–314.

Coutant, C. C., 1987. Thermal preference - When does an asset become a liability. *Environmental Biology of Fishes*, 18(3):161–172.

Cox, B. A., 2003a. A review of currently available in-stream water-quality models and their applicability for simulating dissolved oxygen in lowland rivers. *The Science of The Total Environment*, 314-316:335–377.

Cox, B. A., 2003b. A review of dissolved oxygen modelling techniques for lowland rivers. *The Science of The Total Environment*, 314-316:303–334.

Crittenden, R. N., 1978. Sensitivity analysis of a theoretical energy balance model for water temperatures is small streams. *Ecological Modelling*, 5(3):207–224.

Darley, W. M., 1982. *Algal biology : A physiological approach*. Blackwell Scientific Publications, Blackwell Mosby Book Distributors, Oxford, Boston, St. Louis, MO, 168 pp.

De Smedt, F., W. Brevis, and P. Debels, 2005. Analytical solution for solute transport resulting from instantaneous injection in streams with transient storage. *Journal of Hydrology*, 315(1-4):25–39.

Dehghan, M., 2004a. Numerical schemes for one-dimensional parabolic equations with nonstandard initial condition. *Applied Mathematics and Computation*, 147(2):321–331.

Dehghan, M., 2004b. Weighted finite difference techniques for the one-dimensional advection-diffusion equation. *Applied Mathematics and Computation*, 147(2):307–319.

Dehghan, M., 2005. Efficient techniques for the second-order parabolic equation subject to nonlocal specifications. *Applied Numerical Mathematics*, 52(1):39–62.

Di Toro, D. M., J. J. Fitzpatrick, R. V. Thomann, and I. Hydroscience, 1983. Water Quality Analysis Simulation Program (WASP) and Model Verification Program (MVP) - Documentation. Technical Report EPA-600/3-81-044, Hydroscience, Inc., Westwood, NJ. for USEPA, Duluth, MN, Contract No. 68-01-3872, 156 pp. Web: `http://dspace.udel.edu:8080/dspace/handle/19716/1450`.

Diasty, R. E., 1998. Variable positioning of the sun using time duration. *Renewable Energy*, 14(1-4):185–191.

Fanning, J. L., 1999. Water use in coastal Georgia by county and source, 1997; and water-use trends, 1980-97. Georgia Geologic Survey Information Circular 104, U.S. Geological Survey, Atlanta, GA, 37 pp. Web: `http://ga.water.usgs.gov/pubs/other/ggs-ic104/`.

Gaffield, S. J., K. W. Potter, and L. Z. Wang, 2005. Predicting the summer temperature of small streams in Southwestern Wisconsin. *Journal of the American Water Resources Association*, 41(1):25–36.

Garg, H. P. and G. Datta, 1993. Fundamentals and characteristics of solar radiation. *Renewable Energy*, 3(4-5):305–319.

Gerald, C. F. and P. O. Wheatley, 1989. *Applied numerical analysis*. Addison-Wesley Pub. Co., Reading, Mass. 679 pp.

Gerald, C. F. and P. O. Wheatley, 2004. *Applied Numerical Analysis*. Pearson/Addison-Wesley, Boston, 609 pp.

Gilvear, D. J., K. V. Heal, and A. Stephen, 2002. Hydrology and the ecological quality of Scottish river ecosystems. *The Science of The Total Environment*, 294(1-3):131–159.

Gooseff, M., K. Strzepek, and S. Chapra, 2005. Potential effect of climate change on water temperature downstream of a reservoir: Lower Madison River, Montana. *Climatic Change*, 68(3):331–353.

Gulliver, J. S. and H. G. Stefan, 1984. Stream productivity analysis with dorm–I : Development of computational model. *Water Research*, 18(12):1569–1576.

Hayes, L., M. Maslia, and W. Meeks, 1983. Hydrology and model evaluation of the principal artesian aquifer, Dougherty Plain, southwest Georgia. Georgia Geologic Survery Bulletin 97, 93 pp.

Hendricks, S. P. and D. S. White, 1988. Hummocking by Lotic Chara: Observations on alterations of hyporheic temperature patterns. *Aquatic Botany*, 31(1-2):13–22.

Hewlett, J. D. and J. C. Fortson, 1982. Stream temperature under an inadequate buffer strip in the Southeast Piedmont. *Water Resources Bulletin*, 18(6):983–988.

Higashino, M. and H. G. Stefan, 2005. Sedimentary microbial oxygen demand for laminar flow over a sediment bed of finite length. *Water Research*, 39(14):3153–3166.

Hinkle, S. R., J. H. Duff, F. J. Triska, A. Laenen, E. B. Gates, K. E. Bencala, D. A. Wentz, and S. R. Silva, 2001. Linking hyporheic flow and nitrogen cycling near the Willamette River – a large river in Oregon, USA. *Journal of Hydrology*, 244(3-4):157–180.

Horne, A. J. and C. R. Goldman, 1994. *Limnology, 2nd Edition*. McGraw-Hill, New York, 576 pp.

Hostetler, S. W., 1991. Analysis and modeling of long-term stream temperatures on the Steamboat Creek Basin, Oregon. *Journal of the American Water Resources Association*, 27(4):637–647.

Hyatt, J. A. and P. M. Jacobs, 1996. Distribution and morphology of sinkholes triggered by flooding following Tropical Storm Alberto at Albany, Georgia, USA. *Geomorphology*, 17(4):305–316.

James, A., 1984. *An Introduction to Water Quality Modelling*. Wiley, Chichester, West Sussex, New York, 234 pp.

Jobson, H., 1977. Bed conduction computation for thermal models. *Journal of the Hydraulics Division, American Society of Civil Engineers*, 103(HY10):1213–1217.

Johnson, P. M., A. E. Liner, S. W. Golladay, and W. K. Michener, 2001. Effects of drought on freshwater mussels and instream habitat in Coastal Plain tributaries of the Flint River, southwest Georgia (July-October, 2000). Presented to The Nature Conservancy Apalachicola River and Bay Project, Jones Ecological Research Center, Route 2 Box 2324, Newton, GA, 34 pp. Web: `http://www.jonesctr.org/research/aquatics_research/final_report2.pdf`.

Jonsson, K., H. Johansson, and A. Worman, 2003. Hyporheic exchange of reactive and conservative solutes in streams–tracer methodology and model interpretation. *Journal of Hydrology*, 278(1-4):153–171.

Jury, W. A. and K. Roth, 1990. *Transfer Functions and Solute Movement Through Soil : Theory and Applications*. Birkhuser Verlag, Basel, Boston, 226 pp.

Karim, M. R., M. Sekine, and M. Ukita, 2003. A model of fish preference and mortality under hypoxic water in the coastal environment. *Marine Pollution Bulletin*, 47(1-6):25–29.

Kayombo, S., T. S. A. Mbwette, A. W. Mayo, J. H. Y. Katima, and S. E. Jorgensen, 2000. Modelling diurnal variation of dissolved oxygen in waste stabilization ponds. *Ecological Modelling*, 127(1):21–31.

Knowles, G. and A. C. Wakeford, 1978. A mathematical deterministic river-quality model. Part 1: Formulation and description. *Water Research*, 12(12):1149–1151.

Krajewski, W. F., A. K. Kraszewski, and W. J. Grenney, 1982. A graphical technique for river water temperature predictions. *Ecological Modelling*, 17(3-4):209–224.

LeBlanc, R. T., R. D. Brown, and J. E. FitzGibbon, 1997. Modeling the effects of land use change on the water temperature in unregulated urban streams. *Journal of Environmental Management*, 49(4):445–469.

Lees, M., L. Camacho, and P. Whitehead, 1998. Extension of the QUASAR river water quality model to incorporate dead-zone mixing. *Hydrology and Earth System Sciences*, 2:353–365.

Leonard, B. P., 1979. A stable and accurate convective modelling procedure based on quadratic upstream interpolation. *Comput. Meth. Appl. Mech. Eng.*, 19:59–98.

Li, G. and C. R. Jackson, 2003. Physical and chemical characteristics of streams in the dougherty plain. In Hatcher, K. J., editor, *Proceedings of the 2003 Georgia Water Resources Conference, April 23-24, 2003*, University of Georgia.

Li, G. and C. R. Jackson, 2006. *Development of a Dynamic Dissolved Oxygen and Temperature Model with Groundwater Interactions*. Ph.D. Dissertation, University of Georgia, Athens, GA.

Lin, Y. C., M. S. Chang, and J. M. A. Medina, 2005. A methodology for solute transport in unsteady, nonuniform streamflow with subsurface interaction. *Advances in Water Resources*, 28(8):871–883.

Lind, O. T., 1985. *Handbook of Common Methods in Limnology, 2nd Edition.* Kendall/Hunt Pub. Co., Dubuque, Iowa, 199 pp.

Litrico, X. and V. Fromion, 2004. Analytical approximation of open-channel flow for controller design . *Applied Mathematical Modelling*, 28(7):677–695.

Litrico, X., V. Fromion, J.-P. Baume, C. Arranja, and M. Rijo, 2005. Experimental validation of a methodology to control irrigation canals based on Saint-Venant equations. *Control Engineering Practice*, 13(11):1425–1437.

Liu, W. C., S. Y. Liu, M. H. Hsu, and A. Y. Kuo, 2005. Water quality modeling to determine minimum instream flow for fish survival in tidal rivers. *Journal of Environmental Management*, 76(4):293–308.

Lopes, L. F. G., J. S. A. Do Carmo, R. M. Vitor Cortes, and D. Oliveira, 2004. Hydrodynamics and water quality modelling in a regulated river segment: application on the instream flow definition. *Ecological Modelling*, 173(2-3):197–218.

Maidment, D. R., 1993. *Handbook of Hydrology.* McGraw-Hill, New York, 1424 pp.

Martinez, C. J. and W. R. Wise, 2003. Analysis of constructed treatment wetland hydraulics with the transient storage model OTIS. *Ecological Engineering*, 20(3):211–222.

Matthews, W. J., 1998. *Patterns in Freshwater Fish Ecology.* Chapman and Hall, New York, 756 pp.

McCuen, R. H., 1998. *Hydrologic analysis and design.* Prentice Hall, Upper Saddle River, N.J.

Miller, A. C. and B. S. Payne, 2004. Reducing risks of maintenance dredging on freshwater mussels (Unionidae) in the Big Sunflower River, Mississippi. *Journal of Environmental Management*, 73(2):147–154.

Moatar, F., J. Miquel, and A. Poirel, 2001. A quality-control method for physical and chemical monitoring data. Application to dissolved oxygen levels in the river Loire (France). *Journal of Hydrology*, 252(1-4):25–36.

Mohseni, O. and H. Stefan, 1998. A non-linear regression model for weekly stream temperatures. *Water Resources Research*, 34(10):2685–2692.

Mohseni, O. and H. G. Stefan, 1999. Stream temperature/air temperature relationship: a physical interpretation. *Journal of Hydrology*, 218(3-4):128–141.

Moore, R. D., D. L. Spittlehouse, and A. Story, 2005. Riparian microclimate and stream temperature response to forest harvesting: A review. *Journal of the American Water Resources Association*, 41(4):813–834.

Morton, K. and D. Mayers, 1994. *Numerical Solution of Partial Differential Equations: An introduction*. Cambridge University Press, Cambridge, New York, 227 pp.

Mosner, M. M., 2002. Stream-Aquifer Relations and the Potentiometric Surface of the Upper Floridan Aquifer in the Lower Apalachicola-Chattahoochee-Flint River Basin in parts of Georgia, Florida, and Alabama, 1999-2000. Water-Resources Investigations Report 02-4244, U.S. Geological Survey, 51 pp. Web: `http://ga.water.usgs.gov/pubs/wrir/wrir02-4244/`.

O'Loughlin, E. M. and K. H. Bowmer, 1975. Dilution and decay of aquatic herbicides in flowing channels. *Journal of Hydrology*, 26(3-4):217–235.

Orlob, G. T., 1983. *Mathematical modeling of water quality: streams, lakes, and reservoirs*. Wiley, Chichester, New York.

Park, S. S. and P. R. Jaffe, 1999. A numerical model to estimate sediment oxygen levels and demand. *Journal of Environmental Quality*, 28(4):1219–1226.

Park, S. S. and Y. S. Lee, 1996. A multiconstituent moving segment model for water quality predictions in steep and shallow streams. *Ecological Modelling*, 89(1-3):121–131.

Park, S. S. and C. G. Uchrin, 1988. A numerical mixing zone model for water quality assessment in natural streams: Conceptual development. *Ecological Modelling*, 42(3-4):233–244.

Parkhill, K. L. and J. S. Gulliver, 1999. Modeling the effect of light on whole-stream respiration. *Ecological Modelling*, 117(2-3):333–342.

Parr, L. B., R. G. Perkins, and C. F. Mason, 2002. Reduction in photosynthetic efficiency of *Cladophora glomerata*, induced by overlying canopies of *Lemna spp*. *Water Research*, 36(7):1735–1742.

Pearson, N. and N. O. Crossland, 1996. Measurement of community photosynthesis and respiration in outdoor artificial streams. *Chemosphere*, 32(5):913–919.

Penrod, E. B. and K. V. Prasanna, 1962. Design of a flat-plate collector for a solar earth heat pump. *Solar Energy*, 6(1):9–22.

Power, G., R. Brown, and J. Imhof, 1999. Groundwater and fish - Insights from northern North America. *Hydrological Processes*, 13(3):401–422.

Priest, S., 2004. Evaluation of Ground-Water Contribution to Streamflow in Coastal Georgia and Adjacent Parts of Florida and South Carolina. Scientific Investigations Report 2004-5265, U.S. Department of the Interior; U.S. Geological Survey. Prepared in cooperation with the Georgia Department of Natural Resources, EPA, Atlanta, Georgia, 50 pp. Web: `http://pubs.usgs.gov/sir/2004/5265/`.

Rauch, W., M. Henze, L. Koncsos, P. Reichert, P. Shanahan, L. Somlyody, and P. Vanrolleghem, 1998. River water quality modelling: I. State of the art. *Water Science and Technology*, 38(11):237–244.

Richter, B. D., D. P. Braun, M. A. Mendelson, and L. L. Master, 1997. Threats to imperiled freshwater fauna. *Conservation Biology*, 11(5):1081–1093.

Runkel, R. L., 1998. One-dimensional transport with inflow and storage (OTIS): a solute transport model for streams and rivers. Water-Resources Investigations Report 98-4018, U.S. Geological Survey, Denver, Colorado, 80 pp. Web: `http://co.water.usgs.gov/otis/documentation/primary/wrir98-4018.pdf`.

Rutherford, J. C., S. Blackett, C. Blackett, L. Saito, and R. J. Davies-Colley, 1997. Predicting the effects of shade on water temperature in small streams. *New Zealand Journal of Marine and Freshwater Research*, 31:707–721.

Sabo, M. J., C. F. Bryan, W. E. Kelso, and D. A. Rutherford, 1999. Hydrology and aquatic habitat characteristics of a riverine swamp: I. Influence of flow on water temperature and chemistry. *Regulated Rivers: Research and Management*, 15(6):505–523.

Saltelli, A., 2004. *Sensitivity analysis in practice : a guide to assessing scientific models*. Wiley, Hoboken, NJ.

Schreier, H., W. Erlebach, and L. Albright, 1980. Variations in water quality during winter in two Yukon rivers with emphasis on dissolved oxygen concentration. *Water Research*, 14(9):1345–1351.

Sincock, A. M., H. S. Wheater, and P. G. Whitehead, 2003. Calibration and sensitivity analysis of a river water quality model under unsteady flow conditions. *Journal of Hydrology*, 277(3-4):214–229.

Sinokrot, B. A. and J. S. Gulliver, 2000. In-stream flow impact on river water temperatures. *Journal of Hydraulic Research*, 38(5):339–349.

Sinokrot, B. A. and H. Stefan, 1993. Stream temperature dynamics: Measurements and modeling. *Water Resources Research*, 29(7):2299–2312.

Skidmore, R. E., S. C. Maberly, and B. A. Whitton, 1998. Patterns of spatial and temporal variation in phytoplankton chlorophyll a in the River Trent and its tributaries. *The Science of The Total Environment*, 210-211:357–365.

Sousa, E. and I. Sobey, 2002. On the influence of numerical boundary conditions. *Applied Numerical Mathematics*, 41(2):325–344.

Sridhar, V., A. L. Sansone, J. LaMarche, T. Dubin, and D. P. Lettenmaier, 2004. Prediction of stream temperature in forested watersheds. *Journal of the American Water Resources Association*, 40(1):197–213.

Stamou, A. I., 1992. Improving the numerical modeling of river water quality by using high order difference schemes. *Water Research*, 26(12):1563–1570.

Stefan, H. G. and X. Fang, 1994. Dissolved oxygen model for regional lake analysis. *Ecological Modelling*, 71(1-3):37–68.

Stefan, H. G., J. S. Gulliver, M. G. Hahn, and A. Y. Fu, 1980. Water Temperature Dynamics in Experimental Field Channels: Analysis and Modeling,. Project report no. 193, Prepared for Environmental Research Laboratory, EPA, Duluth, 171 pp.

Stefan, H. G. and E. B. Preudhomme, 1993. Stream Temperature Estimation from Air-Temperature. *Water Resources Bulletin*, 29(1):27–45.

Sturm, T. W., 2001. *Open Channel Hydraulics*. McGraw-Hill, Boston, 493 pp.

Sullivan, K. and T. A. Adams., 1990. An analysis of temperature patterns in stream environments based on physical principles and field data. Weyerhaeuser tech. report.

Sullivan, K., J. Tooley, K. Doughty, J. Caldwell, and P. Knudsen, 1990. Evaluation of prediction models and characterization of stream temperature regimes in Washington. Timber/Fish/Wildlife Rep. No. TFW-WQ3-90-006, Washington Dept. Nat. Resources, Olympia, Washington, 224 pp.

Supriyasilp, T., A. J. Graettinger, and S. R. Durrans, 2003. Quantitatively directed sampling for main channel and hyporheic zone water-quality modeling. *Advances in Water Resources*, 26(9):1029–1037.

Tang, R. and Y. Etzion, 2004. Comparative studies on the water evaporation rate from a wetted surface and that from a free water surface. *Building and Environment*, 39(1):77–86.

Tang, R., Y. Etzion, and I. A. Meir, 2004. Estimates of clear night sky emissivity in the Negev Highlands, Israel. *Energy Conversion and Management*, 45(11-12):1831–1843.

Taniguchi, M., J. Shimada, T. Tanaka, I. Kayane, Y. Sakura, Y. Shimano, S. Dapaah-Siakwan, and S. Kawashima, 1999a. Disturbances of temperature-depth profiles due to surface climate change and subsurface water flow: 1. An effect of linear increase in surface temperature caused by global warming and urbanization in the Tokyo metropolitan area, Japan. *Water Resources Research*, 35(5):1507–1517.

Taniguchi, M., D. R. Williamson, and A. J. Peck, 1999b. Disturbances of temperature-depth profiles due to surface climate change and subsurface water flow: 2. An effect of step increase in surface temperature caused by forest clearing in southwest Western Australia. *Water Resources Research*, 35(5):1519–1529.

Taylor, G. I., 1953. Dispersion of Soluble Matter in Solvent Flowing Slowly through a Tube. *Royal Society of London Proceedings Series A*, 219:186–203.

Theurer, F., K. Voos, and W. Miller, 1984. Instream water temperature model. Instream flow information paper no. 16, USDA Fish and Wildlife Service, Cooperative Instream Flow Service Group, Fort Collins, CO.

Thomee, V., 2001. From finite differences to finite elements: A short history of numerical analysis of partial differential equations. *Journal of Computational and Applied Mathematics*, 128(1-2):1–54.

Torak, L. J., G. S. Davis, G. Strain, and J. Herndon, 1996. Geohydrology and evaluation of stream-aquifer relations in the Apalachicola-Chattahoochee-Flint River Basin, southeastern Alabama, northwestern Florida, and southwestern Georgia. Water-Supply Paper 2460, U.S. Geological Survey, 95 pp. Web: `http://ga.water.usgs.gov/publications/abstracts/wsp2460.html`.

TVA, 1972. Heat and mass transfer between a water surface and the atmosphere. Water Resources Laboratory Report 14, Norris, Tennessee Valley Authority.

USGS, 2000. Droughts in Georgia. Technical report. Web: `http://ga.water.usgs.gov/publications/ofr00-380.pdf`.

Van Orden, G. N. and C. G. Uchrin, 1993. The study of dissolved oxygen dynamics in the Whippany river, New Jersey using the QUAL2E model. *Ecological Modelling*, 70(1-2):1–17.

Wang, H., M. Hondzo, C. Xu, V. Poole, and A. Spacie, 2003. Dissolved oxygen dynamics of streams draining an urbanized and an agricultural catchment. *Ecological Modelling*, 160(1-2):145–161.

Warner, D., J. A. Easoz, and S. Priest, 2002. Ground-Water-Quality Data for Albany and Surrounding Areas, Southwest Georgia, 1951-99. U.S. Geological Survey Open-File Report 02-124, in cooperation with Albany Water, Gas, and Light Commission, Atalanta, GA, 11 pp. Web: `http://ga.water.usgs.gov/publications/ofr02-124/ofr02-124.pdf`.

Warner, D. and S. J. Lawrence, 2005. Ground-Water Flow and Water Quality in the Upper-Floridan Aquifer, Southwestern Albany Area, Georgia, 1998 - 2001. Scientific Investigations Report 2005-5047, U.S. Department of the Interior, U.S. Geological Survey, 77 pp. Web: `http://pubs.usgs.gov/sir/2005/5047/`.

Whitehead, P. G., R. J. Williams, and D. R. Lewis, 1997. Quality simulation along river systems (QUASAR): model theory and development. *Science of The Total Environment*, 194-195:447–456.

Williams, R. J., C. White, M. L. Harrow, and C. Neal, 2000. Temporal and small-scale spatial variations of dissolved oxygen in the Rivers Thames, Pang and Kennet, UK. *The Science of The Total Environment*, 251-252:497–510.

Wool, T. A., R. B. Ambrose, J. L. Martin, and E. A. Comer, 2001. Water Quality Analysis Simulation Program (WASP) Version 6.0 - DRAFT: User's Manual. Technical report, US Environmental Protection Agency, Atlanta, GA, 267 pp. Web: `http://www.epa.gov/athens/wwqtsc/html/wasp.html`.

Young, P. and B. Beck, 1974. The modelling and control of water quality in a river system. *Automatica*, 10(5):455–468.

Zeng, W., 2000. *A Model For Understanding And Managing The Impacts Of Sediment Behavior On River Water Quality*. PhD thesis, University of GA, Athens, GA, 244 pp. Web: `http://getd.galib.uga.edu/public/zeng_wei_200012_phd/zeng_wei_200012_phd.pdf`.

Zeng, W. and M. B. Beck, 2003. STAND, a dynamic model for sediment transport and water quality. *Journal of Hydrology*, 277(1-2):125–133.

Zeng, X., 2001. *Water Quality Modeling in Southeastern Lake Management: A Case Study of Lake Lanier, Georgia*. PhD thesis, University of GA, Athens, GA, 345 pp. Web: `http://getd.galib.uga.edu/hold5yr/zeng_xiao-qing_200112_phd/zeng_xiao-qing_200112_phd.pdf`.

Zeng, X., T. C. Rasmussen, M. B. Beck, A. K. Parker, and Z. Lin, 2005. A biogeochemical model for metabolism and nutrient cycling in a Southeastern Piedmont impoundment. *Environmental Modelling and Software*, In Press.

Zheng, L., C. Chen, and F. Y. Zhang, 2004. Development of water quality model in the Satilla River Estuary, Georgia. *Ecological Modelling*, 178(3-4):457–482.

Appendix A

Model Formulations

A.1 CSTR based model formulations

The CSTR model assumes immediate and perfect mixing. The state variable in output flow is exactly the same as that inside the tank. The diffusion is thought insignificant and often neglected. Based on CSTR model assumptions, the stream reach is segmented into a series of continuously connected CSTRs (Figure A.1).

Flow module

Based on mass balance, the changing rate of the volume for each CSTR is governed by the upstream and tributary inputs, streambed groundwater infiltration, and downstream output. In the formulation, the tributary flow is combined to the upstream input, while The groundwater flow is considered separately:

$$\frac{dV}{dt} = Q_{in} - Q + Q_g \tag{A.1}$$

where, V is water volume inside the CSTR (m); t is time (s); Q_{in} is upstream discharge into the CSTR (m^3/s); Q is downstream outflow discharge out of the CSTR (m^3/s); Q_g is groundwater discharge (m^3/s), positive for a gaining stream and negative for a losing stream;

Equation A.1 requires the following relationships to be solvable:

$$V = AL \tag{A.2a}$$

$$A = \frac{Q}{U} \tag{A.2b}$$

$$U = aQ^b \tag{A.2c}$$

where, A is cross section area (m^2); L is length of the CSTR (m); U is flow velocity (m/s); a and b are coefficients describing relationships between flow velocity and discharge (dimensionless);

Substitute equation A.2a into A.1 and rearrange, the CSTR type streamflow module takes the following form:

$$\frac{dQ}{dt} = \frac{aQ^b}{(1-b)L}(Q_{in} - Q + Q_g) \tag{A.3}$$

Temperature module

Similarly, based on energy balance theory, the CSTR type stream temperature module can be represented as below:

$$\frac{dVT}{dt} = Q_{in}T_{in} - QT + Q_gT_g|_{z\to 0} + A_{bed}\frac{K_{bed}}{C_p}\frac{dT_g}{dz}|_{z\to 0} + A_{surf}\frac{E_s + E_L + E_v + E_c}{C_p} \tag{A.4}$$

where, T is stream water temperature (°C); T_{in} is water temperature of upstream inflow (°C); T_g is ground water temperature in streambed (°C); A_{bed} is streambed surface area of the CSTR (m^2); K_{bed} is streambed heat conductivity (W m^{-1} °C^{-1})); A_{surf} is stream water surface area of a CSTR (m^2); E_s is solar radiation rate (W m^{-2}); E_L is long wave radiation rate (W m^{-2}); E_v is evaporative heat flux rate (W m^{-2}); E_c is convective heat flux rate (W m^{-2}); C_p is volumetric heat capacity of water (J m^{-3} °C^{-1}).

Equation A.4 can be simplified if the following equations are substituted in:

$$\tau = \frac{V}{Q}; \quad \tau_1 = \frac{V}{Q_{in}}; \quad \tau_2 = \frac{V}{Q_g} \tag{A.5a}$$

$$h = \frac{V}{A_{surf}} \approx \frac{V}{A_{bed}} \tag{A.5b}$$

$$D_{T_{bed}} = \frac{K_{bed}}{C_p} \tag{A.5c}$$

where, τ, τ_1, and τ_2 are residence time of residence time of overall flow, upstream inflow, and groundwater infiltration flow respectively (s), and satisfy $\tau = \frac{\tau_1\tau_2}{\tau_1+\tau_2}$; h is hydraulic mean depth (m); $D_{T_{bed}}$ is the effective heat diffusivity of streambed (m^2/s);

The combination of equations (A.4) and (A.4) yields,

$$\frac{dT}{dt} = \frac{T_{in}}{\tau_1} + \frac{T_g}{\tau_2}|_{z\to 0} - \frac{T}{\tau} + \frac{1}{h}(D_{T_{bed}}\frac{dT_g}{dz}|_{z\to 0} + \frac{E_s + E_L + E_v + E_c}{C_p}) \tag{A.6}$$

DO module

Similarly, stream DO module takes the following form:

$$\frac{dC}{dt} = \frac{C_{in}}{\tau_1} + \frac{C_g}{\tau_2}|_{z\to 0} - \frac{C}{\tau} + \frac{1}{h}D_{C_g}\frac{dC_g}{dz}|_{z\to 0} + P_k + P_a - R_a - R_b - Rs \tag{A.7}$$

where, C is dissolved oxygen concentration in stream (mg/L); C_{in} is oxygen level of upstream inflow (mg/L); C_g is oxygen level of groundwater infiltration flow (mg/L); D_{C_g} is effective oxygen diffusivity in groundwater flow (m^2/s); P_k is reaeration rate (mg L^{-1} s^{-1}); P_a is algal photosynthesis rate (mg L^{-1} s^{-1}); R_a is algal respiration rate (mg L^{-1} s^{-1}); R_b is BOD decay rate (mg L^{-1} s^{-1}); R_s is SOD decay rate (mg L^{-1} s^{-1}).

A.2 ADRE based model formulations

Flow module

Open channel flow is simulated with Saint-Venant equations (Sturm, 2001, P_{267}; Chaudhry, 1993, P_{278}):

$$\frac{\partial A}{\partial t} + \frac{\partial Q}{\partial x} - q_g = 0 \tag{A.8a}$$

$$\frac{\partial Q}{\partial t} + \frac{\partial}{\partial x}(\frac{Q^2}{A}) + gA\frac{\partial h}{\partial x} - gA(S_0 - S_f) - q_g U_g cos(\varphi) = 0 \tag{A.8b}$$

where, A is stream cross section area (m^2); Q is stream discharge (m^3/s); q_g is effective groundwater discharge per unit stream reach length, positive for a gaining stream, and negative for a losing stream (m^2/s); t is time (s); x is longitudinal distance (m); g is gravity acceleration (m/s^2); h is hydraulic mean depth (m); S_0 is streambed gradient (dimensionless); S_f is friction slope (dimensionless); U_g is Darcy velocity of groundwater infiltration flow (m/s); φ is the angle between the groundwater flow direction and surface flow direction (rad).

Friction slope in equation (A.8b) is usually modeled with Manning-Strickler formula (Litrico and Fromion, 2004; Litrico *et al.*, 2005):

$$S_f = \frac{n^2|Q|Q}{A^2R^{4/3}} \tag{A.9}$$

where, n is Manning's roughness coefficient (dimensionless); R is hydraulic radius (m), defined as $R = \frac{A}{P}$, where P is wetted perimeter (m).

Plug equation (A.9) into (A.8), approximate $dA = Bdh$, where B is stream water surface width (m), and rearrange, get,

$$B\frac{\partial h}{\partial t} + \frac{\partial Q}{\partial x} - q_L = 0 \tag{A.10a}$$

$$\frac{\partial Q}{\partial t} + \frac{\partial}{\partial x}(\frac{Q^2}{A}) + gA(\frac{\partial h}{\partial x} - S_0) + g\frac{n^2|Q|Q}{AR^{4/3}} - q_gU_gcos(\varphi) = 0 \tag{A.10b}$$

Temperature module

The longitudinal stream heat energy dynamics (indicated by temperature T) along a stream is described by the one-dimensional advection-diffusion equation. The energy balance analysis, including ground water interactions, is illustrated in Figure A.2. From the Figure, the following energy balance equation is derived:

$$\frac{\partial A\Delta xTC_p}{\partial t} + \frac{\partial QTC_p}{\partial x}\Delta x = \frac{\partial}{\partial x}(AK_T\frac{\partial T}{\partial x})\Delta x + B\Delta xK_{T_g}\frac{\partial T_g}{\partial z}|_{z\to 0} + q_gB\Delta xC_pT_g|_{z\to 0} \tag{A.11}$$

where, Δx is reach length towards downstream (m); T is water temperature(°C); T_g is groundwater temperature in streambed (°C); C_p is volumetric heat capacity of water (J m^{-3} °C^{-1}); K_T is heat conductivity of water (W m^{-1} °C^{-1})); B is streambed width, which approximately equal to stream surface width for very small side bank slope (m); K_{T_g} is effective heat conductivity of streambed (W m^{-1} °C^{-1}));

Cancel Δx and let $D_T = \frac{K_T}{C_p}$, and $D_{T_g} = \frac{K_{T_g}}{C_p}$ which are effective stream water heat dispersivity and streambed heat diffusivity respectively (m^2/s), then equation (A.11) changes to:

$$\frac{\partial AT}{\partial t} + \frac{\partial QT}{\partial x} = \frac{\partial}{\partial x}(AD_T\frac{\partial T}{\partial x}) + BD_{T_g}\frac{\partial T_g}{\partial z}|_{z\to 0} + q_gBT_g|_{z\to 0} \tag{A.12}$$

The other source or sink terms, such as heat exchanges due to solar radiation (E_s), long wave radiation(E_L), evaporation(E_v), and convection (E_c), which occur at stream water surface, can be added in as below:

$$\frac{\partial AT}{\partial t}+\frac{\partial QT}{\partial x}=\frac{\partial}{\partial x}(AD_T\frac{\partial T}{\partial x})+BD_{T_g}\frac{\partial T_g}{\partial z}|_{z\to 0}+q_gBT_g|_{z\to 0}+\frac{B}{C_p}(E_s+E_L+E_v+E_c) \quad \text{(A.13)}$$

DO module

The longitudinal stream DO mass transportation dynamics (denoted by DO concentration C) is similar as that for stream heat energy dynamics. An illustration of the integrated stream DO mass transportation for a given reach with groundwater interactions is shown in Figure A.3, from which the following mass balance equation is obtained:

$$\frac{\partial A\Delta xC}{\partial t}+\frac{\partial QC}{\partial x}\Delta x=\frac{\partial}{\partial x}(AD_C\frac{\partial C}{\partial x})\Delta x+B\Delta xD_{C_g}\frac{\partial C_g}{\partial z}|_{z\to 0}+q_gB\Delta xC_g|_{z\to 0} \quad \text{(A.14)}$$

where, C is water dissolved oxygen concentration(mg/L); C_g is oxygen concentration of groundwater in streambed (mg/L); D_C and D_{C_g} are effective mass dispersivity in stream water flow and diffusivity in groundwater flow through the streambed respectively (m^2/s).

Cancel Δx, then equation A.14 changes to:

$$\frac{\partial AC}{\partial t}+\frac{\partial QC}{\partial x}=\frac{\partial}{\partial x}(AD_C\frac{\partial C}{\partial x})+BD_{C_g}\frac{\partial C_g}{\partial z}|_{z\to 0}+q_gBC_g|_{z\to 0} \quad \text{(A.15)}$$

The other source or sink terms, including mass exchange due to atmospheric reaeration (P_k), algal photosynthesis (P_a), respriration (R_a), BOD decay (R_b), and SOD decay (R_s), can be added as below:

$$\frac{\partial AC}{\partial t}+\frac{\partial QC}{\partial x}=\frac{\partial}{\partial x}(AD_C\frac{\partial C}{\partial x})+BD_{C_g}\frac{\partial C_g}{\partial z}|_{z\to 0}+q_gBC_g|_{z\to 0}+A(P_k+P_a+R_a+R_b+R_s) \quad \text{(A.16)}$$

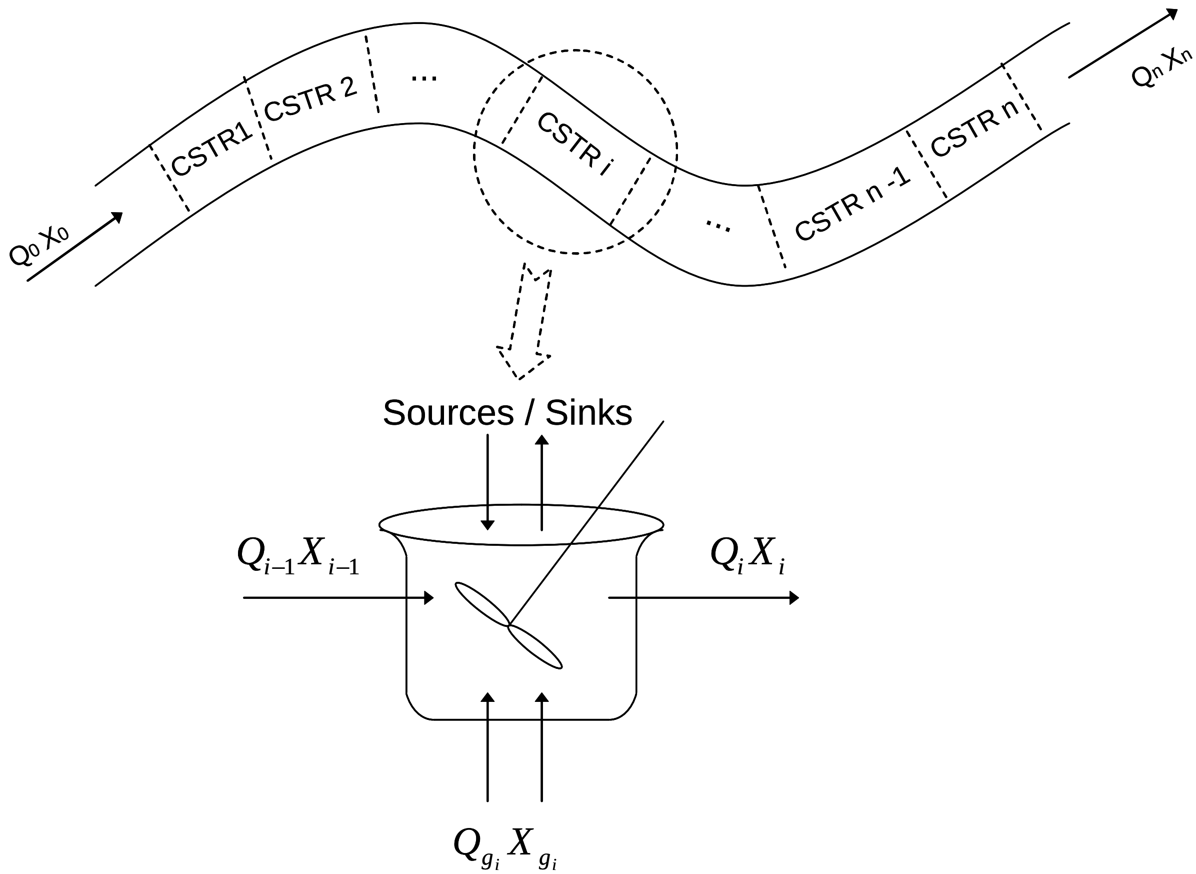

Figure A.1: Schematic of CSTR conceptualization (after Beck and Finney, 1987). Q is stream discharge, X is any state variable of interest, such as temperature or dissolved oxygen. Subscript g means that the indicated variables are for groundwater through streambed.

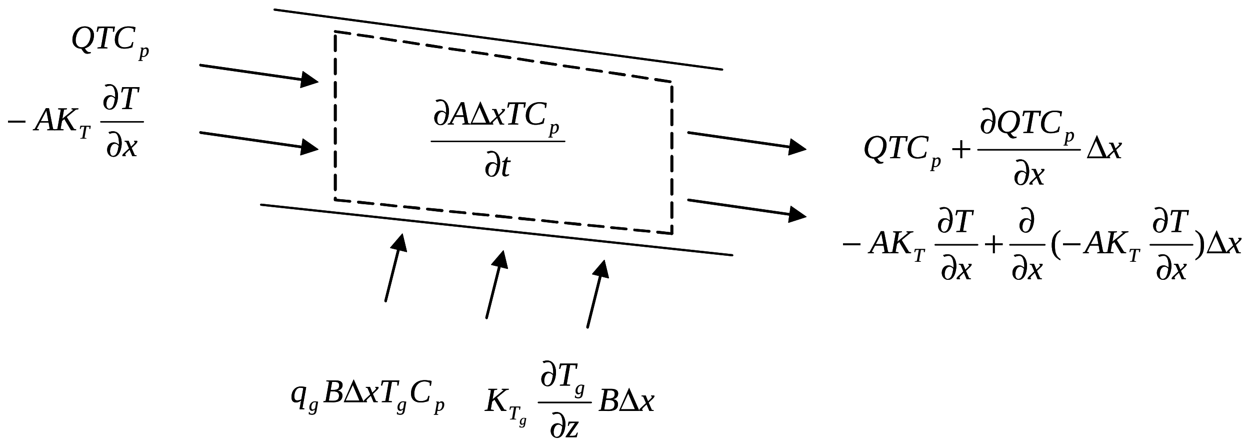

Figure A.2: Schematic of energy transportation along a stream. Where, Q is stream discharge (m^3/s); q_g is effective groundwater discharge per unit stream reach length, positive for a gaining stream, and negative for a losing stream (m^2/s); T is water temperature(°C); T_g is groundwater temperature in streambed (°C); t is time (s); x is longitudinal distance (m); Δx is reach length towards downstream (m); B is streambed width,which approximately equal to stream surface width for very small side bank slope (m); K_T is heat conductivity of water (W m^{-1} °C^{-1})); K_{T_g} is effective heat conductivity of streambed (W m^{-1} °C^{-1})); C_p is volumetric heat capacity of water (J m^{-3} °C^{-1}).

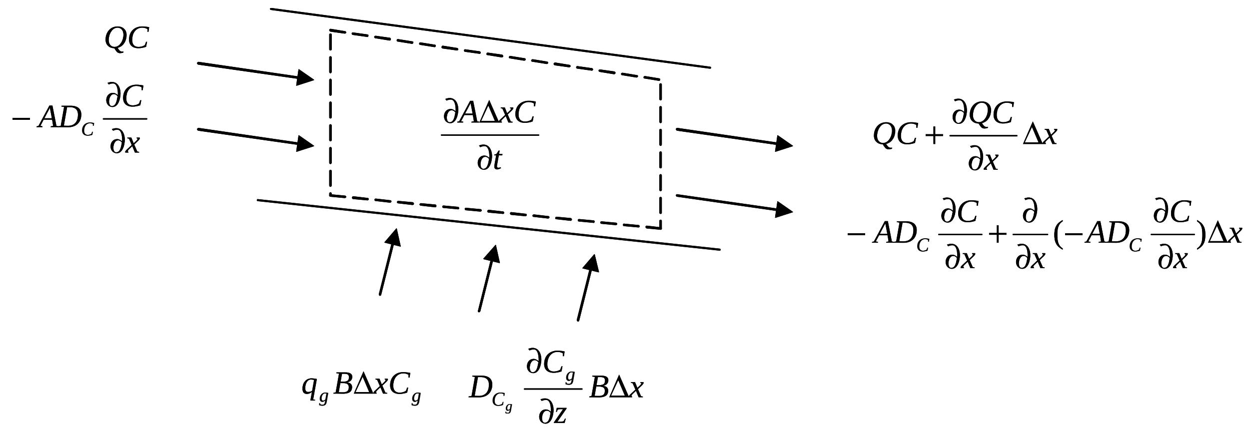

Figure A.3: Schematic of mass transportation along a stream. Where, Q is stream discharge (m^3/s); q_g is effective groundwater discharge per unit stream reach length, positive for a gaining stream, and negative for a losing stream (m^2/s); C is water dissolved oxygen concentration(mg/L); C_g is oxygen concentration of groundwater in streambed (mg/L); D_C and D_{C_g} are effective mass dispersivity in stream water flow and diffusivity in groundwater flow through the streambed respectively (m^2/s); t is time (s); x is longitudinal distance (m); Δx is reach length towards downstream (m); B is streambed width,which approximately equal to stream surface width for very small side bank slope (m).

Appendix B

Numerical Solutions

B.1 Preissmann scheme for solving Saint-Venant equations

Derivation of the scheme

The Preissmann Scheme uses weighted-average discretization for derivative approximation. The spatial and temporal derivatives are evaluated at a point somewhere inside the four points "box" (Fig. B.1), where $f_{i,j}$ denotes any state variable interested at space i and time j. Accordingly, the following equations are used for evulation (Sturm, 2001, P_{315}):

$$\frac{\partial f}{\partial x} = \frac{\theta(f_{i+1}^{j+1} - f_i^{j+1}) + (1-\theta)(f_{i+1}^{j} - f_i^{j})}{\Delta x} \tag{B.1a}$$

$$\frac{\partial f}{\partial t} = \frac{(f_{i+1}^{j+1} + f_i^{j+1}) - (f_{i+1}^{j} + f_i^{j}))}{2\Delta t} \tag{B.1b}$$

$$\bar{f} = \frac{\theta(f_{i+1}^{j+1} + f_i^{j+1}) + (1-\theta)(f_{i+1}^{j} + f_i^{j})}{2} \tag{B.1c}$$

Apply equations (B.1) to equations (A.10), the resulting difference equations are:

$$\bar{B}\frac{h_{i+1}^{j+1} + h_i^{j+1} - h_{i+1}^{j} - h_i^{j}}{2\Delta t} + \frac{\theta(Q_{i+1}^{j+1} - Q_i^{j+1}) + (1-\theta)(Q_{i+1}^{j} - Q_i^{j})}{\Delta x} - q_L = 0 \tag{B.2a}$$

$$\begin{aligned}
&\frac{Q_{i+1}^{j+1} + Q_i^{j+1} - Q_{i+1}^{j} - Q_i^{j}}{2\Delta t} \\
&\quad + \frac{\theta[(\frac{Q^2}{A})_{i+1}^{j+1} - (\frac{Q^2}{A})_{i}^{j+1}] + (1-\theta)[(\frac{Q^2}{A})_{i+1}^{j} - (\frac{Q^2}{A})_{i}^{j}]}{\Delta x} \\
&\quad + g\bar{A}(\frac{\theta(h_{i+1}^{j+1} - h_i^{j+1}) + (1-\theta)(h_{i+1}^{j} - h_i^{j})}{\Delta x} - S_0) \\
&\quad + \frac{gn^2}{\bar{A}\bar{R}^{4/3}}[\frac{\theta}{2}(Q_i^{j+1}|Q_i^{j+1}| + Q_{i+1}^{j+1}|Q_{i+1}^{j+1}|) + \frac{1-\theta}{2}(Q_i^{j}|Q_i^{j}| + Q_{i+1}^{j}|Q_{i+1}^{j}|)] \\
&\quad + q_g U_g cos(\phi) = 0
\end{aligned} \tag{B.2b}$$

Equations (B.2) can be redefined as:

$$G_i(Q_i^{j+1}, h_i^{j+1}, Q_{i+1}^{j+1}, h_i^{j+1}) = 0 \tag{B.3a}$$

$$H_i(Q_i^{j+1}, h_i^{j+1}, Q_{i+1}^{j+1}, h_i^{j+1}) = 0 \tag{B.3b}$$

Apply equations (B.3) to a stream reach with I nodes, get $2(I-1)$ equations, and $2I$ variables. The remaining two equations comes from the two boundary conditions. The upper boundary condition is the upstream flow input, while the downstream boundary assumes longitudinal derivative to be zero:

$$G_0 = Q_1^{j+1} - Q_0^{j+1} = 0 \tag{B.4a}$$

$$G_I = h_I^{j+1} - h_{I+1}^{j+1} = 0 \tag{B.4b}$$

Equations (B.3) and (B.4) completes a nonlinear system that can be solved numerically using Newton-Raphson iteration algorithm. This algorithm is based on Taylor series expansion with truncation of second and higher order derivatives. Let G_i^k denotes k^{th} step estimates at node i, then for step $k+1$, the Taylor series expansion for the multivariate function G takes the following form:

$$G_i^{k+1} \approx G_i^k + \frac{\partial G_i^k}{\partial h_i}(h_i^{k+1} - h_i^k) + \frac{\partial G_i^k}{\partial Q_i}(Q_i^{k+1} - Q_i^k) + \frac{\partial G_i^k}{\partial h_{i+1}}(h_{i+1}^{k+1} - h_{i+1}^k) + \frac{\partial G_i^k}{\partial Q_{i+1}}(Q_{i+1}^{k+1} - Q_{i+1}^k) \tag{B.5}$$

The goal is to obtain $G_i^{k+1} = 0$, Substitute G_i^{k+1} with 0 in equation (B.5), rearrange to yield,

$$\frac{\partial G_i^k}{\partial h_i}(h_i^{k+1} - h_i^k) + \frac{\partial G_i^k}{\partial Q_i}(Q_i^{k+1} - Q_i^k) + \frac{\partial G_i^k}{\partial h_{i+1}}(h_{i+1}^{k+1} - h_{i+1}^k) + \frac{\partial G_i^k}{\partial Q_{i+1}}(Q_{i+1}^{k+1} - Q_{i+1}^k) \approx -G_i^k \tag{B.6}$$

Substitute equation (B.6) into equations (B.3) and (B.4), get the matrix notation of the simultaneous equations:

$$\mathbf{J}\Delta\mathbf{X} = \mathbf{R} \tag{B.7}$$

where, $\mathbf{J}$ is the Jacobian matrix, $\Delta\mathbf{X}$ is step increment vector of unknowns, and $\mathbf{R}$ is residual vector. They take the following forms:

$$\mathbf{J} = \begin{bmatrix} \frac{\partial G_0}{\partial h_1} & \frac{\partial G_0}{\partial Q_1} & & & & & & \\ \frac{\partial G_1}{\partial h_1} & \frac{\partial G_1}{\partial Q_1} & \frac{\partial G_1}{\partial h_2} & \frac{\partial G_1}{\partial Q_2} & & & & \\ \frac{\partial H_1}{\partial h_1} & \frac{\partial H_1}{\partial Q_1} & \frac{\partial H_1}{\partial h_2} & \frac{\partial H_1}{\partial Q_2} & & & & \\ & & \ddots & \ddots & \ddots & & & \\ & & \frac{\partial G_i}{\partial h_i} & \frac{\partial G_i}{\partial Q_i} & \frac{\partial G_i}{\partial h_{i+1}} & \frac{\partial G_i}{\partial Q_{i+1}} & & \\ & & \frac{\partial H_i}{\partial h_i} & \frac{\partial H_i}{\partial Q_i} & \frac{\partial H_i}{\partial h_{i+1}} & \frac{\partial H_i}{\partial Q_{i+1}} & & \\ & & & & \ddots & \ddots & \ddots & \\ & & & & & & \frac{\partial G_I}{\partial h_I} & \frac{\partial G_I}{\partial Q_I} \end{bmatrix}_{2I \times 2I} \tag{B.8}$$

$$\Delta\mathbf{X} = \begin{bmatrix} h_1^{k+1} - h_1^k \\ Q_1^{k+1} - Q_1^k \\ \vdots \\ h_i^{k+1} - h_i^k \\ Q_i^{k+1} - Q_i^k \\ \vdots \\ h_I^{k+1} - h_I^k \\ Q_I^{k+1} - Q_I^k \end{bmatrix}_{2I \times 1} \tag{B.9}$$

$$\mathbf{R} = - \begin{bmatrix} G_0(h_1^k, Q_1^k) \\ G_1(h_1^k, Q_1^k, h_2^k, Q_2^k) \\ H_1(h_1^k, Q_1^k, h_2^k, Q_2^k) \\ \vdots \\ G_i(h_i^k, Q_i^k, h_{i+1}^k, Q_{i+1}^k) \\ H_i(h_i^k, Q_i^k, h_{i+1}^k, Q_{i+1}^k) \\ \vdots \\ G_I(h_I^k, Q_I^k) \end{bmatrix}_{2I \times 1} \tag{B.10}$$

Equation (B.7) gives solution of $\Delta\mathbf{X}$ as below:

$$\Delta\mathbf{X} = \mathbf{J}^{-1}\mathbf{R} \tag{B.11}$$

And the $(k+1)^{th}$ trial values are given by:

$$\mathbf{X}^{k+1} = \mathbf{X}^k + \Delta\mathbf{X} \tag{B.12}$$

The procedure shown by equation (B.11) and (B.12) can be repeated until for the given precision criteria $\delta > 0$, inequation $\Delta = max\{|\frac{X_1^{k+1} - X_1^k}{X_1^k}|, \cdots, |\frac{X_i^{k+1} - X_i^k}{X_i^k}|, \cdots, |\frac{X_I^{k+1} - X_I^k}{X_I^k}|\} < \delta$ is met.

Jacobian matrix calculation

From equation (B.2a), get,

$$\frac{\partial G_i}{\partial h_i^{j+1}} = \bar{B}; \tag{B.13a}$$

$$\frac{\partial G_i}{\partial Q_i^{j+1}} = -\frac{2\Delta t}{\Delta x}\theta; \tag{B.13b}$$

$$\frac{\partial G_i}{\partial h_{i+1}^{j+1}} = \bar{B}; \tag{B.13c}$$

$$\frac{\partial G_i}{\partial Q_{i+1}^{j+1}} = \frac{2\Delta t}{\Delta x}\theta; \tag{B.13d}$$

Derivatives from equation (B.2b) are more complex. These are calculated with following steps.

$$\begin{aligned}
\frac{\partial H_i}{\partial h_i^{j+1}} &= -\frac{\theta}{\Delta x}(Q_i^{j+1})^2 \frac{\partial (A_i^{j+1})^{-1}}{\partial h_i^{j+1}} + g\frac{\partial}{\partial h_i^{j+1}}(\bar{A}\frac{\partial h}{\partial x}) + gn^2 \frac{\partial}{\partial h_i^{j+1}}(\frac{1}{\bar{A}\bar{R}^{4/3}})\bar{Q}^2 \\
&= \frac{\theta}{\Delta x}\frac{(Q_i^{j+1})^2}{(A_i^{j+1})^2}\frac{\partial (A_i^{j+1})}{\partial h_i^{j+1}} + g[\frac{\partial h}{\partial x}\frac{\partial \bar{A}}{\partial h_i^{j+1}} + \bar{A}\frac{\partial}{\partial h_i^{j+1}}(\frac{\partial h}{\partial x})] \\
&\quad + gn^2\bar{Q}^2(\bar{A}^{-1}\frac{\partial \bar{R}^{-4/3}}{\partial h_i^{j+1}} + \bar{R}^{-4/3}\frac{\partial \bar{A}^{-1}}{\partial h_i^{j+1}}) \\
&= \frac{\theta}{\Delta x}(\frac{Q_i^{j+1}}{A_i^{j+1}})^2 B_i^{j+1} + g[\frac{\partial h}{\partial x}\frac{\theta B_i^{j+1}}{2} - \bar{A}\frac{\theta}{\Delta x}] \\
&\quad + gn^2\bar{Q}^2[-\frac{4}{3}\bar{A}^{-1}\bar{R}^{-4/3-1}\frac{\partial \bar{R}}{\partial h_i^{j+1}} - \bar{R}^{-4/3}\bar{A}^{-2}\frac{\partial \bar{A}}{\partial h_i^{j+1}}] \\
&= \frac{\theta B_i^{j+1}}{\Delta x}(\frac{Q_i^{j+1}}{A_i^{j+1}})^2 + g\theta[\frac{B_i^{j+1}}{2}\frac{\partial h}{\partial x} - \bar{A}\frac{1}{\Delta x}] \\
&\quad - \frac{gn^2\bar{Q}^2}{\bar{A}\bar{R}^{4/3}}\theta[\frac{2}{3}\frac{1}{\bar{R}}(\frac{B_i^{j+1}}{P_i^{j+1}} - \frac{A_i^{j+1}}{(P_i^{j+1})^2}2\sqrt{1+s^2}) + \frac{1}{\bar{A}}\frac{B_i^{j+1}}{2}]
\end{aligned} \tag{B.14a}$$

$$\frac{\partial H_i}{\partial Q_i^{j+1}} = \frac{1}{2\Delta t} - \frac{\theta}{\Delta x}\frac{2Q_i^{j+1}}{A_i^{j+1}} + \frac{gn^2\theta Q_i^{j+1}}{\bar{A}(\bar{R})^{4/3}} \tag{B.14b}$$

$$\begin{aligned}
\frac{\partial H_{i+1}}{\partial h_{i+1}^{j+1}} &= \frac{\theta}{\Delta x}(Q_{i+1}^{j+1})^2\frac{\partial(A_{i+1}^{j+1})^{-1}}{\partial h_{i+1}^{j+1}} + g\frac{\partial}{\partial h_{i+1}^{j+1}}(\bar{A}\frac{\partial h}{\partial x}) + gn^2\frac{\partial}{\partial h_{i+1}^{j+1}}(\frac{1}{\bar{A}\bar{R}^{4/3}})\bar{Q}^2 \\
&= -\frac{\theta}{\Delta x}\frac{(Q_{i+1}^{j+1})^2}{(A_{i+1}^{j+1})^2}\frac{\partial(A_{i+1}^{j+1})}{\partial h_{i+1}^{j+1}} + g[\frac{\partial h}{\partial x}\frac{\partial \bar{A}}{\partial h_{i+1}^{j+1}} + \bar{A}\frac{\partial}{\partial h_{i+1}^{j+1}}(\frac{\partial h}{\partial x})] \\
&\quad + gn^2\bar{Q}^2(\bar{A}^{-1}\frac{\partial \bar{R}^{-4/3}}{\partial h_{i+1}^{j+1}} + \bar{R}^{-4/3}\frac{\partial \bar{A}^{-1}}{\partial h_{i+1}^{j+1}}) \\
&= -\frac{\theta}{\Delta x}(\frac{Q_{i+1}^{j+1}}{A_{i+1}^{j+1}})^2 B_{i+1}^{j+1} + g[\frac{\partial h}{\partial x}\frac{\theta B_{i+1}^{j+1}}{2} + \bar{A}\frac{\theta}{\Delta x}] \\
&\quad + gn^2\bar{Q}^2[-\frac{4}{3}\bar{A}^{-1}\bar{R}^{-4/3-1}\frac{\partial \bar{R}}{\partial h_{i+1}^{j+1}} - \bar{R}^{-4/3}\bar{A}^{-2}\frac{\partial \bar{A}}{\partial h_{i+1}^{j+1}}] \\
&= -\frac{\theta B_{i+1}^{j+1}}{\Delta x}(\frac{Q_{i+1}^{j+1}}{A_{i+1}^{j+1}})^2 + g\theta[\frac{B_{i+1}^{j+1}}{2}\frac{\partial h}{\partial x} + \bar{A}\frac{1}{\Delta x}] \\
&\quad - \frac{gn^2\bar{Q}^2}{\bar{A}\bar{R}^{4/3}}\theta[\frac{2}{3}\frac{1}{\bar{R}}(\frac{B_{i+1}^{j+1}}{P_{i+1}^{j+1}} - \frac{A_{i+1}^{j+1}}{(P_{i+1}^{j+1})^2}2\sqrt{1+s^2}) + \frac{1}{\bar{A}}\frac{B_{i+1}^{j+1}}{2}]
\end{aligned} \tag{B.14c}$$

$$\frac{\partial H_{i+1}}{\partial Q_{i+1}^{j+1}} = \frac{1}{2\Delta t} + \frac{\theta}{\Delta x}\frac{2Q_{i+1}^{j+1}}{A_{i+1}^{j+1}} + \frac{gn^2\theta Q_{i+1}^{j+1}}{\bar{A}(\bar{R})^{4/3}} \tag{B.14d}$$

B.2 MacCormack scheme for solving one-dimensional Advection-Dispersion-Reaction equations

B.2.1 General formulation of MacCormack Scheme

The MacCormack Scheme is a predictor-corrector scheme (Chapra 1997, P_{229}; Sturm 2001, P_{310}). The spatial and temporal discretization was shown in Figure B.2, where $f_{i,j}$ denotes any state variable interested at space i and time j. The upper boundary was defined as the observed upstream input, and the lower boundary was extrapolated linearly from previous two nodes. The temporal and spatial derivatives are approximated as below:

Predictor: evaluated at time j

$$\frac{\partial f}{\partial t} = \frac{f_i^{j+1} - f_i^j}{\Delta t} \tag{B.15a}$$
$$\frac{\partial f}{\partial x} = \frac{f_{i+1}^j - f_i^j}{\Delta x} \tag{B.15b}$$
$$\frac{\partial^2 f}{\partial x^2} = \frac{f_{i+1}^j + f_{i-1}^j - 2f_i^j}{\Delta x^2} \tag{B.15c}$$
$$f = f_i^j \tag{B.15d}$$

Let s^p denote the sum of all the other terms than the time derivative, the above discretization leads to the following prediction equation:

$$(f^p)_i^{j+1} = f_i^j + \Delta t \cdot s^p \tag{B.16}$$

Corrector: evaluated at time $j+1$

$$\frac{\partial f}{\partial t} = \frac{f_i^{j+1} - f_i^j}{\Delta t} \tag{B.17a}$$
$$\frac{\partial f}{\partial x} = \frac{f_i^{j+1} - f_{i-1}^{j+1}}{\Delta x} \tag{B.17b}$$
$$\frac{\partial^2 f}{\partial x^2} = \frac{f_{i+1}^{j+1} + f_{i-1}^{j+1} - 2f_i^{j+1}}{\Delta x^2} \tag{B.17c}$$
$$f = f_i^{j+1} \tag{B.17d}$$

Let s^c denote the sum of all the other terms than the time derivative, the above discretization leads to the following prediction equation:

$$(f^c)_i^{j+1} = f_i^j + \Delta t \cdot s^c \tag{B.18}$$

Correction: take the mean

The average of calculations from the above two steps gives the final prediction for variable at node (i, j).

$$f_i^{j+1} = \frac{(f^p)_i^{j+1} + (f^c)_i^{j+1}}{2} \tag{B.19}$$

B.2.2 Using MacCormack Scheme to solve temperature module

Apply equations (B.15) - (B.19) to equation (A.13), get the following difference equations for temperature module:

Predictor: evaluated at time j

$$\begin{aligned} s^p = &-\frac{(QT)_{i+1}^j - (QT)_i^j}{\Delta x} + \frac{D_T \frac{A_{i+1}^j + A_i^j}{2} \frac{T_{i+1}^j - T_i^j}{\Delta x} - D_T \frac{A_i^j + A_{i-1}^j}{2} \frac{T_i^j - T_{i-1}^j}{\Delta x}}{\Delta x} \\ &+ D_{T_g} B_i^j \frac{(T_g)_1^j - (T_g)_0^j}{\Delta z} + q_g B_i^j \frac{(T_g)_1^j + (T_g)_0^j}{2} \\ &+ \frac{B_i^j}{C_p} \{(E_s)_i^j + (E_L)_i^j + (E_v)_i^j + (E_c)_i^j\} \end{aligned} \tag{B.20a}$$

$$(AT)_i^{j+1} = (AT)_i^j + \Delta t \cdot s^p \tag{B.20b}$$

$$T_i^{j+1} = \frac{(AT)_i^j + \Delta t \cdot s^p}{A_i^{j+1}} \tag{B.20c}$$

Corrector: evaluated at time $j+1$

$$\begin{aligned} s^c = &-\frac{(QT)_i^{j+1} - (QT)_{i-1}^{j+1}}{\Delta x} + \frac{D_T \frac{A_{i+1}^{j+1} + A_i^{j+1}}{2} \frac{T_{i+1}^{j+1} - T_i^{j+1}}{\Delta x} - D_T \frac{A_i^{j+1} + A_{i-1}^{j+1}}{2} \frac{T_i^{j+1} - T_{i-1}^{j+1}}{\Delta x}}{\Delta x} \\ &+ D_{T_g} B_i^{j+1} \frac{(T_g)_1^{j+1} - (T_g)_0^{j+1}}{\Delta z} + q_g B_i^{j+1} \frac{(T_g)_1^{j+1} + (T_g)_0^{j+1}}{2} \\ &+ \frac{B_i^{j+1}}{C_p} \{(E_s)_i^{j+1} + (E_L)_i^{j+1} + (E_v)_i^{j+1} + (E_c)_i^{j+1}\} \end{aligned} \tag{B.21a}$$

$$(AT)_i^{j+1} = (AT)_i^j + \Delta t \cdot s^c \tag{B.21b}$$

$$T_i^{j+1} = \frac{(AT)_i^j + \Delta t \cdot s^c}{A_i^{j+1}} \tag{B.21c}$$

Correction: take the mean

$$(T)_i^{j+1} = \frac{(T^p)_i^{j+1} + (T^c)_i^{j+1}}{2} \tag{B.22}$$

B.2.3 Using MacCormack scheme to solve DO module

Apply equations (B.15) - (B.19) to equation (A.16), get the following difference equations for DO module:

Predictor: evaluated at time j

$$\begin{aligned} s^p = &- \frac{(QC)_{i+1}^j - (QC)_i^j}{\Delta x} + \frac{D_C \frac{A_{i+1}^j + A_i^j}{2} \frac{C_{i+1}^j - C_i^j}{\Delta x} - D_C \frac{A_i^j + A_{i-1}^j}{2} \frac{C_i^j - C_{i-1}^j}{\Delta x}}{\Delta x} \\ &+ D_{C_g} B_i^j \frac{(C_g)_1^j - (C_g)_0^j}{\Delta z} + q_g B_i^j \frac{(C_g)_1^j + (C_g)_0^j}{2} \\ &+ A_i^j \{(P_k)_i^j + (P_a)_i^j + (R_a)_i^j + (R_b)_i^j + (R_s)_i^j\} \end{aligned} \tag{B.23a}$$

$$(AC)_i^{j+1} = (AC)_i^j + \Delta t \cdot s^p \tag{B.23b}$$

$$C_i^{j+1} = \frac{(AC)_i^j + \Delta t \cdot s^p}{A_i^{j+1}} \tag{B.23c}$$

Corrector: evaluated at time $j+1$

$$\begin{aligned} s^c = &- \frac{(QC)_i^{j+1} - (QC)_{i-1}^{j+1}}{\Delta x} + \frac{D_C \frac{A_{i+1}^{j+1} + A_i^{j+1}}{2} \frac{C_{i+1}^{j+1} - C_i^{j+1}}{\Delta x} - D_C \frac{A_i^{j+1} + A_{i-1}^{j+1}}{2} \frac{C_i^{j+1} - C_{i-1}^{j+1}}{\Delta x}}{\Delta x} \\ &+ D_{C_g} B_i^{j+1} \frac{(C_g)_1^{j+1} - (C_g)_0^{j+1}}{\Delta z} + q_g B_i^{j+1} \frac{(C_g)_1^{j+1} + (C_g)_0^{j+1}}{2} \\ &+ A_i^{j+1} \{(P_k)_i^{j+1} + (P_a)_i^{j+1} + (R_a)_i^{j+1} + (R_b)_i^{j+1} + (R_s)_i^{j+1}\} \end{aligned} \tag{B.24a}$$

$$(AC)_i^{j+1} = (AC)_i^j + \Delta t \cdot s^c \tag{B.24b}$$

$$C_i^{j+1} = \frac{(AC)_i^j + \Delta t \cdot s^c}{A_i^{j+1}} \tag{B.24c}$$

Average: take the mean

$$(C)_i^{j+1} = \frac{(C^p)_i^{j+1} + (C^c)_i^{j+1}}{2} \tag{B.25}$$

MacCormack Scheme for streambed temperature and DO module as shown in equation (4.1) is more simpler. The upper boundary is the interface between stream water and streambed surface, and the lower boundary is defined at a depth of two meters, where temperature and DO levels are assumed the same as observed levels in groundwater.

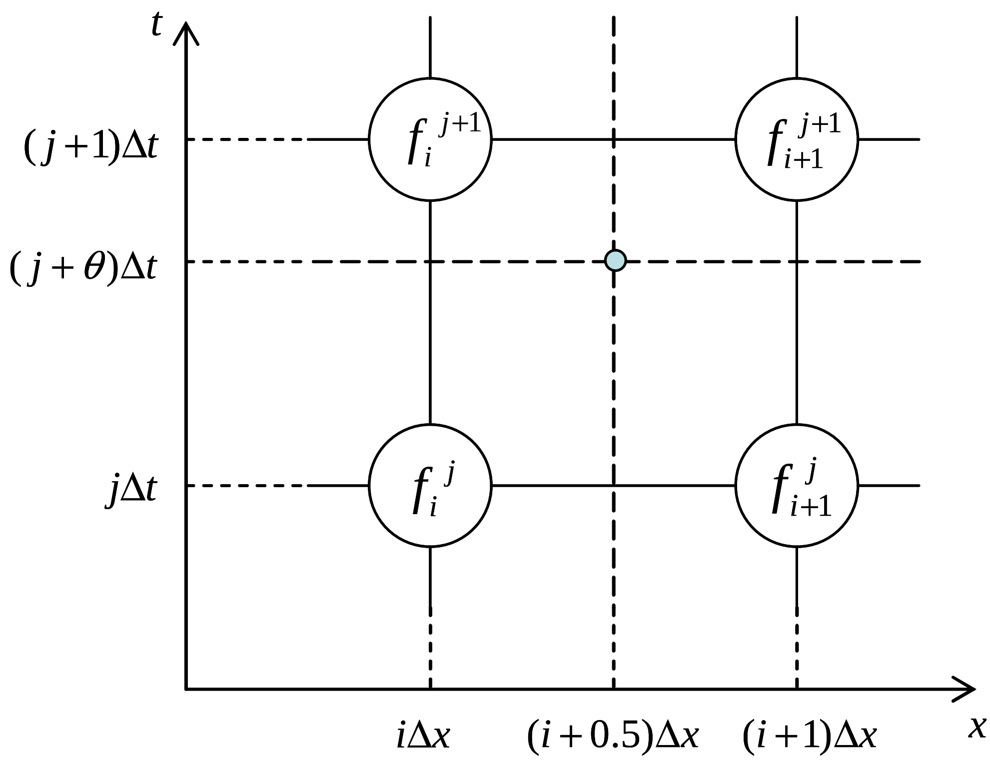

Figure B.1: Discretization of Preissmann schemes

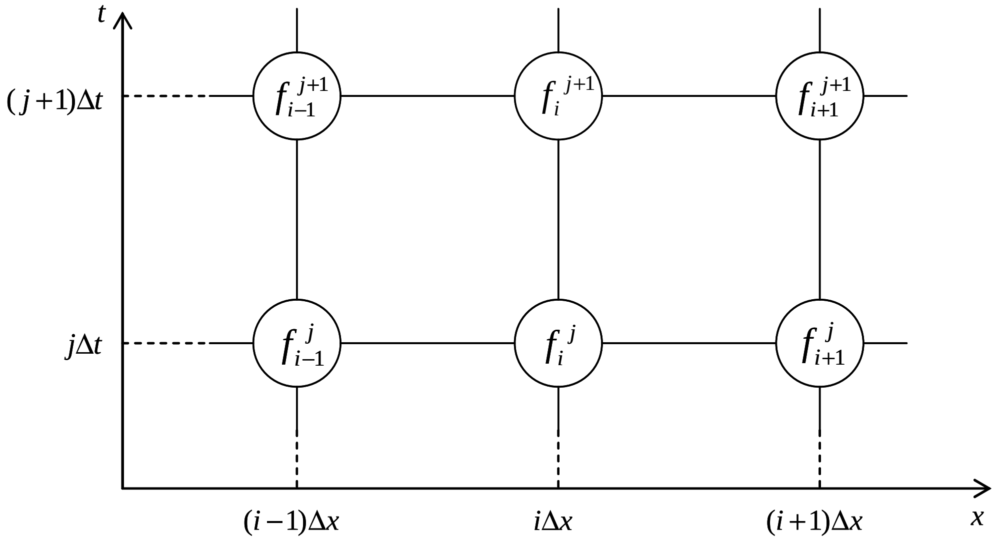

Figure B.2: Discretization of MacCormack schemes

Appendix C

Solar Altitude and Azimuth Angle Calculations

C.1 Solar altitude angle calculation

Refer to Figure C.2, where, O is the center of the Earth; N is the north pole of the Earth; arch NAQ and arch NBT are two meridians of the Earth; arch EQT is the equator; A is the location at the Earth surface where the solar altitude angle is to be calculated; B is the location at the Earth surface from which the Sun looks like right at the zenith of the sky; C is on line OT with $BC \perp OT$; D is on line OQ with $AD \perp OQ$; F is on line AD with $BF \perp AD$. It is not difficult to tell that, $\measuredangle BOC$ is the solar decline angle, $\measuredangle AOD$ is the latitude of point A, $\measuredangle COD$ is the hour angle before noon of point Q, and $\measuredangle AOB$ is the solar zenith angle of point A.

We know that the solar altitude angle is the complementary angle of the solar zenith angle. So the effort is to calculate the zenith angle $\measuredangle AOB$ at point A. This angle can be calculated by using the Law of Cosines:

$$c^2 = a^2 + b^2 - 2ab\cos(\measuredangle C) \tag{C.1}$$

where, a, b, and c are side lengths of the triangle; and $\measuredangle C$ denotes the angle by side a and b.

The Law of Cosines allows to calculate any of the three angle of a triangle if the lengths of the triangle's three sides are all known. For the triangle $\triangle AOB$ in Figure (C.2), by setting the radius of the sphere to be unit, we have the length of 1 for both sides AO and BO. The length of side AB is to be calculated. We can tell the trapezoid $ABCD$ consists of a rectangle $BCDE$ and right triangle ABF. Now if we know the lengths of the right angle sides AF and BF of $\triangle ABF$, the length of the hypotenuse AB will be known by the Pythagorean theorem. Now we use the name of a side/line denotes its length as well, then it can be seen the following relations hold,

$$\begin{aligned}
BF^2 &= CD^2 = OC^2 + OD^2 - 2 \times OC \times OD \times \cos(\measuredangle COD) \\
&= [BO \times \cos(\measuredangle BOC)]^2 + [AO \times \cos(\measuredangle AOD)]^2 \\
&\quad - 2 \times [BO \times \cos(\measuredangle BOC)] \times [AO \times \cos(\measuredangle AOD)] \times \cos(\measuredangle COD) \\
&= [\cos(\measuredangle BOC)]^2 + [\cos(\measuredangle AOD)]^2 \\
&\quad - 2 \times \cos(\measuredangle BOC) \times \cos(\measuredangle AOD) \times \cos(\measuredangle COD) \qquad \text{(C.2a)}\\
AF^2 &= [AD - DF]^2 = [AD - BC]^2 \\
&= [AO \times \sin(\measuredangle AOD) - BO \times \sin(\measuredangle BOC)]^2 \\
&= [\sin(\measuredangle AOD) - \sin(\measuredangle BOC)]^2 \qquad \text{(C.2b)}
\end{aligned}$$

To simplify the notations, define $\alpha = \measuredangle BOC$, $\beta = \measuredangle AOD$, $\Omega = \measuredangle COD$, and $\psi = \measuredangle AOB$. With the new symbols, equations (C.2b)and (C.2b) are represented as,

$$BF^2 = \cos^2\alpha + \cos^2\beta - 2\cos\alpha\cos\beta\cos\Omega \qquad \text{(C.3a)}$$

$$AF^2 = [\sin\beta - \sin\alpha]^2 = \sin^2\beta + \sin^2\alpha - 2\sin\beta\sin\alpha \qquad \text{(C.3b)}$$

From equation (C.3a) and (C.3b), by Pythagorean theorem, the length of AB can be calculated as below,

$$\begin{aligned}
AB^2 &= BF^2 + AF^2 \\
&= [\cos^2\alpha + \cos^2\beta - 2\cos\alpha\cos\beta\cos\Omega] + [\sin^2\beta + \sin^2\alpha - 2\sin\beta\sin\alpha] \\
&= 2 - 2\cos\alpha\cos\beta\cos\Omega - 2\sin\alpha\sin\beta \qquad \text{(C.4)}
\end{aligned}$$

Now for triangle $\triangle AOB$, using Law of Cosine, yield,

$$\begin{aligned}
\cos\psi &= \frac{AO^2 + BO^2 - AB^2}{2 \times AO \times BO} = \frac{1^2 + 1^2 - AB^2}{2 \times 1 \times 1} = \frac{1}{2}[2 - AB^2] \\
&= \frac{1}{2}[2 - (2 - 2\cos\alpha\cos\beta\cos\Omega - 2\sin\alpha\sin\beta)] \\
&= \sin\alpha\sin\beta + \cos\alpha\cos\beta\cos\Omega \qquad \text{(C.5)}
\end{aligned}$$

The hour angle Ω of point Q in the above equation decreases with the rotation of the Earth during the day time. Since Ω is a function of the planet angular velocity ω of the Earth and local time t of point Q, in order to conveniently use ωt to represent the hour angle, the following formula is considered,

$$\cos\Omega = \cos(\pi - \measuredangle QOE) = -\cos(\measuredangle QOE) = -\cos\omega t \tag{C.6}$$

Substitute equation (C.6) into (C.5), get,

$$\cos\psi = \sin\alpha\sin\beta - \cos\alpha\cos\beta\cos\omega t \tag{C.7}$$

The solar altitude angle,Ψ, is the complementary angle of zenith angle ψ, which gives,

$$\cos\psi = \cos(\frac{\pi}{2} - \Psi) = \sin\Psi \tag{C.8}$$

Substitute equation (C.8) into (C.7), we finally get the solar altitude angle formula for point A as below,

$$\sin\Psi = \sin\alpha\sin\beta - \cos\alpha\cos\beta\cos\omega t \tag{C.9}$$

where,

$\Psi =$	solar altitude angle	(rad)
$\alpha =$	solar declination angle	(rad)
$\beta =$	site latitude	(rad)
$\omega =$	earth angular velocity	$(\frac{\pi}{12}h^{-1})$
$t =$	local time $[0, 24)$	(h)

C.2 Solar azimuth angle calculation

Refer to Figure **??**, where, O is the center of the Earth; N is the north pole of the Earth; arch NAQ and arch NBT are two meridians of the Earth; arch EQT is the equator; A is the location at the Earth surface where the solar azimuth angle is to be calculated; B is the location at the Earth surface where the Sun looks like right at the zenith of the sky;

F is the projection of point B on plane AOQ, e.g., $BF \perp AOQ$; C is on line OT with $BC \perp OT$; D is on line OQ with $FD \perp OQ$; by $BF \perp AOQ$, $BF \perp OQ$; by $FD \perp OQ$ and $BF \perp OQ$, $OQ \perp BCDF$; by $OQ \perp BCDF$, $CD \perp OQ$; G is on line AO with $BG \perp AO$; by $BF \perp AOQ$, $BF \perp FG$ and $BF \perp AO$; by $BG \perp AO$ and $BF \perp AO$, $AO \perp BFG$; by $AO \perp BFG$, $FG \perp AO$; by $BG \perp AO$ and $FG \perp AO$, the angle $\measuredangle BGF$ is the angle by planes AOQ and AOB, which is exactly the solar azimuth angle from the due south; meanwhile, it is easy to see that $\measuredangle BOC$ is the solar decline angle, $\measuredangle AOD$ is the latitude of point A, $\measuredangle COD$ is the hour angle before noon of point Q, and $\measuredangle AOB$ is the solar zenith angle of point A.

Our effort is to calculate $\measuredangle BGF$. By $BF \perp FG$, we know the $\triangle BFG$ is a right triangle. For the right triangle $\triangle BFG$, if any two of the three sides are known, then all the three internal angles will be known. It can be seen that, the hypotenuse side BG is the right angle side of another right triangle $\triangle BOG$, with $\measuredangle BOG$ being exactly the zenith angle of point A. Since the zenith angle becomes a known after using formula (C.9), then the length of BG is,

$$BG = BO \times \sin(\measuredangle BOG) = \sin\psi = \sin(\frac{\pi}{2} - \Psi) = \cos\Psi \tag{C.10}$$

It can also be seen that, the polygon $BFDT$ is a rectangle, which enables us to calculate right angle side BF as below,

$$BF = CD = CO \times \sin\Omega = BO \times \cos\alpha \times \sin\Omega = \cos\alpha\sin\Omega \tag{C.11}$$

From equation (C.10) and (C.11), the azimuth angle from due south at point A can be calculated as below,

$$\sin(\measuredangle BGF) = \frac{BF}{BG} = \frac{\cos\alpha\sin\Omega}{\cos\Psi} \tag{C.12}$$

Similarly, in order to conveniently use ωt to represent the hour angle, the following formula is considered,

$$\sin\Omega = \sin(\pi - \measuredangle QOE) = \sin(\measuredangle QOE) = \sin\omega t \tag{C.13}$$

Substitute equation (C.13) to (C.12), get,

$$\sin(\measuredangle BGF) = \frac{BF}{BG} = \frac{\cos\alpha \sin\omega t}{\cos\Psi} \tag{C.14}$$

In our case, we redefine the azimuth angle to be from due east instead of due south, and denote the angle with symbol Φ. It can be seen that Φ is the complementary angle of $\measuredangle BGF$, thus,

$$\sin(\measuredangle BGF) = \sin(\frac{\pi}{2} - \Phi) = \cos\Phi \tag{C.15}$$

Substitute equation (C.15) into (C.14), get the final azimuth equation,

$$\cos\Phi = \frac{\cos\alpha \sin\omega t}{\cos\Psi} \tag{C.16}$$

where,

$\Phi =$	solar azimuth angle from due east	(rad)
$\alpha =$	solar declination angle	(rad)
$\omega =$	earth angular velocity	$(\frac{\pi}{12}h^{-1})$
$t =$	local time $[0, 24)$	(h)
$\Psi =$	solar altitude angle	(rad)

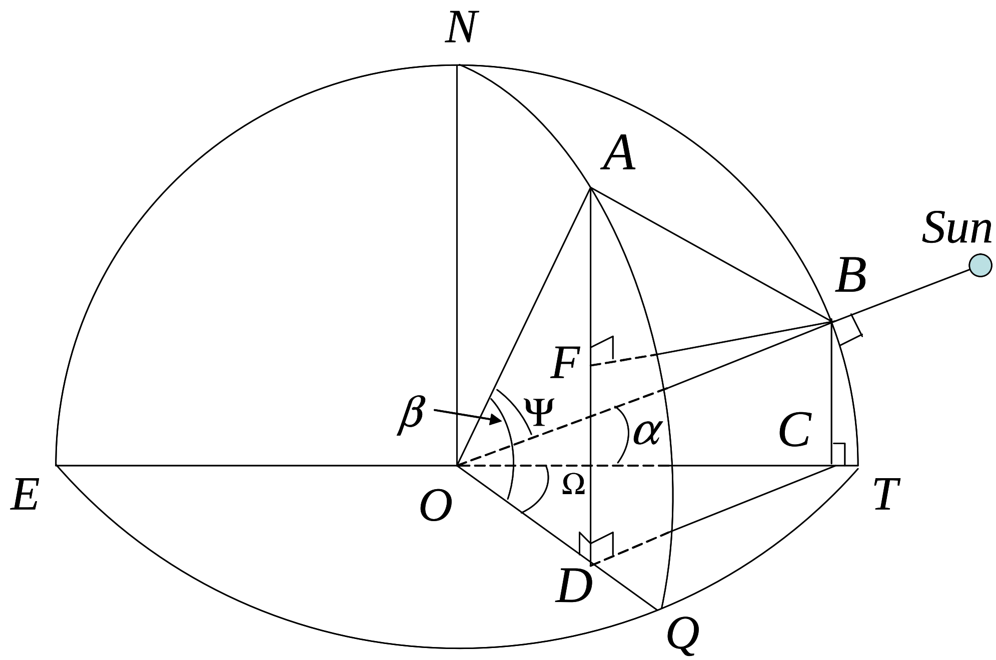

Figure C.1: Schematic of the solar altitude angle at the location A on the North Hemisphere of the Earth. Where, $\alpha = \measuredangle BOC$ is the the solar declination angle, $\beta = \measuredangle AOD$ is the latitude at location A, $\Omega = \measuredangle COD$ is the hour angle at location A, and $\Psi = \measuredangle AOB$ is the solar altitude angle at location A.

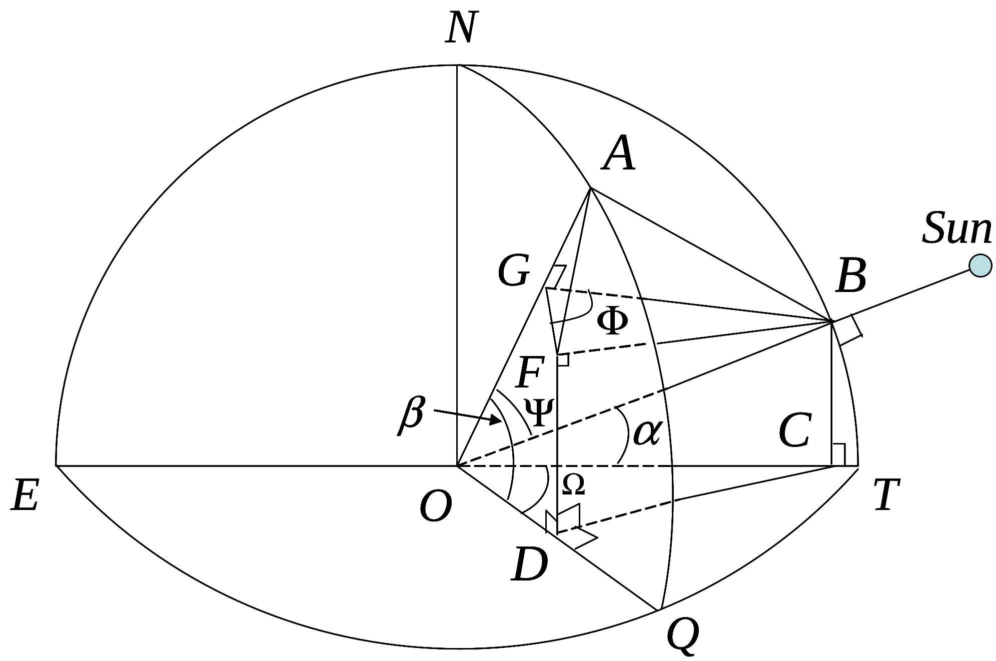

Figure C.2: Schematic of the solar azimuth angle at the location A on the North Hemisphere of the Earth. Where, $\alpha = \measuredangle BOC$ is the the solar declination angle, $\beta = \measuredangle AOD$ is the latitude at location A, $\Omega = \measuredangle COD$ is the hour angle at location A, $\Psi = \measuredangle AOB$ is the solar altitude angle at location A, and $\Phi = \measuredangle BGF$ is the solar azimuth at location A angle from due east.

Appendix D

Matlab Source Code - Tested in Matlab 7.0

D.1 Shared modules

D.1.1 SHADE.m

```
function [SP SE] = SHADE(River_Angle, Tree_hight, Bank_hight, ...
                    Bank_Slope, Bottom_Width, Water_level, ...
                    Water_width, SA, DA, HA, DT)
%%%%%%%%%%%%%%%%%%%%%%%%%%%%%%%%%%%%%%%%%%%%%%%%%%%%%%%%%%%%%%%%%%%%%%%%%%%%
% Function:
%   SHADE.m --- SHADE program for shading ratio on stream water surface;
%
% Output:
%   SP -- Shading rate within [0,1];
%   SE -- Unshading rate, equal to 1-SP;
%
% Input:
%   River_Angle -- river angle beginning from east clockwise; 1 by M;
%   Tree_hight -- row vector: 1 by M;
%   Bank_hight -- row vector: 1 by M;
%   Bank_Slope -- row vector: 1 by M;
%   Bottom_Width -- row vector: 1 by M;
%   Water_level -- water depth: N by M;
%   Water_width -- water surface width: N by M;
%   SA -- solar angle,  within [0, pi/2], =0 after sunset; N by M;
%   DA -- solar decline angle, negative in South Hemisphere; N by M;
%   HA -- solar hour angle, monotonoicaly increase with time; N by M;
%%%%%%%%%%%%%%%%%%%%%%%%%%%%%%%%%%%%%%%%%%%%%%%%%%%%%%%%%%%%%%%%%%%%%%%%%%%%

tg=tan(SA);
% tan of Solar angle, SA is (0 -> pi/2 -> 0). tg=0 after sunset, not
% invseribile; if tg is less than 10^-2, it is around twilight time.
% At this time shadow of trees is really long (100*tree height);
% So we just simply set 100*Tree_hight as the longest shadow,
% which is reasonable enough and easy for inverse;

tol=10^-2;          % tolerance value.
a = (tg<=tol);      % logic eqn: if tg<=tol, a=1, otherwise a=0;
b = (tg>tol);       % logic eqn: if tg>tol,  b=1, otherwise b=0;
tg=tg.*b+a.*tol;    % if tg>0.01, tg = tg; if tg<=0.01, tg = 0.01;
warning off MATLAB:conversionToLogical;     % depress warning info.
ctg=1./tg;          % inverse of tg. ctg*tree_height = shadow length.

[row col] =  size(Water_level);  % Matrix size Water_level;
TH=ones(row, 1)*Tree_hight;      % 1 by M -> N by M;
BH=ones(row, 1)*Bank_hight;      % 1 by M -> N by M;
WL=Water_level;                  % N by M;
H=TH+BH-WL;                      % H is effective hight: N by M;
H = H.*(H>0);                    % if H<0 then H=0;
```

```
SHADE=ctg.*H;        %Shadow length of trees on horizontal plane;

cos_x = cos(DA).*sin(HA)./cos(SA);
% The above eqn is to calulate solar azimuth angle from east direction:
% SA is within [-pi/2, pi/2], however, cos(SA) is always>0 inside this
% range. DA=[-23.45, 23.45], again, cos(DA)>0; thus, cos_x is only
% determined by hour angle HA. during the day, HA is from 0 to pi, cos_x is
% from 1 to -1; at night, HA is from pi to 2pi, cos_x is from -1 to 1.
% cos_x = cos(DA).*cos(HA)./cos(SA);

Theta = acos(cos_x);
% This is to get azimuth angle of solar from east direction.
% Here Theta (arcos(x))is actually day:[0 pi] and night: [pi 0]. but at
% summmer time Theta can be in [pi 0] cycle even before sunset.
% To identify if Theta is already in [pi 0] during daylight,
% the time series trend has to be used. if identified, convert
% to either pi-Theta or Theta-pi.
% since plus or minus does not matter -- abs will be taken anyway.

a = Theta;             % a is tmp variable;
b = (a(2,:)-a(1,:))<0; % Check if first value is already in [pi, 0] cycle.
Theta(1,:) = pi*b - Theta(1,:); %  set it to pi-Theta if it is.

for i=2:row                % Check if the rest values are in [pi, 0] cycle.
    b=(a(i,:)-a(i-1,:))<0; % set them to Theta-pi if they are.
    Theta(i,:)=Theta(i,:)-b *pi;
end
Theta=abs(Theta);      % Take absolute value to calculate angle with river.
% Angle betwn river and shade =solar azimuth angle(from east direction)
% -stream orientation angle(from east direction, which can be <0.
% since sin(-x)=-sin(x), take absolute value of angle.

% Stream oritentaiton from east direction, 1 by N, N CSTRs ;
RA=ones(row, 1)*River_Angle*pi/180;

AG=Theta-RA;        %Angle betwn stream and solar azimuth.
AG=abs(AG);         %sin(AG)*SHADE is actual shadow length on stream.

a=(SA>0);                   % if sun is set, a=0, otherwise a=1;
b=(SA<=0);                  % if sun is set, b=1, otherwise b=0;
sinAG=sin(AG);
sinAG=a.*sinAG+b;           % after sunset, set sinAG to its max=1.
ShadeOnRiver=SHADE.*sinAG;  % so at night ShadeOnRiver = SHADE;

% River shading efficiency:
BS = ones(row, 1)*Bank_Slope;   % 1 by M -> N by M;
a = (BH-WL)>0;
ExposedBank=a.*(BH-WL).*BS;     % Longitudinal bank width;

% if shade on water > 0, set ShadeOnwater to itself
% Otherwise, set ShadeOnwater to 0 -- no shading occurs;
ShadeOnWater=ShadeOnRiver-ExposedBank; a=ShadeOnWater>0;
ShadeOnWater=a.*ShadeOnWater;

ShadingRate=ShadeOnWater./Water_width;
%Make data ready for output
a=ShadingRate<=1;       % If shade<=1, a = 1, otherwise a=0;
b=ShadingRate>1;        % Calculated ShadingRate may >1, set to 1.
SP=a.*ShadingRate+b;    % SP is final shading rate, maximal after sunset.
SE=1-SP;                % SE is final unshaded area rate, 0 after sunset.

return
```

D.1.2 solarC.m

```
function [Phi, Sin_Phi, Alpha, Omega, Beta, SI] = solarC(DT,LD)
%%%%%%%%%%%%%%%%%%%%%%%%%%%%%%%%%%%%%%%%%%%%%%%%%%%%%%%%%%%%%%%%%%%%%%%%%%%
% Function:
%   solarC.m --- Solar angle calculator: SA for any point of the earth;
%                This program generates necessary input for SHADE.m;
%
% Input:
%   DT --- Date to be simulated , n by 1 (matlabdate);
%   LD --- Latitude in degree [SouthPolar, NorthPolar]=[-90, 90],
%          in scalar or 1 by N vector;
%
% Output:
%   Sin_Phi --- Corrected Sin value of Solar angle,
%               e.g., Sin_Phi=0 for night time;
%   Phi     --- Solar angle, Phi=0 after sunset&before sunrise (radian);
%               = Pie/2-solar zenith angle
%   Alpha   --- Solar decline angle ([-23.45 23.45]), (radian);
%               Incidence angle between equator and sunlight (or Latitude
%               of the points where sunlight is perpendicular with
%               earth surface) (positive in northern hemisphere).
%   Omega   --- Hour angle for a day ([0, 2pi]), (radian);  Degree of angle
%               circumrotated from a start point at 6:00am. =(Time
%               6:00am)*2*pi
%               time=[0 6 12 18 24]==> sin(Omega)=[-1, 0 1, 0, -1];
%   Beta    --- Latitude. Latitude where the study points lie (positive in
%               northern hemisphere).
%   SI      --- Expected solar radiation rate under S0=1050W/m^2;
%%%%%%%%%%%%%%%%%%%%%%%%%%%%%%%%%%%%%%%%%%%%%%%%%%%%%%%%%%%%%%%%%%%%%%%%%%%

% Set reference date; to get Julian day of the year.
[year, month, day] = datevec(DT(1));    % get year of the first data;
Day0=datenum(['1-Jan-' num2str(year)]); % or: Day0=DATENUM(2003,1,1,0,0,0);
Julianday=DT-Day0+1;     % JulianDay of the Simulation period, n by 1;
I0=1050;                 % Solar constant is: 1366W/m^2

Alpha=23.45*pi/180*cos(2*pi*(Julianday-172)/365);   % Chen_1998; Garg_1993
Omega=(Julianday)*2*pi;

% matrix expansion to row by col for next step calculation;
row = length(DT); col = length(LD); Alpha=repmat(Alpha, 1, col);
Beta=repmat(LD, row, 1)*pi./180; Omega=repmat(Omega, 1, col);

% -------------------------------------------------------------------------
% Solar angle as a function of decline angle, latitude, and hour angle;
% refer to appendix C of the dissertation
Sin_Phi=sin(Alpha).*sin(Beta)-cos(Alpha).*cos(Beta).*cos(Omega);

a=(Sin_Phi>0);          % a is logic value, =1 if true, =0 if false.
Sin_Phi=a.*Sin_Phi;     % Solar angle is < 0 during night. Set it to be 0;
Phi=asin(Sin_Phi);      % Solar angle in radian, =0 if <0;
% -------------------------------------------------------------------------

% The following steps converts monotoneously increasing hour angle Omega to
% values in [-pi/2, pi/2];
sinOmega = sin(Omega); Omega=asin(sinOmega);

SI = I0*Sin_Phi;    % solar radiation under I0 = 1050W/M^2;

return
```

D.2 DDOT in CSTR structures

D.2.1 Main function - To invoke Q, T, and C models

```
function [DT, Qs Vs Us Ts DOs TBeds DOBeds, ...
          T, DO, WF, WE, Ds, hs, h, BOs] = CSTR;
%%%%%%%%%%%%%%%%%%%%%%%%%%%%%%%%%%%%%%%%%%%%%%%%%%%%%%%%%%%%%%%%%%%%%%%%%%%%
% Function:
%   CSTR.m --- Prepare data to invoke Q, T, and DO model:CSTR_ftdo.m;
%
% Inputs:
%   No explicit inputs;
%
% Outputs:
%   DT --- Date recongizable by Matlab; N by 1;
%   Qs --- Simulated flow (m3/s); N by M;
%   Vs --- Simulated CSTR volume (m3); N by M;
%   Us --- Simulated flow velocity (m/s);
%   Ts --- Simulated Temperature (*C); N by M;
%   DOs --- Simulated DO (mg/L); N by M;
%   TBeds --- Simulated streambed Temperature profile (*C); N by (Mbed*M);
%   DOBeds --- Simulated streambed flow DO profile (mg/L); N by (Mbed*M);
%   T --- Observed T at upper, lower, trib boundaries; N by 3;
%   DO --- Observed DO at upper, lower, trib boundaries; N by 3;
%   WF --- Observed flow at upper, lower, trib boundaries; N by 3;
%   WE --- Observed 7 weather parameters; N by 7;
%   Ds --- Simulated hydrolic water depth (m); N by M;
%   hs --- Simulated water depth (m); N by M;
%   h --- Observed water depth (m); N by M;
%   BOs --- Simulated water surface width (m); N by M;
%%%%%%%%%%%%%%%%%%%%%%%%%%%%%%%%%%%%%%%%%%%%%%%%%%%%%%%%%%%%%%%%%%%%%%%%%%%%

% function obj = CSTR(p); % turn on for potimization;

%   [solar, longwave1air, longwave2wate,  convection, evaporation ]
p = [0.248    0.34    0.2        0.9763      0.2084]; %51.7419 @ tol=1e-4

% IDDO is calibrated coefficient for each component.
% IDDO = [ka,   growth,  respiration, bod,   sod,   half-saturation]
IDDO = [0.03  5.1745  32.4552  0.02  746.9551  211.2586]; % SSE = 17.2870;

if nargin==0    % for result run;
    % close all hidden;clear all;
    savID=0;                % 0 -> no save; 1 -> save;
    tempID=[1 1 1 1 1]*1;
    doID=[0 0 0 0 0 0]+1;
    CSTR=25;
    % disp('No input par');
else            % for optimization;
    modelID=1;
    savID=0;
    tempID=[1 1 1 1 1]*1;
    doID=[0 0 0 0 0 0]+1;
    CSTR=25;
end;

M=CSTR;
TotalDS=25200;              % Total distance of stream reach (m);
DS1=8611;                   % Distance before tributary (m);
n1=round(DS1/TotalDS*M);    % Number of CSTR before trib;
n2=M-n1;                    % Number of CSTR after trib;
L=TotalDS/M;                % Length for each CSTR(m)

% ========================================================================
% Read in observed data;
```

```
WFlow=xlsread('WFlow.xls');
% observed flow (m3/s); format:
% [Time Ichi2_Morgan Ichi2_Morgan Patch Patch Ichi3_Milford Ichi3_Milford];
% [time  Depth   Flow    Depth    Flow    Depth     Flow];
% [time  m       m3/s    m        m3/s    m         m3/s];

WQuality=xlsread('WQuality.xls');
% observed water quality in main stream;
% [Time  Temp   Temp   Temp   DO      DO      DO];
% [Time  *C     *C     *C     mg/L    mg/L    mg/L]

Weather=xlsread('Weather.xls');
% observed weather; format:
% [time airT    Humidity    TotalPres   SolarR  Rain    wind];
% [time *C      %           kpa         W/m2    mm      m/s];
% =========================================================================

DT = WQuality(:,1)+datenum('30-Dec-1899');  % Excel date -> Matlab date;

% sm = ones(1,8)/8;                          % Smoothing parameter;
% WFlow_= filtfilt(sm, 1, WFlow);            % Smooth flow data;
% WQuality_= filtfilt(sm, 1, WQuality);      % Smooth water quality data;
% Weather = filtfilt(sm, 1, Weather);        % Smooth weather data;
WE=Weather;

% --------------------------------------
% Reorganize observed data;
WF(:,2)=WFlow(:,3);     % Ichi2 flow(m3/s)
WF(:,3)=WFlow(:,5);     % Ichi3 flow(m3/s)
WF(:,1)=WFlow(:,7);     % Patch flow(m3/s)

h(:,2)=WFlow(:,2);      % Ichi2 flow(m3/s)
h(:,3)=WFlow(:,4);      % Ichi3 flow(m3/s)
h(:,1)=WFlow(:,6);      % Patch flow(m3/s)

T(:,1)=WQuality(:,2);   % Patch T(Ichi1) (*C)
T(:,2)=WQuality(:,3);   % Ichi2 T (*C)
T(:,3)=WQuality(:,4);   % Ichi3 T (*C)
T=T+273.15;             % *C -> K;

DO(:,1)=WQuality(:,5);  % Patch DO(Ichi1)
DO(:,2)=WQuality(:,6);  % Ichi2 DO
DO(:,3)=WQuality(:,7);  % Ichi3 DO
% --------------------------------------

% display initial conditions [Flow(m3/s) Temp(*C) DO(mg/L)]
% Setup stream geomorphology conditions:
B1=12;       % Streambed width (m) at up boundary Ichi2;
B2=16;       % Streambed width (m) right before the trib joint Patch;
B3=22;       % Streambed width (m) right after the trib joint Patch;
B4=28;       % Streambed width (m) at down boundary Ichi3;

s1=.5;       % side slope at up boundary Ichi2;
s2=.5;       % side slope after trib joint Patch;
s3=.5;       % side slope at down boundary Ichi3;
LD1=31.527;  % Latitude (degree) at up boundary Ichi2;
LD2=31.383;  % Latitude (degree) at down boundary Ichi3;
CV1=0.90;    % Canopy cover (%) at up boudary Ichi2;
CV2=0.75;    % Canopy cover (%) at joint of trib;
CV3=0.5;     % Canopy cover (%) at down boudary Ichi3;
for i=1:M
    if i<n1+1
        k=i/n1;                 % Ratio;
        B(i)=B1*(1-k)+B2*k;     % Streambed width (m);
        s(i)=s1*(1-k)+s2*k;     % Side slope;
        CV(i)=CV1*(1-k)+CV2*k;  % Linear interpolation - Canopy cover (%);
    else
        k=(i-n1)/n2;            % Ratio;
```

```
        B(i)=B3*(1-k)+B4*k;     % Streambed width (m);
        s(i)=s2*(1-k)+s3*k;     % Side slope;
        CV(i)=CV2*(1-k)+CV3*k;  % Linear interpolation - Canopy cover (%);
    end
    k=i/M;
    LD(i)=LD1*(1-k)+LD2*k;      % Linear interpolation - Latitude (degree);
end
B=B';       % 1 by M -> M by 1;
s=s';       % 1 by M -> M by 1;
CV=CV';     % 1 by M -> M by 1;

% ========================================================================
% invoke SolarC.m and Shade.m model;
% ------------------------------------------------------------------------
% Invoke  SolarC.m - Solar angle model ;
% DT-1/24 = remove daylight saving time effect;
[SA, sinSA, DA, HA] = solarC(DT-1/24,LD);
% SA --- Solar angle, SA=0 if <0(sunset&before sunrise) (radian);
% sinSA --- sin of Solar angle, sinSA=0 after sunset & before sunrise;
% DA --- Solar decline angle ([-23.45 23.45]), (radian);
% HA --- Hour angle for a day ([0, 2pi]), (radian);

Phi = SA*180/pi;    % rad -> degree;
Omega = HA;
% ------------------------------------------------------------------------
River_agl(1:2) = 90;        % river orientation (degree);
Tree_height(1:2) = 20;      % tree height (m);
Bank_height(1:2) = [2 3];   % stream side bank height (m);
slp_bank = s';              % stream side slope;

River_agl = River_agl(1) ...
            + [0:M-1]/(M-1)*(River_agl(2) - River_agl(1));
Tree_height = Tree_height(1) ...
            + [0:M-1]/(M-1)*(Tree_height(2) - Tree_height(1));
Bank_height = Bank_height(1) ...
            + [0:M-1]/(M-1)*(Bank_height(2) - Bank_height(1));
slp_bank = s;
pW = B;
pB = [ones(size(DT,1),1)*[pW']]';
ph = [WFlow(:,4)*ones(1,M)]';
canopy = 0.8;   % canopy density;

% SHADE model (SE = % of water surface NOT in shadow);
p1 = River_agl;         % 1 by M;
p2 = Tree_height;       % 1 by M;
p3 = Bank_height;       % 1 by M;
p4 = [slp_bank(:,1)]';  % 1 by M;
p5 = [pW(:,1)]';        % 1 by M;
p6 = ph';               % N by M;
p7 = pB';               % N by M;
p8 = SA;                % N by M;
p9 = DA;                % N by M;
p10 = HA;               % N by M;

% Invoke SHADE.m
SP = SHADE(p1, p2, p3, p4, p5, p6, p7, p8, p9, p10, DT);    % N by M;
SP = SP'*canopy(1);     % M by N; shading percent;
SE = 1-SP;              % M by N; unshading percent;
SE = SE';
% ========================================================================

% positive: aquifer -> stream
% negative: stream  -> aquifer
% groundwater assumption:
Bed=[12 28];

wid_bed(1) = Bed(1);
wid_bed(2) = Bed(2);
```

```
wid_bed_trib = 8;

alpha = pi/4;   % angle between trib and main stem;
bedW1 = wid_bed(1);
bedW2 = ((TotalDS-DS1)*bedW1+DS1*(wid_bed(2) ...
             - wid_bed_trib*cos(alpha)))/TotalDS;
bedW3 = bedW2 + wid_bed_trib*cos(alpha);
bedW4 = wid_bed(2);
bedW = [bedW1 bedW2 bedW3 bedW4];
% ---------------------------------------------------------------------
bedA1 = DS1*mean([bedW(1) bedW(2)]);
bedA2 = (TotalDS-DS1)*mean([bedW(3) bedW(4)]);
qGv = (WF(1, 3)-WF(1, 2)-WF(1,1))/(bedA1 + bedA2)*.6;
% groundwater flow velocity (m/s); 0.6 -> groundwater flow corrector;

F1 = WF(1,2);                                   % flow at up boundary;
F2 = WF(1,2) + qGv*DS1*mean([bedW(1) bedW(2)]); % flow before trib;
F3 = F2 + WF(1,1);                              % flow after trib;
F4 = WF(1,3);                                   % flow at lower boundary;
F_g1 = (F2 - F1)/(n1-1);
F_g2 = (F4 - F3)/(M-n1);

T1 = T(1,2);                                    % T at up boundary;
T2 = T(1,2) + .4;                               % T before trib;
T3 = (T(1,2)*F2+T(1,1)* WF(1,1))/(F3);          % T after trib;
T4 = T(1,3);                                    % T at lower boundary;
T_g1 = (T2 - T1)/(n1-1);
T_g2 = (T4 - T3)/(M-n1);

DO1 = DO(1,2);                                  % DO at up boundary;
DO2 = DO(1,2) - .4;                             % DO before trib;
DO3 = (DO(1,2)*F2+DO(1,1)* WF(1,1))/(F3)-.2;    % DO after trib;
DO4 = DO(1,3);                                  % DO at lower boundary;
DO_g1 = (DO2 - DO1)/(n1-1);
DO_g2 = (DO4 - DO3)/(M-n1);

a1 = 0.247;     % input;  %v=a*Q^b;
b1 = 0.4602;    % input;  %v=a*Q^b;
a4 = 0.1883;    % output; %v=a*Q^b;
b4 = 0.345;     % output; %v=a*Q^b;
a2 = a1 + (a4 - a1)/(B4-B1)*(B2-B1);    % before trib;
b2 = b1 + (b4 - b1)/(B4-B1)*(B2-B1);    % before trib;
a3 = a1 + (a4 - a1)/(B4-B1)*(B3-B1);    % after trib;
b3 = b1 + (b4 - b1)/(B4-B1)*(B3-B1);    % after trib;

a_g1 = (a2 - a1)/(n1-1);
b_g1 = (b2 - b1)/(n1-1);
a_g2 = (a4 - a3)/(M-n1);
b_g2 = (b4 - b3)/(M-n1);

for i=1:M
    if i<n1+1
        x0(i,1)=F1 + (i-1)*F_g1;          % flow
        a(i)=a1 + (i-1)*a_g1;             % v=a*Q^b;
        b(i)=b1 + (i-1)*b_g1;             % v=a*Q^b;
        x0(i,2)=T1 + (i-1)*T_g1;          % temperature
        x0(i,3)=DO1 + (i-1)*DO_g1;        % DO
    else
        x0(i,1)=F3 + F_g2*(i-n1);         % flow
        a(i)= a3 + (i-n1)*a_g2;           % v=a*Q^b;
        b(i)= b3+(i-n1)*b_g2;             % v=a*Q^b;
        x0(i,2)=T3 + (i-n1)*T_g2;         % temperature
        x0(i,3)=DO3 + (i-n1)*DO_g2;       % DO
    end
end
a=a';
b=b';
```

```
% -------------------------------------------------------------------------
qGT(1:M,1) = 20.5;      % groundwater T *C;
qGDO(1:M,1) = 5;        % groundwater DO mg/L
bedM = 21;              % vertical nodes;
bedTg = ([qGT + 273.15 - x0(:,2)])/(bedM-1);  % T gradient;
bedDOg = ([qGDO - x0(:,3)])/(bedM-1);         % DO gradient;
for j=1:bedM
    bedT(:,j) = x0(:,2) + bedTg*(j-1);        % vertical profile: T *C;
    bedDO(:,j) = x0(:,3) + bedDOg*(j-1);      % vertical profile: DO mg/L;
end
bedT = bedT';                    % vertical profile: T (*C);
bedDO = bedDO';                  % vertical profile: DO (mg/L);
bedT = reshape(bedT, [], 1);     % into one column;
bedDO = reshape(bedDO, [], 1);   % into one column;

x0 = [x0(:,1); x0(:,2); x0(:,3); bedT; bedDO];    % initial value for ODE;

% -------------------------------------------------------------------------
%Invoke temperature model ODE
%Setup options for ODE:
[row col]=size(WFlow);
tspan=[1:row];
options=odeset('Reltol',1e-4);
t=1:row;
[t,x]=ode45(@CSTR_ftdo, tspan, x0, options, WF, T, DO, WE, M, n1, ...
        L, a, b, B, s, Phi, Omega, SE, CV,p, IDDO, ...
        tempID, doID, bedM, bedW, TotalDS, DS1);
% -------------------------------------------------------------------------
% output;
T = T-273.15;
x(:,M+1: M*2) = x(:,M+1:M*2)-273.15;
x(:,3*M+1:3*M+bedM*M) = x(:,3*M+1:3*M+bedM*M)-273.15;
[row col]=size(x);
for i=1:M
    x(:,col+i)=L/a(i)*x(:,i).^(1-b(i));   % volume
end

a = ones(row,1)*a';
b = ones(row,1)*b';
B = ones(row,1)*B';
s = ones(row,1)*s';

Us=a.*x(:,1:M).^b;                  % calculate velocity from flow Q (m/s);
As=x(:,1:M)./Us;                    % Cross section area (m2);
hs=(-B+sqrt(B.^2+4*As.*s))/2./s;    % Water depth (m);
B0s=B+2*s.*hs;                      % Top width (m);
Ds=As./B0s;                         % Hydrolic water depth (m);

Qs = x(:,1:M);
Vs = x(:,col+1:col+M);
Ts = x(:,M+1: M*2);
DOs = x(:,M*2+1:M*3);
TBeds = x(:,3*M+1:3*M+M*bedM);
DOBeds = x(:,M*3+M*bedM+1:M*3+M*bedM*2);

% -------------------------------------------------------------------------
% Save simulation results;
if savID==1
    head1 = {'date', 'Flow','T','DO'}
    head2 = {'date', 'm3/s', '*C', 'mg/L'};
    outData = [DT-datenum('30-Dec-1899'), x(:,M), x(:,2*M), x(:,3*M)];

    try, xlswrite('Simulated_T_DO_Flow.xls', head1, 'sheet1', 'a1'), ...
        catch, disp('Not saved to Simulated_T_DO_Flow.csv'), end;
    try, xlswrite('Simulated_T_DO_Flow.xls', head2, 'sheet1', 'a2'), ...
        catch, disp('Not saved to Simulated_T_DO_Flow.csv'), end;
    try, xlswrite('Simulated_T_DO_Flow.xls', outData, 'sheet1', 'a3'), ...
        catch, disp('Not saved to Simulated_T_DO_Flow.csv'), end;
```

```
end
% -----------------------------------------------------------------------
% The following lines are for optimization;
err1 = Qs(:,M) - WF(:,3);
    obj1 = err1'*err1;
err2 = Ts(:,M) - T(:,3);
    obj2 = err2'*err2
err3 = DOs(:,M) - DO(:,3);
    obj3 = err3'*err3

obj = obj2;

return
```

D.2.2 Q, T, and C models (integrated) - ODE equations

```
function [x_rate] = CSTR_ftdo(t, x, WF, T, DO, WE, M, n1, L, a, b, B, ...
                    s, Phi, Omega, SE, CV, p, IDDO, tempID, doID, ...
                    bedM, bedW, TotalDS,DS1)
%%%%%%%%%%%%%%%%%%%%%%%%%%%%%%%%%%%%%%%%%%%%%%%%%%%%%%%%%%%%%%%%%%%%%%%%%%%
% Function:
%   CSTR_ftdo.m --- Integrated Q, T, DO model based on CSTR structures;
%                   Prepare changing rate to ODE solver: ODE45.m;
% Inputs:
%   t --- Time in natural numbers; scalar;
%   x --- Initial conditions of Q, T, and DO; (3*M) by 1 vector;
%   WF --- Observed Q at Trib, Upper, and Lower boundaries (m3/s); N by 3;
%   T --- Observed T at Trib, Upper, and Lower boundaries (*C); N by 3;
%   DO --- Observed DO at Trib, Upper, and Lower boundaries (mg/L); N by 3;
%   WE --- Observed 7 weather parameters; N by 7; Format:
%          [time  airT   Humidity   TotalPres   SolarR   Rain   wind];
%          [time  C      %          kpa         W/m2     mm     m/s]
%   M --- Number of CSTR over the stream reach; scalar;
%   n1 --- Number of CSTR before the tributary; scalar;
%   L --- Length of a single CSTR (m); scalar;
%   a, b --- Velocity coefficient for flow: v=a*Q^b; M by 1;
%   B --- Streambed width for each CSTR (m); M by 1;
%   s --- Stream side slope for each CSTR; M by 1;
%   Phi --- Solar altitude angle (degree); N by M;
%   Omega --- Hour angle (degree); N by M;
%   SE --- % of water surface NOT shaded by tree; N by M;
%   p --- corrector for T; 1 by 5;
%   IDDO --- corrector for DO; 1 by 6;
%   tempID --- process controller for T; 1 by 6;
%   doID --- process controller for DO; 1 by 6;
%   bedM --- number of vertical grids in streambed;
%   bedW --- bed width at upper boundary, before trib, after trib, and
%            lower boundary; 1 by 4;
%   TotalDS --- Total length of stream reach (m); scalar;
%   DS1 --- Total length before trib (m); scalar;
%
% Outputs:
%   x_rate --- changing rate of Q, T, DO; dQ/dt, dT/dt, dC/dt;
%
% Note:
%   The ODE45 solver uses a smaller time step(non-integer) to calculate.
%   In this case, all the needed parameters take values measured at integer
%   t,  e.g., if t is not integer, only use it's integeral part.
%%%%%%%%%%%%%%%%%%%%%%%%%%%%%%%%%%%%%%%%%%%%%%%%%%%%%%%%%%%%%%%%%%%%%%%%%%%

d=floor(t); % cut off decimals;
pp=p;
% pick out current value at time d;
```

```
F=WF(d,:);
T=T(d,:);
DO=DO(d,:);
W=WE(d,:);
SE=[SE(d,:)]';

% Streambed conduction;
D_T = 5.97015E-07;      % diffusivity (m2/s);
D_DO = 1.19403E-07;     % diffusivity (m2/s);
Delta_t = 900;          % 900 s = 15min;
Delta_z = 0.1;          % space step (m)

v = a.*x(1:M).^b;                 % calculate velocity from flow Q (m/s);
A = x(1:M)./v;                    % Cross section area (m2);
h = (-B+sqrt(B.^2+4*A.*s))/2./s;  % Water depth (m);
B0 = B+2*s.*h;                    % Top width (m);
D = A./B0+0.2;            % Hydraulic depth (m), with 0.2m depth Dead Zone;
CP = 4218*1000;                   % Specific heat capacity of water (J/m3);

Phi=Phi(d,:);

F_U=F(2);  % In flow
F_T=F(1);  % Trib flow
F_L=F(3);  % Out flow
% ------------------------------------------------------------------------
% set groundwater input = differences; qG >0 -> aquifer to stream;
bedA1 = DS1*mean([bedW(1) bedW(2)]);
bedA2 = (TotalDS-DS1)*mean([bedW(3) bedW(4)]);
qGv = (F_L - F_U - F_T)/(bedA1 + bedA2)*.6; % velocity (m/s);

% local adjust for groundwater input;
if (d>720) & (d<855)
    qGv =0;
end
if (d>750) & (d<800)
    qGv = .0000008*sin((d-750)*pi/50);
end
% groundwater flow rate in m3/s;
qG(1:M) = qGv*L.*B;    %Here if qG >0 ==> going to stream;
qG = qG';
% ------------------------------------------------------------------------
% surfare runoff effect if exist;
qL(1:M)=0;      %Lateral flow (m^3/s);
TL=273.15+10;   %Runoff temp;
DOL=6;          %Runoff DO (mg/L);
% ------------------------------------------------------------------------
% boundary values of DO;
if qGv > 0;             % qG>0 ==> going from the stream to aquifer;
    DOG=x(2*M+1:3*M);   % bed flow DO (mg/L);  going to aquifer;
else
    DOG(1:M)=5;         % bed flow DO (mg/L);  going to stream;
end
% ------------------------------------------------------------------------
% Initialize x_rate with size of x for each CSTR,
% which is n by 1 column vector.
x_rate=zeros(length(x),1);

% ========================================================================
% The following 3 steps are derivative estimation;
% ========================================================================
% ------------------------------------------------------------------------
% 1. Advection term only (Physical processes):
% ------------------------------------------------------------------------
% CSTR1
x_rate(1)=(F_U+qG(1)+qL(1)-x(1)) ...                            % Q
           /(L/a(1)*x(1)^(-b(1))*(1-b(1)))*Delta_t;
x_rate(M+1)=(F_U*T(2)+qL(1)*TL-(F_U+qL(1))*x(M+1)) ...          % T
           *Delta_t/(L/a(1)*x(1)^(1-b(1))) ;
```

```
x_rate(2*M+1)=(F_U*DO(2)+qL(1)*DOL-(F_U+qL(1))*x(2*M+1)) ...    % DO
            *Delta_t/(L/a(1)*x(1)^(1-b(1)));

% CSTRs before trib
for i=2:n1
    x_rate(i)=(x(i-1)+qG(i)+qL(i)-x(i))...
            /(L/a(i)*x(i)^(-b(i))*(1-b(i)))*Delta_t;            % Q
    x_rate(M+i)=(x(i-1)*x(M+i-1)+qL(i)*TL-(x(i-1)+qL(i)) ...
            *x(M+i))*Delta_t/(L/a(i)*x(i)^(1-b(i)));            % T
    x_rate(2*M+i)=(x(i-1)*x(2*M+i-1)+qL(i)*DOL-(x(i-1)+qL(i)) ...
            *x(2*M+i))*Delta_t/(L/a(i)*x(i)^(1-b(i)));          % DO
end

% CSTR at trib: CSTR=n1+1;
if n1>0
    x_rate(n1+1)=(x(n1)+F_T+qG(n1+1)+qL(n1+1)-x(n1+1)) ...
        /(L/a(n1+1)*x(n1+1)^(-b(n1+1))*(1-b(n1+1)))*Delta_t;     % Q
    x_rate(M+n1+1)=(x(n1)*x(M+n1)+F_T*T(1)+qL(n1+1)*TL-(x(n1) ...
        +F_T+qL(n1+1))*x(M+n1+1))*Delta_t/(L/a(n1+1)*x(n1+1)^(1-b(n1+1)));
    x_rate(2*M+n1+1)=(x(n1)*x(2*M+n1)+F_T*DO(1)+qL(n1+1)*DOL-(x(n1)+ ...
        F_T+qL(n1+1))*x(2*M+n1+1))*Delta_t/(L/a(n1+1)*x(n1+1)^(1-b(n1+1)));
else
    x_rate(n1+1)=(F_U+F_T+qG(n1+1)+qL(n1+1)-x(n1+1)) ...
        /(L/a(n1+1)*x(n1+1)^(-b(n1+1))*(1-b(n1+1)));            % Q
    x_rate(M+n1+1)=(F_U*T(2)+F_T*T(1)+qL(n1+1)*TL-(F_U+F_T+qL(n1+1)) ...
        *x(M+n1+1))*Delta_t/(L/a(n1+1)*x(n1+1)^(1-b(n1+1)));    % T
    x_rate(2*M+n1+1)=(F_U*DO(2)+F_T*DO(1)+qL(n1+1)*DOL-(F_U+F_T ...   %DO
        +qL(n1+1))*x(2*M+n1+1))*Delta_t/(L/a(n1+1)*x(n1+1)^(1-b(n1+1)));
end

% CSTRs after trib
for i=n1+2:M
    x_rate(i)=(x(i-1)+qG(i)+qL(i)-x(i))/(L/a(i) ...
        *x(i)^(-b(i))*(1-b(i)))*Delta_t;                        %Q
    x_rate(M+i)=(x(i-1)*x(M+i-1)+qL(i)*TL-(x(i-1)+qL(i)) ...
        *x(M+i))*Delta_t/(L/a(i)*x(i)^(1-b(i)));                %T
    x_rate(2*M+i)=(x(i-1)*x(2*M+i-1)+qL(i)*DOL-(x(i-1) ...
        +qL(i))*x(2*M+i))*Delta_t/(L/a(i)*x(i)^(1-b(i)));       %DO
end

% -----------------------------------------------------------------------
% 2. Temperature/Energy exchange with its environment:
% -----------------------------------------------------------------------
% Solar energy input:
    Phi=Phi';     % Solar angle from row vector to column vector (degree);
    m=Phi>1.24;   % a is logic vector M by 1;
    n=1-m;        % b is reverse of a;
    % Albedo for solar wave: if Phi<1.24, Albedo=1, else,=1.18*Phi.^(-0.77);
    Albedo_S=(m*1.18+n).*(m.*Phi+n).^(-0.77);
    SLD=W(5).*SE; % solar radiation corrected by exposure (from SHADE.m);
    SR=SLD.*(1-Albedo_S);          % Corrected solar input (J/m2/s);
    T_SR=SR*Delta_t./D/CP*p(1);    % Solar radiation;

% Longwave readiation:
    TA=W(2)+273.15;    % Air Temp (K), scalar; W(2)=Air T, W(3)=Humidity(%);
    SBC=5.67*10^(-8);  %Stefan-Boltzman constant = 5.67e-8 (W/m2/K);
    % Chaupra(P567):saturated vapor pressure at water surface T(mmHg);
    % 1 kpa=10mb = 10*0.02953 inHg = 10*0.02953*25.4 mm = 7.50062mmHg;
    e_air=W(3)/100*4.596*exp(17.27*(TA-273.15)./(237.3+TA-273.15));
    % Chaupra(P570):Emissivity of clear night sky;
    EmissivitySky=0.7+0.031*sqrt(e_air);
    % Tang Runsheng: 0.754+0.0044Tdp; EmissivitySky=0.787+0.0028Tdp;
    % EmissivitySky=0.7+0.045*sqrt(e_air)*p(2);
    % Chaupra(P570),Tang:Emissivity of water(nearly constant) of 0.97;
    EmissivityWater=0.97;
    % Tang: the absorptivity of water for long wave radiation is 0.935;
    Albedo_L=0.065;
    % Long wave radiation rate (W/m^2);
```

```
    T_LR=SBC*(EmissivitySky.*TA^4*(1-Albedo_L)*p(2) ...
        -EmissivityWater.*(x(M+1:2*M).^4)*p(3))*Delta_t./D/CP;

% Conduction and convection (W/m^2):
    Wind=W(7);
    ID='LeBlanc';
    crc=1;  % ratio of between wind over streams and local weather station;
    switch ID
        case 'LeBlanc'
            %LeBlanc(Krajewski, 1982). FU=0.0228*W(4)*Wind
            %W(4)=airPressure(Kpa), Wind=Wind(m/s);
            %Raphael, 1962 T_CV=0.0124*Wind*P(Tw-Ta)
            FU=0.0228*W(4)*Wind*5;
            T_CV=FU.*(TA-x(M+1:2*M))*Delta_t./D/CP*p(4);%.*(1-CV);
        otherwise
            %Chaupra(P571), Wind=wind(m/s), 0.47 is Bowen's coefficient;
            FU1=0.47*(19+0.95*(Wind*crc)^2);
            T_CV=FU1.*(TA-x(M+1:2*M))*Delta_t./D/CP;    %.*(1-CV);
    end

% Evaporation and condensation:Dalton's law. Refer:Runsheng Tang's paper.
    % Latent Heat
    % Wind function, Wind is is wind speed (m/s);
    FU2 = 0.0887+0.07815*Wind;
    % Chapra_1997(P567): saturated vapor pressure at water surface T(mmHg);
    e_water=4.596*exp(17.27*(x(M+1:2*M)-273.15)./(237.3+x(M+1:2*M)-273.15));
    T_EV=FU2.*(e_air-e_water)*133.3*Delta_t./D/CP*p(5); % 1 mmHg=133.3 pa;

% ------------------------------------------------------------------------
% bed effect on T;
    bedT_tmp = x(M*3+1:M*3+M*bedM);           % current vertical T profile;
    bedT_tmp = reshape(bedT_tmp, bedM, M);    % current vertical T profile;
    dTdz = [(bedT_tmp(2,:)- bedT_tmp(1,:))/Delta_z]'; % gradient;
    T_BED1 = D_T*dTdz./D*Delta_t;                     % diffusion;

    bedTM=mean([bedT_tmp(2,:), bedT_tmp(1,:)]); % mean of first two layers;
    m = (qG>0);
    T_BED2 = qG.*(bedTM.*m + x(M+1:2*M).*(1-m) ...          % advection;
       - x(M+1:2*M))./(L./a.*x(1:M).^(1-b))*Delta_t;
    T_BED = T_BED1 + T_BED2;                                % total effect;

% ------------------------------------------------------------------------
% Adding Source/sink terms for temperature model:
x_rate(M+1:2*M) = x_rate(M+1:2*M)+T_SR*tempID(1)+T_LR*tempID(2) ...
                + T_CV*tempID(3)+T_EV*tempID(4) + T_BED*tempID(5);

% ------------------------------------------------------------------------
% 3. DO/Mass exchange with its environment (mg/L/Delta_t):
% ------------------------------------------------------------------------
% Reaeration from atmosphere (/day): (Chapra_1997:P377; EPA_1985:p103-106);
    ID='OD';
    switch ID
        case 'OD'
            % O'Connor-Dobbins, 1956; for D=(0.3 - 9.14m), v=0.15-0.49m/s);
            Ka=3.93*(v.^0.5)./(D.^1.5);
        case 'CH'
            % Churchill et al. 1962; for D=(0.61 - 3.35m), v=0.55-1.52m/s);
            Ka=5.026*v./(D.^1.67);
        case 'OG'
            % Owens and Gibbs, 1964; for D=(0.12 - 0.73m), v=0.03-0.55m/s);
            Ka=5.32*(v.^0.67)./(D.^1.85);
    end
    Ka=Ka/24/4*IDDO(1);  % convert from /day to /15min;
    ThetaKa=1.024;       % T corrector: 1.022-1.024; EPA_1985:P125; (/day);
    Ka=Ka.*(ThetaKa.^(x(M+1:2*M)-20-273.15));
    % EPA, 1985: P91; Cox, 2003: P8 --> Elmore&Hayes, 1960;
    CS=14.652-0.41022*(x(M+1:2*M)-273.15)+0.007991*((x(M+1:2*M) ...
        -273.15).^2)-7.7774*10^-5*((x(M+1:2*M)-273.15).^3);
```

```
    DO_Ka=Ka.*(CS-x(2*M+1:3*M));

% Photosynthesis by Algae (EPA, 1985: P125; 2. Cox, 2003 Review: P24, 27)
    Alg = 0.001;    % (mg/L) By measurements: 0.35~1.4 ug/L (2004, by Li);
    ThetaP = 1.036;   %Parkhill & Gulliver, 1998; Megard et al., 1984);
    MaxGrowth=1/24/4*IDDO(2);   % algae maximum growth rate (/15min);
    SRLimit = IDDO(6);          % saturation light(W/m2)for photosynthesis;
    PSR = (SR<SRLimit).*SR + (SR>=SRLimit)*SRLimit;
    GRate=MaxGrowth.*PSR;       % modified from Xiaoqing's thesis:P185-186;
    AlgToOxy = 138*32/106/12;   % Zeng Xiaoqing's Dissertation: P184,188;
    GRate=GRate.*ThetaP.^(x(M+1:2*M)-20-273.15); %correction by temp
    AlgToOxy=138*32/106/12;     % Zeng Xiaoqing's Dissertation: P184,188;
    DO_P=Alg.*GRate*AlgToOxy;   % EPA_1985: P188;

% Respiration by Algae:
    RRate=1/4/24*IDDO(3); %Maximum respiration rate at 20*C; (/day);
    %Parkhill_Gulliver_1998; Gulliver_Stefan_1984b; Ambrose_et_al_1988:
    ThetaR=1.045;
    AlgConsumeOxy=138*32/106/12; %Zeng Xiaoqing's Dissertation: P184,188;
    DO_R=Alg.*RRate.*(ThetaR.^(x(M+1:2*M)-20-273.15))*AlgConsumeOxy;

% BOD decay;
    ThetaB=1.047;       % Arrhenius coefficient for BOD; Knowles_1978;
    BOD = 4;            % mg/L by field grab samples;
    BODRate = 1/4/24*IDDO(4)*BOD; % BOD decay rate; 1/s;
    BOD_Decay = BODRate*ThetaB.^(x(M+1:2*M)-20-273.15);  % correction by T;
    DO_BOD= BOD_Decay;  % mg/L/s*m^2;

% SOD decay; assuming constant rate corrected by T;
    % http://wilsontxt.hwwilson.com/pdfhtml/02385/am81d/yfh.htm
    % cox,2003, 1.065 for SOD;
    ThetaS=1.065;
    SODRate = 1/4/24*IDDO(5);   % SOD decay rate: mg/m^2/s;
    % correction by T; 0.001 converts from mg/m^3 -> mg/L:
    SOD_Decay = SODRate*(ThetaS.^(x(M+1:2*M)-20-273.15))./D*.001;
    DO_SOD= SOD_Decay;          % mg/L/s*m^2;

% bed effect on DO;
    bedDO_tmp = x(M*3+M*bedM+1:M*3+M*bedM*2); %current vertical DO profile;
    bedDO_tmp = reshape(bedDO_tmp, bedM, M);
    dDOdz = [(bedDO_tmp(2,:)- bedDO_tmp(1,:))/Delta_z]';    % gradient;
    DO_BED1 = D_DO*dDOdz./D*Delta_t;                         % diffusion;

    bedDOM = mean([bedDO_tmp(2,:),bedDO_tmp(1,:)]); % mean of layers 1 & 2;
    m = (qG>0);
    DO_BED2 = qG.*(bedDOM.*m + x(M*2+1:3*M).*(1-m) ...      % advection;
            - x(M*2+1:3*M))./(L./a.*x(1:M).^(1-b))*Delta_t;
    DO_BED = DO_BED1 + DO_BED2;                              % total effect;

% -----------------------------------------------------------------------
% Adding Source/sink terms for DO model:
x_rate(2*M+1:3*M)=x_rate(2*M+1:3*M)+DO_Ka*doID(1)+DO_P*doID(2) ...
    -DO_R*doID(3)-DO_BOD*doID(4)-DO_SOD*doID(4) + DO_BED*doID(6);

% =======================================================================
% Groundwater T/DO profile: FTCS numerical method;
% =======================================================================
% define coefficients;
gam = -qGv*Delta_t/2/Delta_z; % advection number, minus sign added;

lmd_T = D_T/(Delta_z)^2*Delta_t;      % T dispersion number;
lmd_DO = D_DO/(Delta_z)^2*Delta_t;    % DO dispersion number;

aa_T = lmd_T + gam;     % T coefficient for i-1;
bb_T = 1-2*lmd_T;       % T coefficient for i;
cc_T = lmd_T - gam;     % T coefficient for i+1;

aa_DO = lmd_DO + gam;     % DO coefficient for i-1;
```

```
bb_DO = 1-2*lmd_DO;       % DO coefficient for i;
cc_DO = lmd_DO - gam;     % DO coefficient for i+1;

% FTCS scheme to get bed T for next time step;
% bedT_tmp is bedT at current step; bedM by M;
% bedT_x is a bedT for next step; bedM by M;
bedT_x(1,:) = bedT_tmp(1,:);        % up boundary: T = water T;
bedDO_x(1,:) = bedDO_tmp(1,:);      % up boundary: DO = water DO;

for i = 2:bedM-1                    % FTCS in between layers
    bedT_x(i,:) = aa_T*bedT_tmp(i-1,:) ...
                + bb_T*bedT_tmp(i,:)+cc_T*bedT_tmp(i+1,:);
    bedDO_x(i,:) = aa_DO*bedDO_tmp(i-1,:) ...
                + bb_DO*bedDO_tmp(i,:)+cc_DO*bedDO_tmp(i+1,:);
end
bedT_x(bedM,:) = bedT_tmp(bedM,:);   % Lower boundary: T = ground T;(K);
bedDO_x(bedM,:) = bedDO_tmp(bedM,:); % Lower boundary: T = ground T;(mg/L);

% Converting to changing rate of bedT for ODE solver;
% bedT_rate = (newT - oldT)/dt, dt=1;
% top layer T rate = water T rate;
% bedDO_rate the same;
bedT_rate = bedT_x - bedT_tmp;                       %  T: bedM by M;
bedT_rate(1,:) = reshape(x_rate(M+1:M*2),1,[]);      %  T: 1 by M;
bedDO_rate = bedDO_x - bedDO_tmp;                    % DO: bedM by M;
bedDO_rate(1,:) = reshape(x_rate(M*2+1:M*3),1,[]);  % DO: 1 by M;

% put bed T/DO changing rate to ODE solver rates holder;
bedT_rate = reshape(bedT_rate, [], 1);               %  T: bedM*M by 1;
x_rate(3*M+1:3*M+bedM*M) = bedT_rate;                %  T: bedM*M by 1;
bedDO_rate = reshape(bedDO_rate, [], 1);             % DO: bedM*M by 1;
x_rate(3*M+bedM*M+1:3*M+bedM*M*2) = bedDO_rate;     % DO: bedM*M by 1;

return
```

D.3 DDOT in ADRE structures

D.3.1 Main function - To invoke Q, T, and C models

```
function [T, DO, Tbed, DObed, Q, A, B, h, U, QQ, SE, ...
            SA, DT, we, WQuality, WFlow, qGv] = ftdo;
%%%%%%%%%%%%%%%%%%%%%%%%%%%%%%%%%%%%%%%%%%%%%%%%%%%%%%%%%%%%%%%%%%%%%%%%%%%%%
% Function:
%   FTDO.m --- ADRE based modeling (flow, T, DO modules)
%   outputs are M by N matrix, M is space nodes, N is time nodes.
%
% Inputs:
%   No explicit input parameters necessary;
%
% Outputs:
%   T --- simulated temperature (*C);
%   DO --- simulated DO (mg/L);
%   Tbed --- simulated bed temperature profile (*C);
%   DObed --- simulated bed flow DO profile (mg/L);
%   Q --- simulated flow (m^3/s);
%   A --- simulated cross section area (m2);
%   B --- simulated water surface width (m);
%   h --- simulated water stage (m);
%   U --- simulated flow velocity (m/s);
%
%   SE --- simulated exposure percent to direct solar radiation by SHADE;
%   SA --- simulated solar angle by SHADE;
%   DT --- time in format recongizable by Matlab;
```

```
%   we --- weather;
%   WQuality --- observed water quality;
%   WFlow --- observed flow;
%   qGv --- estimated ground water flow rate (m/s);
%
% Boundary conditions:
%   Upboundary is the upstream flow input. Lower boundary is zero
%   derivative of stream water depth. So no observed lower boundary data
%   required.
%%%%%%%%%%%%%%%%%%%%%%%%%%%%%%%%%%%%%%%%%%%%%%%%%%%%%%%%%%%%%%%%%%%%%%%%%%%

% function obj = ftdo(p);       % Enable this line for optimization

if exist('p')
    ID = p                  % for parameter optimization;
else
    ID = ones(1,6)    % for general model run;
end

% ========================================================================
% disp('Loading data from XLS files ...')
% time series flow/stage data;
% col:       1      2     3     4      5     6     7
% row1 = [time  Ichi2 Ichi2 Ichi3  Ichi3 Patch Patch]
% row2 = [timeN Depth Flow  Depth  Flow  Depth Flow ]
WFlow = xlsread('WFlow.xls');

% water quality = [Time upT upDO downT downDO tribT tribDO]
WQuality = xlsread('WQuality.xls');

% geomorphology = [INFO Abbr Upstream Downstream Metric_units]
[geonum geotxt]=xlsread('Geomorphology.xls');

% weather = [timeofyear airT Humidity VaporP TotalPres SolarR TotalSolar
% Rain WindV]
Weather = xlsread('Weather.xls');
%-------------------------------------------------------------------------
% Smoothing
k = 8;
sm = ones(1,k)/k;                        % smoothing parameter
% Weather= filtfilt(sm, 1, Weather_);   % Smooth Temperature data;
% disp('Loading data done!')
% ========================================================================

% convert Excel date to Matlab date;
DT = WFlow(:,1) + datenum('30-Dec-1899');

% -------------------------------------
% This is for code testing;
id = 10;  % let id = 1 for fast testing;
if id == 1
    N=300
    WFlow = WFlow(1:N,:);
    WQuality = WQuality(1:N,:);
    Weather = Weather(1:N,:);
    DT = DT(1:N,1);
end
% -------------------------------------

we = Weather;

[row col] = size(WFlow);

% time series Flow data; only one tributary considered;
h_up = WFlow(:,2);      % upboundary water depth (m);
Q_up = WFlow(:,3);      % upboundary water flow (m^3/s);
h_down = WFlow(:,4);    % downboundary water depth (m);
Q_down = WFlow(:,5);    % downboundary water flow (m^3/s);
```

```
h_trib = WFlow(:,6);    % tributary water depth (m);
Q_trib = WFlow(:,7);    % tributary water flow (m^3/s);

% time series WQ data; only one tributary considered;
T_up = WQuality(:,2);       % upboundary water depth (m);
DO_up = WQuality(:,3);      % upboundary water flow (m^3/s);
T_down = WQuality(:,4);     % downboundary water depth (m);
DO_down = WQuality(:,5);    % downboundary water flow (m^3/s);
T_trib = WQuality(:,6);     % tributary water depth (m);
DO_trib = WQuality(:,7);    % tributary water flow (m^3/s);

% create variables for stream reach geomorphology data;
% see Geomorphology.xls for variables generated by this loop;
[row_geo col_geo]=size(geonum); for i=1:row_geo
    if isnan(geonum(i,2))
        eval([geotxt{i+1,2},'=geonum(i,1);']);
    else
        eval([geotxt{i+1,2},'=geonum(i,:);']);
    end
end

% nodes on mesh: M = space nodes; N = time nodes;
M = round(L/delta_x)+1; N = row;
M_trib = round(L_trib/delta_x)+1;   % location of tributary;

% Parameters examination (initial up/down stream only) (erasable);
A_0 = (wid_bed + slp_bank.*[h_up(1) h_down(1)]).*[h_up(1)
h_down(1)]; P_0 = (wid_bed + 2*[h_up(1) h_down(1)] .*
sqrt(slp_bank.^2+1)); R_0 = A_0./P_0; U_0 =
1.49./n.*R_0.^(2/3).*slp_bed.^(.5); Q_0 =A_0.*U_0;

% Trib flow conditions time series;
A_trib = (wid_bed_trib + slp_bank_trib*h_trib).*h_trib; P_trib =
wid_bed_trib + 2*h_trib.* sqrt(slp_bank_trib^2+1); R_trib =
A_trib./P_trib; U_trib =
1.49./n_trib*R_trib.^(2/3)*sqrt(slp_bed_trib);
%Q_trib = A_trib.*U_trib;

% invoke function to obtain simulated Q and h;
if (M_trib < 3) | (M_trib > M-3 & M_trib<M)
    clc;
    disp(['Error! Not enough nodes between tributary and bounds']);
    disp(['Please change space step size or reach length to correct.']);
    return;
end

% -------------------------------------------------------------------------
% prepare groundwater flow rate in N by M;
% groundwater assumption:
alpha = pi/4;   % angle between trib and main stem;
bedW1 = wid_bed(1); bedW2 = ((L-L_trib)*bedW1+L_trib*(wid_bed(2) ...
        - wid_bed_trib*cos(alpha)))/L;
bedW3 = bedW2 + wid_bed_trib*cos(alpha); bedW4 = wid_bed(2);

bedA1 = L_trib*mean([bedW1 bedW2]); bedA2 = (L-L_trib)*mean([bedW3
bedW4]); qGv(1:N,1) = WFlow(:,10)/(bedA1 + bedA2)*.6;

% - local adjust for groundwater input (m/s);
qGv(720:855) = 0; qGv(750:800) = .000001*sin([0:50]*pi/50);

qGv = qGv * ones(1,M);

n_g = (n(2)-n(1))/(M-1); for i=2:M
    n(:,i) = n(:,1)+(i-1)*n_g;          %Manning's n;
end

% =========================================================================
% invoke flow model;
```

```
% ========================================================================
if M_trib < M;   % with one trib;
    % if trib exists;
    % calculations before trib;
    alpha = pi/4;   % angle between trib and main stem;
    wid(1) = wid_bed(1);
    wid(2) = ((L-L_trib)*wid_bed(1)+L_trib*(wid_bed(2) ...
             - wid_bed_trib*sin(alpha)))/L;

    Q_mid = Q_up;
    h_mid = h_up;
    % initial values adjust;
    Q_up(1) = Q_up(1)-.02;
    Q_mid(1) = Q_mid(1)+.25;
    h_up(1) = h_up(1)-.02;
    h_mid(1) = h_mid(1)-0.05;
    % assuming before trib: Q at trib = Q_up;
    [Q, h, B, A, P, R, U, QQ, W, slp_bank] = ...
            ftdo_flow(Q_up, h_up, Q_mid, h_mid, qGv(:,1:M_trib), ...
            wid, slp_bed, slp_bank, n(:,1:M_trib), delta_x, delta_t, ...
            M_trib, N, tol);

    % calculations after trib;
    wid(1)=wid(2)+wid_bed_trib*sin(alpha);
    wid(2)=wid_bed(2);
    Q_mid = Q(M_trib,:)' + Q_trib;    % redifine up input;
    h_mid = h(M_trib,:)';

    % initial values adjust;
    Q_mid(1) = Q_mid(1)-.15;
    Q_down(1) = Q_down(1);-0.2;
    h_mid(1) = h_mid(1)+.06;
    h_down(1) = h_down(1)+.015;
    [Q_t, h_t, B_t, A_t, P_t, R_t, U_t, QQ_t, W_t, slp_bank_t] = ...
            ftdo_flow(Q_mid, h_mid, Q_down, h_down, qGv(:,M_trib:M), ...
            wid, slp_bed, slp_bank, n(:,M_trib:M), delta_x, delta_t, ...
            M-M_trib+1, N, tol);

    % first column is upboundary conditions of after-trib,
    % which is duplicate of downstream conditions before trib; so removed.
    Q_t(1,:) = [];
    h_t(1,:) = [];
    B_t(1,:) = [];
    A_t(1,:) = [];
    P_t(1,:) = [];
    R_t(1,:) = [];
    U_t(1,:) = [];
    QQ_t(1,:) = [];
    W_t(1,:) = [];
    slp_bank_t(1,:) = [];

    % merge results;
    Q = [Q; Q_t];
    h = [h; h_t];
    B = [B; B_t];
    A = [A; A_t];
    P = [P; P_t];
    R = [R; R_t];
    U = [U; U_t];
    QQ = [QQ; QQ_t];
    W = [W; W_t];
    slp_bank = [slp_bank; slp_bank_t];

else    % if no trib;
    [Q, h, B, A, P, R, U, QQ, W, slp_bank] = ...
            ftdo_flow(Q_up, h_up, Q_up, h_up, qGv, ...
            wid_bed, slp_bed, slp_bank, n, delta_x, delta_t, ...
            M, N, tol);
```

```
end

% ========================================================================
% invoke SolarC and SHADE model;
% ========================================================================
% Solar angle SA, decline angle DA and hour angle HA (N by M matirx).
LD = LD(1) + [0:M-1]/(M-1)*(LD(2) - LD(1));

% DT-1/24 = remove daylight saving time effect for summer time;
[SA, sinSA, DA, HA]=solarC(DT-1/24,LD);     % Solar angle model;
% SA --- Solar angle, SA=0 if <0(sunset&before sunrise) (radian);
% sinSA --- sin of Solar angle, sinSA=0 after sunset & before sunrise;
% DA --- Solar decline angle ([-23.45 23.45]), (radian);
% HA --- Hour angle for a day ([0, 2pi]), (radian);

River_agl = River_agl(1) ...
            + [0:M-1]/(M-1)*(River_agl(2) - River_agl(1));
Tree_height = Tree_height(1) ...
            + [0:M-1]/(M-1)*(Tree_height(2) - Tree_height(1));
Bank_height = Bank_height(1) ...
            + [0:M-1]/(M-1)*(Bank_height(2) - Bank_height(1));

% SHADE model (SE = % of water surface NOT in shadow, eg. exposed);
    p1 = River_agl;         % 1 by M;
    p2 = Tree_height;       % 1 by M;
    p3 = Bank_height;       % 1 by M;
    p4 = [slp_bank(:,1)]';  % 1 by M;
    p5 = [W(:,1)]';         % 1 by M;
    p6 = h';                % N by M;
    p7 = B';                % N by M;
    p8 = SA;                % N by M;
    p9 = DA;                % N by M;
    p10 = HA;               % N by M;
    % invoke SHADE.m
    SP = Shade(p1, p2, p3, p4, p5, p6, p7, p8, p9, p10, DT);   % N by M;
    SP = SP'*canopy(1);     % M by N; shading percent;
    SE = 1-SP;              % M by N; unshading percent;

% ========================================================================
% invoke T and DO models;
% ========================================================================
% prepare data for input;
SA=SA'; sinSA=sinSA'; DA=DA'; HA=HA';  qGv=qGv'; % M by N;

if M_trib < M       % with one trib;
    % --------------------------------------------------------------------
    % calculation before trib;
    Q_tmp = Q(1:M_trib,:);  % time series flow;
    A_tmp = A(1:M_trib,:);  % time series cross section;
    B_tmp = B(1:M_trib,:);  % time series surface width (m);
    h_tmp = h(1:M_trib,:);  % time series water depth;
    U_tmp = U(1:M_trib,:);  % time series water depth;
    W_tmp = W(1:M_trib,:);  % longitudinal streambed width;
    qGv_tmp = qGv(1:M_trib,:);  % longitudinal groundwater flow;
    SE_tmp = SE(1:M_trib,:);    % unshaded percent;
    SA_tmp = SA(1:M_trib,:);    % Solar angle in radius;
    % time series cross section;
    T_down_tmp = T_up + L_trib/L*(T_down - T_up);
    DO_down_tmp = DO_up + L_trib/L*(DO_down - DO_up);
    DO_down_tmp(1) = DO_down_tmp(1)-0.4; %adjust initial of lower boundary;
    % invoke TDO model using corrected MacCormack scheme;
    [T, DO, Tbed, DObed] = MacCormack_c(T_up, DO_up, T_down_tmp, ...
                    DO_down_tmp, Q_tmp, h_tmp, qGv_tmp, TG, DOG, ...
                    D_Tbed, D_DObed, delta_z, ...
                    M_bed, U_tmp, A_tmp, B_tmp, W_tmp, ...
                    M_trib, N, delta_t, delta_x, ...
                    Weather, SE_tmp, SA_tmp, ID);
    % --------------------------------------------------------------------
```

```
    % calculation after trib;
    Q_tmp = Q(M_trib:M,:);
    Q_tmp(1,:) = Q(M_trib,:) + Q_trib';   % correct input Q at trib;
    A_tmp = A(M_trib:M,:);
    A_tmp(1,:) = 2*A_tmp(2,:)-A_tmp(3,:); % int of input A at trib;
    B_tmp = B(M_trib:M,:);
    B_tmp(1,:) = 2*B_tmp(2,:)-B_tmp(3,:); % int of input B at trib;
    h_tmp = h(M_trib:M,:);
    h_tmp(1,:) = 2*h_tmp(2,:)-h_tmp(3,:); % int of input h at trib;
    U_tmp = U(M_trib:M,:);
    U_tmp(1,:) = 2*U_tmp(2,:)-U_tmp(3,:); % int of input U at trib;
    W_tmp = W(M_trib:M,:);
    W_tmp(1,:) = 2*W_tmp(2,:)-W_tmp(3,:); % int of input wid_bed at trib;
    SE_tmp = SE(M_trib:M,:);
    SE_tmp(1,:) = 2*SE_tmp(2,:)-SE_tmp(3,:); % int of input wid_bed at trib;
    qGv_tmp = qGv(M_trib:M,:);
    SA_tmp = SA(M_trib:M,:);            % Solar angle in radius;
    T_up_tmp = ([T(M_trib,:).*Q(M_trib,:)]'+T_trib.*Q_trib) ...
                ./([Q(M_trib,:)]' + Q_trib);
    DO_up_tmp = ([DO(M_trib,:).*Q(M_trib,:)]'+DO_trib.*Q_trib) ...
                ./([Q(M_trib,:)]' + Q_trib);
    DO_up_tmp(1) = DO_up_tmp(1) - .2;  % adjust initials.
    % invoke TDO model using corrected MacCormack scheme;
    [T_t, DO_t, Tbed_t, DObed] = MacCormack_c(T_up_tmp, DO_up_tmp, ...
                    T_down, DO_down, ...
                    Q_tmp, h_tmp, qGv_tmp, TG, DOG, D_Tbed, D_DObed, ...
                    delta_z, M_bed, U_tmp, A_tmp, B_tmp, W_tmp, ...
                    M-M_trib+1, N, delta_t, delta_x, ...
                    Weather, SE_tmp, SA_tmp, ID);

    % first column is duplicate, so removed.
    T_t(1,:) = [];
    DO_t(1,:) = [];
    Tbed_t(:,1,:) = [];
    % ---------------------------------------------------------------------
    % merge results for before and after trib;
    T = [T; T_t];
    DO = [DO; DO_t];
    Tbed = [Tbed Tbed_t];

else    % if no trib;
    [T, DO, Tbed, DObed] = MacCormack_c(T_up, DO_up, T_down, DO_down, ...
                    Q, h, qGv, TG, DOG, D_Tbed, D_DObed, ...
                    delta_z, M_bed, U, A, B, W, ...
                    M, N, delta_t, delta_x, ...
                    Weather, SE, SA, ID);
end     % end temperature and Do model invoke;

% the following 5 lines are objective functions for optimization;

err = [T(M,:)]' - T_down;

obj1 = err'*err;

err = [DO(M,:)]' - DO_down;

obj2 = err'*err;

obj = obj2;

return
```

D.3.2 Flow model - Saint-Venant Equations

```
function [Q, h, B, A, P, R, U, QQ, wid_bed, slp_bank, qG] = ...
```

```
                    ADRE_Flow(Q_up, h_up, Q_down, h_down, qG, ...
                    wid_bed, slp_bed, slp_bank, n, ...
                    delta_x, delta_t, M, N, tol)
%%%%%%%%%%%%%%%%%%%%%%%%%%%%%%%%%%%%%%%%%%%%%%%%%%%%%%%%%%%%%%%%%%%%%%%%%%%
% Function:
%   ADRE_Flow.m --- Open channel flow simulation (Saint-Venant Equations);
%                   Generates flow info for ADRE water quality structures;
%
% Inputs:
%   Q_up --- up boundary time series flow rate (m3/s);
%   h_up --- up boundary time series water depth (m);
%   qL --- lateral/groundwater flow rate (m2/s);
%   bed_wid --- streambed width (m);
%   slp_bank --- stream bank slope (dimensionless);
%   slp_bed --- streambed slope (dimensionless);
%   n --- manning's roughness coefficient (dimensionless);
%   distance --- total length of reach (m);
%   delta_x --- space step interval (m);
%   time --- total time period of simulation (s);
%   delta_t --- temporal step interval (s);
%   Q_down --- down boundary time series flow rate (m3/s);
%   h_down --- down boundary time series water depth (m);
%
% Outputs:
%   Q --- output flow rate (m3/s);
%   h --- output water depth (m);
%   B --- output water surface width (m);
%   A --- output cross section area (m2);
%   P --- output wetted perimeter (m);
%   R --- output hydaulic radius (m);
%   U --- output flow velocity (m/s);
%%%%%%%%%%%%%%%%%%%%%%%%%%%%%%%%%%%%%%%%%%%%%%%%%%%%%%%%%%%%%%%%%%%%%%%%%%%

fprintf('\n'); qG_v = qG';

% obtain vector form parameters along spatial mesh nodes;
wid_bed_t = wid_bed;
slp_bed_t = slp_bed;
slp_bank_t = slp_bank;
n = n/1.49;

% define initial values at time j=1 using linear intepolation;
% gradients;
slp_bed_g = (slp_bed(2)-slp_bed(1))/(M-1);

slp_bank_g = (slp_bank(2)-slp_bank(1))/(M-1); h_g =(h_down(1) -
h_up(1))/(M-1)

Q_g = (Q_down(1)-Q_up(1))/(M-1);             % if no trib;
wid_bed_g = (wid_bed(2)-wid_bed(1))/(M-1);

clear wid_bed slp_bed slp_bank qG;

% linear interpolation to get M by 1 vectors for longitudinal gemorphology;
for i=1:M
    wid_bed(i,1) = wid_bed_t(1) + (i-1)*wid_bed_g;
    slp_bed(i,1) = slp_bed_t(1) + (i-1)*slp_bed_g;
    slp_bank(i,1) = slp_bank_t(1) + (i-1)*slp_bank_g;
    h(i,1) = h_up(1) + (i-1)*h_g;     %water depth (m); at t=1
    Q(i,1) = Q_up(1) + (i-1)*Q_g;     %water flow (m3/s); at t=1
end

% expand vector to matrix for coding convenience;
wid_bed = [wid_bed wid_bed]; \\
slp_bed = [slp_bed slp_bed]; \\
slp_bank = [slp_bank slp_bank]; n = [n' n'];

% base values at j=1 for try is the initial values;
```

```
h_try(:,1) = h; Q_try(:,1) = Q;

% define the next trying values(column 2)the same as the base values;
h_try = [h_try h_try]; Q_try = [Q_try Q_try];

theta = 0.6;   % weight coeffient in preissmann scheme (0.5 < theta <= 1);
g = 9.8;    % gravity (m/s2)

% double loops for grid calculation;
for jj = 2:N     % jj is time steps

    progressbar(jj/N);     % progressbar.m --- progress indicator
    qG(:,1) = qG_v(:,jj-1);
    qG(:,2) = qG_v(:,jj);
    qGr = qG.*wid_bed;      % groundwater flow rate (m2/s);
    cos_phiG= pi/2;         % assuming groundwater perpendicular to stream;
    gw1 = qGr;              % groundwater for continuity eqn;
    gw2 = qGr.*qG*cos_phiG; % groundwater for momentum eqn;

    Q_try(1,2)= Q_up(jj); % upboundary conditions;

    for k = 1:50 % iterations for try and error;
        for i = 1:M
            if Q_try(i,2) < 0;
                Q_try(i,2) =0.001;
            end
        end
        % nodes
        % calculate hydrolic pars;
        B = wid_bed + 2*slp_bank.*h_try;         % surf Wid (m);I by 2;
        A = (wid_bed + slp_bank.*h_try).*h_try;  % cross section area (m2);
        P = wid_bed + 2*h_try.*sqrt(1+slp_bank.^2);  %wetted perimeter (m);
        R = A./P;                                    % hydrolic radius (m);
        QQ_A = Q_try.^2./A;                          % QU(m4/s2);

        % calculate averages:
        for i = 1:M-1
            B_bar(i,1) = (theta*(B(i,2) + B(i+1,2)) ...
                + (1-theta)*(B(i,1) + B(i+1,1)))/2;
            A_bar(i,1) = (theta*(A(i,2) + A(i+1,2)) ...
                + (1-theta)*(A(i,1) + A(i+1,1)))/2;
            R_bar(i,1) = (theta*(R(i,2) + R(i+1,2)) ...
                + (1-theta)*(R(i,1) + R(i+1,1)))/2;
            QQ_bar(i,1) = (theta*(Q_try(i,2).^2 + Q_try(i+1,2).^2) ...
                + (1-theta)*(Q_try(i,1).^2 + Q_try(i+1,1).^2))/2;
            gw1_bar(i,1) = (theta*(gw1(i,2) + gw1(i+1,2)) ...
                + (1-theta)*(gw1(i,1) + gw1(i+1,1)))/2;
            gw2_bar(i,1) = (theta*(gw2(i,2) + gw2(i+1,2)) ...
                + (1-theta)*(gw2(i,1) + gw2(i+1,1)))/2;
            n_bar(i,1) = (theta*(n(i,2) + n(i+1,2)) ...
                + (1-theta)*(n(i,1) + n(i+1,1)))/2;
            slp_bed_bar(i,1) = (theta*(slp_bed(i,2) ...
                + slp_bed(i+1,2)) + (1-theta)*(slp_bed(i,1) ...
                + slp_bed(i+1,1)))/2;
            slp_bank_bar(i,1) = (theta*(slp_bank(i,2) ...
                + slp_bank(i+1,2)) + (1-theta)*(slp_bank(i,1) ...
                + slp_bank(i+1,1)))/2;

            pQpx(i,1) = (theta*(Q_try(i+1,2) - Q_try(i,2)) ...
                + (1-theta)*(Q_try(i+1,1) - Q_try(i,1)))/delta_x;
            pQQ_Apx(i,1) = (theta*(QQ_A(i+1,2) - QQ_A(i,2)) ...
                + (1-theta)*(QQ_A(i+1,1) - QQ_A(i,1)))/delta_x;
            phpx(i,1) = (theta*(h_try(i+1,2) - h_try(i,2)) ...
                + (1-theta)*(h_try(i+1,1) - h_try(i,1)))/delta_x;

            phpt(i,1) = (h_try(i+1,2) + h_try(i,2) ...
                        - h_try(i+1,1) - h_try(i,1))/2/delta_t;
            pQpt(i,1) = (Q_try(i+1,2) + Q_try(i,2) ...
```

```
                    - Q_try(i+1,1) - Q_try(i,1))/2/delta_t;
end

gnAR = g*n_bar.^2./A_bar./R_bar.^(4/3);

% calculate function G & H at try step k,
% which are also called residuals ;
G = B_bar.*phpt + pQpx - gw1_bar;
H = pQpt + pQQ_Apx + g*A_bar.*(phpx - slp_bed_bar) ...
        + gnAR.*QQ_bar - gw2_bar;

% combination into one variable;
GH(1,1) = Q_try(1,2) - Q_up(jj);
for i = 1:M-1   % i is space index;
    j=2*i;      % j is time index;
    GH(j,1) = G(i);
    GH(j+1,1) = H(i);
end

% downstream boundary - Saulyev type (diagonal)
GH(2*M,1) = h_try(M,2) +h_try(M-2,1) -h_try(M-1,1) -h_try(M-1,2);

% Calculation for Jacobian matrix;
pGph1 = B_bar/delta_t;
pGpQ1 = -theta/delta_x*ones(M-1,1);
pGph2 = pGph1;
pGpQ2 = -pGpQ1;

pGpQh = [pGph1, pGpQ1, pGph2, pGpQ2];

pHph1 = theta/delta_x*B(1:M-1,2) ...
        .*(Q_try(1:M-1,2)./A(1:M-1,2)).^2 ...
        + g*theta.*(B(1:M-1,2).*phpx/2 - A_bar/delta_x) ...
        - gnAR.*QQ_bar.*theta.*(2/3./R_bar ...
        .*(B(1:M-1,2)./P(1:M-1,2) - A(1:M-1,2)./P(1:M-1,2).^2) ...
        .*sqrt(slp_bank_bar)/2 + B(1:M-1,2)./A_bar/2);

pHpQ1 = 1/2/delta_t - theta/delta_x*2*Q_try(1:M-1, 2) ...
        ./A(1:M-1, 2) + gnAR*theta.*Q_try(1:M-1, 2);

pHph2 = -theta/delta_x*B(2:M,2) ...
        .*(Q_try(2:M,2)./A(2:M,2)).^2 ...
        + g*theta.*(B(2:M,2).*phpx/2 + A_bar/delta_x) ...
        - gnAR.*QQ_bar.*theta.*(2/3./R_bar ...
        .*(B(2:M,2)./P(2:M,2) - A(2:M,2)./P(2:M,2).^2) ...
        .*sqrt(slp_bank_bar)/2 + B(2:M,2)./A_bar/2);

pHpQ2 = 1/2/delta_t + theta/delta_x*2*Q_try(2:M, 2) ...
        ./A(2:M, 2) + gnAR*theta.*Q_try(2:M, 2);

pHpQh = [pHph1, pHpQ1, pHph2, pHpQ2];

% jacobian matrix;
J = zeros(2*(M-1)); % initialization: (2M-2) by (2M-2);
J(1,1:2) = [0 1];
for i = 1:M-1
    j=2*i;          %index
    J(j,j-1:j+2) = pGpQh(i,:);
    J(j+1,j-1:j+2) = pHpQh(i,:);
end
j=2*M;
J(j,j-1:j) = [1, 0]; % for downstream conditions

% calculate increment for next try;
new_try = -inv(J)*GH;

% pick out increment for new try;
for i=1:length(J)/2
```

```
            h_try_delta(i) = new_try(2*i-1);
            Q_try_delta(i) = new_try(2*i);
        end

        % update try values by adding increment;;
        h_try(:,2) = h_try(:,2) + h_try_delta';
        Q_try(:,2) = Q_try(:,2) + Q_try_delta';

        % stop trying criteria - relavant precision:
        delta_rel = max(abs([h_try_delta' Q_try_delta'] ...
                    ./[h_try(:,2) Q_try(:,2)]));

        if delta_rel < tol  % stop criteria;
            break;
        end
    end     %end loop k, finish iteration for time j;

    h = [h h_try(:,2)];     % collect results for output;
    Q = [Q Q_try(:,2)];     % collect results for output;

    % base(c1)/try(c2) values for next time step;
    h_try = [h_try(:,2) h_try(:,2)];
    Q_try = [Q_try(:,2) Q_try(:,2)];

end     %end loop jj, finish calculation for all time steps;

% more terms to be returned;
% Parameters testing (initial up/down stream only);
B = wid_bed(:,1)*ones(1,N) + 2*slp_bank(:,1)*ones(1,N).*h;  %surface width
A = (wid_bed(:,1)*ones(1,N) + slp_bank(:,1)*ones(1,N).*h).*h; P =
(wid_bed(:,1)*ones(1,N) + 2*h .*
sqrt((slp_bank(:,1)*ones(1,N)).^2+1)); R = A./P; U =
1./(n(:,1)*ones(1,N)).*R.^(2/3).*(slp_bed(:,1)*ones(1,N)).^(.5); \\
QQ = U.*A;

return
```

D.3.3 Temperature and DO models (integrated) - ADRE equations

```
function [T, DO, Tbed, DObed] = MacCormack_c(T_up, DO_up, ...
                    T_down, DO_down, Q, h, qG, TG, DOG, ...
                    D_Tbed, D_DObed, delta_z, M_bed, U, A, B, wid_bed, ...
                    M, N, delta_t, delta_x, Weather, SE, SA, ID);
%%%%%%%%%%%%%%%%%%%%%%%%%%%%%%%%%%%%%%%%%%%%%%%%%%%%%%%%%%%%%%%%%%%%%%%%%%%%
% Function:
%   TDO_MacCormack_c.m --- temperature and DO models using corrected
%                           MacCormack numerical scheme.
%
% Inputs:
%   T_up --- upper boundary time series temperature (*C); N by 1;
%   DO_up --- upper boundary time series DO (mg/L); N by 1;
%   T_down --- lower boundary time series temperature (*C); N by 1;
%   DO_down --- lower boundary time series DO (mg/L); N by 1;
%   Q --- simulated flow by Flow model (m3/s); M by N;
%   h --- simulated water stage by Flow model (m); M by N;
%   qG --- groundwater flow (m/s); positive if into stream; M_bed by M;
%   TG --- groundwater temperature in aquifer (20.5*C); scalar; 1 by 1;
%   DOG --- groundwater DO in aquifer (mg/L); scalar; 1 by 1;
%   D_Tbed --- Heat dispersive coefficient in streambed;
%   D_DObed --- Mass dispersive coefficient in streambed flow;
%   delta_z --- vertical space step size in streambed;
%   M_bed --- number of space grids in bed;
%   U --- simulated flow velocity by flow model (m/s); M by N;
%   A --- simulated cross section area by flow model (m^2); M by N;
```

```
%   B --- simulated water surface width (m); M by N;
%   wid_bed --- bed width (m);  M by 1;
%   M --- total number of space grid of stream reach; scalar; 1 by 1;
%   N --- total number of time grid of time series data; scalar; 1 by 1;
%   delta_t --- time step length (s); scalar; 1 by 1;
%   delta_x --- space step length of stream reach (m); scalar; 1 by 1;
%   Weather --- weather data; N by 7; but will be 7 by N for use;
%   SE --- simulated exposure of stream to direct solar radiation; M by N;
%   SA --- simulated solar angle (rad); M by N;
%   ID --- correction coefficients for T module; 1 by 6;
%
% Outputs:
%   T --- simulated temperature (*C);
%   DO --- simulated DO (mg/L);
%   Tbed --- simulated bed temperature profile (*C);
%   DObed --- simulated bed flow DO profile (mg/L);
%%%%%%%%%%%%%%%%%%%%%%%%%%%%%%%%%%%%%%%%%%%%%%%%%%%%%%%%%%%%%%%%%%%%%%%%%%%%

% ID=ID(1:6)     % turn on for T model optimization;
% IDDO=ID        % turn on for DO model optimization;

% ID: [gw, solar, longwave1, convection, evaporation longwave2]
ID = [1.0000    0.262    0.21   4.7932    0.2281   0.1457];% SSE = 45.4186;
% The above cofficients are calibrated values for T correction;

% set to 1/0 to include/exclude numerical dispersion effect;
numerical=1;

A=A+B.*ones(size(A))*0.2;   % correction for equivalent deadzone effect;

D_T = 100;       % heat dispersivity in main channel;
D_DO = 100;      % mass dispersivity in main channel;
fprintf('\n');
fprintf('Main stream Dispersion number = %2.3f \n',D_T*delta_t/delta_x^2);
fprintf('Main stream Advection number = %2.3f \n',0.4*delta_t/delta_x);
fprintf('Streambed Dispersion number = %2.3f \n',D_Tbed*delta_t/delta_z^2);
fprintf('Main stream Advection number = %2.3f \n',qG(1)*delta_t/delta_x);

D_bed_n1 = delta_z/2*qG(1)*numerical;     % num dispersion for Bkwd Space;
D_bed_n2 = delta_t/2*qG(1)^2*numerical;   % num dispersion for Bkwd Time;

CP=4218*1000;   % Specific heat capacity of water (J/m3);

% Linear interpolation for initials;
% Linear interpolation of T/DO along logitudinal reach grids;
T = ones(M,1)*T_up(1) + ([0:M-1]')/(M-1)*(T_down(1) - T_up(1)); DO =
ones(M,1)*DO_up(1) + ([0:M-1]')/(M-1)*(DO_down(1) - DO_up(1));
A_tmp =  (A(1:M-1,:) + A(2:M,:))/2; % mean for diffusion;

% initial values for vertical/longitudinal streambed temperature/DO.
Tbed = ones(M_bed,1)*T' + ([0:M_bed-1]')/(M_bed-1)*(TG - T'); DObed
= ones(M_bed,1)*DO' + ([0:M_bed-1]')/(M_bed-1)*(DOG - DO');

% Weather data;
Weather = Weather';  % N by 7 -> 7 by N
DT = Weather(1,:);   % Time;
TA = Weather(2,:);   % air temperature (*C));
HM = Weather(3,:);   % air humidity %;
TP = Weather(4,:);   % air total pressure (Kpa);
SR = Weather(5,:);   % solar radiation (W/m^2);
RN = Weather(6,:);   % rain (mm);
WN = Weather(7,:);   % wind (m/s);

% =========================================================================
% ---------------------------------------------------------------------
% Solar radiation;
SR = ones(M, 1)*SR.*SE;     % Correct solar(J/m^2/s) with shading effect;
SA = SA/pi*180;             % convert solar angle from rad to degree;
```

```
m=(SA>1.24);                % m is logic vector N by 1;
n=1-m;                      % a is reverse of a;
Albedo_S=(m*1.18+n).*(m.*SA+n).^(-0.77); % Anderson_1954; LeBlanc_1997;
SR=SR.*(1-Albedo_S);        % Correct solar with reflection (J/m^2/s);
T_SR=SR.*B/CP;              % Contribution to temp;

% ----------------------------------------------------------------------
% Longwave radiation;
sbc=5.67*10^(-8);  % Stefan-Boltzman C = 5.67 x 10 -8 Watts /m^2/K;
%Chaupra(P567):saturated vapor pressure (mmHg) at water surface
% Temperature; 1 kpa=10 mb = 10 * 0.02953 inHg = 10 * 0.02953 *
%25.4 mm =7.50062mmHg; 1mmHg=133.3pa;
e_air=(HM/100).*4.596.*exp(17.27*TA./(237.3+TA))*133.3; % pa=N/M^2;
% Chaupra_1997(P570):Emissivity of clear night sky;
EmissivitySky = 0.7+0.031*sqrt(e_air/133.3);    % 0.5 ~ 0.7
%EmissivitySky = 1
% Chaupra(P570),Tang(2004): Emissivity of water = 0.97;
EmissivityWater = 0.97;
% Tang: absorptivity of water for long wave radiation is 0.935;
% Chaupra(P570): reflection coefficient is generally small (~=0.03);
Albedo_L = 0.065;     % 0.03 ~ 0.065;
J_LR=sbc*EmissivitySky.*(TA+273.15).^4*(1-Albedo_L); % Long wave radiation;
T_LR = ones(M, 1)*J_LR.*B/CP;               % Contribution to temp;

% ----------------------------------------------------------------------
%Conduction & Convection at water surface: wind function;
IDC='LeBlanc'; switch IDC
    case 'LeBlanc'
        % LeBlanc(Krajewski, 1982), 1996: F(w)=0.0228*TP*Wind
        % TP = airPressure(Kpa), Wind=WindSpeed(m/s);
        WNC=0.0228*TP.*WN;
    otherwise
        % Chaupra(P571), Wind=wind(m/s), 0.47 is Bowen's coefficient;
        WNC=0.47*(19+0.95*WN.^2);
end

% ----------------------------------------------------------------------
% Latent Heat: Evaporation and condensation: Dalton's law.
% Refer:Runsheng Tang(2004)(Carrier, 1918): WN(m/s), P(N/M^2);
WNE = 0.0887+0.07815*WN; % Wind function, WN = wind speed (m/s);

% ======================================================================
% ----------------------------------------------------------------------
% correctors for DO model;
%IDDO = [ka, solar, respiration, bod, sod, half-saturation]
IDDO = [0.03    4.1745   32.4552    0.085  300.9551  200.2586]; % SSE = 27

% ----------------------------------------------------------------------
% Reaeration from atmosphere(/day): (Chapra_1997:P377; EPA_1985:p103-106)
ID_DO='OD';
switch ID_DO    %(/day)
    case 'OD'
        % O'Connor-Dobbins, 1956; for D=(0.3 - 9.14m), v=0.15-0.49m/s);
        Ka=3.93*(U.^0.5)./(h.^1.5);
    case 'CH'
        % Churchill et al. 1962;  for D=(0.61 - 3.35m), v=0.55-1.52m/s);
        Ka=5.026*U./(h.^1.67);
    case 'OG'
        % Owens and Gibbs, 1964; for  D=(0.12 - 0.73m), v=0.03-0.55m/s);
        Ka=5.32*(U.^0.67)./(h.^1.85);
end
Ka=Ka/3600/24*IDDO(1);       % from /day to /s;
% Temperature correction: 1.022 ~ 1.024; EPA, 1985: P125;
ThetaKa=1.024;

% ----------------------------------------------------------------------
% Photosynthesis by Algae (EPA, 1985: P125; 2. Cox, 2003 Review: P24, 27)
Alg=.001;    %(mg/L) By measurements: 0.35~1.4 ug/L (2004, by Li);
```

```
ThetaP=1.036;   %Parkhill & Gulliver, 1998; Megard et al., 1984);
MaxGrowth=1/3600/24*IDDO(2); %algae maximum growth rate (/day);
SRLimit = IDDO(6); PSR = (SR<SRLimit).*SR + (SR>=SRLimit)*SRLimit;
GRate=MaxGrowth.*PSR;   % modified from Xiaoqing's Dissertation: P185-186;
AlgToOxy = 138*32/106/12;   % Zeng, Xiaoqing's Dissertation: P184,188;

% ----------------------------------------------------------------------
% Respiration by Algae:
RRate=1/3600/24*IDDO(3); %Maximum respiration rate at 20*C; (/day);
% Parkhill_Gulliver_1998; Gulliver_Stefan_1984b; Ambrose_et_al_1988;
ThetaR=1.045;
AlgConsumeOxy=138*32/106/12; %Zeng Xiaoqing's Dissertation: P184,188;

% ----------------------------------------------------------------------
% BOD decay;
ThetaB=1.047;    % Arrhenius coefficient for BOD; Knowles_1978
BOD = 4;        %mg/L by field grab samples;
BODRate = 1/3600/24*IDDO(4)*BOD; % BOD decay rate; 1/s;
% ----------------------------------------------------------------------
% SOD decay; % Arrhenius coefficient for BOD;
ThetaS=1.065; %http://wilsontxt.hwwilson.com/pdfhtml/02385/am81d/yfh.htm
% cox_2003, 1.065 for SOD;
SODRate = 1/3600/24*IDDO(5); % SOD decay rate: mg/m^2/s;

D_Tbed_ID = 1;  % control if add in straembed heat diffusion effect;
D_DObed_ID = 1; % control if add in straembed DO diffusion effect;

% ======================================================================
% Begin loop:
% ======================================================================
for jj = 2:N
    progressbar(jj/N);              % progress indicator;
    qGr = qG(:,jj).*wid_bed(:,1);   % groundwater in per unit length(m^2/s);
    qGv = ones(M_bed, 1)*qG(:,jj)'; % expand matrix to M_bed by M;
    % initial values for vertical/longitudinal streambed temperature/DO.
    if qGv(1)>0
        qGv_gain = 1;    % aquifer -> stream;
        qGv_loss = 0;    % stream -> aquifer;
    else
        qGv_gain = 0;    % aquifer -> stream;
        qGv_loss = 1;    % stream -> aquifer;
    end

% --------------------------------------------------------------------------
% step1: FTFS - stream reach T/DO;
% --------------------------------------------------------------------------
    % Upboundary conditions = up input;
    T(1,jj) = T_up(jj);     % upstream input T;
    DO(1,jj) = DO_up(jj);   % upstream input DO;

    % ----------------------------------------------------------------------
    % T/Energy exchange with its environment;
    % ----------------------------------------------------------------------
    % streambed T/DO gradient;
    dTdz = [(Tbed(2,:,jj-1) - Tbed(1,:,jj-1))/(delta_z)]';
    dDOdz = [(DObed(2,:,jj-1) - DObed(1,:,jj-1))/(delta_z)]';
    TG_mean = [(Tbed(2,:,jj-1) + Tbed(1,:,jj-1))/2]';
    DOG_mean = [(DObed(2,:,jj-1) + DObed(1,:,jj-1))/2]';
    % ----------------------------------------------------------------------
    % Longwave radiation by water;
    TW = T(2:M-1,jj-1)+273.15;         % water Temp (K);
    J_WR = sbc*EmissivityWater*TW.^4;  % Long wave radiation;
    T_WR = -J_WR.*B(2:M-1,jj-1)/CP;     % Contribution to temp;
    % Nodes in between up and lower boundary.
    % ----------------------------------------------------------------------
    % Conduction & Convection at water surface: wind function Contrib to T;
    T_CN = WNC(jj-1)*(TA(jj-1)-T(2:M-1,jj-1)).*B(2:M-1,jj-1)/CP;
    % ----------------------------------------------------------------------
```

```
% Latent Heat: Evaporation and condensation: pa=N/M^2;
e_water = 4.596.*exp(17.27*T(2:M-1,jj-1)./(237.3+T(2:M-1,jj-1)))*133.3;
T_EV = WNE(jj-1).*(e_air(jj-1)-e_water).*B(2:M-1,jj-1)/CP;

% ---------------------------------------------------------------------
% DO/Mass exchange with its environment -- inside loop;
% ---------------------------------------------------------------------
% Reaeration by atmosphere(1/t):(Chapra,1997: P377; EPA,1985: p103-106)
Kajj = Ka(2:M-1,jj-1).*(ThetaKa.^(T(2:M-1,jj-1)-20)); %correction by T;
CS=14.652-0.41022*T(2:M-1,jj-1) ...          % EPA, 1985: P91;
        +0.007991*(T(2:M-1,jj-1).^2) ...     % Cox, 2003: P8 -->
        -7.7774*10^-5*(T(2:M-1,jj-1).^3);    % --> Elmore&Hayes, 1960;
DO_Ka=Kajj.*(CS-DO(2:M-1,jj-1)); % Effect on DO(mg/L/s);
% ---------------------------------------------------------------------
% Photosynthesis by Algae (EPA,1985: P125; Cox,2003: P24,27)
Growth=GRate(2:M-1,jj-1).*(ThetaP.^(T(2:M-1,jj-1)-20)); % correct by T;
DO_P=Alg.*Growth*AlgToOxy;   % EPA, 1985: P188;(mg/L/s*m^2);
% ---------------------------------------------------------------------
% Respiration by Algae(mg/L/s*m^2):
Respiration = RRate*(ThetaR.^(T(2:M-1,jj-1)-20));    % correction by T;
DO_R= Alg.*Respiration*AlgConsumeOxy;                % EPA, 1985: P188;
% ---------------------------------------------------------------------
% BOD decay; assuming constant rate corrected by T;
BOD_Decay = BODRate*(ThetaB.^(T(2:M-1,jj-1)-20));    % correction by T;
DO_BOD= BOD_Decay;                                   % mg/L/s*m^2
% ---------------------------------------------------------------------
% SOD decay; assuming constant rate corrected by T;
% correction by T; here 0.001 convert g/m3 to mg/L;
SOD_Decay = SODRate*(ThetaS.^(T(2:M-1,jj-1)-20))./h(2:M-1,jj-1)*0.001;
DO_SOD= SOD_Decay;    % mg/L/s*m^2;
% ---------------------------------------------------------------------
D_n1 = -U(2:M-1,jj-1)*delta_x/2*numerical;    %num disp for Bkwd Space;
D_n2 = -U(2:M-1,jj-1).^2*delta_t/2*numerical; %num disp for Bkwd Time;
% ---------------------------------------------------------------------
T_slp1(2:M-1,1) = -1/delta_x.*(Q(3:M,jj-1).*T(3:M,jj-1) ...
         - Q(2:M-1,jj-1).*T(2:M-1,jj-1)) ...
         + (D_T-D_n1-D_n2)./(delta_x^2) ...
         .* (A_tmp(2:M-1,jj-1).*(T(3:M,jj-1) - T(2:M-1,jj-1)) ...
         - A_tmp(1:M-2,jj-1).*(T(2:M-1,jj-1) - T(1:M-2,jj-1))) ...
         + ID(1)*D_Tbed_ID*D_Tbed*wid_bed(2:M-1,1).*dTdz(2:M-1,1) ...
         + ID(1)*qGr(2:M-1,1).*(qGv_gain*TG_mean(2:M-1,1) ...  % gwA;
         + qGv_loss*T(2:M-1,jj-1)) ...                      % gwA;
         + ID(2)*T_SR(2:M-1,jj-1) ...                       % solar;
         + ID(3)*T_LR(2:M-1,jj-1) + ID(6)*T_WR ...          % Longwave;
         + ID(4)*T_CN ...                                   % Convection;
         + ID(5)*T_EV;                                      % Evaporation;
DO_slp1(2:M-1,1) = -1/delta_x.*(Q(3:M,jj-1).*DO(3:M,jj-1) ...
        - Q(2:M-1,jj-1).*DO(2:M-1,jj-1)) ...
        + (D_DO-D_n1-D_n2)./(delta_x^2) ...
        .* (A_tmp(2:M-1,jj-1).*(DO(3:M,jj-1) - DO(2:M-1,jj-1)) ...
        - A_tmp(1:M-2,jj-1).*(DO(2:M-1,jj-1) - DO(1:M-2,jj-1))) ...
        + D_DObed_ID*D_DObed*wid_bed(2:M-1,1).*dDOdz(2:M-1,1) ...
        + qGr(2:M-1,1).*(qGv_gain*DOG_mean(2:M-1,1) ...
        + qGv_loss*DO(2:M-1,jj-1)) ...
        +A(2:M-1,1).*( ...
        + DO_Ka ...
        + DO_P ...
        - DO_R ...
        - DO_BOD ...
        - DO_SOD);
% results;
T(2:M-1,jj) = (A(2:M-1,jj-1).*T(2:M-1,jj-1) ...
                + T_slp1(2:M-1,1).*delta_t)./A(2:M-1,jj);
DO(2:M-1,jj) = (A(2:M-1,jj-1).*DO(2:M-1,jj-1) ...
                + DO_slp1(2:M-1,1).*delta_t)./A(2:M-1,jj);
% Lower boundary = 2Ci - C(i-1);
T(M,jj) = 2*T(M-1,jj) - T(M-2,jj);
DO(M,jj) = 2*DO(M-1,jj) - DO(M-2,jj);
```

```
    DO(:,jj) = (DO(:,jj)>0).*DO(:,jj);  % if DO <0 then set to 0;
% ------------------------------------------------------------------------
% step1: FTFS - Streambed T/DO profile;
% ------------------------------------------------------------------------
    Tbed(1,:,jj) = T(:,jj)';      % streambed surface temperature;
    DObed(1,:,jj) = DO(:,jj)';    % streambed surface DO;
    % in between - slp; Please note no minus sign before qGv since qGv is
    % defined positive from aquifer to stream
    Tbed_slp1(2:M_bed-1,:)  = qGv(2:M_bed-1,:)./delta_z  ...
                 .*(Tbed(3:M_bed,:,jj-1)-Tbed(2:M_bed-1,:,jj-1)) ...
                 + (D_Tbed+D_bed_n1+D_bed_n2)/(delta_z^2) ...
                 * (Tbed(3:M_bed,:,jj-1) - 2*Tbed(2:M_bed-1,:,jj-1) ...
                 + Tbed(1:M_bed-2,:,jj-1));
    DObed_slp1(2:M_bed-1,:)  = qGv(2:M_bed-1,:)./delta_z  ...
                 .*(DObed(3:M_bed,:,jj-1)-DObed(2:M_bed-1,:,jj-1)) ...
                 + (D_DObed+D_bed_n1+D_bed_n2)/(delta_z^2) ...
                 * (DObed(3:M_bed,:,jj-1) - 2*DObed(2:M_bed-1,:,jj-1) ...
                 + DObed(1:M_bed-2,:,jj-1));
    Tbed(2:M_bed-1,:,jj) = Tbed(2:M_bed-1,:,jj-1) ...
                    + Tbed_slp1(2:M_bed-1,:).*delta_t;
    DObed(2:M_bed-1,:,jj) = DObed(2:M_bed-1,:,jj-1) ...
                    + DObed_slp1(2:M_bed-1,:).*delta_t;
    % streambed bottom conditions;
    Tbed(M_bed,:,jj) = TG;
    DObed(M_bed,:,jj) = DOG;

% ------------------------------------------------------------------------
% step2: BTBS - stream reach T/DO;
% ------------------------------------------------------------------------
    % Upboundary conditions = up input;
    T_tmp(1,1) = T_up(jj);
    DO_tmp(1,1) = DO_up(jj);

    % --------------------------------------------------------------------
    % T/Energy exchange with its environment:
    % --------------------------------------------------------------------
    % streambed T/DO gradient;
    dTdz = [(Tbed(2,:,jj) - Tbed(1,:,jj))/(delta_z)]';
    dDOdz = [(DObed(2,:,jj) - DObed(1,:,jj))/(delta_z)]';
    TG_mean = [(Tbed(2,:,jj) + Tbed(1,:,jj))/2]';
    DOG_mean = [(DObed(2,:,jj) + DObed(1,:,jj))/2]';
    % --------------------------------------------------------------------
    % Longwave radiation by water;
    TW = T(2:M-1,jj)+273.15;          % water Temp (K);
    J_WR = sbc*EmissivityWater*TW.^4; % Long wave radiation;
    T_WR = -J_WR.*B(2:M-1,jj)/CP;     % Contribution to temp;
    % --------------------------------------------------------------------
    % Conduction & Convection at water surface: wind function;
    T_CN = WNC(jj)*(TA(jj)-T(2:M-1,jj)).*B(2:M-1,jj)/CP; % T;
    % T_CN = k*(T(2:M-1,jj) - TA(jj)).*B(2:M-1,jj)/CP; % T;
    % --------------------------------------------------------------------
    % Latent Heat: Evaporation and condensation: pa=N/M^2;
    e_water = 4.596.*exp(17.27*T(2:M-1,jj)./(237.3+T(2:M-1,jj)))*133.3;
    % T_EV = WNE(jj-1).*(e_air(jj-1)-e_water).*B(2:M-1,jj-1)/CP;
    T_EV = WNE(jj).*(e_air(jj)-e_water).*B(2:M-1,jj)/CP;

    % --------------------------------------------------------------------
    % DO/Mass exchange with its environment -- inside loop;
    % --------------------------------------------------------------------
    % Reaeration by atmosphere(1/t):(Chapra,1997: P377; EPA,1985: p103-106)
    Kajj = Ka(2:M-1,jj).*(ThetaKa.^(T(2:M-1,jj)-20));  % correction by T;
    CS = 14.652-0.41022*T(2:M-1,jj) ...         % EPA, 1985: P91;
        + 0.007991*(T(2:M-1,jj).^2) ...    % Cox, 2003: P8 -->
        - 7.7774*10^-5*(T(2:M-1,jj).^3);   % --> Elmore&Hayes, 1960;
    DO_Ka=Kajj.*(CS-DO(2:M-1,jj)); % Effect on DO(mg/L/s*m^2);
    % --------------------------------------------------------------------
    % Photosynthesis by Algae (EPA,1985: P125; Cox,2003: P24,27)
    Growth = GRate(2:M-1,jj).*(ThetaP.^(T(2:M-1,jj)-20)); %correction by T;
```

```
    DO_P=Alg.*Growth*AlgToOxy;   % EPA, 1985: P188;(mg/L/s*m^2);
    % ----------------------------------------------------------------------
    %Respiration by Algae(mg/L/s*m^2):
    Respiration = RRate*(ThetaR.^(T(2:M-1,jj)-20));      % correction by T;
    DO_R= Alg.*Respiration*AlgConsumeOxy; % EPA, 1985: P188;
    % ----------------------------------------------------------------------
    % BOD decay; assuming constant rate corrected by T;
    BOD_Decay = BODRate*(ThetaB.^(T(2:M-1,jj)-20));      % correction by T;
    DO_BOD= BOD_Decay;    % mg/L/s*m^2
    % ----------------------------------------------------------------------
    % SOD decay; assuming constant rate corrected by T;
    % correction by T; here 0.001 convert g/m3 to mg/L;
    SOD_Decay = SODRate*(ThetaS.^(T(2:M-1,jj)-20))./h(2:M-1,jj)*0.001;
    DO_SOD= SOD_Decay;    % mg/L/s*m^2
    % ----------------------------------------------------------------------

    D_n1 = U(2:M-1,jj)*delta_x/2*numerical;   %num disper for Bkwd Space;
    D_n2 = U(2:M-1,jj).^2*delta_t/2*numerical; %num disper for Bkwd Time;
    % Nodes in between.
    T_slp2(2:M-1,1)  = -1/delta_x.*(Q(2:M-1,jj).*T(2:M-1,jj) ...
            - Q(1:M-2,jj).*T(1:M-2,jj)) ...
            + (D_T-D_n1-D_n2)./(delta_x^2) ...
            .* (A_tmp(2:M-1,jj).*(T(3:M,jj) - T(2:M-1,jj)) ...
            - A_tmp(1:M-2,jj).*(T(2:M-1,jj) - T(1:M-2,jj))) ...
            + ID(1)*D_Tbed_ID*D_Tbed*wid_bed(2:M-1,1).*dTdz(2:M-1,1) ...
            + ID(1)*qGr(2:M-1,1).*(qGv_gain*TG_mean(2:M-1,1) ...  % gwA
            + qGv_loss*T(2:M-1,jj)) ...                         % gwA
            + ID(2)*T_SR(2:M-1,jj) ...                          % solar;
            + ID(3)*T_LR(2:M-1,jj) + ID(6)*T_WR ...             % Longwave;
            + ID(4)*T_CN ...                                    % Convection;
            + ID(5)*T_EV;                                       % Evaporation;
    DO_slp2(2:M-1,1)  = -1/delta_x.*(Q(2:M-1,jj).*DO(2:M-1,jj) ...
            - Q(1:M-2,jj).*DO(1:M-2,jj)) ...
            + (D_DO-D_n1-D_n2)./(delta_x^2) ...
            .* (A_tmp(2:M-1,jj).*(DO(3:M,jj) - DO(2:M-1,jj)) ...
            - A_tmp(1:M-2,jj).*(DO(2:M-1,jj) - DO(1:M-2,jj))) ...
            + D_DObed_ID*D_DObed*wid_bed(2:M-1,1).*dDOdz(2:M-1,1) ...
            + qGr(2:M-1,1).*(qGv_gain*DOG_mean(2:M-1,1) ...
            + qGv_loss*DO(2:M-1,jj)) ...
            + A(2:M-1,2).*( ...
            + DO_Ka ...
            + DO_P ...
            - DO_R ...
            - DO_BOD ...
            - DO_SOD);
    % results;
    T_tmp(2:M-1,1) = (A(2:M-1,jj-1).*T(2:M-1,jj-1) ...
                    + T_slp2(2:M-1)*delta_t)./A(2:M-1,jj);
    DO_tmp(2:M-1,1) = (A(2:M-1,jj-1).*DO(2:M-1,jj-1) ...
                    + DO_slp2(2:M-1)*delta_t)./A(2:M-1,jj);
    % Lower boundary = 2Ci - C(i-1);
    T_tmp(M,1) = 2*T_tmp(M-1,1) - T_tmp(M-2,1);
    DO_tmp(M,1) = 2*DO_tmp(M-1,1) - DO_tmp(M-2,1);
    DO_tmp(:,1) = (DO_tmp(:,1)>0).*DO_tmp(:,1);  % if DO <0 then set to 0;

% ----------------------------------------------------------------------
% step3: Correction - stream reach T/DO;
% ----------------------------------------------------------------------
    t1 = T(1:M-1,jj);
    T(1:M,jj) = (T(1:M,jj)+T_tmp(1:M,1))/2;
    DO(1:M,jj) = (DO(1:M,jj)+DO_tmp(1:M,1))/2;
    t2 = T(1:M-1,jj);

% --------------------------------------------------------------------------
% step2: BTBS - Streambed T/DO profile;
% --------------------------------------------------------------------------
    % streambed T profile at time = jj;
    % streambed surface conditions;
```

```
    Tbed_tmp(1,:,1) = T_tmp';
    DObed_tmp(1,:,1) = DO_tmp';
    % in between - slp; Please note no minus sign before qGv since qGv is
    % defined positive from aquifer to stream
    Tbed_slp2(2:M_bed-1,:)  = qGv(1:M_bed-2,:)./delta_z ...
                    .*(Tbed(2:M_bed-1,:,jj)-Tbed(1:M_bed-2,:,jj)) ...
                    + (D_Tbed-D_bed_n1-D_bed_n2)/(delta_z^2) ...
                    *(Tbed(3:M_bed,:,jj) - 2*Tbed(2:M_bed-1,:,jj) ...
                    + Tbed(1:M_bed-2,:,jj));
    DObed_slp2(2:M_bed-1,:)  = qGv(1:M_bed-2,:)./delta_z ...
                    .*(DObed(2:M_bed-1,:,jj)-DObed(1:M_bed-2,:,jj)) ...
                    + (D_DObed-D_bed_n1-D_bed_n2)/(delta_z^2) ...
                    * (DObed(3:M_bed,:,jj) - 2*DObed(2:M_bed-1,:,jj) ...
                    + DObed(1:M_bed-2,:,jj));
    Tbed_tmp(2:M_bed-1,:,1) = Tbed(2:M_bed-1,:,jj-1) ...
                    + Tbed_slp2(2:M_bed-1,:).*delta_t;
    DObed_tmp(2:M_bed-1,:,1) = DObed(2:M_bed-1,:,jj-1) ...
                    + DObed_slp2(2:M_bed-1,:).*delta_t;
    % streambed bottom conditions: constant;
    Tbed_tmp(M_bed,:,1) = TG;
    DObed_tmp(M_bed,:,1) = DOG;

% ---------------------------------------------------------------------
% step3: Correction - Streambed T/DO profile;
% ---------------------------------------------------------------------
    Tbed(:,:,jj) = (Tbed_tmp(:,:,1) + Tbed(:,:,jj))/2;
    DObed(:,:,jj) = (DObed_tmp(:,:,1) + DObed(:,:,jj))/2;
end     % end T and DO iteration;

return
```